Dynamic Performance of Cemented Rockfill under Blast-Induced Vibrations

Muhammad Zaka Emad

Doctor of Philosophy

Department of Mining and Materials Engineering,
Faculty of Engineering

McGill University
Montreal, Quebec, Canada
December 2013

A thesis submitted to McGill University in partial fulfillment of the requirements for the degree of Doctorate of Philosophy

ABSTRACT

Sublevel stoping methods with delayed backfill are a popular choice for mining tabular steeply dipping ore deposits. Cemented rockfill (CRF) or consolidated rockfill is a type of backfill that is composed of sized or un-sized aggregates coated with binder slurry having an overall cement content of 4 to 6%. Development waste rock can be used in lieu of aggregates or can be blended with aggregates. Some inherent issues associated with CRF practice include high operational cost, difficulty to tight-fill, segregation and heterogeneity of the mixture, and failure into adjacent stopes causing ore dilution. A CRF block receives dynamic load due to blast vibrations from adjacent production stopes. The most commonly observed mode of CRF failure is a wedge shape located at the top of the exposed fill face. The cause of wedge failure has been reported to be induced by blast vibrations. A CRF block may also fail due to blast-hole drilling inaccuracy and the CRF is accidently blasted with the production blast. Another mode of observed CRF failure is due to over-break of primary stope resulting in an awkward giant belly shaped stope, when backfill is placed. The belly-shape backfill block is destabilized when exposed during mining of adjacent stopes.

The stability analyses of backfill are conventionally performed using the Fill Strength Requirement (FSR) Models or limit equilibrium method. However, it has been verified from CRF operations and numerical modelling studies that relying absolutely on FSR may not warrant complete understanding of mechanical behaviour of the CRF. This is because FSR models are based on static strength only and this approach neglects many important factors like mining method, mining sequence, stope inclination, material properties, segregation, cold joints and blast induced vibrations from adjacent production stopes. Numerical modelling helps in verifying and extending limit equilibrium analysis by adding site and case specific scenario. Numerical modeling is a useful tool for understanding backfill behaviour under static and dynamic loading conditions. When the CRF is subjected to blast-induced vibrations from adjacent stope production, a dynamic analysis is required. Advanced computational codes like FLAC3D-Dynamic allow the user to model such dynamic effects as blast vibration propagation. This gives more detailed depiction of blast-induced damage than is possible by the use of charge-weight scaling laws.

In this thesis, a new methodology for the design of CRF under static and dynamic loading conditions is developed. First a comprehensive literature review of the backfill material is

accomplished which included a review of CRF operations and laboratory testing programs. This is followed by a review of numerical modelling studies performed on CRF. Based on the findings from literature review, two numerical models for CRF are developed using FLAC3D code. One of the models considers stopes to be inclined at about 67 degrees and the other considers vertical stopes. The numerical models are then used to study different aspects of CRF practice including the loading conditions, blast-induced vibrations from adjacent production stopes, vertical block mining method, CRF properties, CRF placement method and segregation. A case study mine CRF model is then constructed in accordance with site conditions and the geomechanical data provided by the mine. The case study mine numerical model is calibrated with in-situ stress measurements previously conducted at the case study mine. Mining and backfilling sequence is simulated with the calibrated model and the secondary stope is mined out in three lifts.

In-situ blast vibration monitoring experiment in CRF is performed at the case study mine. Two geophones are installed: one inside CRF and the other on the surface of the CRF, and all three production blasts of the adjacent secondary stope are recorded. The detailed procedure, installation and results are presented in the thesis. The results are also used for numerical model calibration. To calculate damping coefficient for the model and blast load magnitude an equivalent cavity model is constructed. The equivalent cavity model is applied with reduced borehole pressure and the model is compared with charge-weight scaling law. The blast load and damping coefficients are extracted from equivalent cavity model and applied as input parameters for the CRF model. The numerical model is calibrated using blast load and damping coefficients obtained from the equivalent cavity model by computing the blast vibrations at a location similar to the one on site. The model is calibrated for all three blast lifts and results are presented.

Finally, a CRF failure control study is carried out which encompasses the base case scenario of a planned stope at the case study mine, selective mining strategy for mining high grade ore, strategy of leaving an ore skin, tactically varying CRF properties vertically in CRF. In addition a parametric study is conducted to improve CRF stability by varying CRF properties and possible trends are presented. All results compare static loading versus blast loading scenario on CRF. The results include comparison of backfill stresses and profiles of peak particle velocity. Results of all analyses are presented along with the findings, conclusions, suggestions for future work and statement of contribution.

RÉSUMÉ

La méthode d'abattage de chantiers ouverts avec remblayage retardé est populaire les gisements tabulaires à fort pendage. Le remblai rocheux cimenté (CRF) est un remblai composé d'agrégat dimensionné ou non dimensionné recouvert d'une couche de boue cimentée, atteignant une teneure globale de ciment entre 4 et 6%. Les résidus du développement minier peuvent aussi remplacer l`agrégat ou être mélangés avec l'agrégat. Les problèmes inhérents liés à l'utilisation du CRF incluent un haut cout opérationnel, la difficulté de remplissage étanche, la ségrégation et l'hétérogénéité de la mixture, et l'affaissement du CRF dans un chantier adjacent menant à la dilution du minerai. Un bloque de CRF reçoit des contraintes dynamiques dues aux vibrations de tir lors de l'abattage des chantiers de production adjacents. Le mode de rupture le plus observé est un tétraèdre situé en haut de la face exposé du remblai. La cause de l'affaissement du tétraèdre est reportée comme étant les vibrations de tir du chantier adjacent. Un bloque de CRF peut aussi l'affaisser dans le cas ou les trous de mine sont imprécis et le CRF est accidentellement abattu. Une autre mode d'affaissement observé a lieu lorsqu'il y a over-break dans le chantier primaire abattu. L'excès de remblai placé dans le chantier primaire est déstabilisé lorsque que le chantier adjacent est ouvert.

L'analyse de stabilité pour le remblai est conventionnellement exécutée avec des modèles de force requise du remblai (FSR) basé sur l'équilibre statique de forces. Par contre, il est vérifié par les opérations qui se servent du CRF et par la modélisation numérique que se fier uniquement aux modèles FSR peut mener à une connaissance incomplète du comportement mécanique du remblai. Notamment, les modèles FSR sont basés seulement sur l'équilibre des forces statiques et ignorent d'autres facteurs tels que la méthode d'abattage, la séquence d'abattage, l'inclinaison du chantier, les propriétés le la roche, la ségrégation du remblai, les joints froids, et les vibrations de tir induites par l'abattage d'un chantier adjacent. La modélisation numérique aide à vérifier et à compléter l'analyse de l'état d'équilibre limite. La modélisation numérique est un outil utile pour comprendre le comportement du remblai sous des contraintes statiques et dynamiques. Quand le CRF est soumis à des vibrations de tir, une analyse dynamique est requise. Des codes de calcul sophistiqués tel que FLAC3D-Dynamic permettent l'utilisateur de modéliser les effets dynamiques tel que la détonation d'explosifs et la propagation de l'onde de choc. Ceci donne une représentation plus détaillé des dégâts provoqués par le tir que peut être obtenu avec l'utilisation des chartes empiriques.

Dans cette thèse, une nouvelle méthodologie pour la conception de CRF sous des contraintes statiques et dynamiques est développée. Premièrement, un examen de la littérature existante à été accompli. Les opérations minières employant le CRF sont examinées ainsi que les programmes d'essai en laboratoire et les études de modélisation numérique effectuées pour le CRF. Basés sur l'examen de la littérature existante, deux modèles numériques pour le CRF on étés développé en utilisant FLAC3D. Le premier modèle considère un pendage de 67 degrés pour les chantiers, lorsque l'autre considère des chantiers verticaux. Ces modèles numériques sont ensuite utilisés pour l'étude de différents aspects de la pratique du CRF tels que les conditions de chargement, les vibrations de tir, les propriétés du CRF, la méthode de placement du CRF, ainsi que la ségrégation du CRF. Un modèle pour la mine de l'étude de cas est ensuite construit en tenant en compte les conditions du site ainsi que les données geo-mecaniques fournies par la mine. Le modèle pour la mine de l'étude de cas est calibré selon les mesures des contraintes in-situ effectués à la mine. La séquence d'abattage et de remblayage est ensuite simulée avec le modèle numérique calibré et les chantiers secondaires sont extraits en trois étapes.

Les vibrations de tir in-situ sont mesurées à la mine de l'étude de casé. Deux géophones sont installés : un à l'intérieur du CRF et l'autre à la surface du CRF, et les trois sautages de production du chantier adjacent sont enregistrés. La procédure de l'installation et les résultats obtenus avec le géophone sont présentés dans la thèse. Les résultats sont utilises pour valider le modèle numérique. Le chargement de tir ainsi que les coefficients d'amortissement sont extraits d'un modèle de cavité en calculant les vibrations de tir à la même position que celle du site. Le modèle est validé pour les 3 étapes de l'abattage du chantier et les résultats sont présentés.

Finalement, une étude sur le contrôle de stabilité du CRF est effectuée. Cette étude englobe un scenario de base d'un chantier planifié à la mine de l'étude de cas, une stratégie d'abattage sélectif du minerai de haute teneure, une stratégie ou une couche de minerai est laissée dans le chantier, et une variation verticale planifiée des propriétés du CRF. De plus, une étude paramétrique est conduite pour améliorer la stabilité du CRF en variant les propriétés du CRF. Les tendances possibles sont présentées. Tous résultats comparent le chargement statique avec le chargement dynamique sur le CRF. Les résultats incluent une comparaison des contraintes du remblai ainsi que le profile de la vitesse de crête des particules. Les résultats de toutes les analyses sont présentés avec les constatations et conclusions.

LIST OF PUBLICATIONS

REFEREED JOURNALS:

- Emad, M. Z.,., H. S. Mitri, J.G. Henning (2012). "Effect of blast vibrations on the stability of cemented rockfill." International Journal of Mining, Reclamation and Environment 26(3): 233-243.
- Emad, M. Z., H. S. Mitri, and C. Kelly (2013). "Effect of blast-induced vibrations on fill failure in vertical block mining with delayed backfill." Submitted to Canadian Geotechnical Journal in August 2013
- Emad, M. Z., H. S. Mitri, and C. Kelly (2013). "State-of-the-art review of backfill practices for sublevel stoping systems." International Journal of Mining Reclamation and Environment (Accepted in December 2013)

PEER REVIEWED CONFERENCES:

- Emad, M. Z., H. Mitri, (2013). Backfill practices for sublevel stoping system. Proceedings of the 22nd International Symposium on Mine Planning and Equipment Selection MPES 2013 held on 14 – 19 October 2013 in Dresden Germany.. C. Drebenstedt and R. Singhal (Eds) 391–402
- Emad, M. Z., and H. Mitri, (2013). Modelling dynamic loading on backfilled stopes in sublevel stoping systems. SINOROCK 2013 – 3rd ISRM Symposium on Rock Mechanics, "Rock Characterisation, Modelling and Engineering Design Methods". F. Tan. Shanghai, China, CRC Press 2013: 351–356.
- Emad, M. Z., H. Mitri, and J.G. Henning (2012). "Effect of Backfill Placement Method on Its Stability: A Dynamic Modelling Case Study." 21st Canadian Rock Mechanics Symposium, RockEng12 Edmonton AB 5 - 9, May 2012: Chris Hawkes, Derek Kinakin, Sam Proskin and Denis Thibodeau (Eds.) 187 - 196.
- Emad, M. Z., H. S. Mitri, et al. (2011). "Some factors affecting cemented rockfill failure in longhole mining." Proceedings of the Twentieth International Symposium on Mine

Planning and Equipment Selection MPES 2011, A. Zharmenov, R.Singhal, S.Yefremova (Eds): 163–174.

- Bagde, M. N., M. Z. Emad, et al. (2011). "Examining the influence of stope dimensions and mining sequence on backfill dilution: a review with case study " In Int. Conf. on Technological Challenges and Management issues for sustainability of Mining Industries (TMSMI), August 04-06, 2011, organized by Dept. of Mining Eng., NIT Rourkela, India, B. K. Pal and S. Chatterjee (Eds): 13–28.

ACKNOWLEDGMENTS

First and foremost, I am thankful to Almighty Allah, by His grace and bounty, I am able to complete my PhD thesis. I ask sincerity in all my actions from Allah and I quote the verse from the Holy Quran "Say, Indeed, my prayer, my rites of sacrifice, my living and my dying are for Allah, Lord of the worlds" (Al-'An'am, verse 162).

I would like to express my sincere gratitude to my PhD thesis advisor Prof. Hani Mitri for the continuous support of my Ph.D study and research, for his patience, motivation, enthusiasm, and immense knowledge. His guidance helped me in all the time of research and writing of this thesis. I could not have imagined having a better advisor and mentor for my Ph.D study.

I am grateful for the joint financial support of this work by the Natural Sciences and Engineering Research Council of Canada (NSERC) and Vale Canada under the CRD grant. My sincere thanks also go to Ms. Cecile Kelly, Mr. Rob Van Drunen, Dr. Denis Thibodeau, Dr. John G. Henning, Mr. Donald Mitchell, Mr. Wei Wei, Mr. Elliot Hyska, Mr. David Carsewell, Mr. Tomasz Bak and Mr. Micheal Grossman for their useful suggestions, support and guidelines during my PhD research and experimentation at the Birchtree mine.

I thank my fellow lab mates in the Mine Design Laboratory of McGill University: Dr. Shahe Shnorhokian, Dr. G.D. Raju, Dr. Wael Abdellah, Atsushi Sainoki, Rory Hughes, Jenyfer Mosquera, Isaac Vennes, Dr. Yann Gunzburger, Dr. Tarek Hamade, Anand Musunuri, Davide Munari, Guillaume Lafonte and Luc Archer and, for the stimulating discussions, and for all the fun we had in the last three years.

Last but not the least I thank my wife Sidra, my son Muhammad and my parents Mr. Muhammad Anees and Mrs Fauzia Khannum, for their patience, guidance and support throughout my life, especially during my PhD research.

TABLE OF CONTENTS

LIST OF FIGURES

LIST OF TABLES

1 INTRODUCTION

1.1 GENERAL

Many Canadian metal mines employ sublevel stoping mining method or one of its variations, such as blast hole stoping, vertical crater retreat (VCR), or vertical block mining (VBM) for the extraction of steeply dipping ore bodies [1]. In these methods, the ore body is divided into blocks or stopes, which are mined out while following a pyramidal mining sequence in transverse-retreat and longitudinal retreat directions. In VBM, stope production is carried out in three or four blasts lifts. Each lift is blasted and mucked out before blasting the next one. Backfill is required to fill the empty stopes once they are completely mined out. Backfill can be defined as, the filling of an excavation with waste material. It is used as a filling material for stopes in cut and fill and sublevel stoping mining methods. Backfilling is a widespread practice in Canadian metal mines. It has proven to be a good passive support in hard rock metal mines and it decreases ore dilution from hanging-wall and footwall slough while maximizing ore recovery [2, 3]. Backfill dilution is a prime concern while mining adjoining stopes for pillar-less mining. The stability of exposed backfill face is governed by multiple factors, some of them include stope dimensions, stiffness of backfill, cohesion, interlocking of particles, exposure and blast induced vibrations from adjacent stope being mined [4-6]. The main drawbacks of backfill include backfill failure causing dilution of precious ore, as shown in Figure 1-1, high operational cost, high pressure, pipeline wear, and drainage problems for hydraulic backfill [4].

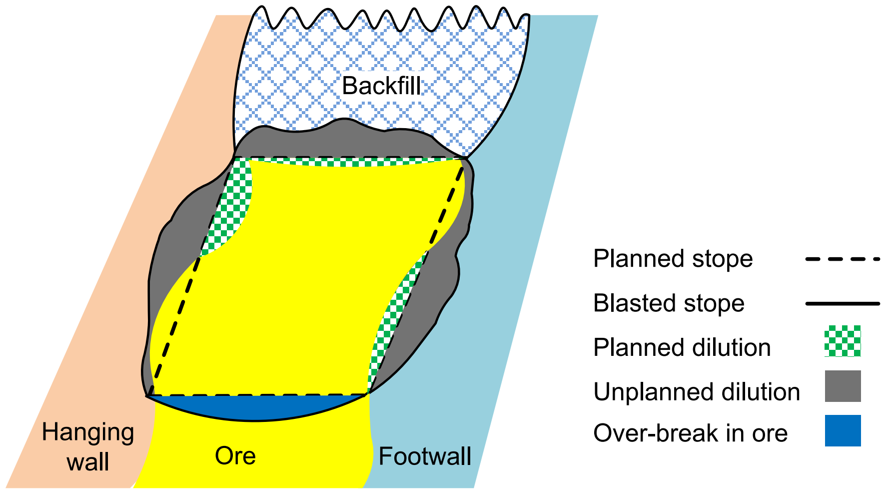

Figure 1-1 – Plan view of a typical stope showing planned and unplanned dilution

Backfill is made by mixing binding agent and bulk inert materials. Binding agent may include ordinary Portland cement, fine slag and fly ash. Bulk material can be coarse slag, mine developmental waste rock, aggregates, coarse sand, and mill tailings. Sometimes additives are also mixed with backfill to enhance its strength, flowing properties and to control settling time of backfill [5, 7].

Backfill can be classified into following three main types:

a) Slurry or hydraulic backfill
b) Paste fill
c) Rockfill

Higher stiffness is required for better wall control and greater recovery. Rockfill attains greater stiffness when cement slurry is mixed with it. The cementation enables rockfill to stand on its own weight when it is subjected to vertical exposures and cementation also enables bearing blast vibrations from adjacent stopes [2, 8]. The quantity of cementation in backfill governs the strength of backfill, which is generally computed from the limit equilibrium methods known as fill strength requirement (FSR) models [9]. If the backfill is exposed to an adjacent stope that is being mined then the backfill stope fails under gravity or blast load, which causes backfill dilution as shown in Figure 1-1 [2, 10-12].

Dilution can be defined as, the mixing of ore with barren waste [13]. Dilution is the most common mine disease [14]. Dilution has a negative impact on profitability, as it lowers the quantity of mineral that is mined [15]. Scoble and Moss [16] termed dilution as the sum of planned and unplanned dilution. So, backfill dilution can be designated as the unplanned dilution component. The cementation enables rockfill to stand on its own weight when it is subjected to vertical exposures and blast-induced vibrations. The quantity of cement in backfill governs the strength of backfill, which can be computed from the fill strength requirement (FSR) models, discussed in Chapter 2. The FSR models are based on the static strength of backfill and they do not incorporate major factors like segregation, geo-mechanical properties (deformational modulus, poisson's ratio), mining method, backfill placement methods, blasting effects on backfill and blast design. Figure 1-2 presents different failure modes identified from the literature review and cavity monitoring survey data. Backfill failure modes can be classified into three main types that are failure due to:

a) Blast induced vibrations from production blasting [10]
b) Drill hole deviations
c) Irregular shape of backfill mass due to over-break [10]

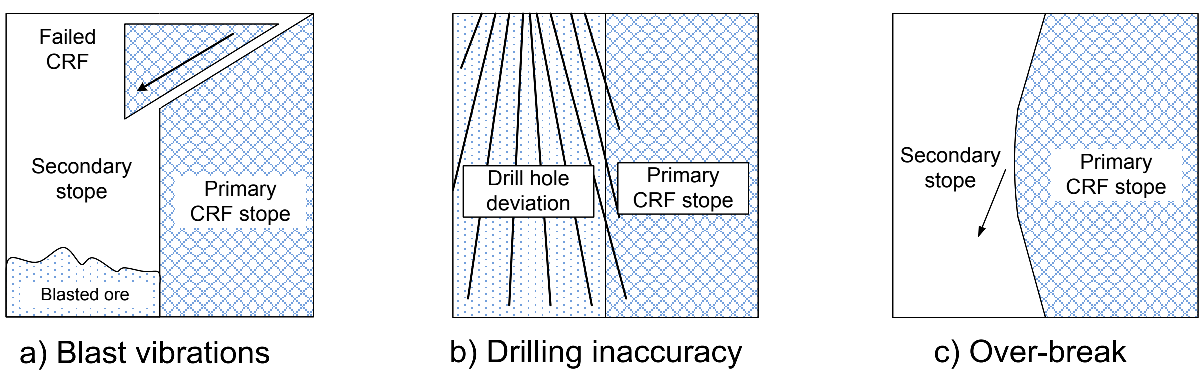

Figure 1-2 – Backfill failure modes identified from CMS data analysis

The irregular stope shape may fail under gravity loading when it is completely exposed, as the bulged out stope is hanging out without any supports. It was found by many researchers [5, 17, 18] that cemented rockfill is the most challenging filling method and causes more dilution than any other backfill method. It has also been reported that cemented rockfill failures were being initiated due to segregation, size of aggregates, mixing, water quality, placement method, impact damage, blast induced vibrations, lack of quality control, improper design strength and lack of cementation [5, 7, 17, 19].

A recent study by Emad et al. [6] has shown that blast induced vibrations can have an impact on adjacent CRF stopes. The blast induced vibrations produce significant tensile stresses in the top most region of the exposed CRF stope, causing ore dilution by failure of CRF into adjacent stope being mined. The development of tensile stress is dependent on critical parameters, such as the CRF practice, placement method, interlocking in fill, water to cement ratio, blast induced vibrations [2, 5-7, 20]. Other parameters that could play an equally important role in the stability of backfilled stope include size of stope, dip of orebody, depth of the orebody, CRF properties, aggregate properties, binder properties, water content, water quality, particle size distribution, quality control, mining method, cold joint, backfill failures in nearby stopes, impact damage, excess or deficiency of fines [5, 7, 19]. When CRF is exposed and it fails, the ore present in secondary stope will be diluted making the mine less profitable. Once the ore is diluted, it cannot be separated before processing, adding extra costs for haulage, grinding, processing and backfilling. To minimize dilution from CRF requires enhancement of CRF design and current CRF practices, to improve its properties. Thus it would be extremely advantageous to know ahead of time which primary stope will receive dilution with current practices and what precautions to take, prior to mining a secondary stope.

Numerical methods such as the finite difference method have been increasingly used in recent years as a tool for geo-mechanical mine planning and design. Such tools can be used to predict potential ground caving and failure in active mining areas. As a result of recent advances in computer technology, it is now possible to handle large-scale problems involving complex material and geometric nonlinearities of underground mining problems at an affordable computational cost.

1.2 STUDY PROBLEM

Backfill dilution due to backfill failure into adjacent stope being mined is very common in underground metal mines [5, 7, 17, 18, 21]. Since 1940’s CRF has been in practice, and a lot of research is going on for development of low cost CRF mix design. Many researchers have made efforts to understand CRF failure. Some empirical designs for static loading have been presented but so far they are unable to simulate CRF failure mechanism. Numerical modeling static analysis has also been used by a number of researchers, but so far it failed to eliminate backfill dilution due to CRF failure [18, 20, 22-29]. It has been proposed by many researchers that blast induced vibrations are accountable for backfill failure, particularly from the top most part of the exposed face in wedge shape [2, 5, 17-19, 21, 30]. The backfill failure schematic is presented in Figure 1-3. Figure 1-4 and 1-5 presents observed failures at some of the other CRF operations, it can be clearly seen that the fill is failing from the top of the exposed face. The phenomenon of fill failure from top of the exposed face is unknown to date. Not much work has been done on dynamic analysis to incorporate effect of blast vibrations on backfill failure. However some two dimensional (2D) dynamic models of backfill have been developed which do not explain the wedge failure from the exposed fill face. The work done so far is inadequate to address the backfill failure problem. The current research work is proposed to address the issue of ore dilution due to backfill failure being initiated by blast induced vibrations.

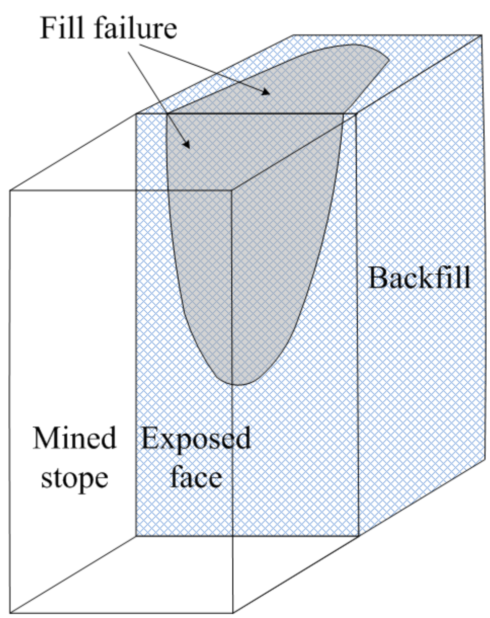

Figure 1-3 – Location of fill failure when fill is exposed

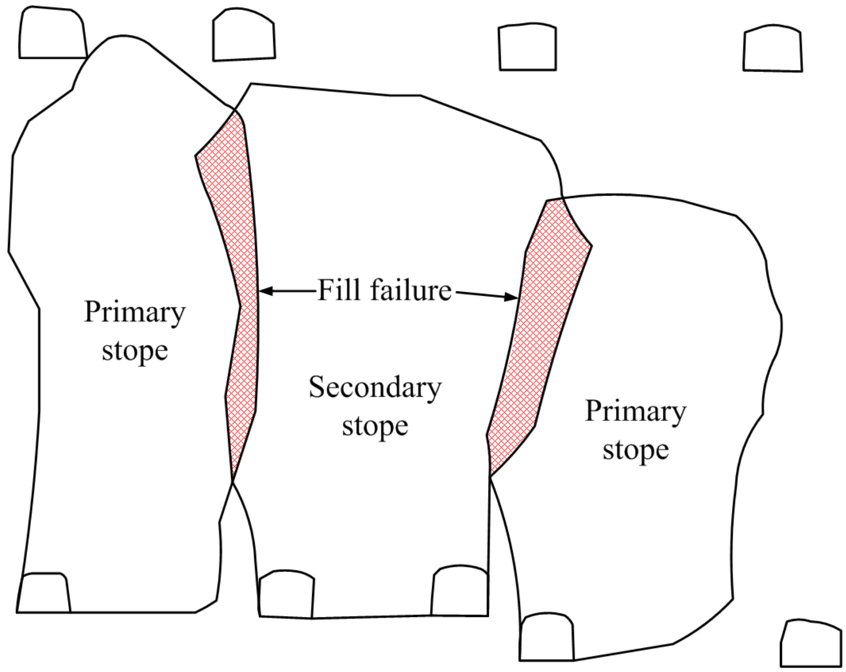

Figure 1-4 – Fill failure as observed at Darlot Gold mine [18]

Figure 1-5 – Fill failure observed at a CRF operation [30]

1.3 SCOPE AND OBJECTIVES

The scope of this work is focused on metal mines practicing sublevel stoping mining method with delayed backfill. Cemented rockfill is found to be the most prone to failure due to blast induced vibrations, so CRF has been chosen as a backfill material for this study. Figure 1-6 presents sublevel stoping mining method.

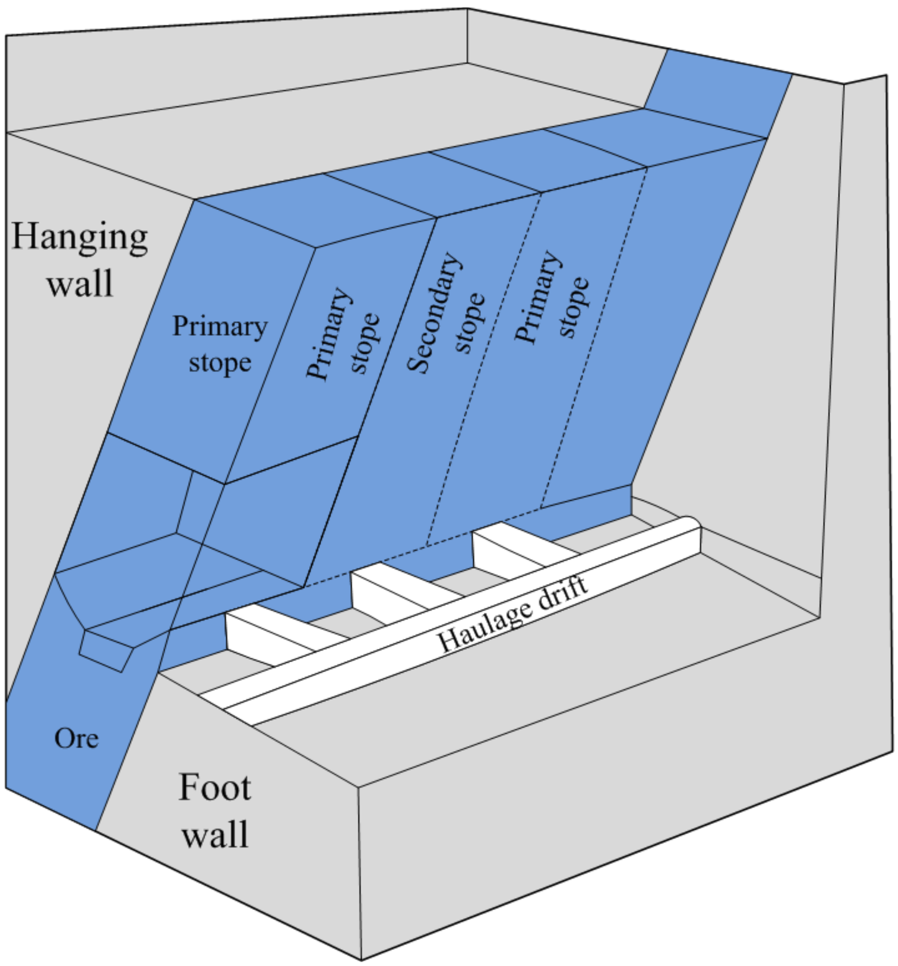

Figure 1-6 – Sublevel mining method [31]

The main objective of this research is to develop a new mine planning methodology capable of designing cemented rockfill stopes for static and dynamic loading conditions. Additional goals of this research include:

i. Review of CRF practices and properties
ii. To study the effect of blast induced vibrations on ore dilution due to backfill failure

iii. To develop a 3D dynamic model for the simulation of mine backfill material behavior under blast-induced vibrations
iv. To monitor blast-induced vibrations inside CRF stope
v. To calibrate the 3D numerical model with field measurements for detailed numerical modelling study

1.4 THESIS ORGANIZATION

Chapter 1 presents brief background information on backfill failure problem. The chapter also presents a brief review different failure mechanism of backfill in order to define the problem. Scope and objectives of the research are also outlined in this introductory chapter. Chapter 2 contains a detailed review of backfill, types, practices, properties, failure profiles, design criteria, previous numerical modelling studies on backfill, issues with CRF and some applications. Chapter 3 emphasizes on dynamic model setup, dynamic loading and failure condition for CRF stopes. The chapter also contains results of dynamic loading on CRF incorporating a parametric study. Chapter 4 presents the case study mine, location, geological setting, ore zone study area, mining method, backfill system, study problem, and geotechnical data. Chapter 5 encompasses in-situ blast vibration monitoring experimental program, site location, experimental setup, and monitoring results. Chapter 6 explains numerical model calibration for the case study mine stopes. The chapter also presents a detailed numerical modelling study on controlling backfill failure. Chapter 7 sums up output of the research. Limitations and recommendations for future work are also presented in this Chapter. Summary is presented at the end of each chapter. References cited in this research are found at the end of the thesis after the statement of contribution.

2 REVIEW OF BACKFILL PRACTICE

2.1 INTRODUCTION

Backfill can be defined as, the filling of an excavation with waste material. It is being used as a filling material for mined out stopes in cut and fill and sublevel stoping mining methods. Backfill is used as a passive support in underground mines since stope walls are not subjected to any stresses from backfill material. Backfill is used to support stope walls and it does not permit further displacements [4, 22]. Figure 2-1 presents purpose of using backfilling with respective percentages in underground mines.

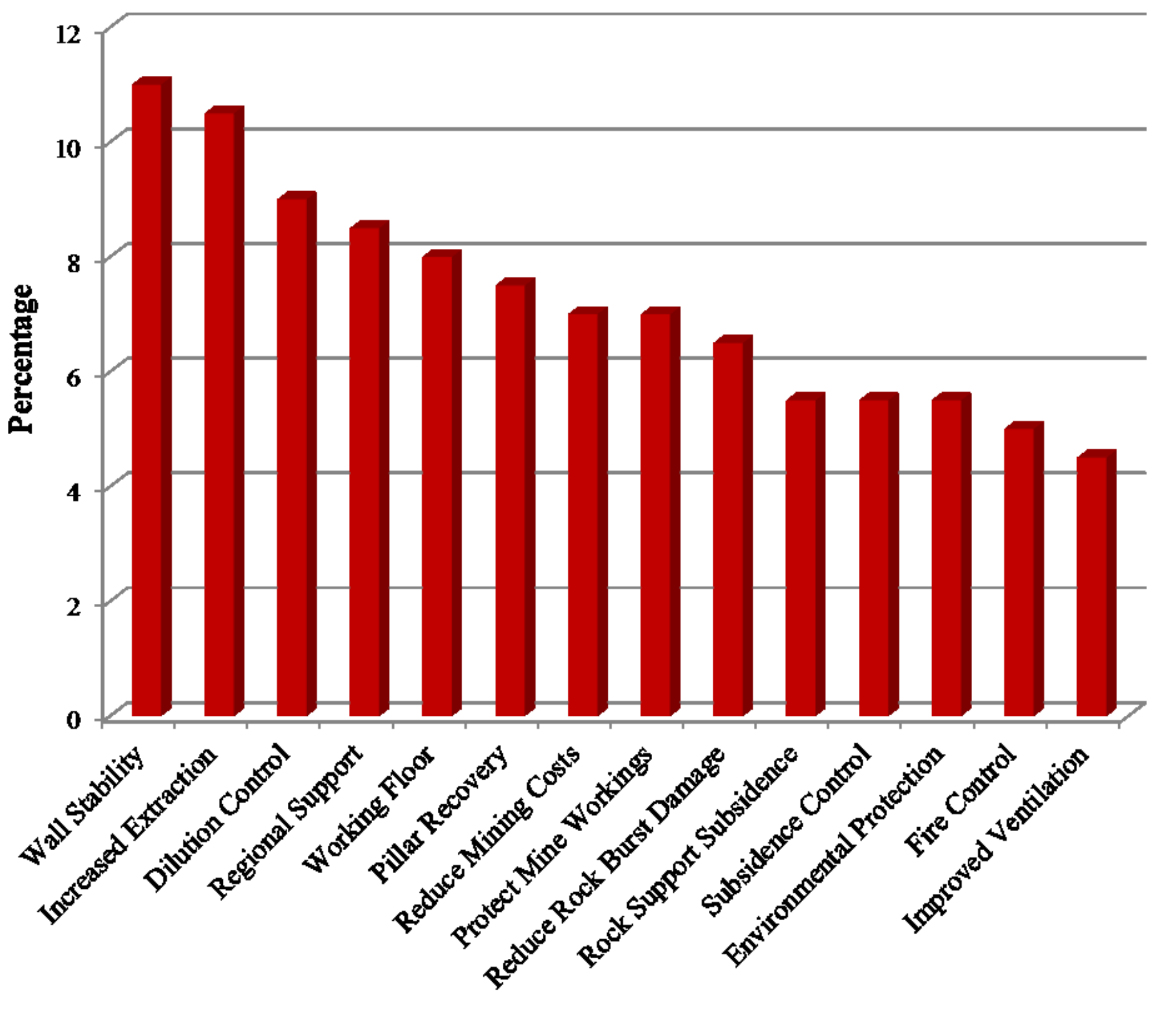

Figure 2-1 – Purpose of backfilling [22]

Backfill helps in reducing ore dilution by good ground control, while enabling maximum recovery of ore. It also provides working surface for cut and fill mining operations [4, 32] and for mucking ore from upper stopes in open stoping methods. As previously mentioned, backfill can be classified into three categories: hydraulic backfill, paste fill, and rockfill. Below is a brief review of each type.

2.1.1 Hydraulic Backfill

Hydraulic backfill also known as slurry backfill, it is composed of a classified, permeable, low density blend of mill tailings, sand, rock and water having and average pulp density of around 60% to 70% solids by weight [4, 19]. Fill must be transported through a network of pipelines at high velocity while maintaining turbulence to achieve suspension of solids. Extensive transport water is required for conveying fill through the mine backfill transportation system. Consequently, there is considerable water seepage from stopes after placement, which must be pumped back to surface [4, 19, 33]. The finer particles are not accommodated in this system and are rejected to surface in a tailings pond. Figure 2-2 presents hydraulic backfill being poured in the open stope [34].

Figure 2-2 – Hydraulic backfill being pumped in the open stope [34]

Hydraulic backfill may or may not incorporate a binder, depending on the future backfill exposure. Hydraulic fill requires a strong barricade to contain fill mass and additional drainage is required to drain out seeped water from fill [4, 33]. This method requires huge binder quantities as most of the binder seeps out of the stope with water. Cured hydraulic backfill is generally very weak as compared to other backfill types. That is why it is practiced for overhand cut and fill operations and is not considered as very good backfill for mines practicing open stoping methods with higher and greater exposures [4, 33, 35].

2.1.2 Paste Fill

Paste backfill is composed of thickened mill tailings generated during mineral processing which are mixed with additives such as Portland cement, lime, pulverized fly ash, and smelter slag. Paste fill utilized full range of tailings and rejects are lesser compared to hydraulic fill [4, 33, 35]. It includes sand/mine tailings, water and cement is added where it is required to enhance strength properties of fill or when there is a risk of liquidation of paste. Paste fill contains 75 – 80% solids by weight. It is relatively consistent backfill having high pulp density with about 15% minus 45 microns (325 mesh) fines content. Its consistency is very similar to a tooth paste. It is the most popular backfilling method used for open stoping mining method with delayed backfill. It requires mill tailings to be used as a raw material, a backfill plant to be employed for paste thickening and storage of thickened tailings. A network of pipelines is also required for delivery and placement of backfill. Backfill plant accepts mill tailings from the mine mill or tailings pond, reduces their water contents using paste fill thickener technology [4]. It then mixes binder and additives for achieving desired properties of paste fill. A network of pipes with valves and pumps are required for delivering paste fill underground. Paste fill is the most popular backfilling method for massive ore bodies employing sublevel mining systems. It has higher initial costs and moderate operational costs, with a much cleaner operation. Figure 2-3, shows the physical appearance of paste fill.

Figure 2-3 – Paste fill physical appearance [34]

Gravity driving for paste is generally preferred [19], which requires a range of bulk density. The main paste fill line should be drilled and cased separately from other mine services; however some operations prefer it to go through the mine shaft. This is done to avoid production delays in case of blowout of main fill line. Backfill plant monitoring and pipeline monitoring system is also required to avoid system failure. Design of backfill plant and paste fill line is based on backfilling rate and pipeline wear. Mine backfill team must have a plan to deal with any kind of blockage, plugging or blowout of pipeline [36]. Pressure losses are higher in paste fill systems (10MPa/Km) and lower for hydraulic fill systems (2 MPa/Km). Variable pipeline diameters for different sections should be eliminated to decrease pipe wear and shock losses [36, 37]. Pipeline wear can also be reduced by increasing percentage solids [19]. A simplified layout of paste fill system is shown in Figure 2-4 [38].

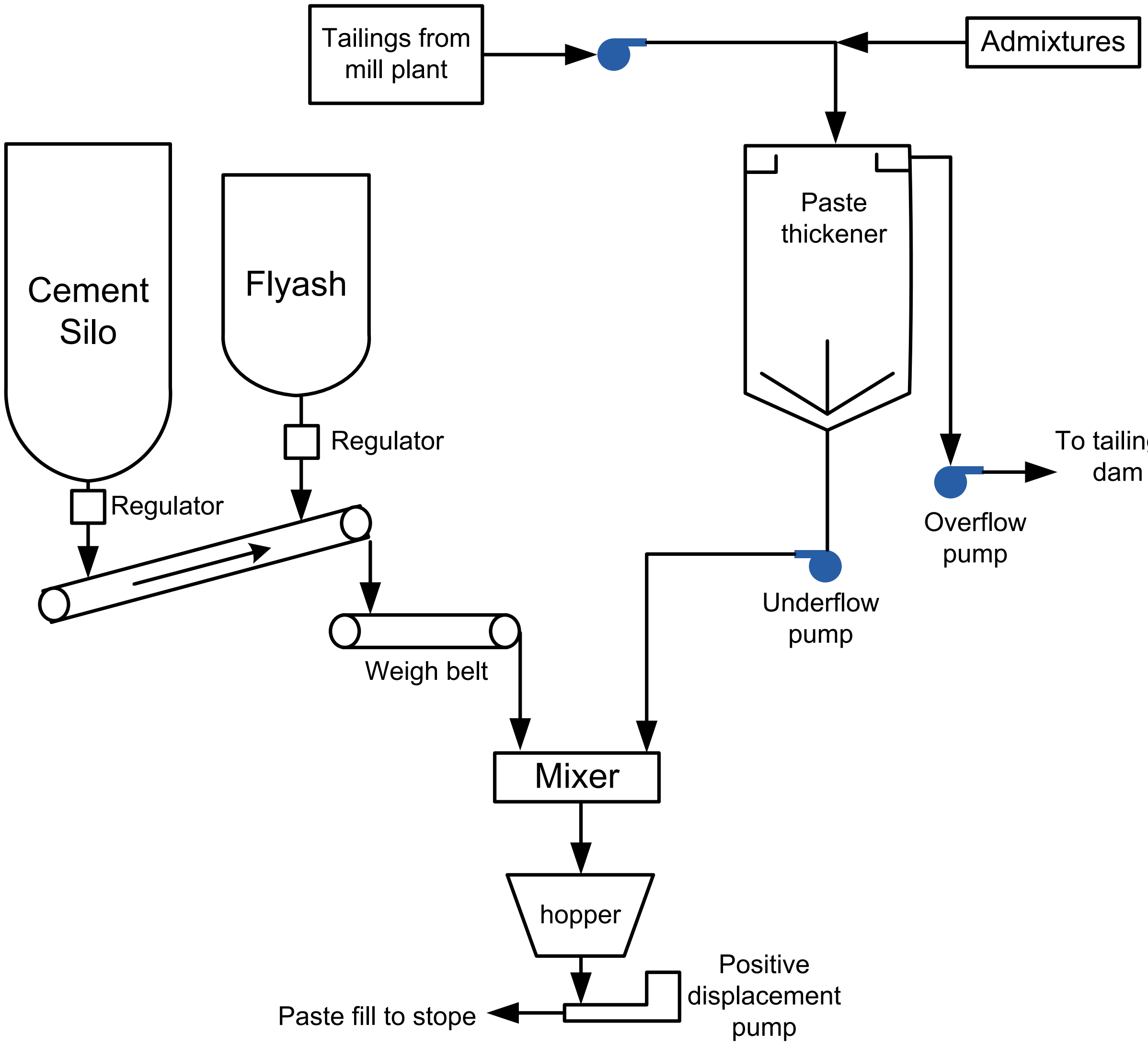

Figure 2-4 – Paste fill processing inside a backfill plant [38]

Increasing solids in fill increases the strength of backfill [37], which means that paste fill is much stronger than hydraulic fill. Paste fill provides flexibility to mine adjacent, underneath or through the fill [19, 20]. High solid contents in paste fill above 70% require a positive displacement pump rather than centrifugal pump for horizontal transport of fill. The relationship between percentage solids, strength and pumps is presented in Figure 2-5.

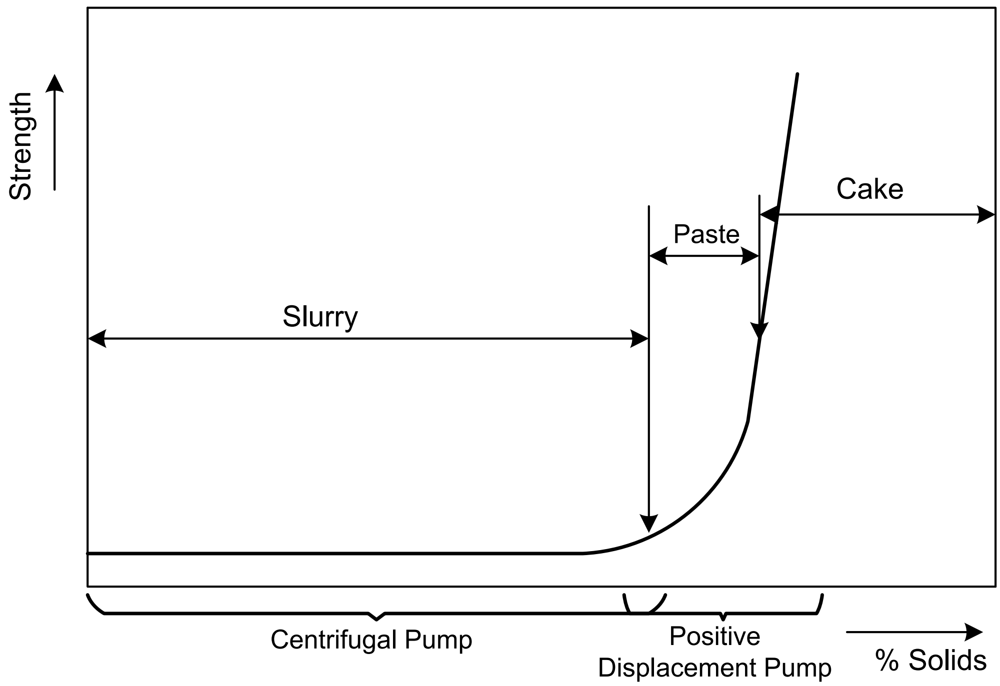

Figure 2-5 – Effect of percentage solids on pumping requirements

Pumps are not generally preferred for paste fill operations and gravity flow is the choice by decreasing horizontal distance. Paste fill is generally used for large operations having higher mining rates and long mine life. There can be many more advantages of using paste fill as a backfill material, some of them are as follows [4, 20]:

1. It is non-segregating backfill
2. It reduces mining cycle due to an early development of compressive strength and continuous filling
3. It reduces binder utilization due to its homogeneous fill nature
4. It consumes the whole range of mill tailings
5. No critical velocity is required to keep backfill in suspension [33, 35]
6. Its operation is cleaner
7. It provides flexibility
8. It reduces long term environmental impacts [39]
9. Better mixing can be achieved [40]

10. Lower cost for constructing a barricade and also there is no drainage from stope [39]

The disadvantages of using paste fill include [4, 41]:

1. Technical supervision and monitoring is essential for successful operation [41]
2. There is a need for better dewatering technology from stopes for better performance [4]
3. High pipeline pressures at greater depths leading to pipeline blow-out and pipe wear [4, 37]
4. Higher exposures of paste fill may lead to backfill dilution
5. Pipelines can get plugged due to slow sedimentation of fill
6. Sticky tailings can pose problems in handling and pumping [19]
7. Fill may leak through jointed rock when poured in an uncased hole[40]
8. Dynamic loading from adjacent production stope may incur dilution of precious ore and may initiate liquidation in paste [40]
9. High dynamic loads on pipeline may lead to failure [33]
10. Blended tailings may segregate when placed in stope [33]
11. Tailings exposed to weather conditions may change properties [41]
12. Some quantity of binder is required even if the paste fill will not be exposed in future

2.1.3 Rockfill (RF)

Rockfill consists of graded or ungraded waste rock, obtained from quarries or underground developmental work. Rockfill is used for passive support in mines and a very limited ground control can be achieved. It is a low cost fill material and its placement is simple, it contains no binding agent but it can be consolidated at a later stage by injection or percolation of cement slurry, if required. The rockfill without post consolidation cannot be exposed at a later stage. Following are the variations of the rockfill to increase the rockfill performance underground:

2.1.3.1 Cemented Rockfill (CRF)

Cemented rockfill (CRF) is also known as consolidated rockfill. It is composed of sized or un-sized aggregates coated with binder slurry having overall cement contents of 4 – 6%. Binder contents below 4% are inappropriate for binder coating on aggregate. Binder contents greater than 6% are less economical for open stoping mining methods. However, higher binder contents are generally employed for drift and fill mining methods for stability. Developmental waste can also be used in place of aggregates or can be blended with aggregates in CRF [4, 19]. A view of in-situ cured CRF is presented in Figure 2-6.

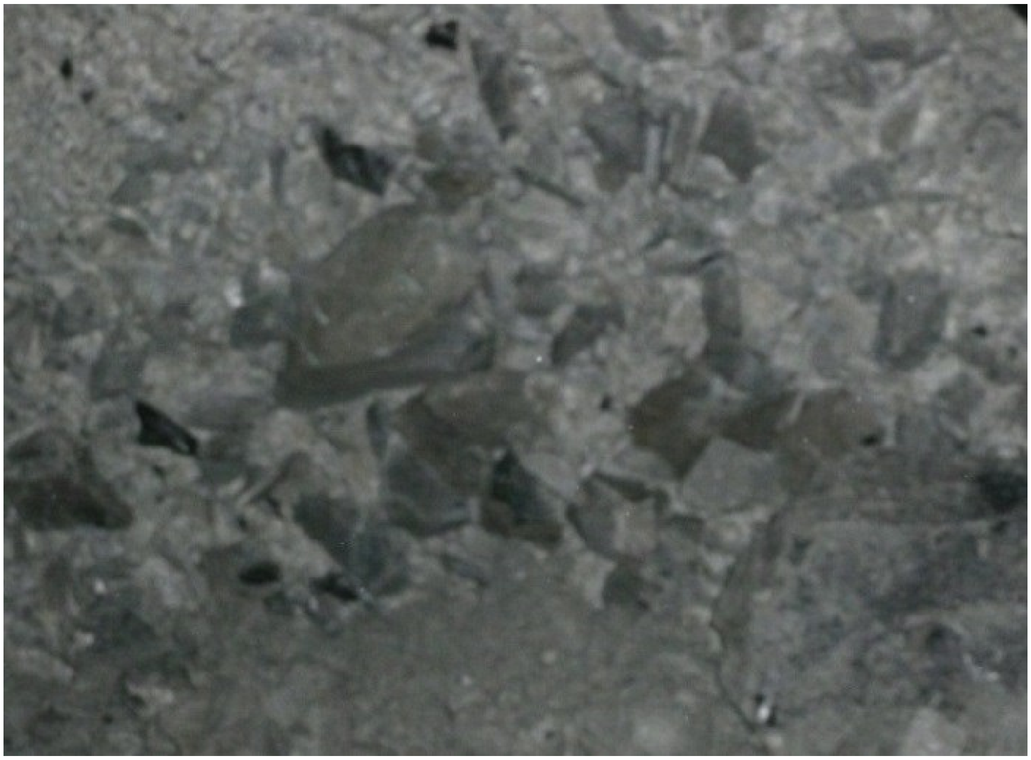

Figure 2-6 – In-situ cured cemented rockfill

CRF is capable of bearing active pressures, providing not only ground support but also improves wall rock stability. No additional drainage is required for CRF systems and high strengths can be achieved by proper placement. Quality control and segregation can be difficult to control. Some of the critical parameters for CRF stability include stope access, backfill raise orientation, binder contents, particle size distribution, water to binder ratio, segregation, placement method and quality control [18, 19, 33]. Sometimes, Portland cement is blended with fine slag or fly ash for cost effectiveness, but inclusion of flyash increases curing time of CRF. CRF has higher strength than paste fill and hydraulic fill, when properly practiced [19, 33]. CRF is generally employed for intermediate to smaller operations having lower mining rate, smaller mining life or for mines having no source of sand or mill tailings. Figure 2-7 presenting cemented rockfill placement in an open stope using a load haul dump machine (LHD) and cured CRF underground.

a) LHD machine dumping CRF

b) Cured CRF

Figure 2-7 – CRF being placed in stope and cured CRF are shown [42]

2.1.3.2 Cemented Sand Rockfill (CSRF)

In cemented sand rockfill (CSRF) 5 – 10% sand is added by weight and mixed with CRF to attain greater strength by filling void spaces in fill. Generally, sand is added to counteract dynamic loading on backfill due to blasting, as sand increases tensile strength of fill Yu [5]. Sand is not increased by more than 10% as it decreases the strength, because up till 10% sand acts as void filler and above 10% cement takes away all the binder contents causing decrease in strength [5]. CSRF decreases segregation, and enables flexibility in raise design. Density of CSRF is more than CRF and has a lesser angle of repose but stope access is critical for placement.

2.1.3.3 Cemented Sand Waste Fill (CSWF)

CSWF is the process of consolidating rockfill. It is practiced by leaving waste in-place in excavated stopes and cement slurry with a pulp density of 65 – 85%, and 18% sand slurry with a 65 – 75% pulp density are poured over waste which percolates in rock aggregates to form CSWF. Overall cement contents are generally kept at 5% by weight. CSWF improves ground support, it decreases dilution due to waste and it improves wall support. It does not require good stope access. Sand slurry flow is difficult to control underground, quality, and quantity controls are critical.

2.1.4 Issues with Cemented Rockfill

The following are the issues associated with CRF:

i. High operational costs
ii. Difficulty to tight fill
iii. Segregation
iv. Improper placement causes reduction in strength
v. Failure into adjacent stopes causing dilution

2.1.5 Backfill Failure Modes

Backfill failure modes and their causes have been reported and discussed by some authors [2, 5, 6, 8, 10, 18, 29]. It has been reported by many authors that CRF failure is a product of multiple factors with a major factor of blast-induced vibrations [2, 5-7, 21, 43]. They discussed that static strength of CRF is not enough to sustain the blast load when the stopes adjacent to CRF are blasted. The dynamic loading on structures induces huge strains $10^5 – 10^6$ compared to static loading strains of less than 10^{-3}[44]. Aitchison et al. [2] were amongst the first to claim that CRF failure profile is in the shape of wedge and the failure is located at the top most part of exposed face. Later Chen et al. [18] and Ran and Watunga [30] published CRF failure profiles in a paper on Darlot Gold mine CRF operation. The profiles clearly showed that the CRF stopes failed in wedge shape as discussed by Aitchison et al. [2], Chen et al. and Ran and Watunga [30]. Emad et al. [6] presented their FLAC^{3D} model of CRF column which showed that blast vibrations may lead to a wedge failure on top of the exposed backfill face. They applied blast induced vibrations on CRF in combination with gravitational loading. The results clearly showed that the CRF column was stable under static loading conditions and was failing when blast load was applied. Notably the dynamic analysis of CRF showed wedge failure again initiating at the top of the backfill. Other than dynamic loading CRF can also fail due to drilling inaccuracy and CRF is fired. Another mode of CRF is when there is big overbreak in primary stope and when the stope is filled, the shape of CRF destabilizes it when exposed by mining of adjacent stopes. Besides wedge failure, small scabbing failures have also been observed in backfill. It is believed that these failures are initiated due to grinding between blasted ore and CRF walls when ore is drawn. CRF failure modes have been presented in Figure 1-2.

2.1.6 Fill Structural Design

Structural design is necessary for optimization of binder contents to reduce rockfill failure. Theoretical techniques such as fill strength requirements (FSR) for structural design consider backfill as a homogeneous material and these methods incorporate only the static loading on backfill. Static loading is only due to backfill weight due to gravity and a backfill must be capable of sustaining shear and tensile forces developing due to gravitational loads. Generally, circular failure also known as wedge shape failure is observed in cemented rockfill and location of failure is near the top of the exposed face [18, 29], contrary to the common believe that backfill needs more strength at the bottom. The failure is presented in Figure 2-9. When a secondary stope is mined the backfill face is exposed and failure can take place. Advanced techniques, such as numerical modelling is employed to design a backfilled stope. Numerical modelling enables a mine planner to enhance backfill design by simulating the site specific scenario in terms of mining method, mining sequence, segregation in fill, fill placement method, multiple exposures, dynamic loading due to blast vibrations and many more. A review of fill strength requirements and numerical modelling is presented in the following sections.

2.1.6.1 Fill Strength Requirement

Fill strength requirement also known as limit equilibrium method is the minimal compressive strength required by backfill to stand on its own weight, it is computed for the determination of binder quantity to be placed. FSR can be related with binder requirements as the more the FSR value more binder will be required and vice versa. The computation of FSR is based on the following models for different scenarios.

2.1.6.1.1 Simple Block Wedge Failure Model

The two dimensional model was presented by Yu [9]. The model considers that the cracks on fill surface are initiating a wedge failure in fill as shown in accompanying figure. It has been presumed that there is no arching effect, failure starts at the toe of the moving block and the fill is acted upon by gravity as shown in Figure 2-8. Now minimal factor of safety or cohesion required to avoid fill failure can be given by:

$$F = \frac{\left(\frac{cB}{\cos\beta} + W\cos\beta\tan\phi\right)}{W\sin\beta} \qquad (2\text{-}1)$$

Where:

F is safety factor

c = cohesion of fill (KN/m^2)

B = width of the fill block (m)

ϕ = friction angle of fill

W = weight of sliding wedge

β = dip of the sliding plane = $45 + \phi/2$

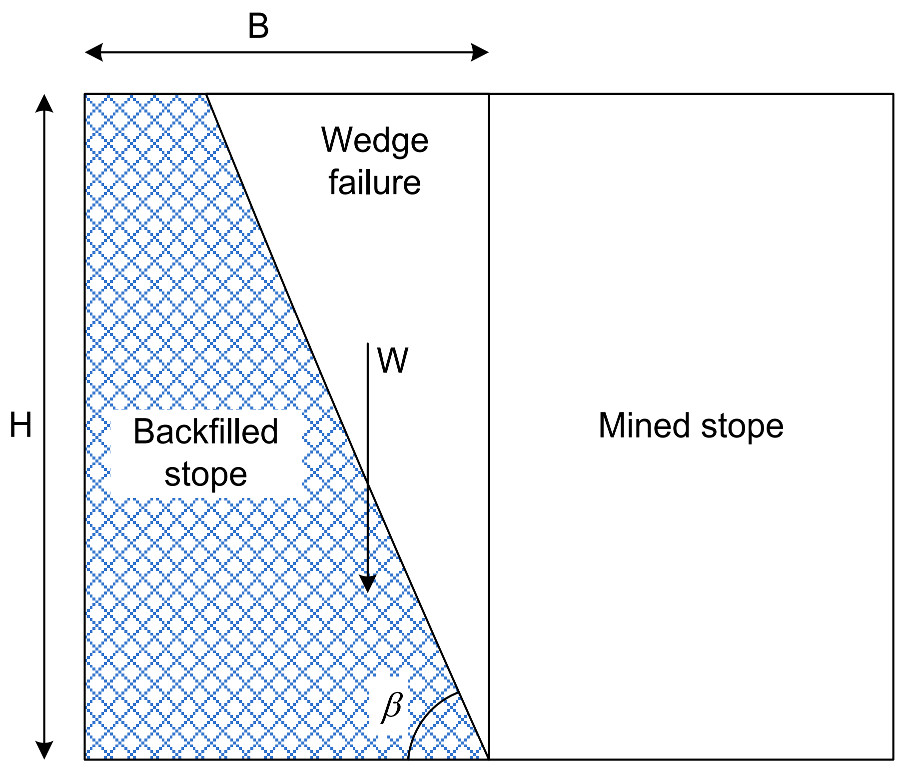

Figure 2-8 – Simple block wedge failure model [9]

2.1.6.1.2 Tension Crack Wedge Failure Model

If the backfill is settled under gravitational loads, then there must be some tension cracks on the upper fill face. A model test indicated that such cracks are evident at one-third the height of fill failure from exposed face [11]. In this model vertical tension cracks are assumed to be intersecting the shear failure plane as shown in Figure 2-9. The factor of safety can be calculated as:

$$F = \frac{\left(\frac{cB}{\cos\beta} + W_f \cos\beta \tan\phi\right)}{W_f \sin\beta} \tag{2-2}$$

Where:

F is safety factor

c = cohesion of fill (KN/m^2)

B = width of the fill block (m)

ϕ = friction angle of fill

β = dip of the sliding plane $= 45^0 + \frac{\phi}{2}$

W_f = Weight of failure wedge/unit length= $B\gamma_f \left(0.5H - \frac{B\tan\beta}{8}\right)$

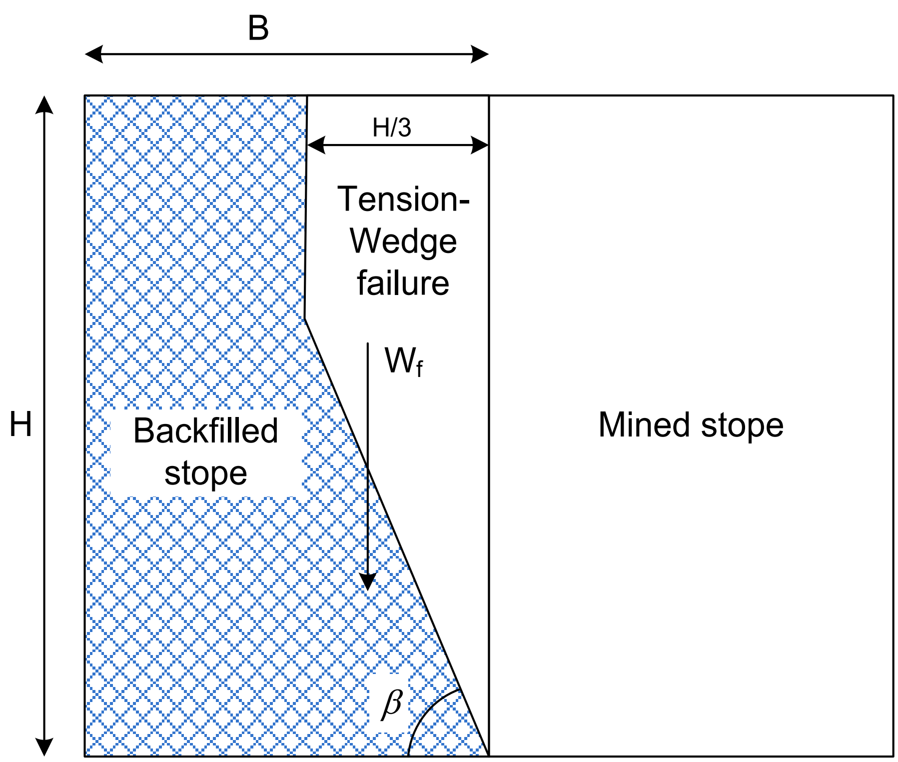

Figure 2-9 – Tension crack wedge failure model [11]

2.1.6.1.3 UCS Model

The fill can lose confinement when pillars around are blasted away [9]. It is assumed that the fill has at least two exposed faces as illustrated in the Figure 2-10. Following relationship can be used:

$$UCS_{design} = F(\gamma_f H_f) \tag{2-3}$$

Where:

F = Factor of safety

γ_f = density of fill (kN/m^3)

H_f = height of fill

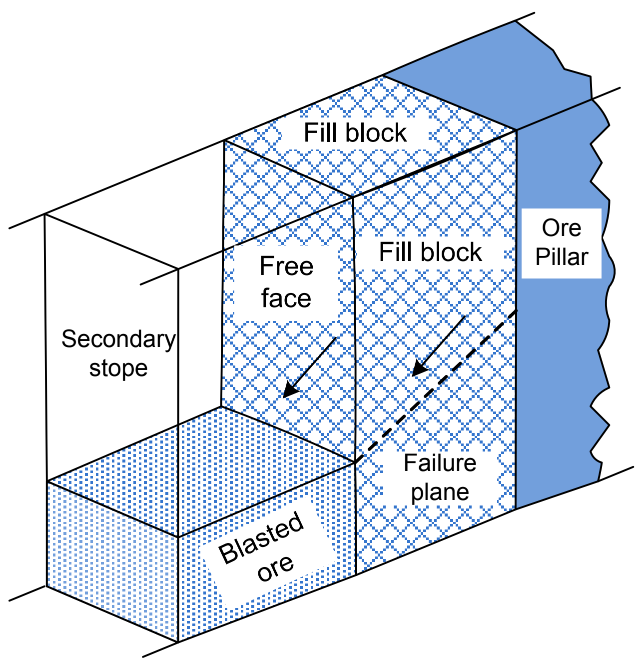

Figure 2-10 – Unconfined compressive strength model [9]

2.1.6.1.4 Modified Terzaghi's Vertical Loading Model

Askew [45] modified Terzaghi's vertical model for a three dimensional analysis presented by Terzaghi and Coates [46, 47]. The model considers arching effects on fill. The scenario in Figure 2-11 defines the circumstances. Following is the formulation for modified Terzaghi's model.

$$UCS_{design} = F\frac{1.25B}{2k\tan\phi}\left[\gamma - \frac{2c}{B}\right]\left[1 - \exp\left(-\frac{2Hk\tan\phi}{B}\right)\right] \qquad (2\text{-}4)$$

Where:

B = width of fill (m)

H = height of fill (m)

F = safety factor

ϕ = friction angle

c = cohesion

γ = density of fill (kN/m^3)

K = horizontal stress to vertical stress ratio

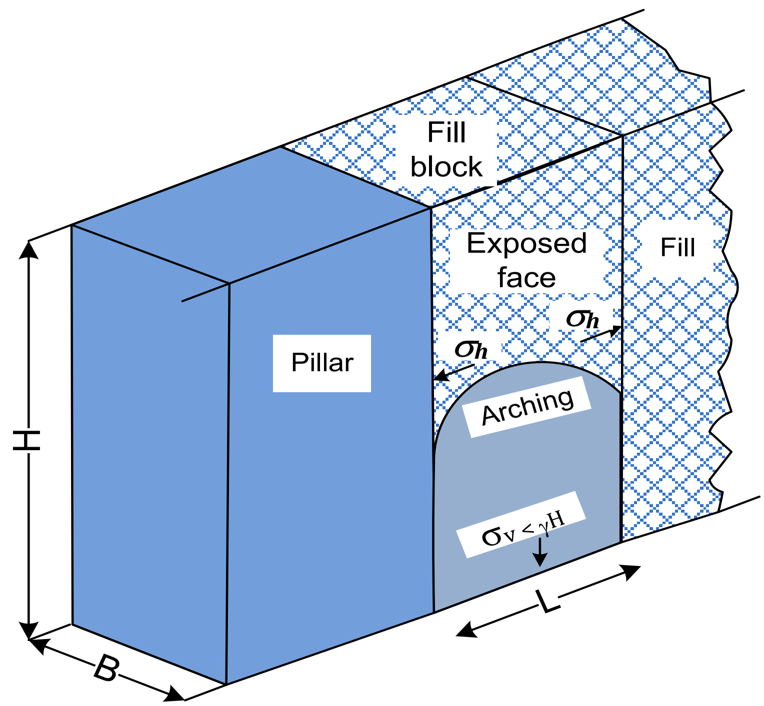

Figure 2-11 – Terzaghi's vertical loading model [45-47]

2.1.6.1.5 Confined Block with Cohesion Model

The three dimensional confined block with cohesion model is shown in Figure 2-12. This model has been quoted by Smith and Mitchell [11, 48]. This model assumed that at least two walls of stope are against fill faces, exposed face is not long enough to consider a 2D scenario and the faces of fill have no friction with walls.

$$UCS_{design} = F\frac{[\gamma L-2c]\left(H-\frac{B}{2}\right)sin(45^0)}{L} \quad (2\text{-}5)$$

Where:

L = length of fill (m)

B = width of fill (m)

H = height of fill (m)

c = cohesion of fill

F = safety factor

γ = density of fill (kN/m^3)

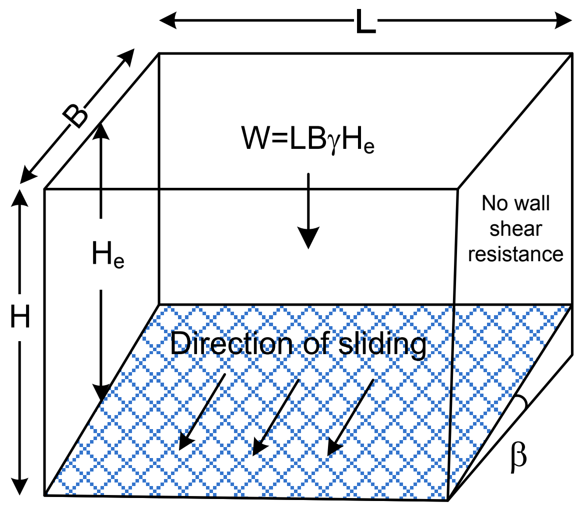

Figure 2-12 – Confined block with cohesion model [11, 48]

2.1.6.1.6 Confined Block with Friction and Cohesion Model

The confined block with friction and cohesion model was presented by Yu [9]. It is an extension of the previous model. It was assumed that at least two walls of stope and fill are attached to each other with considerable amount of friction in between. Figure 2-13 represents the 3D scenario of the model.

$$UCS_{design} = F\frac{(\gamma L-2c)\left[H-\frac{B}{2}\tan\left(45^0+\frac{\phi}{2}\right)\right]\sin\left(45^0+\frac{\phi}{2}\right)}{L} \quad (2\text{-}6)$$

Where:

L = Length of Backfilled Stope (m)

B = Width of Backfilled Stope (m)

H = Height of Exposed Face (m)

H_e = Effective Height of Exposed Fill (m)

γ = Unit weight (kN/m^3)

c = cohesion (MPa)

β = Failure angle through fill (^{o})

F = factor of safety

ϕ = Angle of Internal Friction (^{o})

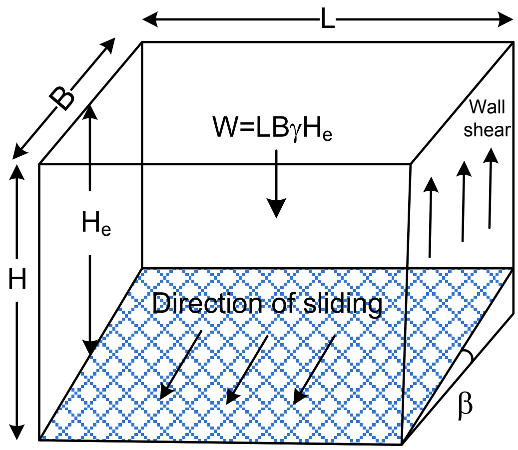

Figure 2-13 – Confined block with cohesion and friction model [11, 48]

2.1.6.2 Review of Numerical Modelling Studies on Backfill

Numerical modelling helps in verifying and extending limit equilibrium design, field studies and physical models. Numerical modeling is high-quality tool for understanding backfill material under static loading due to gravity, and dynamic loading conditions when backfill is subjected to blast induced vibrations and sudden loss of confinement. The advanced computational codes allows a user to model explosives detonation and blast vibration propagation, this gives a more detailed prediction of blast damage than is possible by the use of charge-weight scaling laws [20]. The numerical models are much more complex as compared to the limit equilibrium methods and charge-weight scaling laws, as they incorporate most of the variables like rock mass properties, velocity of detonation, nearby free faces reflecting blast induced waves. Numerical modeling has been used a number of authors for modeling and analyzing mine backfill materials [6, 20, 22-25, 49]. Following text reviews the modelling technique employed for modelling backfill material.

Cundall [50] and Donze [51] modelled backfill by considering backfill as sandwich pillar between hanging-wall and footwall in transverse mining. They used yielding and vertical stresses as failure criteria. The backfill layers were exposed and stability of backfill was assessed. Displacement contours showed that maximum displacement on backfill face was near the top of the backfill. Figure 2-14 presents yield and active failure in backfill pillar.

According to Mitchell [52], cementation increases the brittleness of backfills, making them more prone to cracking under blast loadings and to rupture under local rock deformation. Thus, forces, displacements and energy dissipation should be considered in backfill design. However, it was found from the reported literature that when designing backfill, only gravity loading or self-weight of the backfill is considered using simple wedge model originally provided by Mitchell [53].

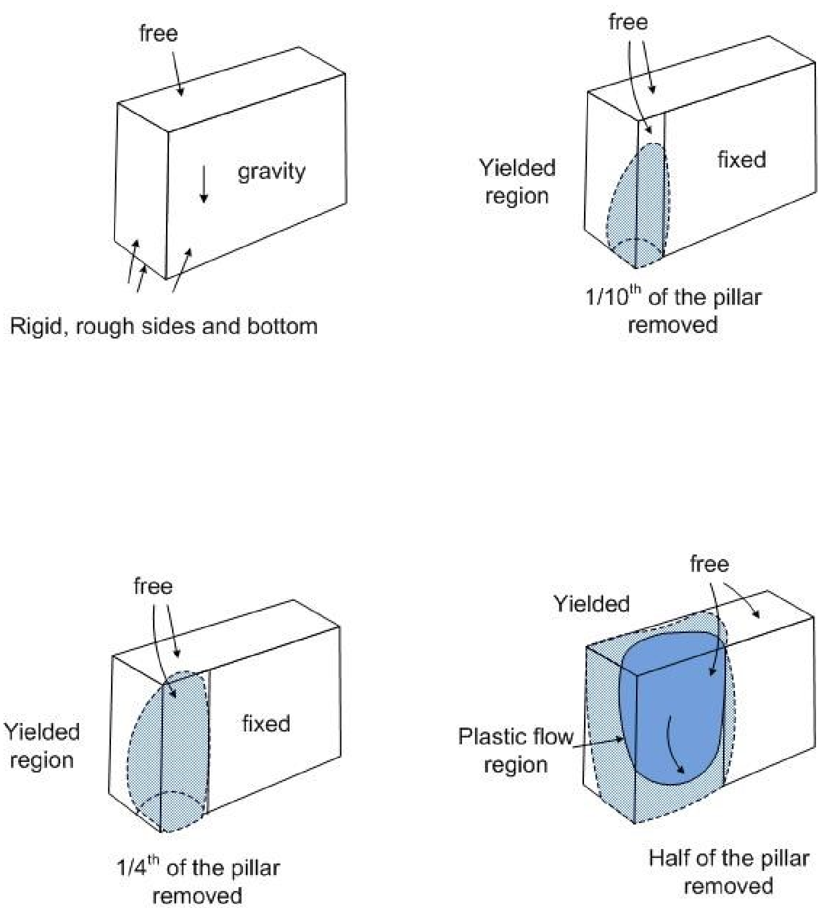

Figure 2-14 – Yield and active failure in backfill [51]

Coulthard [27] modeled underground mining problems and stresses in cemented rockfill, the model was computed during filling an open stope. The stability of exposed CRF stope was studied using FLAC^{3D} code. He modeled 40 square meter columns with approximately 200 meter high exposures to predict stresses. He used vertical and shear stress profiles along centerline of stopes, to present results. The model clearly showed arching which means that some stresses were transferred to walls of the stopes. Figure 2-15 presents profile of vertical and horizontal stresses in backfilled stope when exposed.

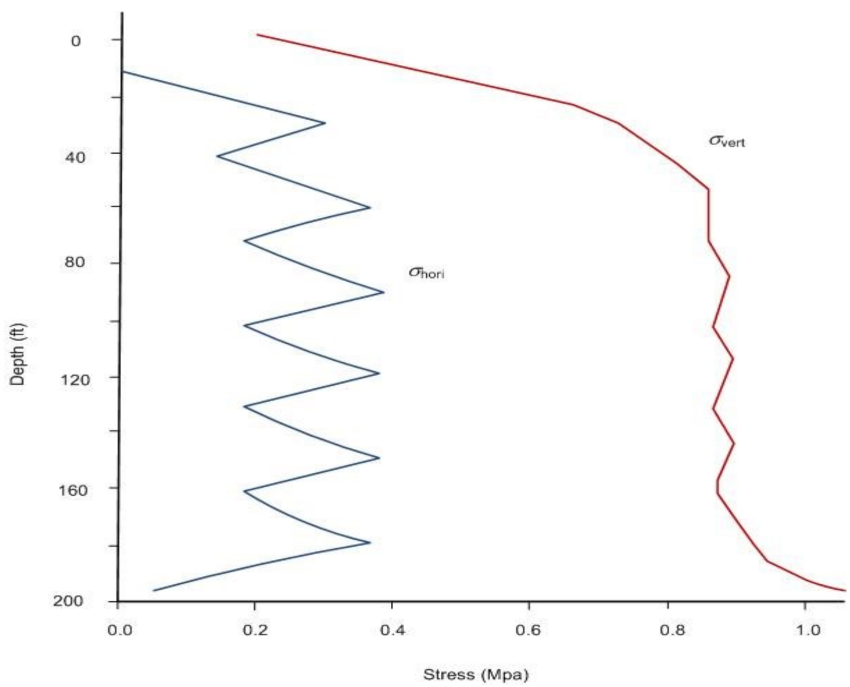

Figure 2-15 – Presenting vertical stress and horizontal stress profiles in backfill

Brady and Brown [54] presented a review study carried out of two hydraulic fill stopes which experienced barricade failures at Osborne copper gold mine located 195 km south east of Mount Isa was the case study employed for this work. Underground mining methods used at the Osborne mine were up-hole retreat panel stoping in flat dipping areas of the ore body and up-hole retreat bench stoping where the dip of the ore body is greater than 40 degrees. They have carried out test work on probe samples of fill taken from with 3E S stope. This data was used by them to analyze the potential for liquefaction under dynamic loading due to either crown failure or mass blasting. Their preliminary findings indicated that Osborne's old specification fill had a low relative density, low effective stress and high potential for liquefaction under dynamic loads.

An issue highlighted by the review process was that a mine's hydraulic fill system must be fully integrated with mine planning due to its requirements and the constraints it places on mine design and scheduling.

Dirige [55] used a laboratory test program for physical characterization of the Golden Giant mine tailings material used in the preparation of paste fill. The strength and deformation behavior of paste backfill in standard static physical model tests were investigated. He investigated the stability, behavior and mechanisms of failure of the paste backfill using analytical, numerical and centrifuge physical modeling. Through his comprehensive studies, he observed that the principal failure modes in paste fill exposed faces are shear failure followed by sliding block, somewhat resembling a circular slip. He also reported that failure modes in sill mats were slip failure, sill rotation and caving and that the stability of fill materials improves when placed in narrow stopes, with rough wall conditions, relative to those placed in wider stopes. The yield and displacement contours of backfill are presented in Figure 2-16. Both the blocks are presenting failure at the central right part of the backfill.

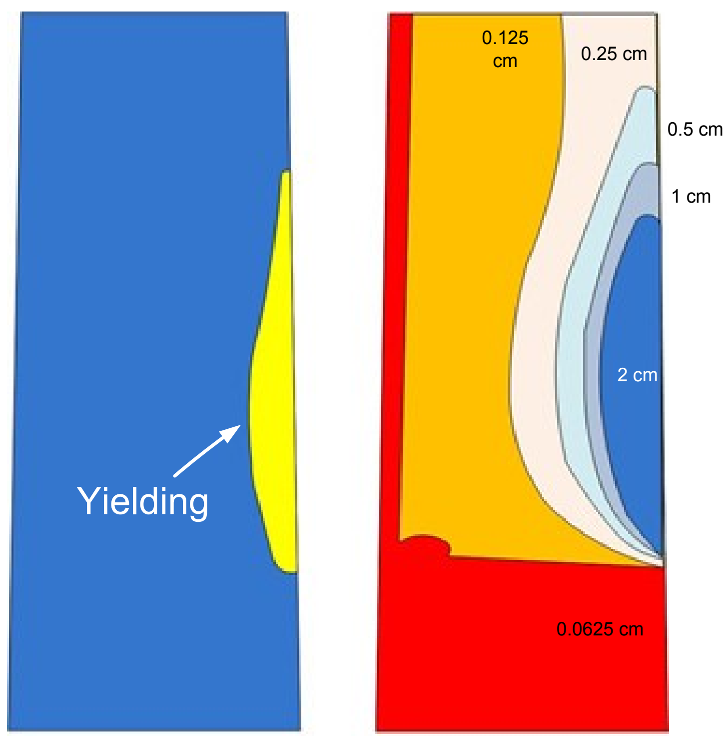

a) Yielding b) Lateral displacement

Figure 2-16 – Results of modelling backfill material [55]

Li et al [56] modeled narrow rectangular backfilled stopes using $FLAC^{2D}$ software. Interface elements were wrapped around backfilled stopes to simulate interface between fill and rock, which is found to be more realistic representation. They plotted vertical stress in backfill and the results showed arching in backfilled stopes.

Rankine [57] studied the effects of mining sequence using $FLAC^{3D}$ model. Paste fill has been modelled as homogeneous material and was investigated for large exposures. Vertical stresses were used to assess stability of backfill when exposed. Interface elements were also used around backfill. The model also showed arching in backfill and it was shown that a three dimensional model gives more realistic representation of backfill and better results are achieved using a three dimensional approach.

Doerner [22] used $FLAC^{2D}$ for modeling cemented rockfill spans at Musslewhite mine. He reported that vertical stress contours are amongst the critical parameters in assessing backfill material as some load is transferred to rockmass, and it has been reported that the key parameter in modeling backfill was found to be horizontal to vertical stress ratio (K). Rockmass was modeled as linear elastic material and cemented rockfill was modeled as elasto-plastic material to enable deformations and yielding. The analysis by Doerner does not incorporate wall convergence before backfilling a stope. Map3D code was used to assess stress in CRF sill matts. It was found that maximum stress in backfill was a factor of vertical height, friction angle and fill density. Backfill yielding in tension and shear were chosen as failure criteria. A factor of safety of 1 was considered to be transition state for backfill. Open stoping longitudinal mining model or AVOCA mining was also constructed and vertical tall columns of CRF were assessed for stability when exposed for pillar-less mining. Vertical and horizontal stresses were plotted along with stope height and width. Effect of stope undercutting was also studied in the thesis. The models were very good for initial assessment of backfill but they lack detailed analysis. Blast-induced damage was not considered in this analysis. $FLAC^{2D}$ was recommended to be highly suitable for modeling backfill material. Incorporation of blast induced vibrations on backfill was highly recommended in this work. It was recommended that cavity monitoring surveys can be used for calculating blast induced damage in CRF.

Zhou and McNearny [58] used PFC3D for shear characterization of CRF test specimens. In this work the authors simulated a failure surface. CRF gradation and void size of the specimen were also included in this analysis. The initial model was constructed with spheres, and particles were assumed to be spheres only. In the later part the angular pieces of aggregates were modelled by a combination of many spheres. The CRF samples modelled are presented in Figure 2-17. The model shows the inclination and position failure surface, based on direction of moving particles in the sample. Figure 2-18 presents modelling of weaker plane in CRF sample. The orientation of the weaker plane has also been varied and the effect of orientation has also been studied.

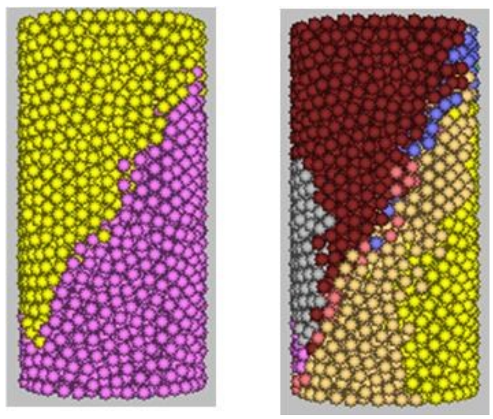

Figure 2-17 – Cemented rockfill sample testing showing failure surface [58]

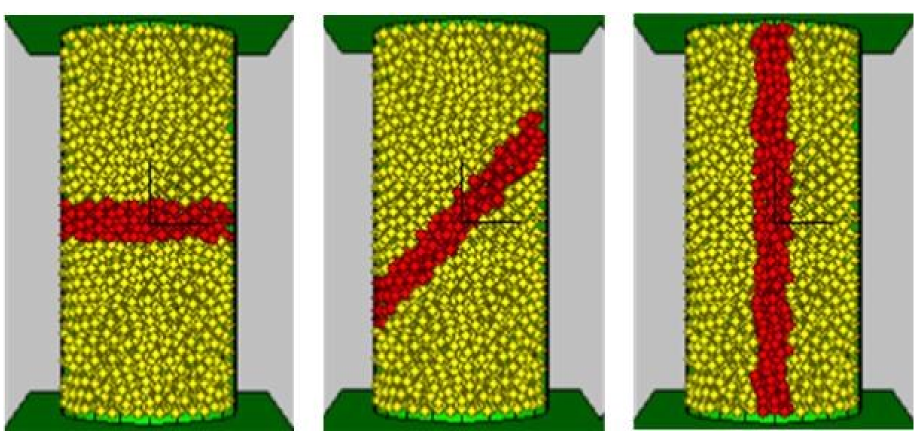

Figure 2-18 – Simulating plane of weakness in CRF test specimen [58]

Kockler [24] modeled CRF sill spans for stability, and they used FLAC^{2D} static model to achieve the goals. He used elasto-plastic model and mohr-coulomb failure criterion. The model was calibrated with laboratory testing values of CRF beams tested and field observations. Vertical stresses were plotted and vertical stress versus lateral thrust and beam deflections. Full scale model was also constructed and CRF stability was assessed in terms of vertical stress. He recommended that a three dimensional analysis is required for complete assessment of backfill. Incorporation of blast induced vibrations in the model will elaborate backfill failure mechanism in detail. The results of model in terms of vertical stress are presented in Figure 2-19.

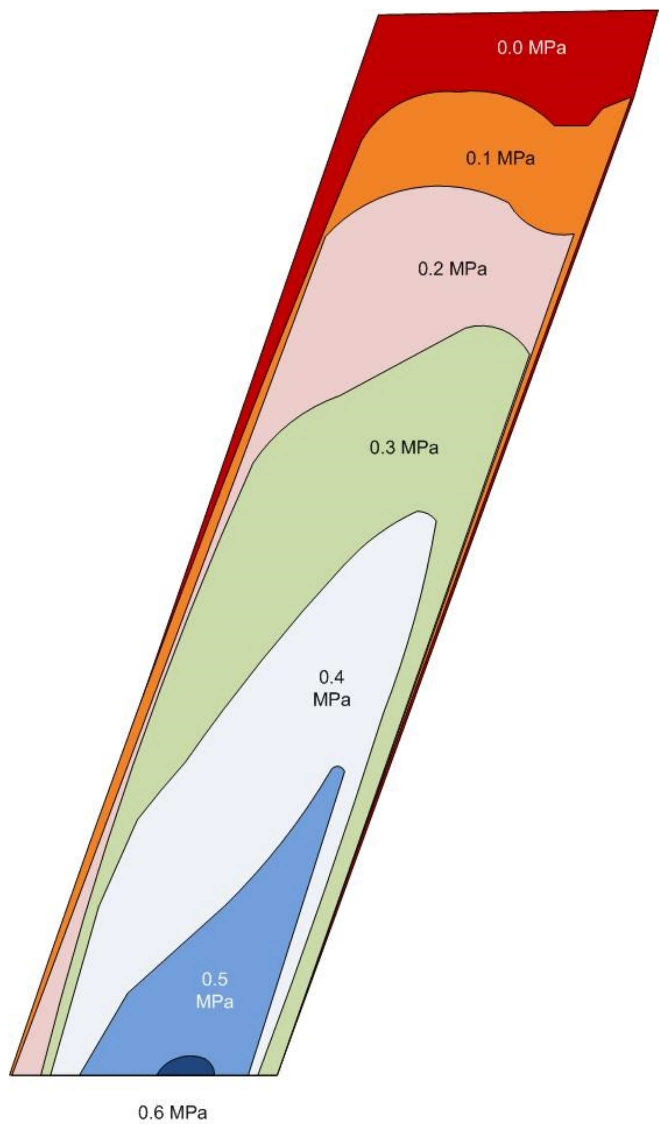

Figure 2-19 – Vertical stress contours on exposed face of an inclined stope [55]

Pirapakaran [49] used FLAC^{2D} and FLAC^{3D} codes to model circular and rectangular axisymmetric backfilled stopes. The backfill was assessed for arching effect, and a parametric study was performed. Rockmass was modeled as linear elastic and backfill was modelled as elasto-plastic material. Interface elements were used around the backfill and a small void was left on top of the backfill. Vertical stresses were plotted and the stopes were analyzed for arching. The model was compared with laboratory observations, in-situ testing and analytical solutions. Notably a small gap is left on top of the backfill. Two dimensional plane strain model is shown in Figure 2-21 and the results of vertical stress contours are presented in Figure 2-21.

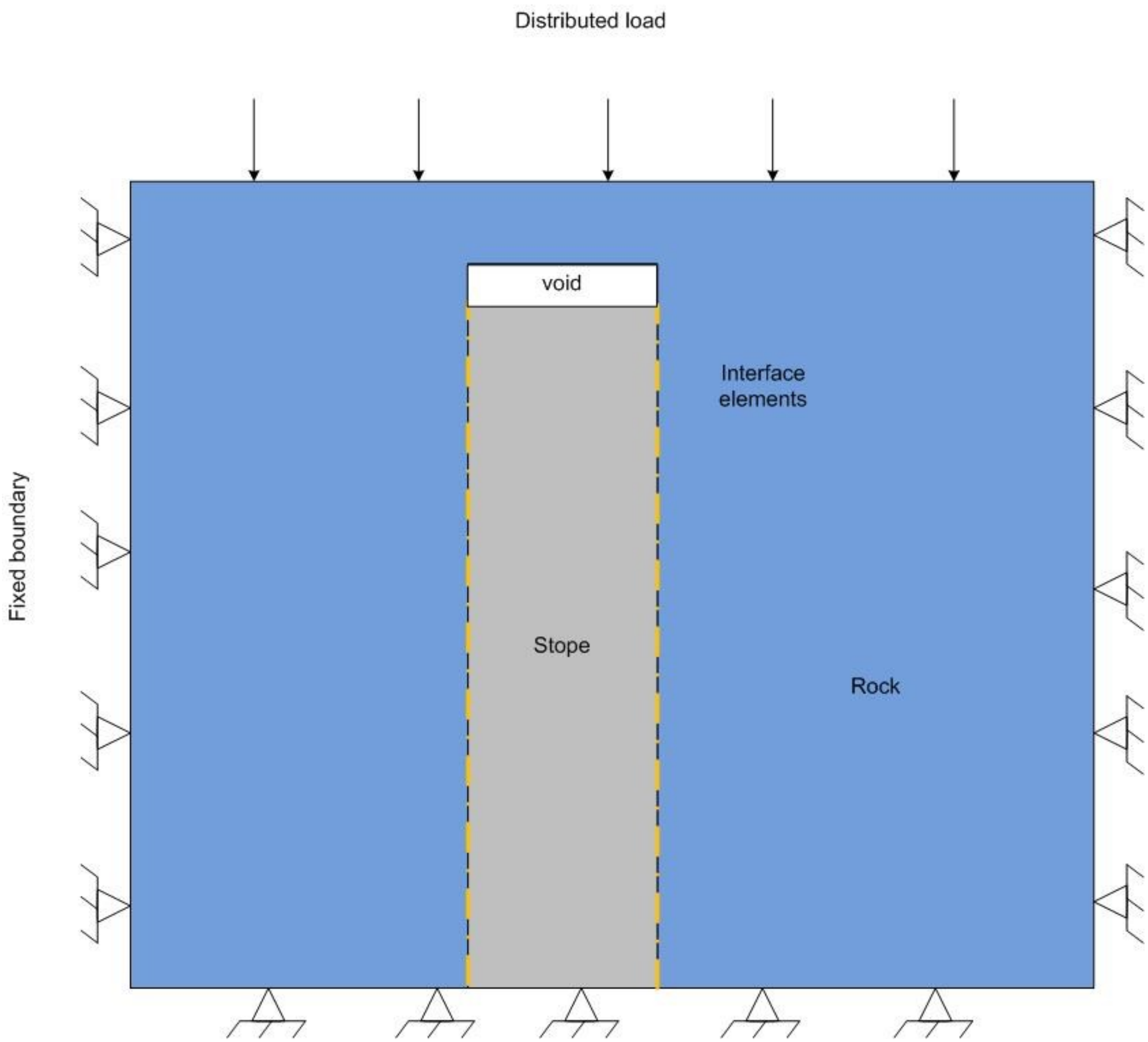

Figure 2-20 – FLAC^{2D} model showing numerical model and boundary conditions [49]

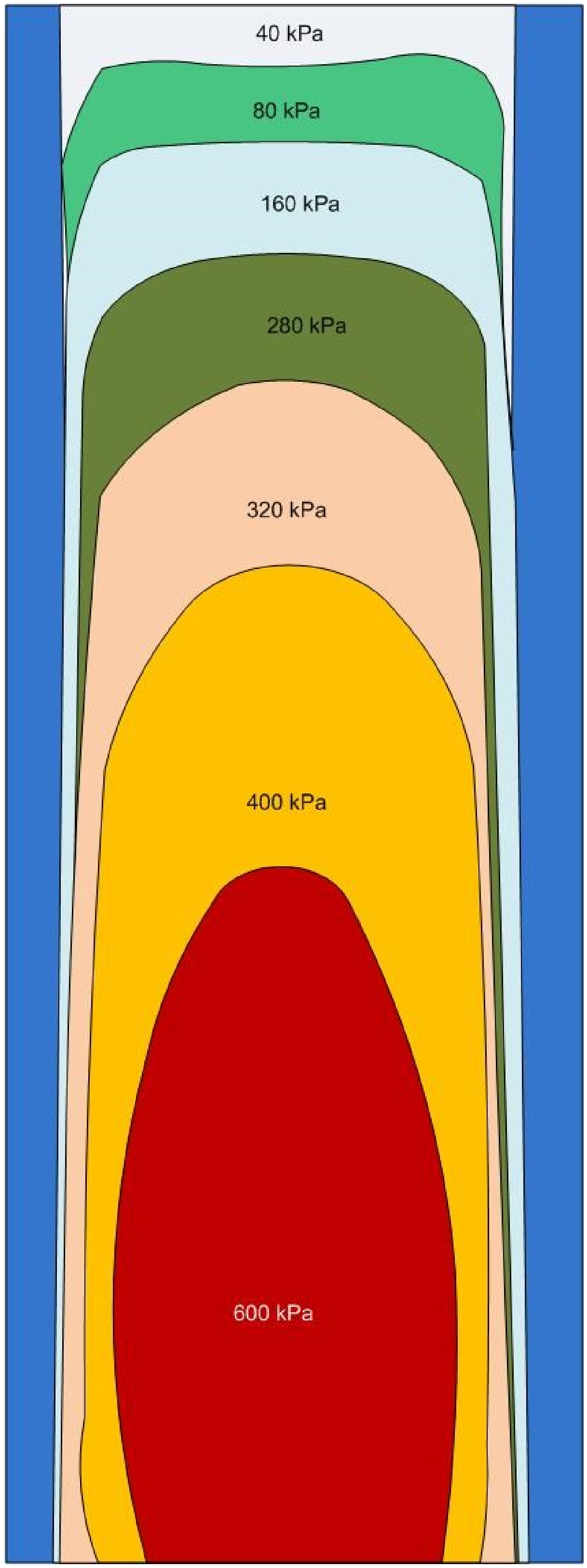

Figure 2-21 – Vertical stress contours in backfilled stope [49]

2.2 REVIEW OF CEMENTED ROCKFILL PRACTICES

2.2.1 Kidd Creek Mine

The following text has been extracted from published work by Yu [5]. The Kidd Creek mine is located approximately 27 Km north of the city of Timmins, Ontario. The operation is producing four and a half million tonnes of ore per annum. Mining method is sublevel stoping, with delayed backfill. There are two mines classified as No. 1 mine and No. 2 mine, with stope dimensions 22 to 65 m long, 18 m wide and 90 to 135 m height for the No. 1 mine, and 30 m long, 15 m wide and 60 m height for No. 2 mine. CRF was placed after the ore recovery and curing time of at least 3 months was practiced before exposing CRF for No. 1 mine and for No.2 mine the stopes were smaller and a curing time of at least 3 weeks was observed before exposure of CRF [5]. The waste rock from open pit was the primary source for the backfill. Initially, aggregate was crushed and graded to coarse (15 cm – 1 cm) and fines (under 1 cm). The coarse to fine ratio is maintained at 3:1 respectively. A number of backfill failures were observed during winter. These failures were due to freezing of binder resulted in poor coating and an increase in time to cure. To counteract this situation 2% calcium chloride was used with binder, which not only lowered the freezing point but it also provided heat for curing of CRF. It was also observed that an increase in depth and re-handling produces surplus fines due to attrition of particles. To counterbalance this problem Kidd Creek removed secondary and tertiary crushers from the circuit. It has been observed that segregation in CRF is unavoidable but can be reduced by better particle size distribution, placement method and proper mixing. CRF stopes were tested underground and it was established that fines occur near the impaction part during placement resulting in a high stiffness zone, as fines contain higher cement contents. Cementation is lesser in coarse particles that are placed at stope perimeter, resulting in a weaker zone. Water contents in the fill also impact the strength as excessive water contents will flush away the binder to the bottom of the stope, which leads to heterogeneity in CRF, and a lower water contents will make a sticky CRF and will decrease flow-ability. Location and orientation of backfill raise was found to be an important aspect for uniform distribution and to decrease segregation. Two raises at the center of stopes are necessary to decrease segregation in CRF. Coating of binder on aggregates is important for a consolidated fill, and coating on aggregate is a factor of mixing binder slurry and aggregates. At No. 1 mine mixing of CRF is done by a 1.2 m diameter by 2 m long steel vessel with three baffles for mixing, and placement of CRF into stope was done with 0.7 m diameter raise. In No. 2 mine the aggregate is hauled by 11.8 tonne trucks, which are loaded from a chute the binder is sprayed on the aggregates while dumping in the raise, and CRF get mixed in raise itself by rolling and dumping, this produces an average strength CRF. Earlier in No 2 mine, there was a fill mixing chamber which contains two $5m^3$ drums with baffles. The mixing station had a capacity of 3000 tpd. The method was one of best for CRF mixing. Impact damage can be a concern when there is a problem of cold joints, a retardant can be used to avoid cold joints. A decrease in water quality due to addition of oil, grease, chemicals and dissolved salts can have an influence on strength of CRF. Laboratory testing results of CRF with 5% OPC showed that the shear strength of CRF was almost 1 MPa. UCS of CRF cylinders is easy to measure in the laboratory. A 15 cm diameter cylinder with 28 days curing time has shown a relationship with binder contents:

$$Q_u = 1.5e^{0.25\,C} \qquad (2\text{-}7)$$

Where

C = binder content by weight % of minus 4 cm aggregate

Q_u = Compressive strength of fill

A proper proportion of sand is known to improve dynamic tensile strength of CRF column. 5% sand in aggregates will increase strength up to 40% and further increase in sand will decrease the strength of CRF.

2.2.2 Meikle Mine

The following text has been extracted from the published work by Stone 2007, Sacrison and Roberts 2001 [7, 59]. The Meikle Mine is owned and operated by Barrick Gold. It is located in Elko County, Nevada USA. It is a shallow ore deposit being mined out mainly by open stoping mining method with delayed backfill and cut and fill mining method is used to mine out nearby irregular ore bodies. The production is 2800 tonnes per day. There are two backfilling plants primary and secondary. Primary plant is responsible for serving as the main backfilling plant and secondary plant is used as a backup and is used during maintenance and repairing of primary plant. The primary plant comprise of 7.65 m^3 on-site shaft ribbon mixer, located 328 m underground. System control is through various programmable logic controllers (P.L.C.) for flexibility, control and higher degree of automation. Rock aggregates are mined from the open pit and are shipped to a crushing and sizing plant. It has been observed that rock aggregates having UCS of less than 70 MPa or higher are generally suitable for CRF. Particle size distribution has the largest impact on CRF strength and density. Excessive fines will take away most of the binder and deficiency of fines lead to higher void ratio. Fines in CRF are particles less than 10 mm diameter. The sized aggregate consists of 70% coarse particles within a range of 3.81 cm x 1 cm (1½" x 3/8") and 30% fine particles less than -1 cm (- 3/8"). A circuit of grizzlies, screens, sieves and crushers were employed to achieve the desired particle size distribution. The aggregate can be graded to maximize CRF density for increased strength based the Talbot distribution curve developed for concrete. The aggregates were transferred dry to underground backfill plant through pipes installed in ventilation shaft. The pipes terminate in a rock-box, transfer raises and end up in silos. The binder is composed of Type II cement and Fly ash, and 6% binder is used in CRF. Concrete mixing technology is being employed for mixing CRF for better performance. Placement is done by 6.1 m^3 remote controlled LHD's dumping CRF into stopes. CRF strength of 2.8 MPa is targeted for primary stope where the fill will not be undercut at a later stage. CRF strength of 5.5 MPa is the targeted strength for undercut stopes. The secondary CRF slurry plant located adjacent to the primary mixing plant consists of a colloidal mixer. Different rock aggregates were used at the Meikle Mine and it was found that generally hard metamorphic and igneous rocks perform better than sedimentary rocks. However, weak and slabby materials are very bad for CRF. CRF admixtures have also been employed to increase strength and water reducer was employed. Overall water contents were constantly monitored and water to cement ratio was kept between 0.9 – 1.2 depending upon weather conditions. It was observed that fill density has a direct relationship with strength and fill density is a factor of particle size distribution, and fill placement method. Quality control is an important aspect and Meikle engineering department collects random samples for different tests of aggregates from binder line, crusher output, CRF mixer output, in-situ placed CRF and water used for slurry preparation. The binder is tested for quantity and quality, rock is tested for impact and aggregates are passed through sieves and water quality is tested frequently. Two CRF cylinders are prepared per shift and cured for 28 days for UCS testing. Diamond drill cores from in-situ CRF stopes are also drilled for UCS testing.

2.2.3 Mount Isa Mine

The following text has been extracted from published work by Mathews [12]. Mount Isa is a copper mine located near Mount Isa in north-west Queensland, Australia. The total ore reserves exceed 100 million tonnes. The ore body was mined out using sublevel stoping mining method with delayed backfill. Cemented hydraulic fill, cemented rockfill and cemented slag fills were used as backfill materials. The fill strength requirements were used to design the CRF columns. It was determined that a UCS of 1-1.4 MPa is sufficient for an exposure of 36-40 m, stope height. A safety factor of 2 was anticipated in the design for blast-induced vibrations. CRF was prepared by crushing rock aggregate to +25 mm –300mm size. The rock was then placed in stopes simultaneously with cemented hydraulic fill via conveyors. An overall cement content was around 1.3%, well below the common practice values. It was observed during in-situ testing program that the strength of CRF was highest (2 MPa) amongst the fill types in use. Segregation was the major problem encountered at Mount Isa mine. Several drop down tests for cemented rockfill showed that a decrease in particle size may range from 50% to 70%. It was then decided that no stopes will be filled directly from surface. CRF percolation test showed that there is a percolation of slurry up to 3 meters for +25 mm material. Core drilling and driving a drift through CRF showed larger particles and slurry deposition near the stope parameters. Fine and dense material was near the dumping point due to impaction of CRF. In-situ plate test showed modulus values of 350 MPa for CRF.

2.2.4 Cayeli Mine

The following text has been extracted from published work by Yumlu [21]. Cayeli mine is located in the north eastern region of Turkey in the Rize province. The mine is 8 km away from the town of Cayeli. The mining method used is long hole stoping with delayed backfill producing 2800 tonnes of ore per day. Stope is developed by driving 7 m x 5 m sill drifts to hanging-wall and foot-wall or to the boundary of cut-off grade. The average length of sill drift is nearly 35 m. Stope is formed by extracting the 15 m high bench between the sill drifts. The CRF is made with 5 % cement only, which sometimes varies with availability and stope requirements; while waste is filled in secondary stopes. When the mine was shallow, trucks were used for hauling the CRF, one surface plant and two backfill mixing plants were used to make CRF. When the trucks are being loaded with aggregates, cement slurry is sprayed over; additional mixing was done during transport to stope. The CRF in-situ strength was nearly 1.5 MPa after 28 days curing period. It was observed that almost 4% backfill dilution was inevitable, and was caused by blast induced vibrations. It was recommended that low explosives and a change in blast design can lower the blast damage on fill.

2.2.5 Hishikari Mine

The following text has been extracted from published work by Kurakami [32]. The Hishikari mine is located in the south of Japan near the district Kyushu. Until 2007 the mine has produced 183000 tonnes of gold with grade of 46 grams per tonne. The mining method used there is by drifting and bench stoping with delayed backfill. Cemented rockfill is used for primary stopes and un-cemented rockfill is used for those secondary stopes which are not likely to be exposed. Rock used for backfill came from developmental work and the waste rock was graded to 20 – 50 mm before placement and 4.5% whereas, Portland cement was used as a binder. The dip of ore body is 70 degrees, stope height varies from 19 m to 24 m, width is 0.5 m to 5 m and length of stope was around 13m. The mine experienced some dilution, which was believed to be due to improper mixing and placement.

2.2.6 Lamefoot Mine

The following text has been extracted from published work by Reschke [60]. Lamefoot mine is located in the north-west of Washington State. It uses longhole mining method with delayed backfill to produce 1350 tpd. Cemented rockfill is used for maximize the extraction of this high grade ore. Stope size is generally 25 m long, 45 m high and 15 m wide. Cement slurry (water: cement = 0.8: 1) is processed in the surface plant and is then sprayed over rock aggregate contained by haul trucks having a capacity of 21.2 tonnes. Rock aggregate particle size is not more than 45 cm, and it comes from developmental work only. At Lamefoot mine there is some dilution from CRF, which is due to segregation and large exposures. Laboratory and in-situ tests are performed consistently and results were incorporated in design to avoid major fill failures.

2.2.7 Polaris Mine

The following text has been extracted from published work by Reschke [60]. Polaris mine is located on the Cornwallis Island in the Canadian High Arctic in Nunavut Canada. The sublevel longhole mining method with delayed backfill has been enforced. Generally the size of stope is 100 – 150 m in length, 15 m wide and 60 – 110 m in height, mined in lifts of 30 m. Raises are used for the placement of cemented rockfill in the mined out stopes. The utilization of CRF was a challenge in conditions where surface temperature was – 55^{o}C in winter to +10 ^{o}C in summer. Rock aggregate was made of quarried and waste rock in 50:50, screened to 12.5 – 200 mm. The rock aggregate was mixed with 5% type 30 Portland cement, and 2.5% calcium chloride. The water to cement ratio was selected to be 0.7:1. Calcium chloride was used as an accelerator, and it was found that aggregate heating was necessary for attaining greater strengths. To achieve this, a 3 MW hot water aggregate heating circuit was designed to bring the temperature from – 30 ^{o}C to + 15 ^{o}C. Slurry was produced in a surface plant which was also been heated by heating circuit. The aggregate was transported by insulated chute into the backfill raises and cement slurry is sprayed on it while dumping. This method was not very good due to freezing problems, so now the method of placement has been replaced by truck box. The CRF mixture is hauled by trucks with heated dump boxes; on reaching the raise the trucks dump CRF in the raise. With the new system the backfill dilution is kept under 5%, earlier it was way over 10%. The success of placement depends on the fact that the placement of raise is right next to the secondary stope to be mined.

2.2.8 Williams Mine

The following text has been extracted from Farsangi [17]. Williams mine is located near Marathon in Ontario, Canada. It was one of the largest gold producers in Canada. Its daily production was about 5500 tonnes per day with annual gold production was 500,000 oz. The mine employed longhole open stoping mining method with delayed backfill. Levels were located at every 105 meters and each sublevel was located at 25 meters. Stope dimensions practiced were 20 m in length, 25 m in width and 25 m in height. Cemented rockfill was used by the mine for greater stiffness. Rock was mined from quarry and then was sized to coarse and fine. Coarse content was sized to – 15 cm + 1 cm (–6” +3/8”) and fine content was – 1 cm (–3/8”) in ratio 3:1.

The rock was transported underground by aggregate raise, which is filled to the surface. Conveyors were used for placement of CRF underground, to open stope or fill raise. For smaller stope a 26 tonne truck is used instead of conveyor and binder slurry is showered on top of the truck. Binder was composed of a blend of ordinary Portland cement and fly ash in ratio 45 to 55 and a total of 4.2% binder was used to prepare binder slurry.

2.2.9 Namew Lake Mine

The following text has been extracted from Reschke [43]. Namew lake mine is located 60 km south of Flin Flon in the province of Manitoba in Canada. The massive ore body is located under the Namew Lake in central Manitoba. It was mined using longhole stoping with delayed backfill. Stope dimensions practiced were 20 m in length by 2 – 30 m in width and 180 m in height, the dip of ore body is 48 degrees. Cemented rockfill was employed as the primary backfill method for supporting hanging wall. Rock aggregate was mined from quarry and was then crushed to – 200 mm and 2 – 6 % fines were added before transporting underground. The rock was sized in accordance with 8" Talbot curve. The binder was prepared by an automated plant with 3 percent cement and 2% fly ash. The water to cement ratio was maintained at 0.8. The placement was achieved with 20 tons truck. The dilution levels were under control and a total dilution of less than 5% was maintained. Occasional large failures were also experienced and the causes were segregation, excessive water in recipe, blasting practice, lack of mixing, aggregate largest particle size and use of frozen aggregate. Research on CRF was also conducted for optimization of backfill.

2.3 REVIEW OF MECHANICAL PROPERTIES OF CEMENTED ROCKFILL

Cemented rockfill is made by mixing binding agent, water and rock aggregate or waste rock Hassani and Archibald [4] which makes it similar to concrete. Portland cement contents vary with design of backfill from 4% to 7%, producing a compressive strength of 1 MPa to 6 MPa. CRF can be termed as a weak concrete with a UCS much lower than regular concrete. Engineering properties of cemented rockfill are very important for planning, design and quality control. CRF samples are generally tested for compressive strength, but other engineering properties like shear strength, tensile strength and Young's modulus are very important for understanding backfill and for conducting a numerical modelling study. Some empirical relationships were developed by Kosmatka [61] for concrete may be applied to CRF as well are presented as follows:

Tensile strength:

$$\sigma_t \approx 12\% \; of \; \sigma_c^{0.5} \qquad (2\text{-}8)$$

Shear Strength:

$$\sigma_{sh} \approx 20\% \; of \; \sigma_c \qquad (2\text{-}9)$$

Young's modulus:

$$E \approx 33\, W^{1.5} \;\; \sigma_c^{0.5} \qquad (2\text{-}10)$$

Farsangi [17] in his research recommended measures to control properties of CRF. It was reported that factors like aggregate size range, fill placement, transportation, quantity of materials and binding agent etc. can be varied to control CRF properties. In addition it has been recommended that quantity of binder slurry should be sufficient enough to coat the surface of aggregates. Moisture contents of rock aggregates also play a vital role for achieving desired properties. It has also been reported that use of mine water for preparation in CRF may reduce strength of CRF to 60%. He reports that Kidd Creek mine prepared CRF with mine effluent water and regular water to check the effect on strength, while keeping everything constant. It was found that the mine effluent water samples had half the strength of regular CRF. The use of recycled water also produced lower cohesive strength. [62]. [5, 63, 64] presented relationships to calculate compressive strength (σ_c) of CRF based on the cement contents (C_v) and porosity (n). The relationships were based on the exhaustive laboratory testing and are presented as follows:

Swan [63]: $$\sigma_c \propto C_v^{2.36} \qquad (2\text{-}11)$$

Yu [5]: $$\sigma_c = 1.5e^{0 \cdot 25C_v} \qquad (2\text{-}12)$$

Lilley [64]: $$\sigma_c \approx 63(C_v \,/\, n)^{1.54} \qquad (2\text{-}13)$$

In-situ strength of CRF may vary from 1.3 MPa to 11 MPa, depending upon the magnitude of segregation [62]. Yu and Counter [8] did a series of dump tests on CRF material and coring through CRF shed light on segregation. Testing of cores led to a wide range of CRF strengths from 6 MPa to 10.3 MPa. They also performed chemical analysis on those cores and it was found that cement were inconsistent throughout the CRF column. The results of cylinder testing and core testing results published by different authors have been presented in Table 2-2.

The following section covers four different projects on CRF laboratory investigations. The work of CANMET's Sudbury Mining Research Laboratories [65, 66], Lafarge Canada Limited [67] and THROW Ontario Limited [68] has been presented. CRF was tested for physical and mechanical properties. Unconfined compressive strength values have been presented in Figure 2-22 and Figure 2-23. The two Figures compare the UCS values when the binder has been changed from 100% ordinary Portland cement (OPC) to 65% ordinary Portland cement and 35% flyash (FA). It can be observed that UCS improved with quantity of cement curing period from both the Figures. It can be inferred that 28 day strength is sufficient for static loading conditions. When Figures 2-15 and 2-16 are compared it can be seen that flyash enhance the strength of CRF but it decreases the curing period. When considering economics 4% binder choice is better than 5% or 7% binders as it gives slightly better strength than 5% but lesser than 7% for the particular recipe used for this testing program.

Table 2-1 – Core and cylinder testing of cemented rockfill materials

Reported by	Sample	Density (Kg/m^3)	Curing period	Average Compressive Strength (MPa)	Elastic Modulus (GPa)
Yu and Counter [8] for Kidd Creek mine	3 cores d = 15 cm	2000	28 days	6.9	0.002
	3 cyl. d = 15 cm	2500	28 days	6.1	-
	9 cores d = 8.4 cm	2300	3 months	10.3	0.0031
	Dump cone test	2400	4 years	11.0	0.0038
	Core from impaction zone	-	4 years	8.5	-
	Core from intermediate zone	-	4 years	3.5	-
	Core from coarse zone	-	4 years	1.3 (estimated)	-
Reschke [43] for Namew lake mine	Cyl d = 15 cm, 5% cement, Aggregates < 2 cm	-	28 days	4.35	-
Seppanen [69]	Cyl.	1650	28 days	9	-
Annor [70]	Cyl. d = 15.2 cm	-	28 days	5.9	9.8
	Cyl. d = 45.7 cm	-	28 days	3.2	1.1
Wang and Villaescussa [71]	3%OPC + Dolerite	2240	28 days	4.3	-
	4%OPC + Dolerite	2260	28 days	6.3	-
	5%OPC + Dolerite	2290	28 days	9.2	-
	6%OPC + Dolerite	2340	28 days	12.8	-
	4%OPC + Marble	2410	28 days	4.98	-
	3%OPC + Dolerite	2240	28 days	2.25	-
	4%OPC + Dolerite	2260	28 days	2.28	-
	5%OPC + Dolerite	2290	28 days	2.32	-
	6%OPC + Dolerite	2340	28 days	2.37	-
Yumlu [21]	Cyl.	-	28 days	1.5	-
Kockler [24]	Cyl.	2114	28 days	3.3 – 4.2	0.74 – 0.82

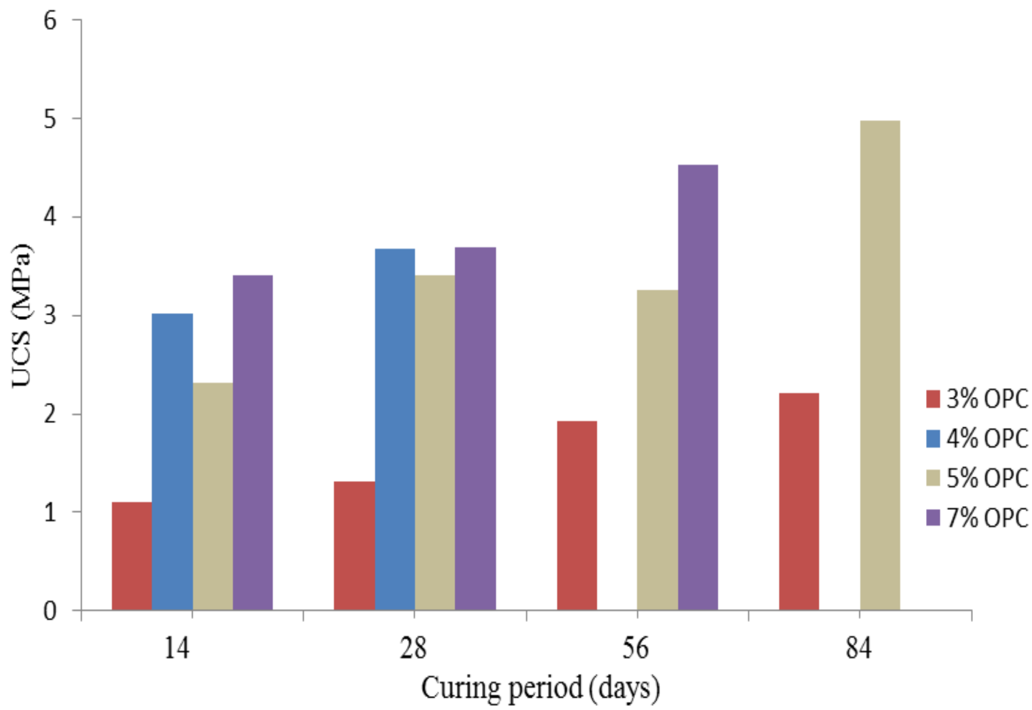

Figure 2-22 – UCS versus Curing time for different %age of binders [65, 67, 72]

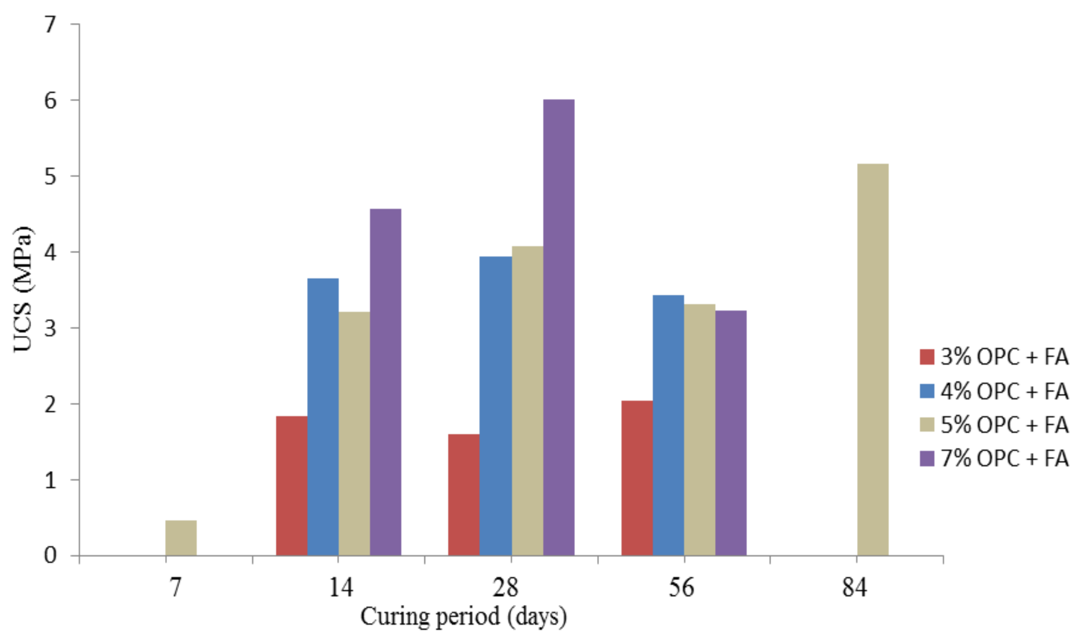

Figure 2-23 – UCS versus Curing Period for different binders [65, 67, 72]

2.4 SUMMARY

This chapter presents a detailed review of backfill types, design, issues, failure mechanisms, case studies and mechanical properties. A detailed review of cemented rockfill system, CRF failure modes and CRF design criteria is also presented along with different CRF operations around the world. Literature review on numerical modelling of backfill material has shed light on backfill material modeling techniques and concepts, adopted by practitioners and researchers. It can be concluded from a review of CRF practices that backfilling with CRF is a very complex process with many issues. CRF failure has been observed to be in wedge shape and it is a product of multiple factors. Some of the prime factors include placement method, recipe, mixing method, blast-induced vibrations and segregation. The laboratory test results of CRF testing published in the literature have been compiled. CRF engineering properties prediction equations have also been presented. This will be very useful for numerical modelling of backfill material. Laboratory testing results of unpublished work has also been presented and trends have been discussed. The section on numerical modelling suggests modelling CRF as elasto-plastic material while wrapping interface elements all around it. Results of past numerical modeling studies are presented in terms of stresses and yielding in tension.

3 DYNAMIC MODELLING OF CEMENTED ROCKFILL STOPES

3.1 INTRODUCTION

Literature review of backfill material showed that the dynamic loading is one of the prime causes of destabilization in fill mass. Numerical modelling codes with dynamic analysis option enable a user to compute the stability of backfill, while incorporating blast loading from adjacent production stopes. Dynamic modelling for mining and civil engineering structures has been in practice, and it has been considered as the integral part of a complete structural analysis, when dynamic loading conditions exist. This is due to the fact that dynamic loading induces high strains level (10^5) compared to static or quasi-static loading on structures (10^{-6} to 10^{-3}) [44]. Blast loading on backfill material has been reported to be one of the prime causes of fill failure in open stoping mining methods with delayed backfill [2, 5-8, 20, 21, 32, 73-76]. This Chapter presents numerical modelling solution for dynamic analysis, followed by dynamic modelling setup. This is followed by numerical modelling studies of CRF material under blast loading. This Chapter also encompasses numerical modelling of backfill and a compilation of backfill studies including variation in dynamic loading conditions, segregation and blasting method.

3.2 NUMERICAL MODELLING SOLUTION FOR DYNAMIC ANALYSIS IN FLAC^{3D}

Dynamic module in FLAC^{3D} by ITASCA [77] enables fully dynamic analysis of any model. The calculations are based on the explicit finite difference procedure, which employ lumped grid-point masses computed from actual masses unlike fictitious masses used in static analysis. The whole formulation is affixed to the structural element model, enabling study of geo-mechanical materials and structure interaction due to impulsive loadings and vibrations. FLAC^{3D} employs both fully non-linear approach and equivalent linear method from earth-quake engineering [78]. Equivalent linear method is a very simple and user friendly unlike non-linear approach. In order to carry out simulations for dynamic analysis, explicit dynamics framework is required [77].

The following equation is used to solve the equation of equilibrium equilibrium [79]

$$M\ddot{u} + C\dot{u} + Ku = P(t) \qquad (3\text{-}1)$$

Where:

u = displacement $\dot{u}$ = velocity

$\ddot{u}$ = acceleration

Acceleration: $$\ddot{u} = \frac{\dot{u}\left(t+\frac{\Delta t}{2}\right)-\dot{u}\left(t-\frac{\Delta t}{2}\right)}{\Delta t} \tag{3-2}$$

Velocity: $$\dot{u} = \frac{u\left(t+\frac{\Delta t}{2}\right)-u\left(t-\frac{\Delta t}{2}\right)}{\Delta t} \tag{3-3}$$

M: mass

3.2.1 Dynamic Modelling Setup

The following must be considered for conducting dynamic analysis:

1) Dynamic timestep
2) Boundary conditions
3) Dynamic loading
4) Damping

3.2.1.1 Dynamic Timestep

The calculation of dynamic timestep is given in the Dynamic Analysis manual of FLAC^{3D} by ITASCA [77]. It is calculated by using a factor of 0.5 and the equation for critical timestep when there is no stiffness proportional damping in the system. The equation is presented as follows,

$$\Delta t_d = 0.5\, min\left\{\frac{V}{C_p A^f_{min}}\right\} \tag{3-4}$$

If stiffness proportional damping is used in the model then the timestep is to be reduced for stability of numerical analysis. Belytschko [80] provided a formula for computing the timestep for stiffness proportional damping.

$$\Delta t_\beta = \Delta t_d\left(\sqrt{1+\lambda^2}-\lambda\right) \tag{3-4}$$

$$\lambda = \frac{0.4\beta}{\Delta t_d} \tag{3-5}$$

$$\beta = \xi_{min/\omega_{min}} \quad (3\text{-}6)$$

Where ξ_{min} and ω_{min} are damping fraction and angular frequency designated for Rayleigh damping.

3.2.1.2 Boundary Conditions

A material under internal dynamic loads should be bounded by dynamic boundary condition at the model boundary or inside the model grid points. Failure to do so will result in reflection of wave at the boundaries. The dynamic boundary conditions are:

1. Quiet or viscous boundaries
2. Free-field boundaries

The types of dynamic boundary conditions are shown schematically in the accompanying Figures. The boundary conditions used during a static analysis must be freed before applying the dynamic boundaries. The static load applied on the boundaries must be applied by the same magnitude load in opposite directions. Boundary conditions are not required if the model is infinitesimally large to absorb the entire dynamic loading applied in the model.

3.2.1.2.1 Quiet Boundary Conditions

This is generally applied to geo-mechanical problems involving impulsive loading, which are generally correspond to unrestrained condition. In case of a static analysis the fixed boundaries' effects vanishes at some particular distance, however in dynamic analysis the same boundaries may reflect the dynamic waves resulting in increasing the magnitude of vibrations. Reflection of blast loading from model boundaries transforms into tensile stress and this leads to huge deformations along the model boundaries. The magnitude of the deformation is proportional to the magnitude of the load reflected. To deal with this situation is to use quiet boundaries (also known as absorbing or viscous) as shown in Figure 3-1. Many formulations have been presented for modeling quiet boundaries [81]. Quiet boundaries are applied with dashpots at normal and shear directions, which are very effective at absorbing waves accurately up to angle of incidence greater than 30 degrees. Waves at angles below 30^o are also absorbed but the efficiency to absorption reduces significantly.

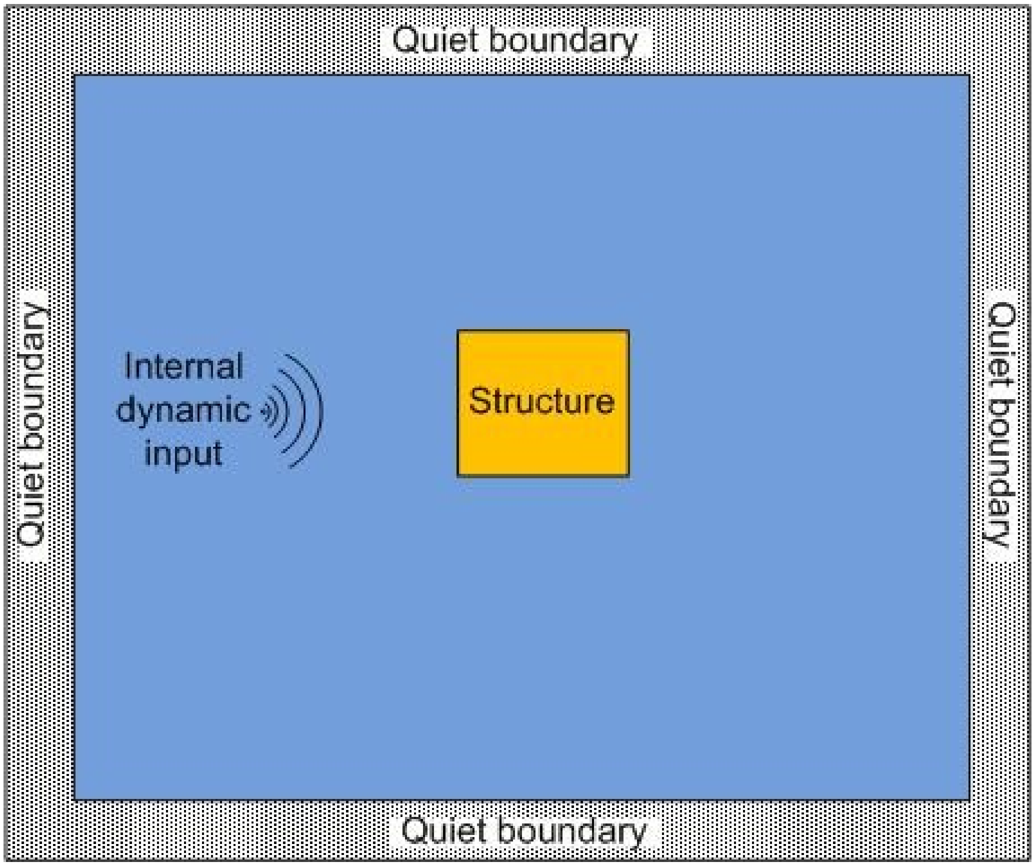

Figure 3-1 – Schematic presenting quiet boundaries [77]

The advantage of this method is it operates within the time domain. It is very effective in both finite element models and finite difference models [82]. The traction of dashpots can be represented by,

$$t_n = -\rho C_p v_n \tag{3-7}$$

$$t_s = -\rho C_s v_s \tag{3-8}$$

Where v_n and v_s are the normal and shear components of the velocity at the boundary, ρ is the mass density. C_p and C_s are the p-wave and s-wave velocities of the material. The tractions t_n and t_s are computed and applied in the same way as boundary loads are applied. The only potential problem concerns are the viscous forces computed from velocities, which lags by half a time-step.

3.2.1.2.2 Free-Field Boundaries

The following text is extracted from ITASCA [77]. When it is required to apply dynamic load as a boundary condition then free-field boundaries are very suitable. The main grid is attached to sub-grids or free field grids by means of viscous dashpots, which makes it a quiet boundary, and the unbalanced forces of the free-field grid are applied back at the main grid, as shown in Figure 3-2. So the model behaves as almost an infinite one. If motion of the main grid is different from free-field grid then dash pots will absorb waves and behave similar to a quiet boundary. To apply free field boundary conditions the model is orientated to make the base horizontal and its normal in z-axis.

If dynamic load is not vertical then orientation of the model should be done with respect to dynamic load and gravitational or other loads are taken at an angle to model. The formulation for free field boundary condition is given as:

$$F_x = -\rho C_p\left(v_x^m - v_x^{ff}\right)A + F_x^{ff} \tag{3-9}$$

$$F_y = -\rho C_s\left(v_y^m - v_y^{ff}\right)A + F_y^{ff} \tag{3-10}$$

$$\boldsymbol{F_z = -\rho C_s\left(v_z^m - v_z^{ff}\right)A + F_z^{ff}} \tag{3-11}$$

Where,

F_x, F_y and F_z are unbalanced forces in main grids

F_x^{ff}, F_y^{ff} and F_z^{ff} are unbalanced forces from free field grids

ρ is the density of zone

C_p and C_s are p-wave and s-wave velocities

v_x^m, v_y^m and v_z^m are velocity components in main grid in x, y and z axis

v_x^{ff}, v_y^{ff} and v_z^{ff} are velocity components in free field grids in x, y and z axis and

A is the x-sectional area of boundary.

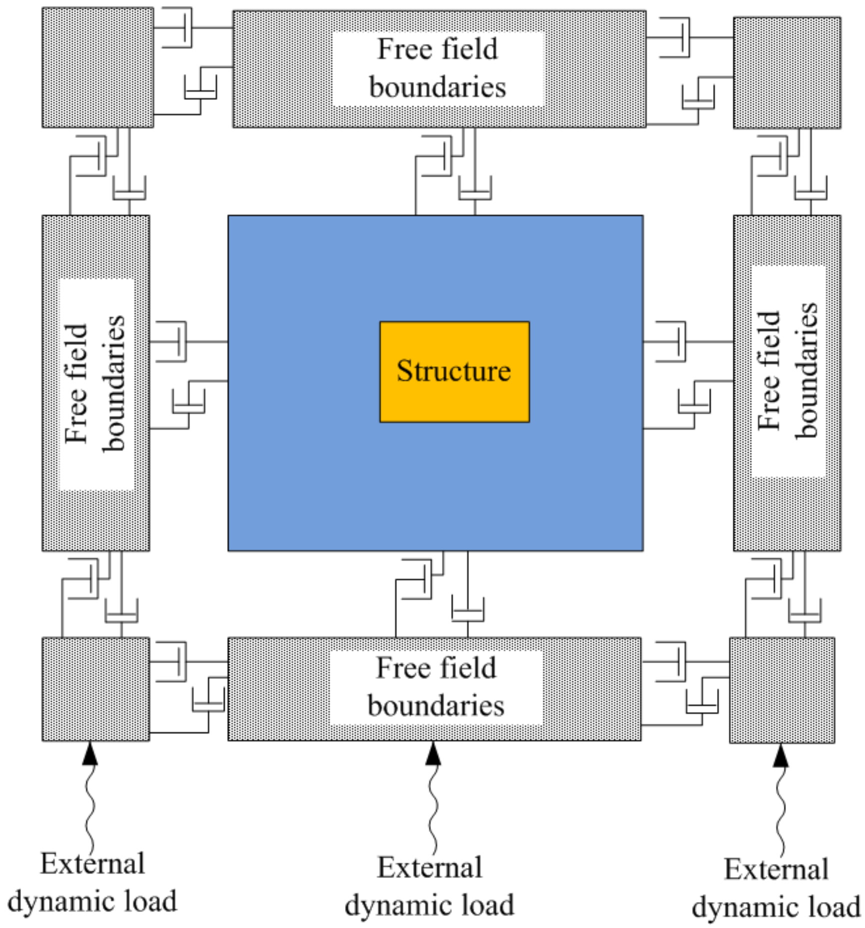

Figure 3-2 – Free field grid and main grid with structure [77]

3.2.1.3 Review of Dynamic Load Application

There are two broad profiles of explosives, which are ideal detonation and non-ideal detonation. The ideal detonation profile can correspond to emulsion type explosive and non-ideal detonation can correspond to ANFO type explosives where the rise in pressure is fast and fall from peak is much slower than emulsion type explosives [83].

Numerical modelling employs one of the following three methods to apply pressure:

a. Equation of State (EOS)

EOS defines a material's response in high-rate intense pressure scenario and the equation accommodates different parameters as a single function of others. The JWL equation [84] relates volume, energy and detonation pressure simultaneously.

b. Decay functions

Many authors reported the use of decay functions [85-89]. These equations reproduce the wave forms, but they assume certain parameters whose physical importance is not known. Figure 3-3 presents the profile of decay function used for applying blast load in a numerical model.

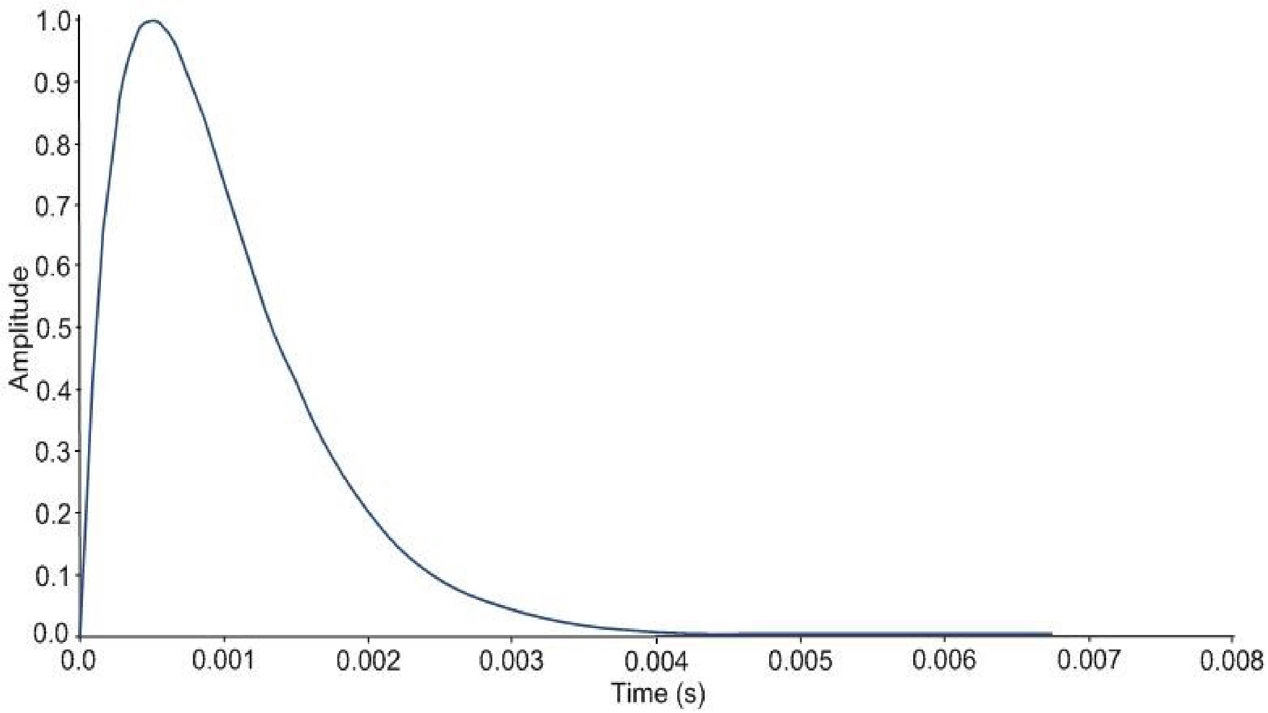

Figure 3-3 – Blast load profile for a decay function

c. Direct input of dynamic pressure

This is the most simplified and organized way of reproducing the blast hole loading profiles. It has some advantage over the above methods, as it is similar to the real loading. Generally two functions are used that are triangular and Gaussian, presented in Figure 3-4.

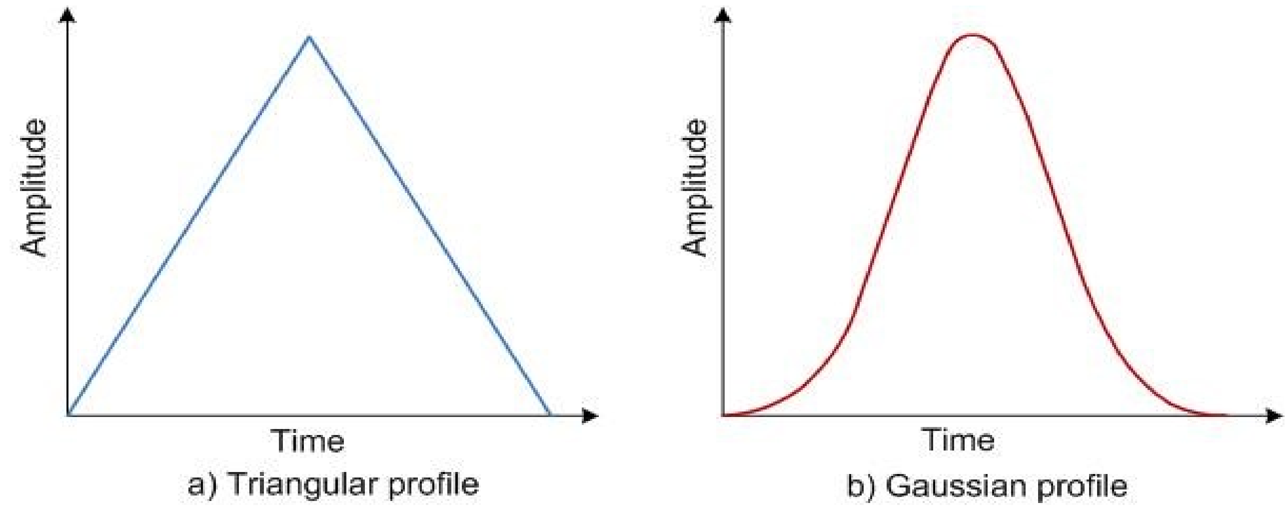

Figure 3-4 – Dynamic blast loading input profiles

The dynamic load in FLAC3D can be applied using one of the following ways,

(a) Acceleration
(b) Velocity
(c) Stress (or pressure)
(d) Force

The acceleration and velocity loads can only be applied with free field boundary and stress or force load can be applied with quiet boundaries. Velocity loading on a boundary can be converted into stress loading by the formula:

$$\sigma_n = 2\rho C_p v_n \qquad (3\text{-}12)$$

$$\sigma_s = 2\rho C_s v_s \qquad (3\text{-}13)$$

Where

σ_n and σ_s are normal and shear components of traction

ρ is density of zone,

C_p and C_s is p and s-wave velocities respectively,

v_n and v_s are normal and shear components of velocity at boundary.

3.2.1.4 Damping

Damping is the loss of energy by propagation of waves through any material. Some level of damping is already present in every material by nature. Geo-materials are considered as very good dampers due to their internal resistance, friction, sliding and slip. All four parameters are responsible for energy loss from the system. For dynamic modeling the loss of energy should be reproduced accurately to represent damping behavior of the material. In geo-materials the damping is hysteretic in nature as it accommodates strain modulus and damping functions directly into a model and generally it is independent of frequency. Hysteretic damping is not easy to simulate as this type of damping does not damp all the components of frequency when several waves are superimposed. Also, the hysteretic damping is path dependent, which is again very difficult to simulate. To simulate the exact conditions to the field some additional damping is be required along with hysteretic damping. Rayleigh damping can be used over a short range at which it is independent of frequency. At a low cycle strain the hysteric damping gives no dissipation of energy, which is unrealistic. To avoid it a little Rayleigh damping is added in a dynamic system. Local damping cannot properly capture the energy loss of multiple frequency cyclic loading and thus it is unsuitable for seismic analysis.

3.2.1.4.1 Rayleigh damping

Rayleigh damping is used with elastic materials models. The coefficients are either computed from ppv observed from site or estimated in between 1 – 15 % [90]. The coefficient of damping should not be more than 0.5 % if a linear failure model is used. Also, Germant [91] found that the natural damping of rock and soil is independent of frequency. It has been reported that the frequency dependent damping sometimes misrepresents the results due to over-damping of low frequencies [92]. It was originally used for the analysis of structures and elastic continua for damping the natural oscillations. It is given by the following expression:

$$[C] = \alpha[M] + \beta[K] \tag{3-14}$$

α = mass proportional damping and β = stiffness proportional damping constants,

α is like a dashpot connecting zones to ground and β *is* like a dashpot connecting across zones. Rayleigh damping can become constant over a restricted range. Damping for geological material is in range 2 – 5% of the critical damping, for structures it is 2 – 10 %. For analysis with large strains only a small percentage of damping is required.

3.2.1.4.2 Hysteretic Damping

Hysteretic damping is independent of frequency of vibrations. It is generally used for earthquake simulations but it does not account for the nonlinear effects directly. In this method a couple of assumptions are made which are to incorporate some of the non-linear effects that are strain-dependent. Modulus and damping functions are taken as an average value. It can be used in combination with other forms of damping like Rayleigh damping for removal of high frequency noise and hysteretic damping for absorbing the dynamic load. The damping formulation is not a constitutive model and it should be used as a supplement to the other built-in models. It operates independent of all other forms of damping that are being applied.

$$\boldsymbol{\tau = M_s \gamma} \tag{3-15}$$

$$M_t = \frac{dt}{dr} = M_S + \gamma \frac{dM}{d\gamma} \tag{3-16}$$

Where

M_s and M_t are the secant and tangent modulus of the zones

γ is the shear strain τ is the shear stress

The calibration of tangent modulus function can be done by comparing the function results with target-shear modulus reduction curve, and also with targeted damping ratio curve. Some noise is found if the damping curves by numerical modeling are compared to the laboratory values. The noise does not affect the results but for cosmetic purpose a small amount of Rayleigh damping can be used to eliminate it.

3.2.1.5 *Blast-induced Load Transmission*

Modelling setup may distort and destabilize a model due to blast load propagation during a dynamic analysis. Blast wave speed characteristics of the model and frequency of input may affect numerical accuracy of load transmission. Lysmer [81] studied the wave propagation through the model, and they found that the element size (Δl) of the model must be less than one-tenth or one-eighth wavelength of the highest frequency of input wave.

$$\Delta l \leq \frac{\lambda}{10} \tag{3-17}$$

Where, λ is the wavelength with highest frequency component containing appreciable amount of energy.

3.3 REVIEW OF BLAST LOAD MODELING ON BACKFILL

Many researchers and practicing engineers have been studying the behavior of backfill under different loading conditions in underground environment [5, 8, 21, 22, 24, 32, 33, 93-96]. Simulation of blast loading requires a deep understanding of dynamic loading input parameters. A review of explosive blast loading is performed and presented in Section 3.3.1. A brief review of current modelling practices is presented in Section 3.3.2. A review of blast loading on backfill is presented in Section 3.3.3.

3.3.1 Numerical Modelling of an Explosive Blast

3.3.1.1 *Equivalent Cavity*

Sharpe [97] developed a technique to model spherical explosive charge and the stress distribution around the opening. He applied the transient cavity pressure on the walls of the sphere, of equivalent cavity to blast hole. It was ensured that the strength of material is greater than the shockwave of blast, so only elastic wave should propagate outside this cavity. It was found that the results were very similar to field measurements. A similar model has been included in FLAC^{3D} Dynamic Analysis manual [77] and examples and it is presented in Figure 3-5. ITASCA [78] has modeled one-eighth of the problem as presented in the Figure. Stress wave can be seen in the model.

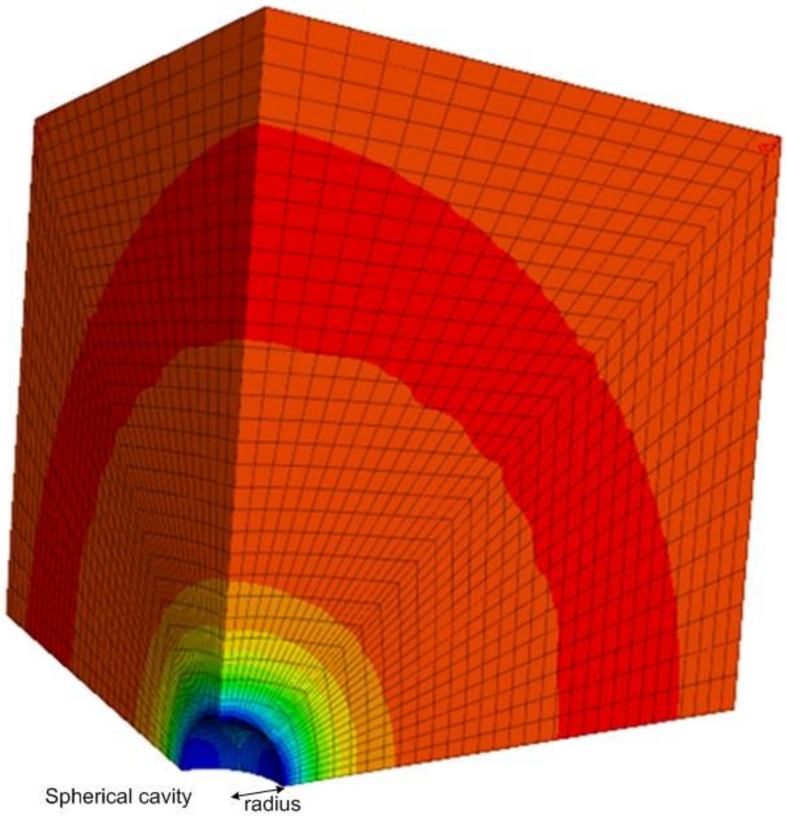

Figure 3-5 – Modelling blast loading on spherical cavity with FLAC^{3D} code [77]

The model was further modified by Kutter and Fairhurst [98]. They computed the optimum radius of the cavity to be modeled. It was found that for a spherical charge the blast damage spreads to six times the sphere diameter and for a cylindrical charge it spreads to nine times the diameter of cylindrical charge. The explosive charge was modeled by applying the pressure to the walls of the equivalent cavity. To model cracks-free process the cavity was sized properly, as the cracks are produced when dynamic compressive strength of material is less than the applied pressure. So, the pressure must be kept equal to dynamic compressive strength at walls of the cavity, and the blast load application area is at 4 times the radius of cavity for spherical and six times the diameter for cylinder charge.

3.3.1.2 Cylinder Charge

Spherical charge is a simplification of blasting process and it cannot be used for modelling blasting process, so a cylindrical charge for modelling has been considered by Starfield and

Pugliese, Harries and Blair and Jiang [99-101]. A cylindrical charge can be modeled by discretizing the charge into spherical segments each representing explosive charge. The blast load was modeled by applying a pressure with a sine wave function to the cavity, the stresses and strains can be determined numerically. The predicted values from this model were found to be in good agreement [99]. One quarter of the blast hole has been modelled by Wilcox [102] and is presented in Figure 3-6.

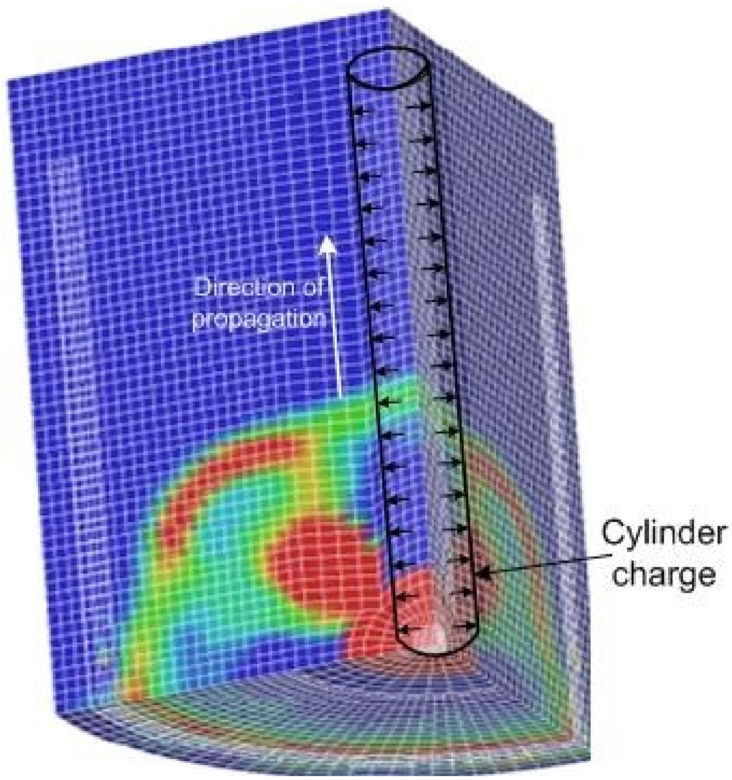

Figure 3-6 – Numerical modelling of a cylinder charge [102]

Harries [100] modeled a cylindrical charge by considering a string of spherical charge. He found that in order to model a dynamic load due to blasting correctly attenuation and dispersion must be taken into account. This can be achieved by using Kjartansson [103] model and taking a Q-value of 4.5, the results were found to be very good theoretically. Blair and Jiang [101] modeled a column of explosive by using the axis symmetry and concept of equivalent cavity, and showed that the stacked spheres do not represent an explosive column. They further studied the effect of charge length on blast induced vibrations and found that the peak particle velocity becomes constant at a critical length of explosive column.

3.3.1.3 Blast Load

Consideration of a blast load in a numerical model is a critical parameter. The method of blast loading depends on the purpose of the model. That is either to study the shattering effects or to study the effects of expansion of gases on rock mass and it is very difficult to model both the effects [104]. The present work is related to blast vibrations and stress loading, which can be accomplished by applying a time varying pressure on walls of equivalent cavity [83].

3.3.1.3.1 Stress loading on equivalent cavity

To consider stress loading on rock due to blasting, the exact value of pressure load to be applied must be known, which can be applied as a time varying load. The load must increase very quickly to maximum value and then decreases to zero for simulating blast loading [83]. If the load is unknown then in-situ blast monitoring may help determining the blast load. The advantages of this method include shorter solving time that is it is numerically efficient and it models the surroundings of a cracked region accurately. The disadvantage is that it cannot predict blast loading effects in deformed regions. Blair and Jiang, Jiang and Blair, Jian and Michinton, and Michinton and Lynch [101, 105-107] used the following function for stress loading. Figure 3-3 presents the profile of the following function, which can be termed as blast loading decay function.

$$p(t) = p_0 e^{-\phi t} \qquad (3\text{-}18)$$

Where:

$p\ (t)$ = pressure as a function of time

p_o = maximum pressure

t = time

ϕ = decay factor

Jiang and Blair [105] modeled elastic and visco-elastic material and used spherical charges with the above relationship. Blair and Jiang [101] used an explosive column to model surface vibrations using equivalent cavity concept of Sharpe [97]. It was found that peak particle velocity (ppv) increases with ϕ for n = 1, and ppv decreases with n for ϕ = 2000.

3.3.1.3.2 Stress Loading on Blast hole Walls

In this method stress history is applied directly on blast hole walls. This method can be used to accurately model the blast loading effects on rock mass including the cracked region around the blast hole. The method requires more memory due to complex cracking and small mesh size is required. This method is not generally used for large scale models.

3.3.1.3.3 Chemical Reaction in Blast hole

This is the third method of applying a blast load to a numerical model. Generally, JWL (Jones Wilkens Lee) equation of state [84] is used for modeling chemical reaction in blast hole. In this method the chemical reaction of explosive is modeled, and the stress wave and gas pressures, both are applied at the same time. It requires huge computations due to complexity and fine meshing around the blast hole and coupled process.

3.3.1.4 Modelling a Single Blast hole

Saharan [83] modeled a single blast hole to study the effects of destress blasting in hard rock using a 2D model. A 20 m by 20 m graded mesh was made with 38 mm blast hole in the center was modelled with roller boundaries. The boundaries were placed more than 250 times the area of interest, to ensure full absorption of blast vibrations in the model. The material model was brittle cracking which takes plasticity into account therefore no damping was initialized in the model. He also applied dynamic load on the walls of the blast hole in the form of triangular blast load profile, computed from the bore hole pressure equations. The dynamic load history was also derived from the same equations.

Saharan [83] also found that ANFO requires lesser stress to open the first crack than emulsion, also ANFO produced smaller crushing zone as compared to the emulsions. Extent of fracturing zone computed from the model was well in accordance with the empirical methods in use. It was also found that the energy utilization in fracturing is very little, which is also in accordance with the literature. A plot of ppv and distance from blast hole was prepared to predict fracturing zone, the prediction was found to be very accurate and in close agreement with existing literature. Figure 3-7 shows a 2D model of a single blast hole applied with static pressure of 2GPa, area under observation has been constructed with fine mesh.

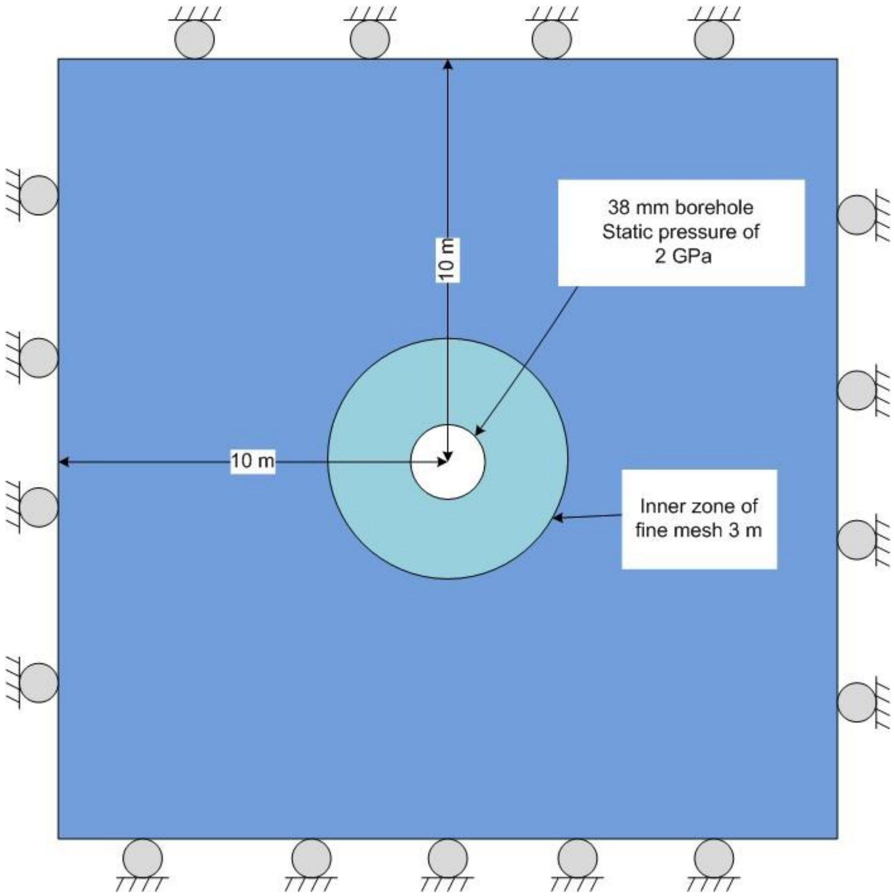

Figure 3-7 – Two dimensional model showing a single blast hole [83]

3.3.1.5 Blasting Multiple Charges

Generally, axis-symmetry is utilized to model a cylindrical column of explosive. The same approach can be used to model for multiple blast holes. Preece [108] used this approach to simulate detonation timings and its impact on fragmentation and dynamic fractures. The model was based on tensile failure and was unable to incorporate the compressive and shear failure mechanisms. The holes were bottom primed and controlled initiation base was used for detonation velocity. They modeled only two blast holes and the model took four days of computation, this approach was found to be inappropriate for multiple explosive columns.

3.3.2 Prevalent Practices for Rock Blasting Simulation

There are two approaches to simulate blasting process with numerical modeling that are continuum and dis-continuum approach. The first approach or the continuum approach does not takes into account the fractures, discontinuities, joints etc. while the dis-continuum approach accommodates them. The aim of continuum approach is to estimate the extent of weakening in the material around the source and local fracture growth is not characterized. Rock material is treated as perfectly elastic or damage in tension as an indication of fracturing in continuum approach. Smooth wall blasting and effects of weak planes was modelled by Piciacchia [109], which comprised of 2D finite element analysis. He used tensile stress to designate failure in their model. He applied blast hole pressure on faces of zones during a static analysis and dynamic analysis was not used. The selection of modelling plane has been done very carefully in this work but one of the shortcomings of this work includes the lack of fully dynamic analysis. Linear elastic are simplified analysis and are generally over-conservative as static analysis represent higher damage level [44]. Seppanen [110] and Schimizee [111] used the same static linear elastic 2D model with inherent fractures. Fracturing in the model was assessed by displacement magnitudes.

Lima [87] and Schimizee [111] used a 2D elastic continuum model for application of dynamic pressure and an implicit algorithm was used for application of load. Lima [87] used the concept of fracture energy for extending pre-existing fractures. Schimizee [111] employed principal stress contours to define extension of fractures. Blast source functions have also been applied as stress and velocity history in continuous elastic or continuous damage models. Some authors [51, 112] faced difficulties when trying to model exact blast loading functions with finite difference (FLAC) and distict element codes. The difficulties included unrealistic results and numerical instability. The difficulties can be coped with using the Gaussian function or blast load profile for applying blast loading. The Gaussian function does not match pressure pulse of blast load exactly and it is an approximation of blast load profile. Taylor [113] reported that scalar damage variable is associated by poisson's ratio of the material in continuum damage models. Many researchers claim that volumetric strain [76, 104, 114, 115], Young's modulus [116-118] and global energy [118] may also be used to report scalar damage in continuum damage models. Repetto [119] reported some sweeping assumptions in geometry and distribution of fractures to be made in homogenizing a cracked solid. There are few objections to continuum modelling approach which includes determination of properties of cracked solid under dynamic loading [120], propagation of blast load between fractures and the failure of brittle material is governed by growth of cracks [119].

Discontinuum approach for simulating blast loading has also been adopted using distinct element codes [51, 74, 121, 122], boundary element codes [123] and finite element codes [86, 124]. Mortazavi [122] provided zero value for cohesion and tension for rock material in their discontinuous deformation analysis code. The problem was 3D and was misrepresented as a 2D problem. Discrete element method also limited the model from producing practical results. The results were unrealistic and Hazzard [29] reported that the cause of unrealistic results is unrealistic assumptions and input data. Ryu [112] also claimed that the stiffness, material damping, boundary conditions and algorithm to solve such problems are amongst the influencing factors. Napier [28] reported poor accuracy with spherical elements in distinct element code used by Donze and Magnier [51, 74]. A 500 MPa pressure history was applied on a 93 mm diameter drill hole using linear elastic boundary element technique [123]. Results of the model presented post-blast fractures. Napier [28] constructed a model with preplaced fractures, this describes an approach but it has no practical significance. The model suffered from limitations of linear elastic model, but the model presented contains bedding planes with zero cohesion [123]. Cho [124] used finite element continuum model to simulate discrete fracture networks. They applied reduced stress history in the model as blast load to avoid numerical instability. The results were affected by boundary value problems, as reflection of pressure pulse from material boundaries did not show any scabbing failures, as observed in the field. They incorporated stress variation with the help of a statistical function in their model. Jung [86] presented a similar model which has a close resemblance with field investigation data. They modelled a high peak pressure of around 1 GPa on 8 mm hole walls, and the load profile was similar to the one observed on the field. The incorporated dynamic compressive and tensile strengths for fracture generation in the model, which were equal to 4.5 times the static strengths. The stability of the numerical model was not discussed in the paper.

3.3.3 Dynamic Modelling of Backfill Material

According to Mitchell [52] cementation increases the brittleness of backfill, making it more prone to cracking under blast loadings and to rupture under local rock deformation. Thus, forces, displacements and energy dissipation should be considered in backfill design. However, it was found from the reported literature that backfill is generally designed while considering only gravity loading or self-weight of backfill, using simple wedge model originally provided by

Mitchell [53]. O'Hearn and Swan [26] used UDEC to model a cemented hydraulic fill sill mat, which is a thin bedded plug below weak backfill and used to support the overlying fill when mining underneath. It was anticipated that the dynamic loading was responsible for failure. They applied sinusoidal pressure pulse with duration of 10 ms and a frequency 100 Hz. It was found that dynamic loading was responsible for failure, only when the ppv was in the range between 200 and 300 mm/s in the fill. The blast was modeled 20 m away from fill. Lilley [125] studied the effects of blasting on cemented hydraulic fill. He developed a mathematical model for dynamic loading of cemented hydraulic fill, but the likelihood of failure was very low. Lilley [25] used cylindrical source, and predicted a plastic deformation with blast loading at a ppv of 1500 mm/s, for a source located 5 m away from cemented hydraulic fill and ore interface. Lilley [25] studied damage due to production blasting adjacent to cemented hydraulic fill (CHF) stopes. They developed a vibration amplitude transfer function to model the transmission of blast vibrations from the source, through ore, across the ore to CHF interface and into the CHF mass. A simple application of the amplitude transfer model indicates that a zone of plastically deformed CHF would be produced, and would extend to a distance of approximately 0.5 meters from the interface into the CHF. The sensitivity analysis indicated that the amplitude of vibrations in CHF was influenced by the initial blast vibration amplitude, the interface amplitude transmission efficiency, the propagation distance in CHF and the rock quality factor of CHF. Given appropriate conditions, the zone of plastic deformation could extend considerably further than 0.5 meters. Pierce [126] used $FLAC^{2D}$ and $FLAC^{3D}$ codes to simulate exposed fill and impact loading on backfill by blasting. Fish is a programming language in FLAC3D which allows a user to set new variables and functions within FLAC and FLAC3D. Fish functions were used for modeling CRF, and model was compared with laboratory testing results. The two dimensional model was applied with a velocity pulse at the center of the pillar. Many parameters were assumed to simplify the model. The model was good enough for initial assessment only. McNearny and Li and Li et al [30, 127] modelled backfilled stopes in sublevel stoping method with delayed backfill. They assessed the backfilled stopes for a lesser curing time that is 3 days and 7 days. FLAC2D, FLAC/SLOPE, PFC2D and PFC3D were used to study the behaviour of backfill. Tension in rockmass and backfill was used as failure criteria. They applied the gravity loading and blast-induced loading for this analysis. They found that the backfill was stable for both the loading conditions studied when backfill was cured for 7 days. Backfill model was again analyzed for 3 day curing time, and it was found that backfill was unstable under dynamic loading. The mine used a relationship for estimating blast-induced vibrations in backfill. The relationship came from the experience at Carr Fork Mine [16] which is not very reliable. Stress plot of backfilled stope from FLAC is presented in Figure 3-8. Results of shear stress in FLAC/SLOPE are presented in Figure 3-9.

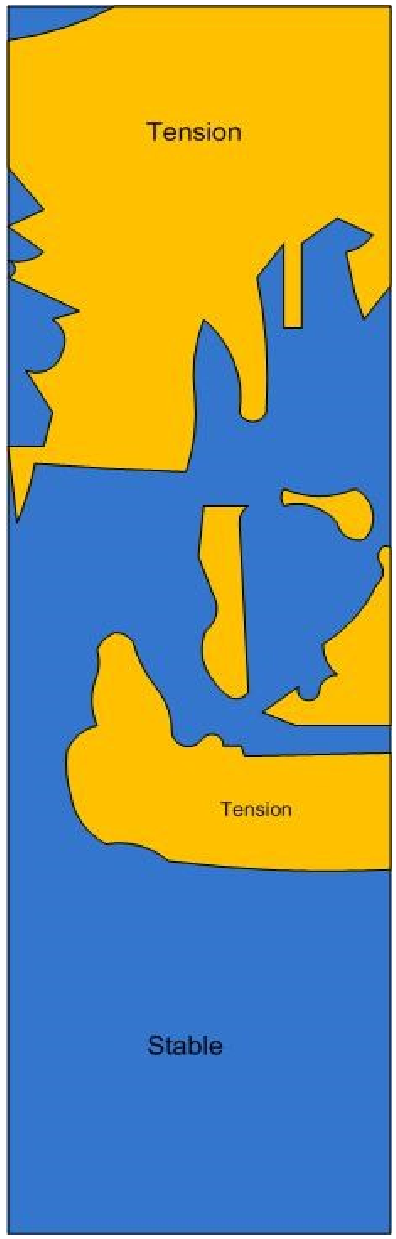

Figure 3-8 – FLAC2D stress plot of backfill [30]

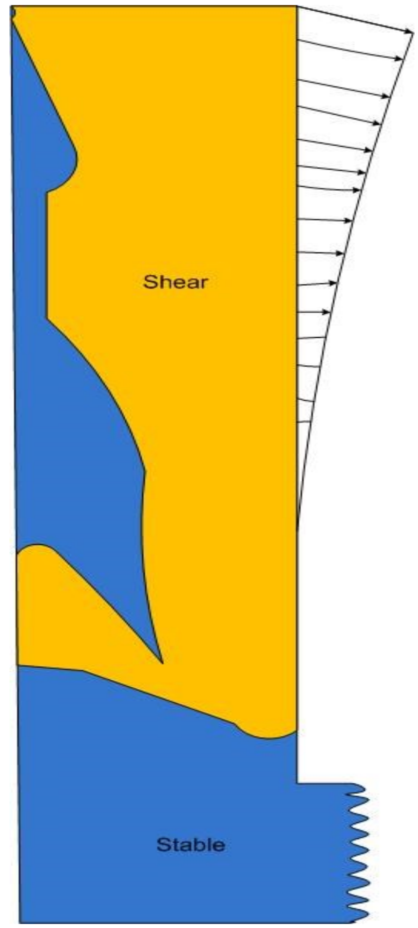

Figure 3-9 – Shear stress FLAC/SLOPE results of backfill [127]

Villaescusa et al. [128] presented the results of a comprehensive monitoring program designed to investigate the extent of blast induced damage experienced by rock masses extracted by bench stoping method. Peak particle velocity, hanging wall deformation measurements and stope surveys were used to develop a site specific damage model that allowed engineers to assess drilling and blasting configurations to minimize the extent of pre-conditioning and damage. The study also included the analysis of the frequency response, displacements and accelerations experienced by the excavation as extraction and mine filling progressed. This work aimed at understanding of the influence of blasting on the dynamic behavior of stope hanging walls. They found that dynamic loading imparted on an exposed hanging wall from subsequent stope blasting was also expected to contribute to rock mass weakening. They also found that mine filling was crucial to arrest further deterioration to hanging wall and footwall. From their findings they concluded that the frequency experienced by an exposed wall was much higher than that experienced by a closed wall for the same blasting event. They were also of the opinion that an increase in dominant frequency could be expected as the strike length of the stope is extended. They demonstrated that larger openings were more susceptible to dynamic loading.

The most recent work conducted by Gool [20] in PhD work titled “the effects of blast loading on paste fill” were studied. The work consisted of experimental and numerical modeling and field work at Cannington mine in Australia. ABAQUS/Explicit numerical modeling package based on finite element method was used to model the behavior of paste fill due to adjacent blasting in an underground mine. The model was run for a variety of loading conditions for static and dynamic loading due to blasting conditions to observe the changes in paste fill behavior due to different blasting conditions. Model results showed that the peak particle velocity and therefore the damage to the paste fill reduced for increased cement contents of fill. The model results also indicated that the order of detonation and the delay time between the detonations of blast holes has little effect on the damage to the paste fill. It was also observed both from the field data and numerical model that once a wave enters a paste fill stope, it stays within that stope and attenuates within the paste fill. In order to reduce the damage to paste fill, smaller diameter boreholes should be used for blast designs located within 5 m of paste fill and greater delays are necessary to reduce damage to the nearby paste fill during blasting. The wave attenuated faster in the paste fill once it had fully cured and reached its full strength. Therefore, in order to reduce the damage observed in paste fill during blasting, the paste fill should be allowed to fully cure before it is exposed to nearby blasting. Based on observations from the field monitoring, the field tests and work by others, the ppv at which damage to paste fill begins to occur was estimated to be in the vicinity of 250 to 350 mm/s. She studied the paste fill properties and monitored the blast vibrations in backfill for calibration of model. The mine drove a drift through paste fill for installation of geophones and they measured the blast induced vibrations by placing series of geophones inside the paste fill and in rock to model the paste fill and rock interface. The mine blasted several rounds in paste fill and recorded vibration data for model calibration. After calibration of model following results were presented,

1. PPV in the paste fill decreases with increase in strength of fill or the cement contents.
2. Most of the blast-induced vibrations reflect back at the interface between rock and paste fill, and some of the vibrations get penetrated in fill.

3. Blast-induced vibrations penetrating inside the fill travel with a much slower velocity than the reflected ones.
4. Damage to paste fill decreases with increase in perpendicular distance of paste fill from blast source
5. Greater diameter blast-holes produce greater peak particle velocity (ppv) and thus greater damage to fill.
6. The location of blast hole has almost no influence on ppv inside paste fill
7. The blast induced waves are constantly reflected inside a paste fill column until they die out.
8. Multiple charges have a greater impact on paste fill, even if detonated with delay
9. Fan pattern produces more ppv and more damage than parallel hole pattern
10. Delay time has almost no influence on damage in paste fill column

Max principal stress contours while blasting right next to paste fill are presented in Figure 3-10 and Figure 3-11. It can be seen that the stress pulse starts to propagate in backfill after a lag of 90 milliseconds.

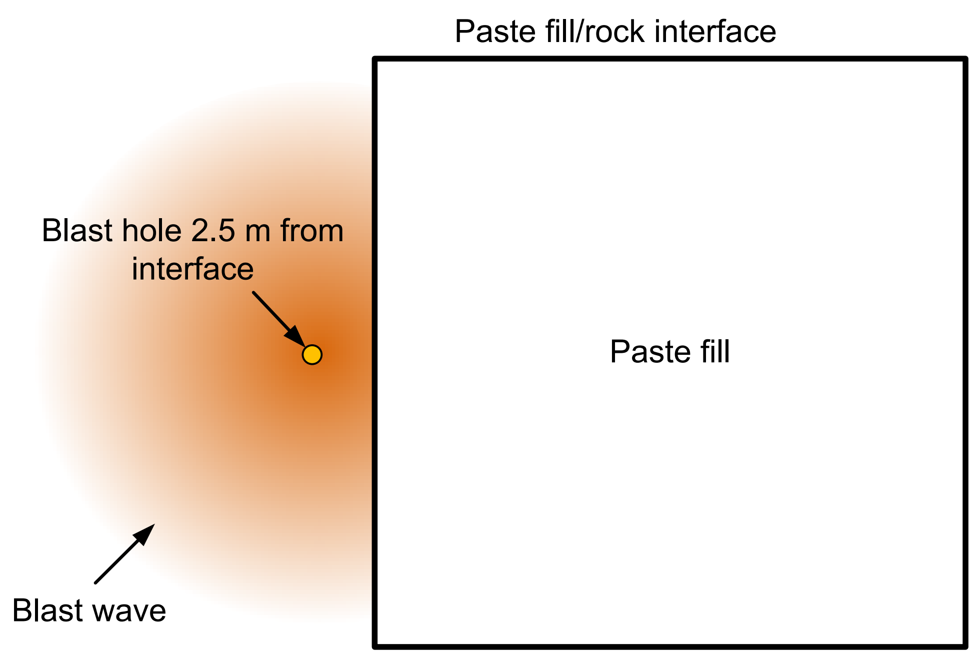

Figure 3-10 – Blast wave propagation after 5 milliseconds [20]

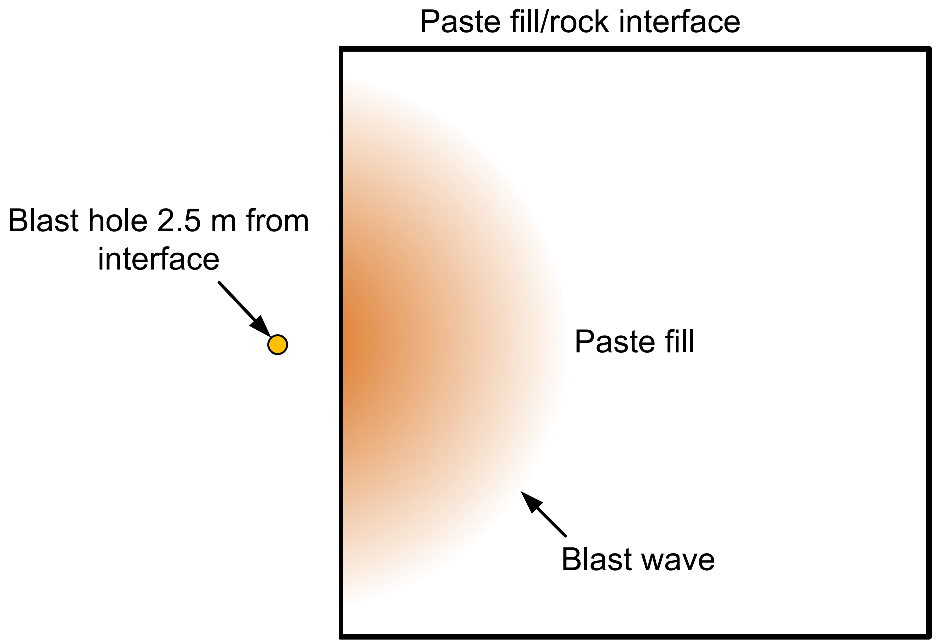

Figure 3-11 – Blast wave propagation after 90 milliseconds [20]

3.4 LIMITATIONS OF THE CURRENT BACKFILL DESIGN

The above review of literature shows that the current backfill design methods (FSR methods) are inadequate. This is due to the fact that FSR methods do not consider complex scenarios especially blast-induced vibrations. A higher safety factor using FSR methods does not necessarily guarantee a stable CRF face under blast vibrations. Cavity monitoring survey profiles show failure of such stopes as well. Thus, there is a need to develop a design methodology to consider the effect of blast-induced vibrations on backfill.

3.5 DYNAMIC MODELING OF CEMENTED ROCKFILL

The review of backfill material and numerical modelling encourage simulation of blast load on backfill. To study the stability of cemented rockfill, a dynamic numerical model is developed with FLAC3D code to simulate static and dynamic load while following primary-secondary mining and backfilling sequence. Initially two models were constructed for two different case study mines and effect of different parameters like stope dimensions, material properties, segregation in fill, mining method, dynamic loading and blast vibration magnitude were studied. Two stopes were created with very fine mesh for both the case studies for simulating primary secondary sequence. An interface was created around the stopes to simulate rock/fill interface scenario by constructing a very thin zone with no tensile strength and no cohesion. Model boundaries were fixed and in-situ stress tensor values were initialized in the model. The material properties applied for the rockmass and in-situ stress tensor values used for each case study are presented in the following section. Gravity was also applied in addition to the stress load. Material properties used for the CRF are extracted from Hassani and Archibald [4] presented in Table 3-1 [4]. The models were run through mesh sensitivity analysis, and it was found that around 150,000 elements are enough to produce consistent results in terms of displacements and stresses.

Table 3-1 – Cemented rockfill properties used in numerical models [4]

Property	CRF	Weak CRF	Interface Zones
Rock mass Deformation Modulus(GPa)	2.50	1.25	0.25
Poisson's Ratio	0.35	0.40	0.45
Tensile Strength (MPa)	0.03	0.015	0.00
Cohesion (MPa)	1.10	0.55	0.00
Angle of Internal Friction (^{o})	37	37	20
Dilation Angle (^{o})	9.20	0	0
Density (kg/m^3)	1800	1200	200

3.5.1 BLAST LOADING

Blast loading in the model is a critical parameter, many authors [83, 112, 129] have used both stress and velocity history profiles for applying blast loading on the free faces of models. All the models studied throughout this chapter have been applied with stress history on the face of exposed backfill. The stress or velocity history in any model is applied by choosing the decay function profile for blast loading. The blast pulse applied in the model is presented in Figure 3-3. The maximum blast load applied in both models is 45 MPa calculated from the field and laboratory experimentation of peak particle velocity (PPV) monitoring in backfill conducted by Gool [20]. Maximum material damping value of 15% was used for some of the models and model boundaries were transformed into viscous boundaries to eliminate blast wave reflection. Reflection of blast load from model boundaries leads to tensile failure in the model.

3.5.2 FAILURE CONDITION

Several failure conditions have been considered by researchers to represent failure in dynamic models due to blast-induced vibrations. Quite a few authors have used yielding as the failure criteria to define failure. Lateral displacement in backfill has also been used to define backfill failure, but such models lack validation from underground case study mines. Backfill material has been reported to fail with development of relaxation zones or transformation of compressive stress into tensile stress in backfill. This is due to the fact that CRF is very weak in tension. Practically it has very low tensile strength as the in-situ strength of CRF varies a lot from the laboratory determined values due to segregation, improper mixing and placement [4, 5]. Throughout this work vertical stresses in backfill have been used to define failure in backfill. Reportedly, backfill fails when there is tensile stress development, as backfill is weak in tension and tensile stress development in backfill is considered as failure condition.

3.5.3 Mine – A

The case study mine-A is located in Manitoba. The massive ore bodies are being mined out with the vertical block mining (VBM) method with delayed backfill which is a variation of sublevel stoping mining. Stopes are being mined out transversely in panels. Each panel is composed of three stopes with a common draw point for ore. The whole ore body is divided into primary and secondary stopes with sublevels at approximately every 30 meters, while following pyramidal mining sequence. Stopes are generally drilled and blasted with the help of an access drift right above the stope. A lower sill drift beneath the stope is used for mucking out the blasted ore. CRF is also placed from a top access drift by using a load haul dump machine (LHD). Ore adjacent to CRF is blasted at least after 28 days or after CRF is cured. The vertical block mining blasting sequence is also employed for extraction of secondary stopes as presented in Figure 1-6. CMS is employed for monitoring the stope profiles and to compute stope over-break in ore, rock and CRF. To analyse a secondary stope for blast induced vibration damage, one of the failed CRF stope has been used. The stope is located below a depth of 1050 meters. The two stopes presented were modelled with FLAC^{3D} for this work. The material properties for ore, footwall and hanging-wall are presented in Table 3-2, and in-situ stress tensor values at a depth of 1050 meters are presented in Table 3-3. The cavity monitoring surveying system (CMS) profile of a failed stope from the case study mine has been used for model calibration.

Table 3-2 – Rockmass properties for case study mine A

Property	Ore	Footwall	Hanging-wall
Rock Mass Deformation Modulus (GPa)	28.1	32	32.5
Poisson's Ratio	0.3	0.29	0.3
Tensile Strength (MPa)	0.4	0.6	0.4
Cohesion (MPa)	4.0	4.9	4.3
Angle of internal friction (^{o})	30.7	29	32
Dilation angle (^{o})	9.78	13.6	7.3

Table 3-3 – In-situ stress tensor values for case study mine A at level 2750

Stress Tensor	Magnitude (MPa)	Orientation
σ_1	31.80	Normal to ore body strike
σ_2	26.70	Parallel to ore body strike
σ_v	15.00	Vertical

3.5.4 Mine – B

The case study mine-B is an underground Canadian gold mine located in northern Quebec. A steeply dipping tabular ore body was mined by open stoping mining method with delayed backfill. The entire ore body was divided into primary and secondary stopes with sublevels at every 30 meters. To mine a primary stope a 1.2 meter slot is created and later enlarged using parallel hole blasting, fan drilling pattern was used for secondary stopes. After blasting, the ore was mucked from drifts, normal to the ore body strike. CRF was placed from top drift or from a backfill raise right after mucking of the ore. The cavity monitoring surveying system (CMS) was employed for monitoring the stope profiles and to compute stope over break in ore, rock and CRF. To analyze a secondary stope for blast induced vibrations, an isolated area of case study was chosen at depth of 1084 meters. Table 3-4 shows the material properties for ore, footwall and hanging-wall and Table 3-5 presents in-situ stress tensor values for mine B at a depth of 1084 meters.

Table 3-4 – Rockmass properties for the case study mine B [10]

Property	Ore	Footwall	Hanging-wall
Rock mass deformation modulus (GPa)	95.2	25.8	12.6
Poisson's Ratio	0.1	0.15	0.21
Tensile Strength (MPa)	0.7	0.25	0.17
Cohesion (MPa)	6.8	5	4.5
Angle of internal friction (^{o})	39	37	35
Dilation angle (^{o})	12	9.8	9.5

Table 3-5 –In-situ stress tensor values for the case study mine B [130]

Stress Tensor	Magnitude	Orientation
σ_1	$2.24*\sigma_v$	Normal to ore body strike
σ_2	$1.50*\sigma_v$	Parallel to ore body strike
σ_v	$0.027*$depth	Vertical

3.6 INITIAL DYNAMIC MODELLING RESULTS

The initial dynamic model is developed to model CRF material and study the effect of different parameters including stope dimensions, material properties, loading conditions, variation in blast vibration magnitude, segregation due to poor mixing and the vertical block mining method. The initial model considered several factors based on literature review of numerical modelling study on backfill material. The results of the factors considered are presented in the following sections.

3.6.1 Modelling the Effects of Dynamic Loading on CRF Stopes

This work was presented by Emad and Mitri [131] in the 3rd ISRM symposium on Rock Mechanics (SINOROCK2013). Three approaches were used to study backfill under static stress due to gravity, dynamic loading on fill due to loss of confinement and dynamic loading due to blast loading on fill. Mine A was used as a case study for this work. After constructing the model geometry stresses and boundary conditions were applied, gravity loading conditions and density was initialized and finally material properties were assigned to different geological units, the model is solved for equilibrium. On reaching equilibrium the mining sequence was followed by mining out primary stope solving the model and then backfilling it. Backfill was assigned with cemented rockfill values presented in Table 3-1. Tensile stress in backfill was considered as a failure condition for this analysis, which was verified by the failure profiles and yielding contours in CRF stope, while considering a value of less than 1 as failure. Yielding contours in this analysis are based on the definition of safety factor that is the ratio between strength and stress. Displacement was also computed but the results of lateral displacements were not found to be in-accordance with the field observations and CRF failure profiles. The secondary stope was then mined under static or gravity loading conditions and results are presented in Figures 3-12 to 3-14. Mined out secondary stope is presented as transparent block in this paper. Figure 3-12 presents vertical stress in CRF stope, it can be seen that the vertical stress contours are almost horizontal with no tensile stress in backfill. Figure 3-13 presents yielding in backfilled stope during static analysis. It shows that yielding is present at the lower most part of the exposed face, which is converse to the failure of CRF shown in CMS profile. Figure 3-14 presents lateral displacements in CRF stopes, which again indicates slight movement of CRF at the toe of the exposed face. This has not been observed in CRF stopes on site and thus the results of displacements are considered inappropriate for quantifying backfill failure. The results of strength to stress ratio in FLAC3D is termed as yielding for this analysis and a yielding value of less than 1 is considered as failure.

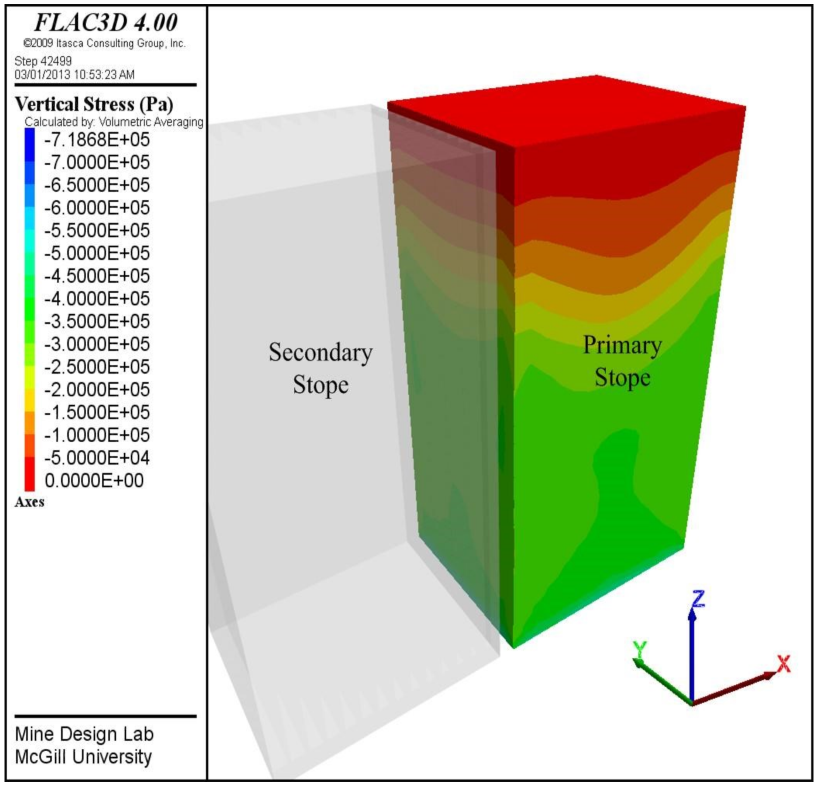

Figure 3-12 – Vertical stress contour for CRF stope - static analysis

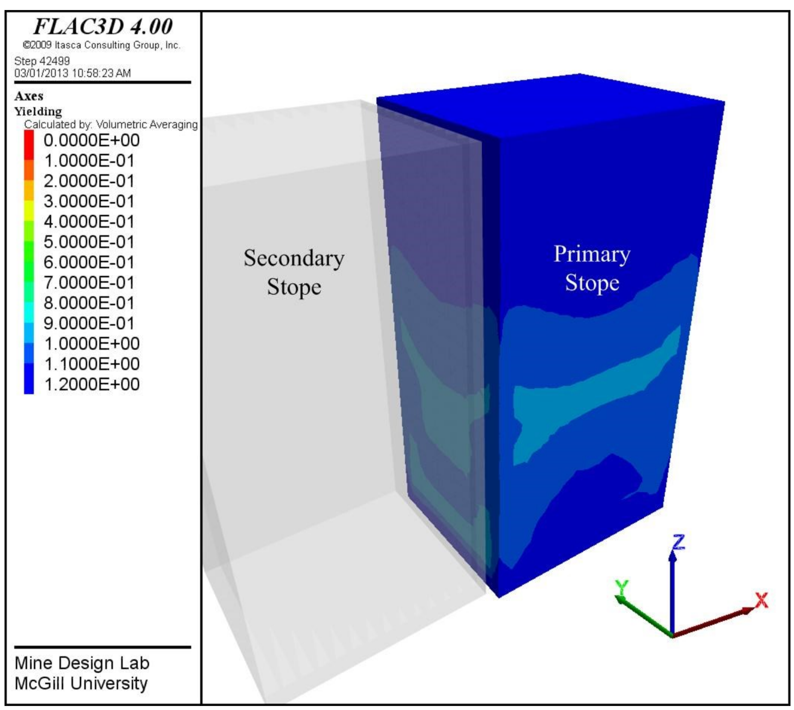

Figure 3-13 – Yielding contour for CRF stope - static analysis

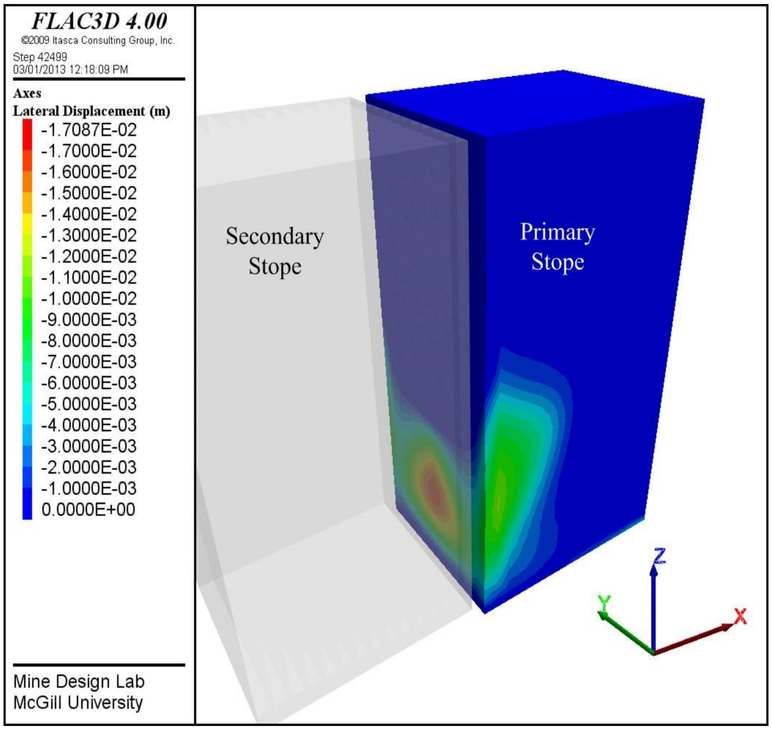

Figure 3-14 – Lateral displacement contour for CRF stope - static analysis

To simulate and analyze the dynamic unloading or sudden loss of confinement by CRF stope, the adjacent secondary stope was mined out while enabling dynamic analysis mode in FLAC^{3D}. The model was solved and results of this analysis have been presented in Figures 3-15 to 3-17. The vertical stress contours are presented in Figure 3-15, and it can be observed that there is no tensile stress development which is an indication of failure in CRF due to dynamic unloading or sudden loss of confinement. Yielding contours presented in Figure 3-16 also show no yielding in CRF stope. The lateral displacement contours have been presented in Figure 3-17, and it can be seen that the results of vertical stresses and yield in CRF show no deterioration of the block however, the results of lateral displacement show that almost the entire stope has moved significantly towards the mined out secondary stope, with maximum movement at the bottom of the stope.

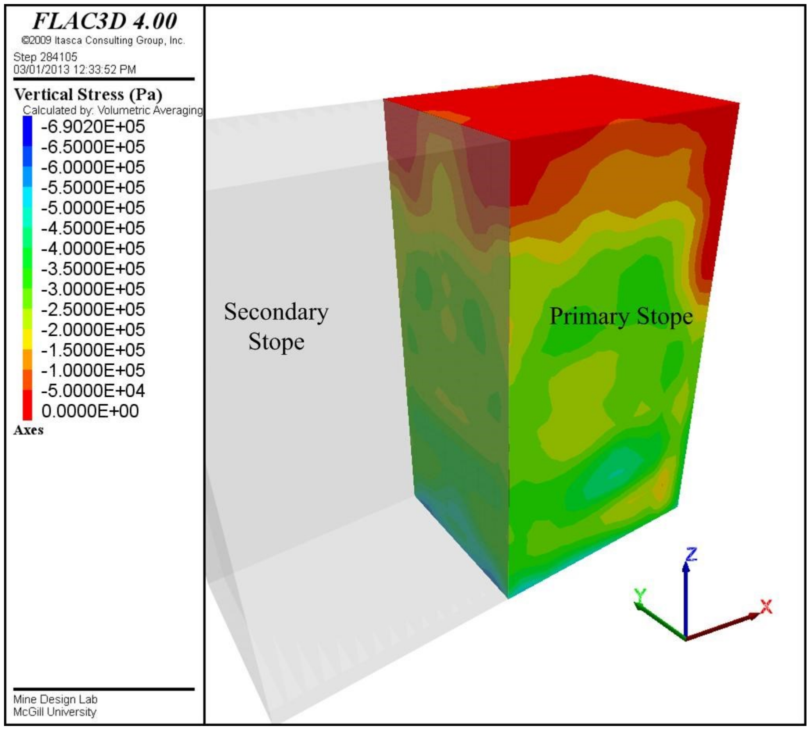

Figure 3-15 – Vertical stress contours for CRF stope - dynamic analysis for loss of confinement

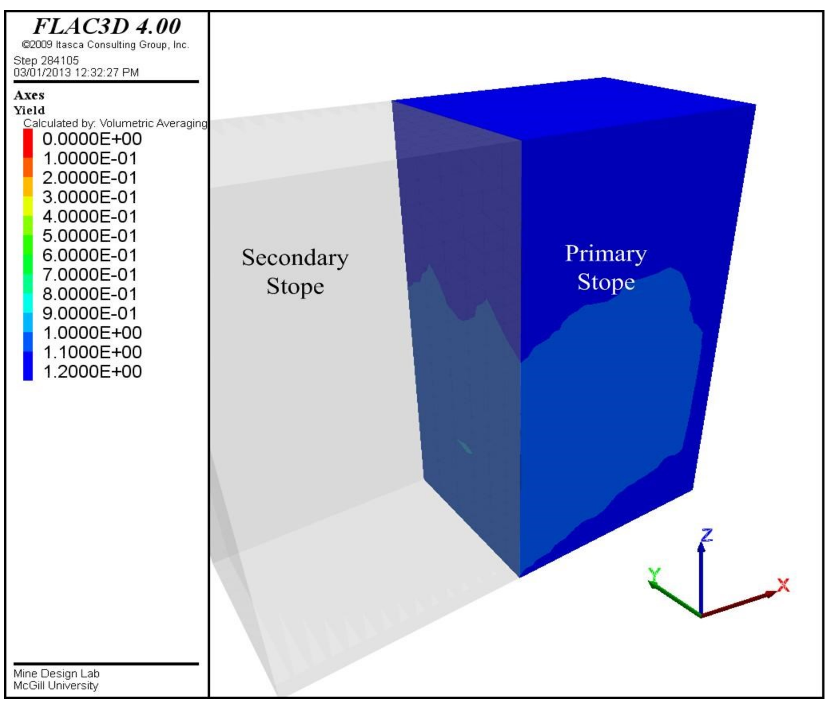

Figure 3-16 – Yielding contours for CRF stope - dynamic analysis for loss of confinement

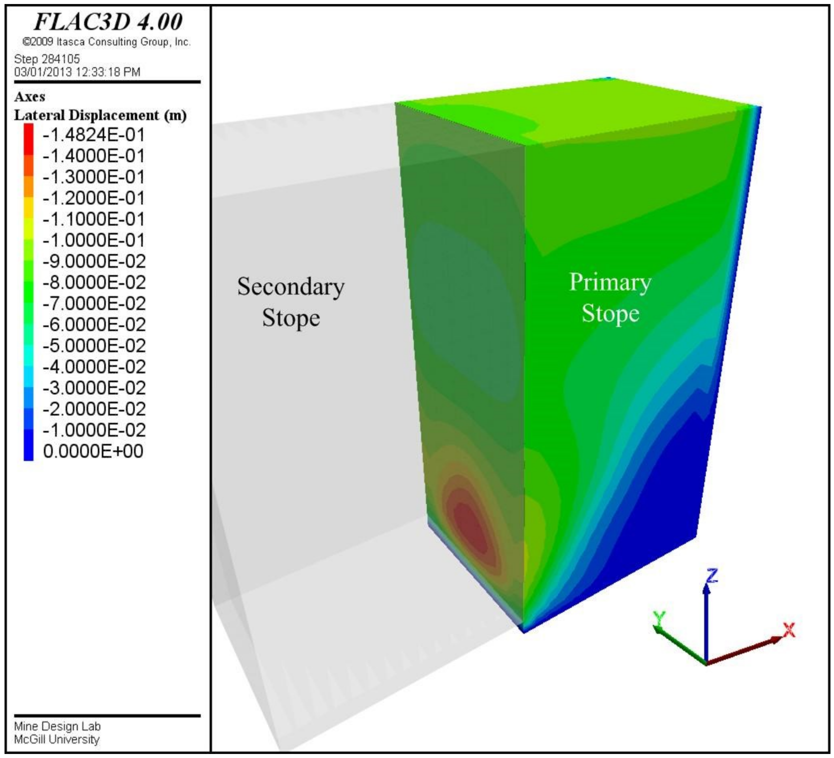

Figure 3-17 – Lateral displacement contours for CRF stope – dynamic analysis for the case of loss of confinement

For the blast loading scenario CRF stope has been applied with dynamic impulse load due to production blasting in adjacent stope. To simulate the effects of blasting a dynamic pressure pulse history load from the work of Gool [20] was applied on the face of backfill and the model was then solved for equilibrium. The results of simulation are presented in Figures 3-18 to 3-20. Vertical stress contours are presented in Figure 3-18, and it can be seen that the CRF stope have tensile stress development on top of the exposed CRF stope face. The results are in accordance with the CMS profile of the CRF stope and Yielding contours presented in Figure 3-19. The yielding contours and vertical stress contours show CRF failure in similar zone. Figure 3-20 presents the displacement contours after applying the blast load on CRF. It can be seen that the displacement contours show movement of exposed CRF towards the mined out secondary stope. When compared the displacement contours are indicating CRF failure at the center and lower portion of the exposed face. This is again converse to the failure indicated by CMS profiles and field observations.

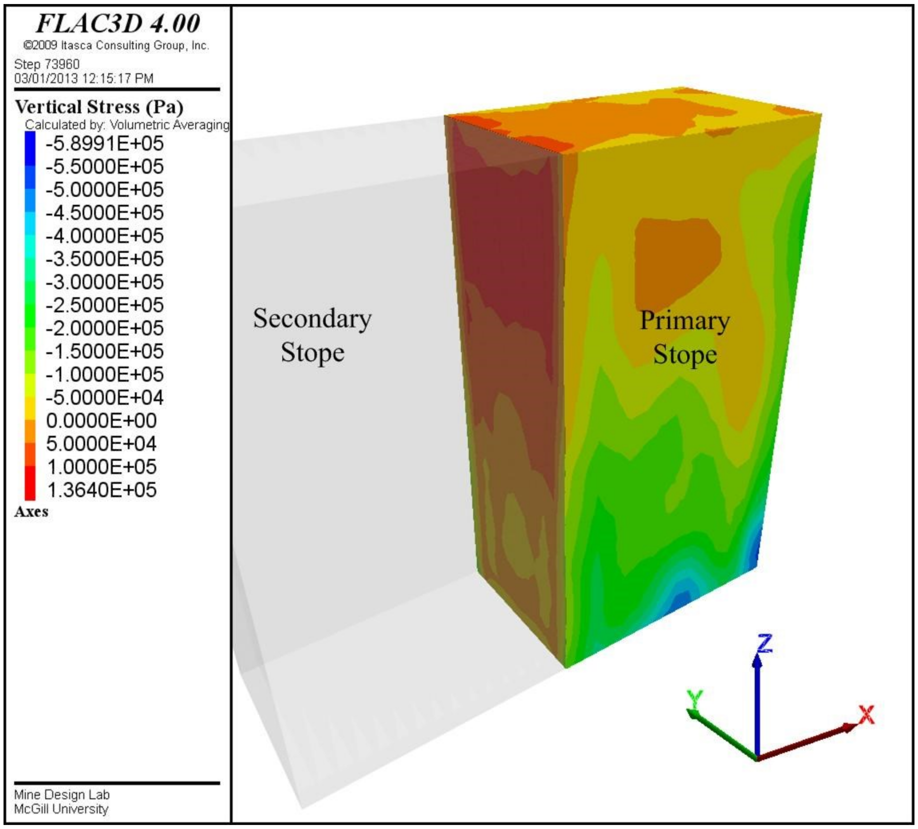

Figure 3-18 – Vertical stress contours for CRF stope - dynamic analysis for blast loading

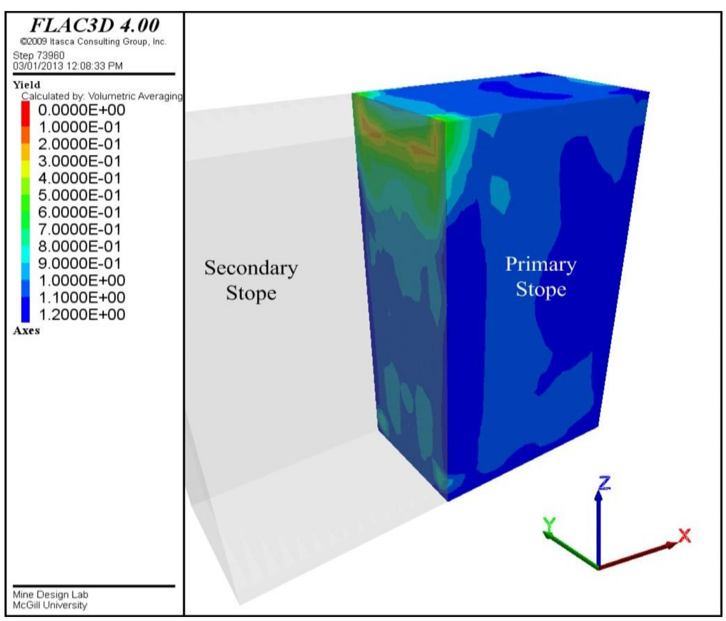

Figure 3-19 – Yielding contours for CRF stope - dynamic analysis for blast loading

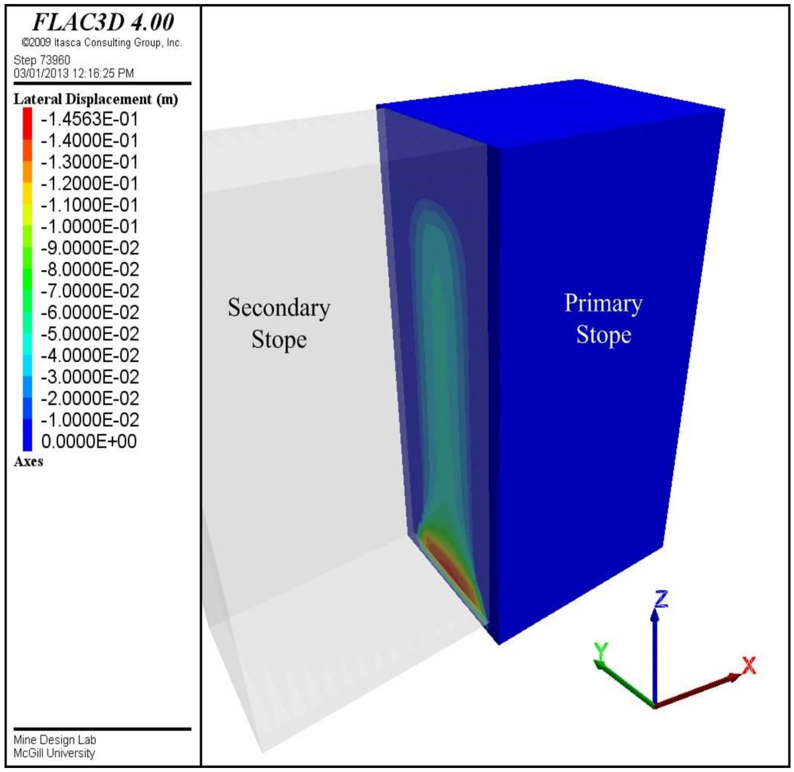

Figure 3-20– Lateral displacement contour for CRF stope - dynamic analysis for blasting loading

The results of vertical stress contours for the three analyses are compared in Figure 3-21, tensile stress region represent failure zones. Vertical stresses were plotted against stope depth along the centerline of stope. It can be seen that static analysis and dynamic analysis results did not show any failures, as these two lines remain in low compression region or stable region in the chart. The results of dynamic loading, due to blast-induced vibrations show failure from a depth of 0 m to 7 m in CRF stope at the exposed face. It can be noticed that the maximum compressive stress in backfill remains under 0.5 MPa for gravity and blast loading, and it increases to 0.7 MPa for the case of sudden loss of confinement by CRF. In all the three cases the compressive stress in backfill does not exceed more than 1 MPa, which is the minimal designed strength.

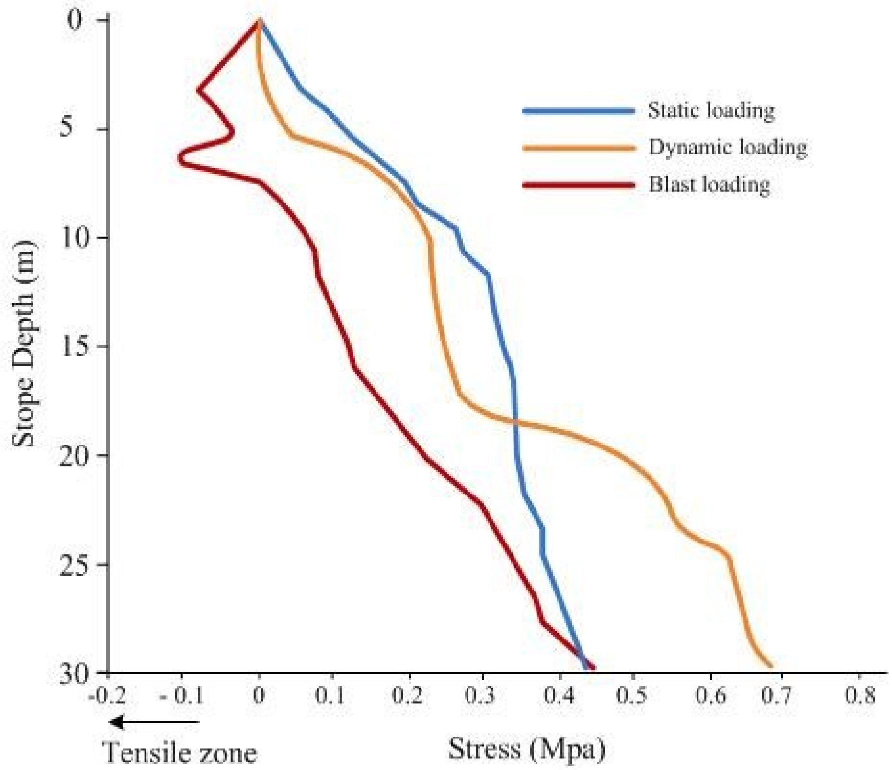

Figure 3-21 – A comparison between vertical stresses for the three analyses

3.6.2 Effect of Stope Dimensions, Engineering Properties and Blast Vibration Magnitude

This work has been published by Emad et al. [6, 132]. These papers discuss factors which are believed to be affecting backfill stability. Dynamic load has also been applied when CRF is exposed for maximum recovery. Mine B has been used as a case study. Parameters like stope length, width, height, cohesion and rockmass deformation modulus have been studied in this research work. The model was analyzed for static loading initially. Afterwards the same model was used for applying blast-induced vibrations on CRF. Blast load has also been varied in magnitude. The results for the vertical stresses, lateral displacements and yielding in backfill are presented in Figure 3-22, 3-23 and 3-24 for static and dynamic analysis. Stope on the right is the primary stope or the backfilled stope, and on the left is secondary stope, which has been excavated. The vertical stresses shown in Figure 3-22 have a maximum value at the bottom of the backfill which is less than 0.7 MPa for static analysis. The dynamic analysis presents a similar scenario except the development of tensile stress on top of the exposed face. The tensile stress in backfill has been used to present failure in CRF. The contour shows that the failure in

CRF is in the wedge shape, which has been advocated by many authors [18, 43, 96]. Lateral displacement contours in backfill have been presented in Figure 3-23 for both static and dynamic analysis. It can be seen that static analysis show that the exposed face of CRF is quite stable. The dynamic analysis results shows that the free face of backfill is moving towards the mined stope. Figure 3-24 shows the yielded state of backfilled stope after static analysis and dynamic analysis. The backfill failure is quantified by the yielding in backfill. A value less than 1 is considered as yielded and value greater than or equal to 1 is stable. Yielding here is based on safety factor which is ratio of strength to stress in CRF. It can be seen that the static analysis presented yielding inside the CRF near the bottom. However the dynamic analysis results of yielding showed failure at the top of the stope. The yield contours in CRF are verifying the dynamic loading vertical stress results. The effects of stope dimensions on CRF column are presented in Figures 3-25. From the Figure, it is evident that the yielded backfill volume increases linearly with increase in the length and width of primary stope. The height of backfilled stope has a little effect on yielding in backfill, within the range 29 to 31 meters and after 31 meters yield increases with stope height. The effects of stiffness and cohesion on backfill are presented in Figure 3-26. Cohesion has inverse impact on yielded elements. The stiffness of backfill have some impact on backfill failure but has a direct relationship with yielding.

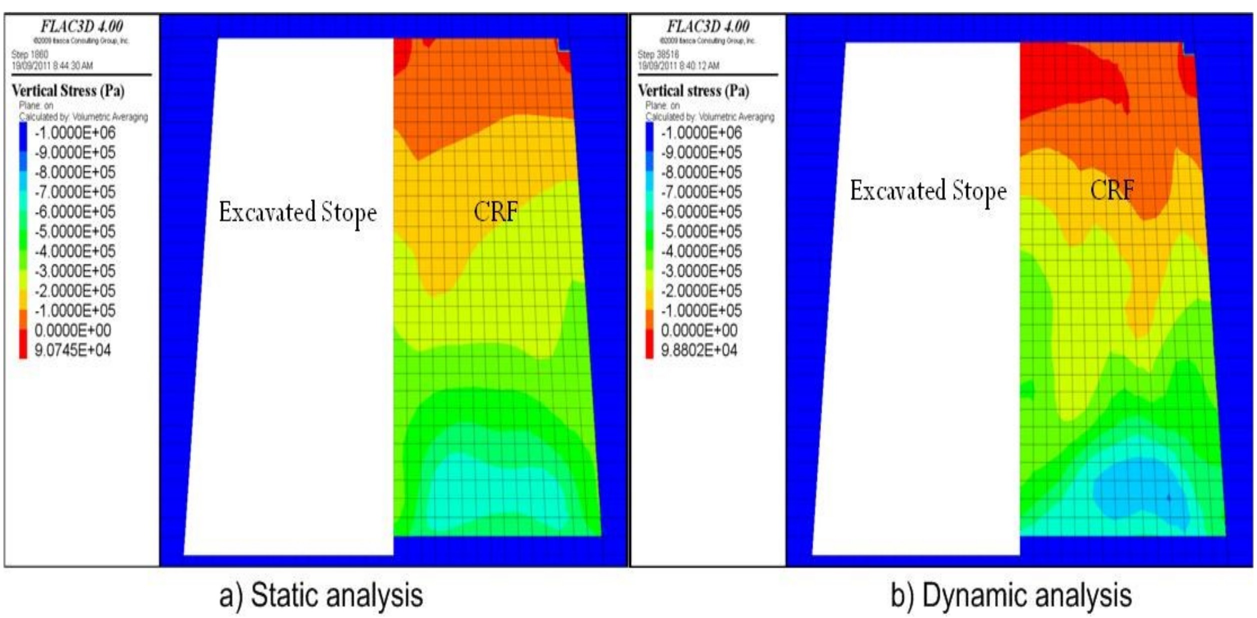

Figure 3-22 – Vertical stress contours for the backfilled stope after extraction of secondary stope

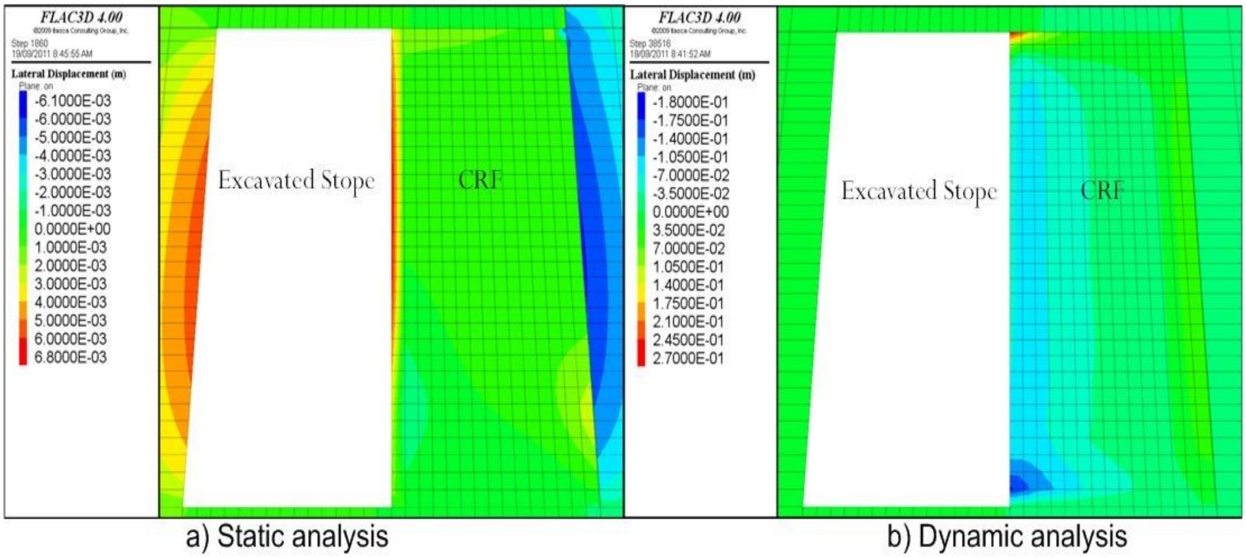

Figure 3-23 – Lateral displacement contours for the backfilled primary stope after extraction of the secondary stope

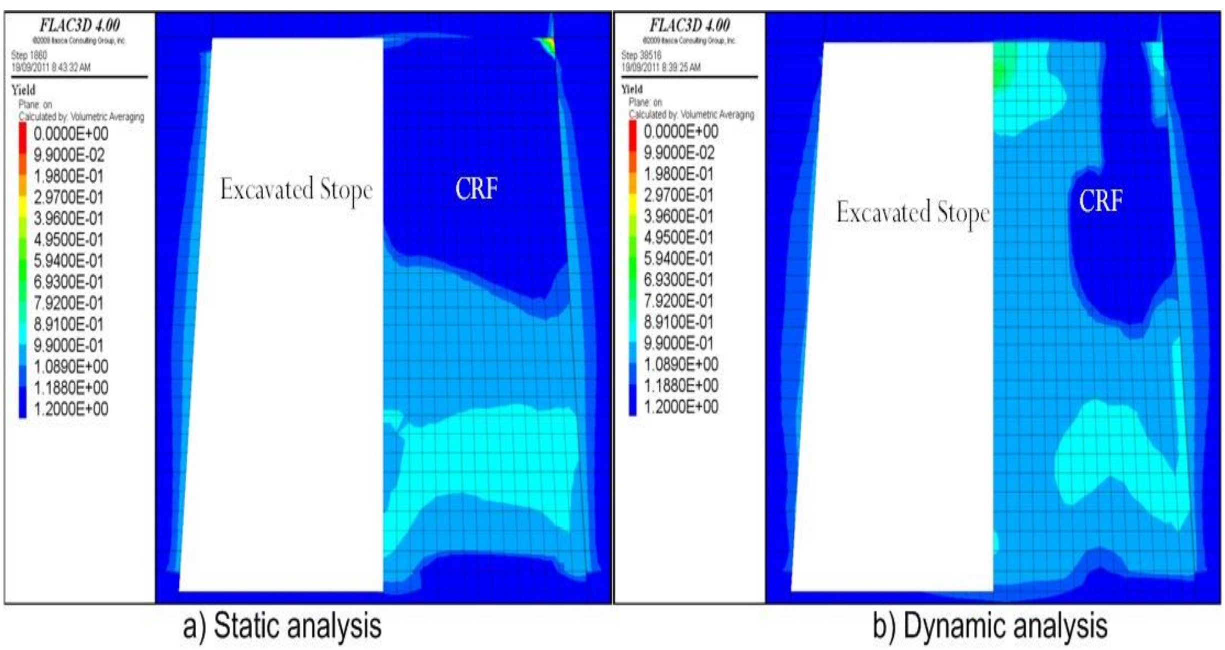

Figure 3-24 – Yield zones for the backfilled primary stope after extraction of secondary stope

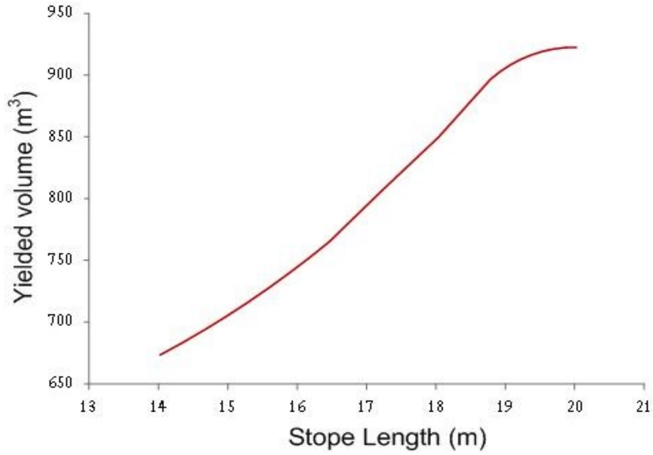

a) Stope length versus yielded volume

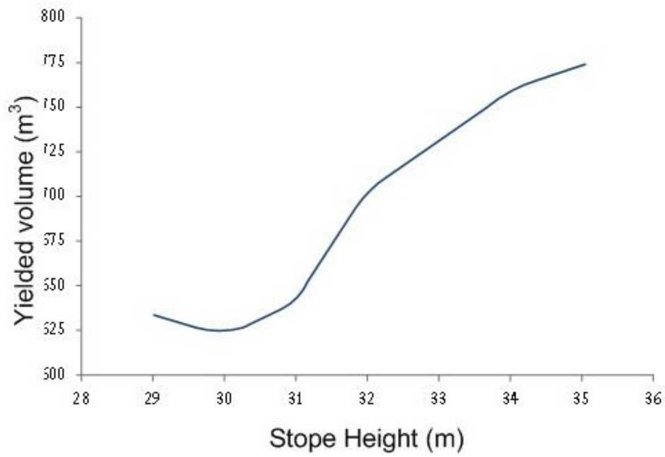

b) Stope height versus yielded volume

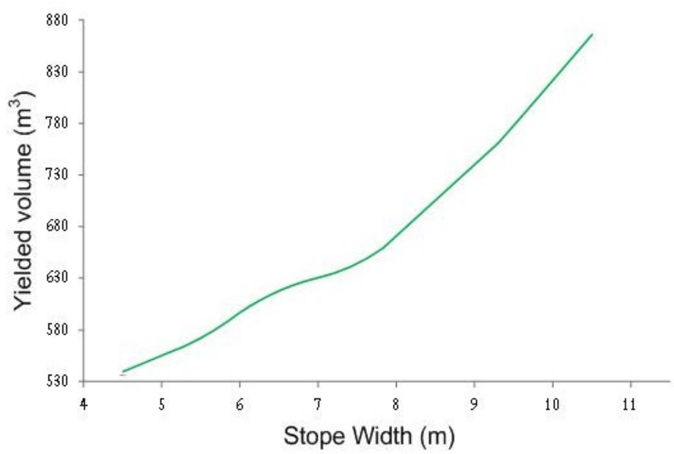

c) Stope length versus yielded volume

Figure 3-25 – Effect of stope dimensions on yielded volume in cemented rockfill

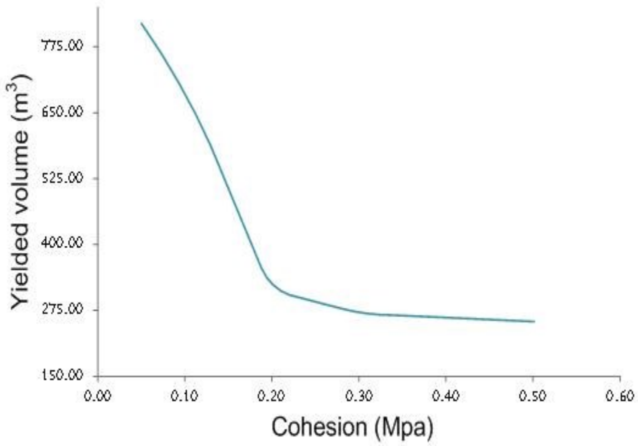

a) Cohesion versus yielded volume

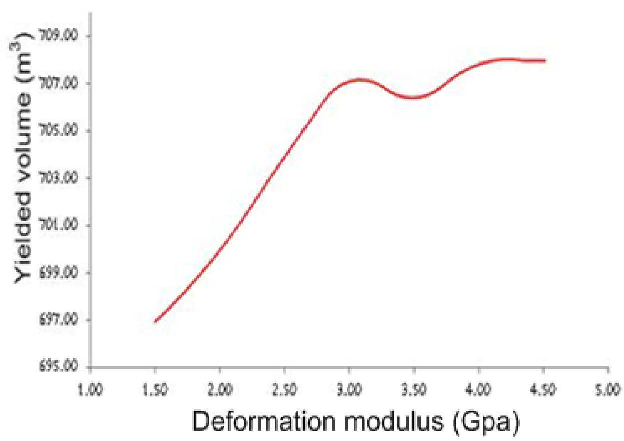

b) Deformation modulus versus yielded volume

Figure 3-26 – Effect of engineering properties on yielded volume in cemented rockfill

In the next stage magnitude of blast vibrations is lowered to 25%, 50%, 75% and 100% of the original blast load, the results are presented in Figure 3-27. The results of yield zones in backfill were compared and it can be seen that yield zones are absent at a lower magnitude of blast vibrations that are 25% and 50%. Yield zones start to develop after 75% of the applied load and a further increase to 100% may lead to greater yielding.

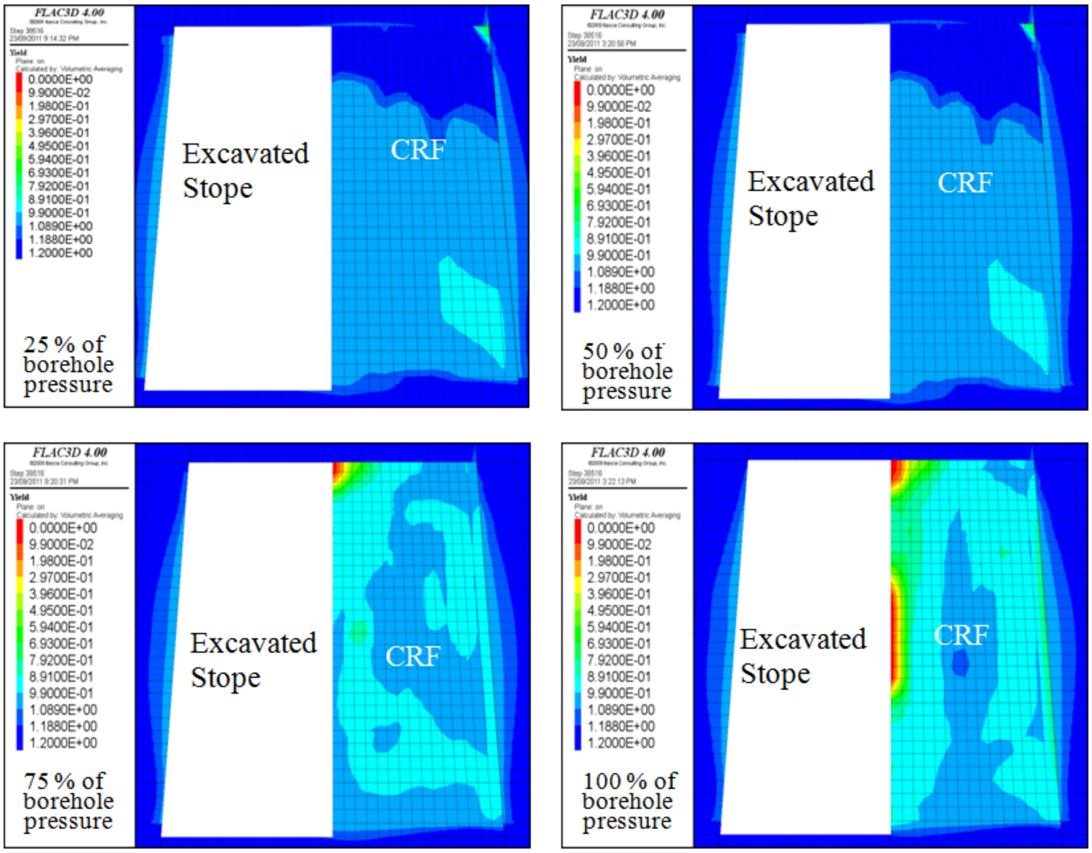

Figure 3-27 – Dynamic yielding in the CRF column due to variation in blast load intensity

3.6.3 Modelling the Effects of Segregation in Cemented Rockfill

This work was presented by Emad et al. [133] in the 21st Canadian Rock Mechanics Symposium, RockEng12 Edmonton AB held between May 5 – 9, 2012. Segregation in CRF is a well-known phenomenon, and the problem of segregation has been highlighted and discussed by a number of researchers [5, 7-9, 17, 19, 21, 31, 59, 73, 95, 134-136]. Many backfill practitioners reported that un-mixed CRF may develop a cement slurry pool away from the dumping point [8]. It has been observed that CRF stopes have different cement concentrations [31]. The cement slurry will seep-out of the aggregate and will make a slurry pool having high strength as compared to the rest of the CRF column. In such a case there will be different sub-zones within the CRF mass having high and low strength regions. The problem of segregation due to improper mixing has been modeled using the case study mine B. High strength zones were assigned CRF properties and low strength zones were assigned weak CRF properties from Table 3-1. Before considering segregation, CRF was considered as a homogeneous material for the base case. The

CRF failure in the modeled homogeneous stope (334 tonnes) was compared with the ore dilution volume from the CRF observed from the cavity monitoring survey (361 tonnes). The following sections present results for static and dynamic loading on the CRF column, considering homogeneity in Section 3.5.3.1 and heterogeneity caused by the combination of improper mixing of the CRF and the placement method in Section 3.5.3.2.

3.6.3.1 Homogeneity in CRF column

3.6.3.1.1 Gravity or static loading on CRF

Before modeling heterogeneity in the CRF, it was assumed that the CRF has been mixed properly before placement and hence the CRF column is assumed to be homogenous. The model was generated and executed while taking into account homogeneity in the CRF. The contours of vertical stresses and yielding after static analysis are presented in Figures 3-28 and 3-29 respectively. Figure 3-28 presents vertical stress contours and it did not show any zones of relaxation and Figure 3-29 presents yield contours, showing no yielding or failure in the CRF. Yielding is based on the factor of safety (ratio of strength to stress), and for this work a threshold yield value of 0.9 and below are considered as failure in the CRF.

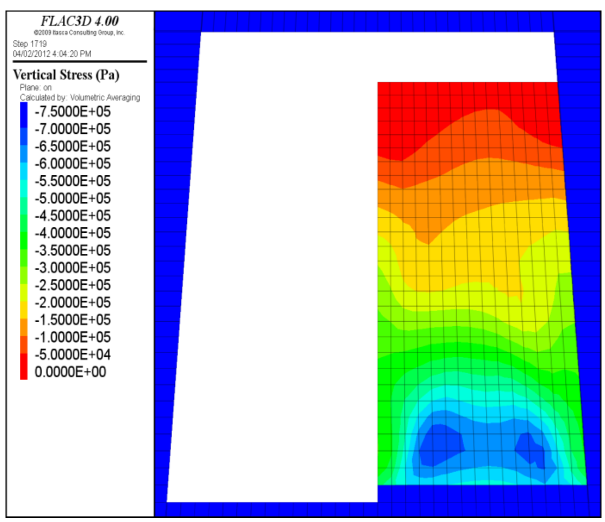

Figure 3-28 – Vertical stress contours for a homogeneous CRF column after static analysis

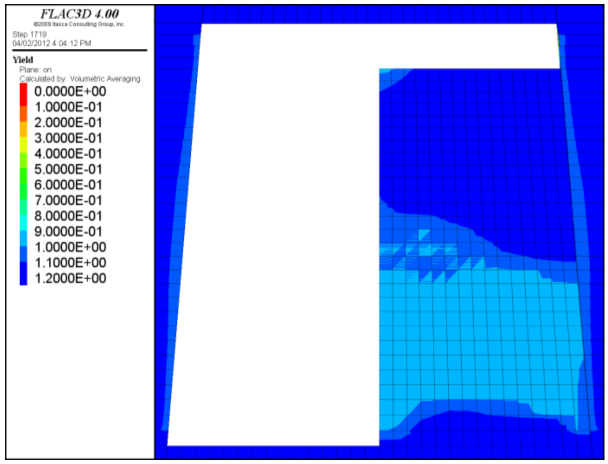

Figure 3-29 – Yield contours for a homogeneous CRF column after static analysis

3.6.3.1.2 Blast loading or dynamic loading on CRF

The CRF column was applied with time varying stress load using the FLAC3D dynamic module to produce inertial forces due to blasting adjacent to the CRF. The dynamic modelling conditions discussed earlier were applied and the model was solved for a period of one second after blasting. Figures 3-30 and 3-31 present vertical stress contours and yield contours after solving the model for a one second interval. In Figure 3-30 it is notable that there is a tensile stress development at the top of the stope, which indicates a zone of relaxation in the CRF causing wedge failure at the top of the CRF column. The yield contours after dynamic analysis verifies the failure from the top of the column.

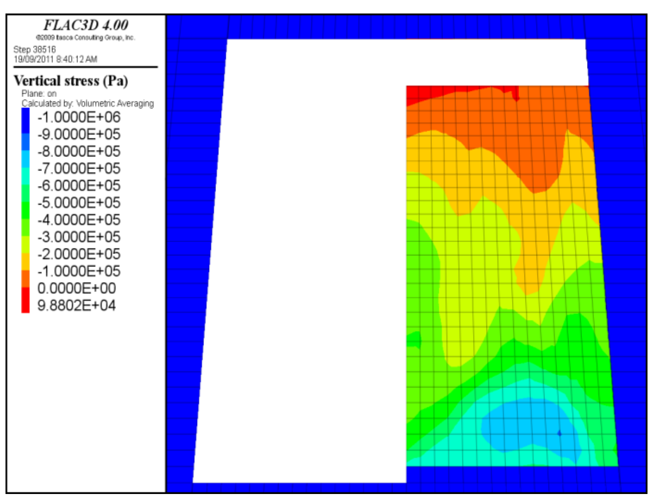

Figure 3-30 – Vertical stress contours for a homogeneous CRF column after dynamic analysis

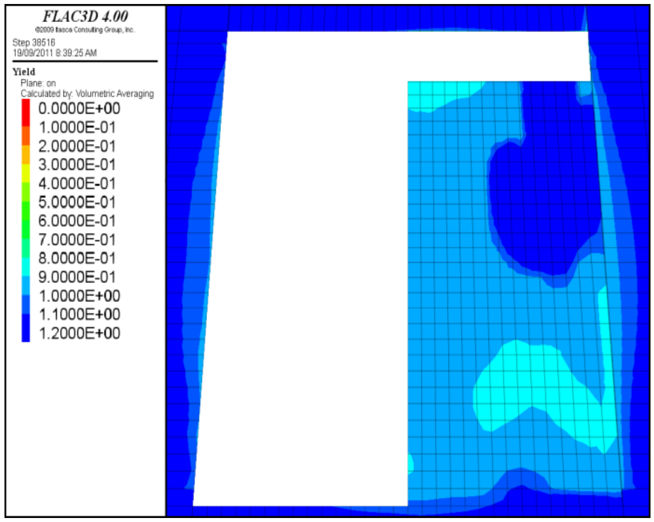

Figure 3-31 – Yield contours of a homogeneous CRF column after dynamic analysis

3.6.3.2 Segregation in CRF column

As discussed earlier the CRF column can become heterogeneous if mixing of the CRF before placement is improper. On the basis of two placement methods, discussed earlier, two different models were generated. The models were loaded for static loading first and then dynamic analysis was performed to accommodate blast induced vibrations. The results are presented in the following sections.

3.6.3.2.1 CRF placement by raise

CRF placement by backfill raise generates two major zones in the CRF column that are the high strength zone located near the hanging-wall and the low strength zones near the footwall. The strong zone properties were doubled in magnitude and the weak zones properties were reduced to two third of the original properties. The two zones have been modeled and analyzed for static loading. Figures 3-32 and 3-33 present the results for vertical stress contours and yield contours. In Figure 3-32, it can be noted that there are no significantly high compressive and tensile stress zones in the CRF, which suggests that improper mixing in combination with this placement method have almost no influence on CRF failure. Figure 3-33 shows some yielding in the CRF but the majority of zones are stable under dynamic load. The same CRF column was analyzed under the dynamic load following the procedure explained earlier.

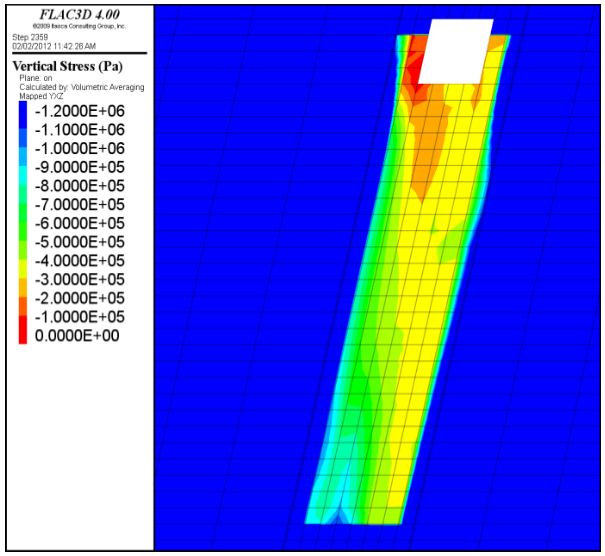

Figure 3-32 – Vertical stress contours for a CRF column filled by raise after static analysis

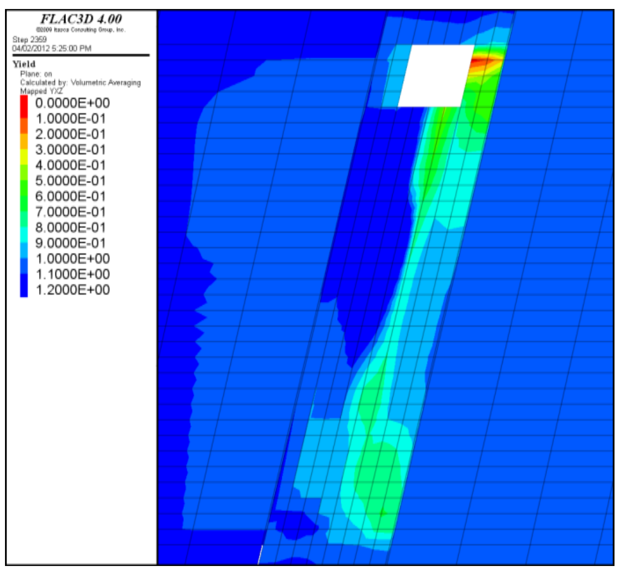

Figure 3-33 – Yield contours for a CRF column filled by raise after static analysis

Figures 3-34 and 3-35 present the vertical stress contours and yield contours after dynamic analysis. It was found that the vertical stress contour shows a tension zone at the low strength zone in the CRF column, indicating relaxation. The yield contour also show yielded zones in the low strength zones of the CRF column, thus verifying CRF failure. When compared with static analysis, the results of dynamic analysis are more realistic and are in accordance with field observations.

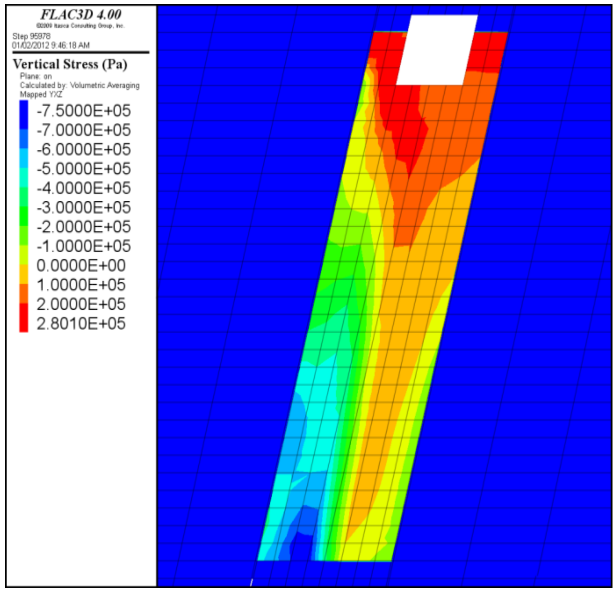

Figure 3-34 – Vertical stress contours for a CRF column filled by raise after dynamic analysis

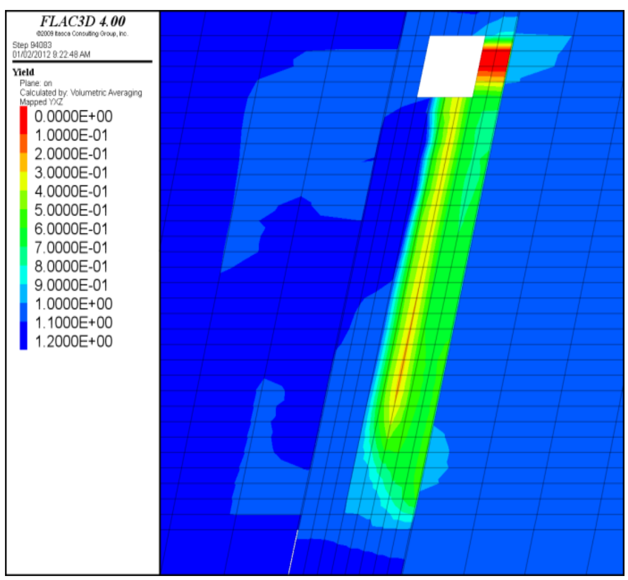

Figure 3-35 – Yield contours for a CRF column filled by raise after dynamic analysis

3.6.3.2.2 CRF placement using LHD

CRF placement using LHD generates three major zones of sub columns. The three zones with different strengths were modeled and the zones nearest the exposed CRF face were considered as the weakest zones, and the zones furthest away from dumping point were considered as the strongest, as discussed earlier. The results of static modeling for vertical stresses and yield are presented in Figures 3-36 and 3-37 respectively. The static results for vertical stresses show that the CRF column is stable as there are no relaxation zones but the yield contours show CRF failure in some of the weaker zones.

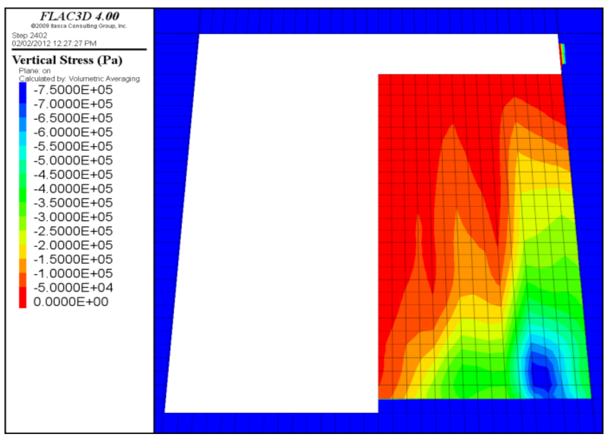

Figure 3-36 – Vertical stress contours for a CRF column filled by LHD after static analysis

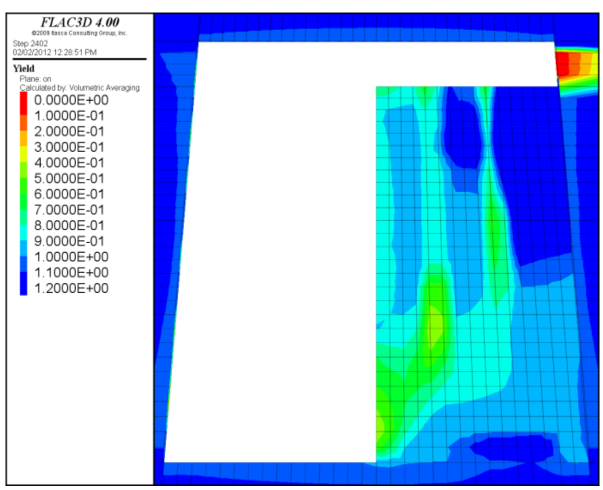

Figure 3-37 – Yield contours for a CRF column filled by LHD after dynamic analysis

The column was then applied with blast-induced load and dynamic analysis is performed. The results for vertical stresses and yield contours are shown in Figures 3-38 and 3-39. The low stress regime at the exposed face signifies CRF failure, which was the weakest zone in the CRF column. The yield contours also confirm yielding in the low strength zones. Yielding in backfill is based on the same failure criteria of safety factor value of less than 0.9.

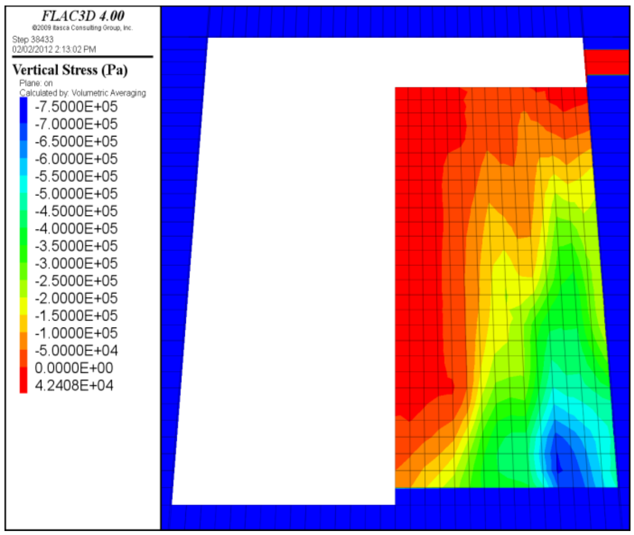

Figure 3-38 – Vertical stress contours for a CRF column filled by LHD after dynamic analysis

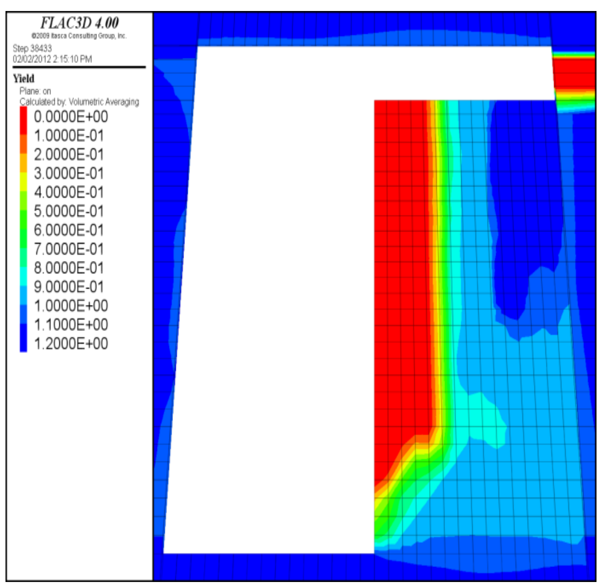

Figure 3-39 – Yield contours for a CRF column filled by LHD after dynamic analysis

3.6.4 Effect of Blast Vibrations in Vertical Crater Retreat Method

This work was presented by Emad et al. [96] in 65th Canadian Geotechnical Conference – GeoManitoba2012 held in Winnipeg MB between September 30th to October 3. Vertical block mining method or vertical crater retreat mining method is the blasting method employed for most of the tabular steeply dipping ore bodies. Mine A was used as a case study for this work. One of the stopes was selected from mine A and a FLAC^{3D} model was constructed. After constructing the model geometry, applying boundary conditions, gravity loading and stresses, assigning material properties and density in accordance with case study mine, the model is solved for equilibrium. On reaching equilibrium the mining sequence is followed by mining out primary stope and backfilling it. The secondary stope was then mined in three lifts one after the other, while following VBM method. After extraction of each lift model was analyzed and dynamic analysis was performed to incorporate the blast loading on CRF.

In the first step, bottom lift is mined from the secondary stope and the vertical stress contours of CRF stope for static analysis and dynamic analysis are presented in Figure 3-40 and 3-41 respectively. The two Figures are similar and both the Figures show a maximum compressive stress of less than 1 MPa located at the bottom of the stope. Notably there is no tensile stress in CRF stope, which implies that there are no backfill failures for the first lift. The lowest compressive stress in backfill remains in between 0 – 0.05 MPa and is located on top most part of CRF. Dynamic analysis results for the 1st lift are similar to static loading on backfill. This means that a compressive strength of 1 MPa or more in CRF is sufficient during blasting and mucking of first lift.

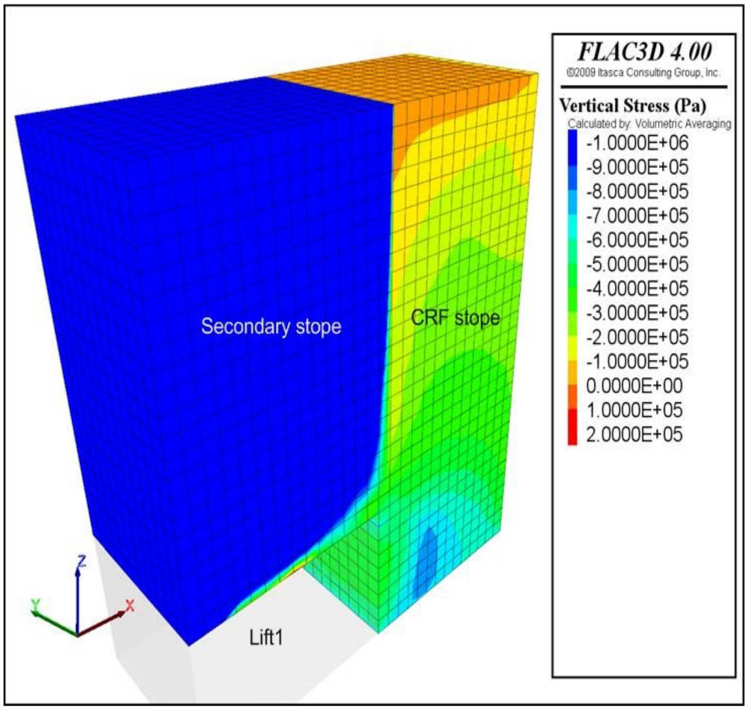

Figure 3-40 – Vertical stress contours of CRF after extraction of 1st lift from the secondary stope – static analysis

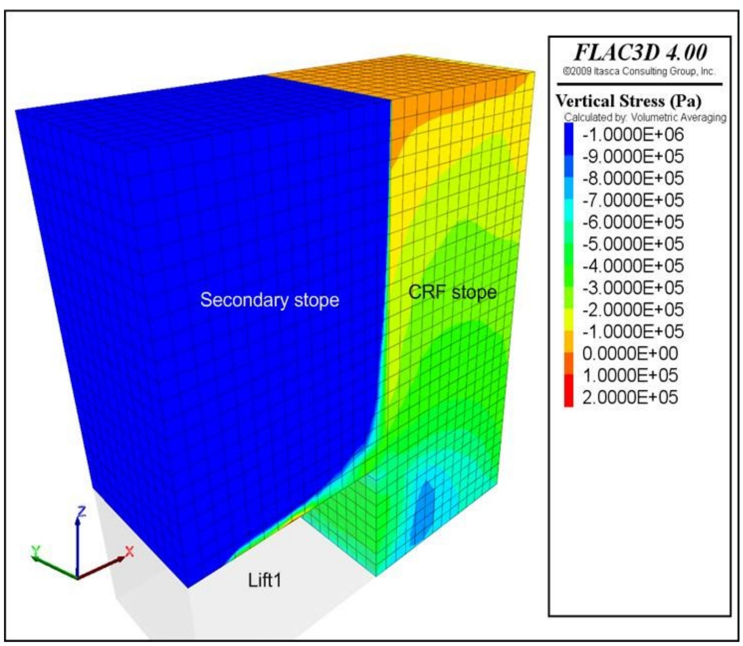

Figure 3-41 – Vertical stress contours of CRF after extraction of 1st lift from the secondary stope – dynamic analysis

In the next step second lift or central block of the secondary stope was mined out and model was solved for static loading due to gravity and dynamic loading due to production blasting in adjacent stope. The results of the vertical stresses contours in CRF stope are presented in Figure 3-42 and 3-43 for static and dynamic analysis respectively. As can be seen, the maximum compressive stress in CRF stope remained the same at 1 MPa located at the bottom of CRF stope, for both static and dynamic analyses after mining the second lift. The minimum stress in CRF remained at 0 MPa for static analysis. Dynamic loading on CRF produced a narrow band of tensile stress near top left corner of backfill that is just starting to develop in the CRF as shown in Figure 3-44. The tensile stress development in CRF is an indication for the development of low confinement zone, leading to failure in CRF.

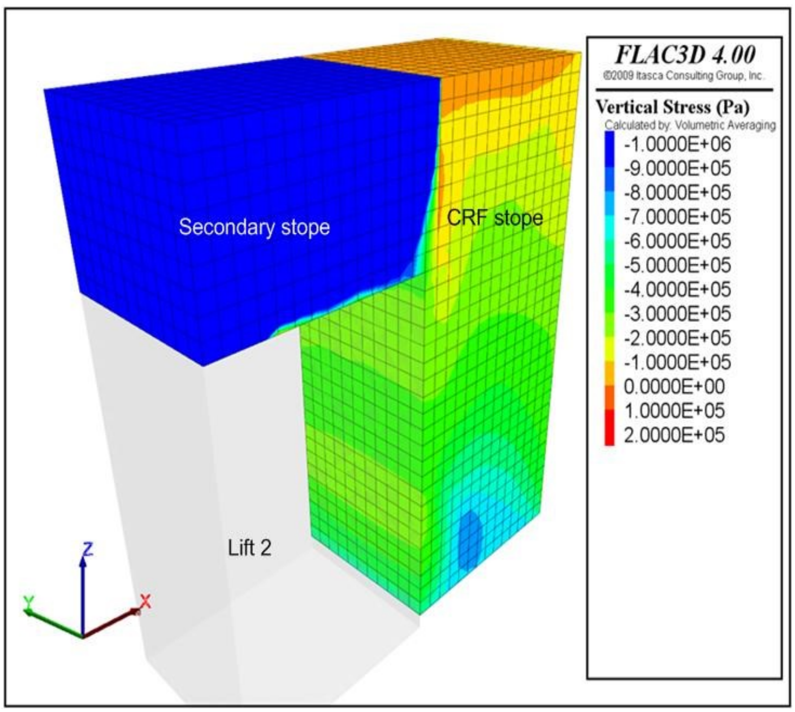

Figure 3-42 – Vertical stress contours of CRF after extraction of 2nd lift from the secondary stope – static analysis

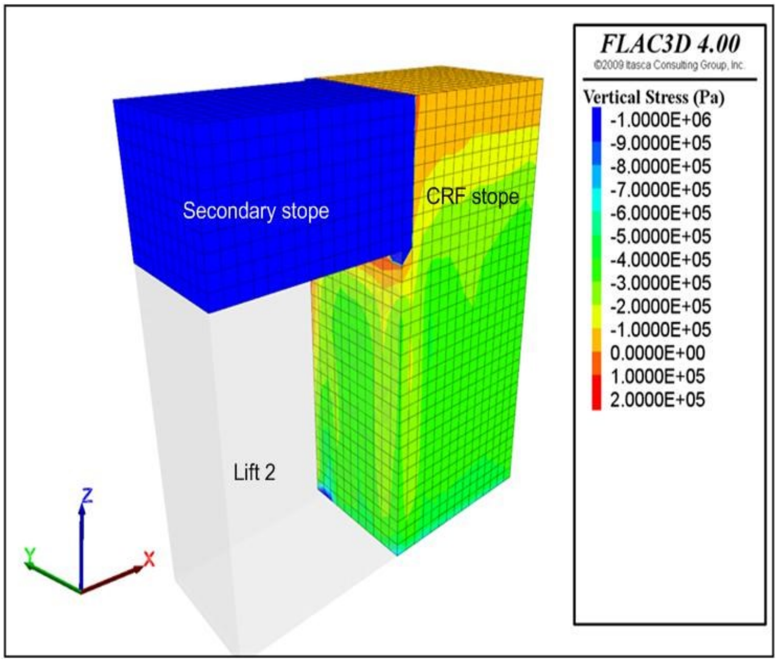

Figure 3-43 – Vertical stress contours of CRF after extraction of 2nd lift from the secondary stope – dynamic analysis

The third lift or last stage is the complete extraction of remaining secondary stope and repeating the exercise which is to solve for static loading first and then applying dynamic loading on CRF. The vertical stress contours for static loading are presented in Figure 3-44. The gravity loading on CRF after the complete extraction of secondary stope shows that the maximum compressive stress remains at less than 1 MPa at the bottom of CRF. Figure 3-44 show that a minimum compressive stress in backfill is still 0 MPa for static loading only. The static loading on backfill shows that there are no failed zones in CRF even after complete extraction of secondary stope. The vertical stress contours for dynamic analysis are presented in Figure 3-45 which shows that the compressive stress in CRF is 1 MPa located at the bottom of stope, but the lowest stress in CRF is now tensile and it is located at the top corner of exposed CRF face. This implies that a zone of relaxation in CRF is developing and is leading to failure in adjacent stopes. Figure 3-45 presents failure from top of the exposed face, in the shape of wedge which is similar to the one presented in CMS profiles.

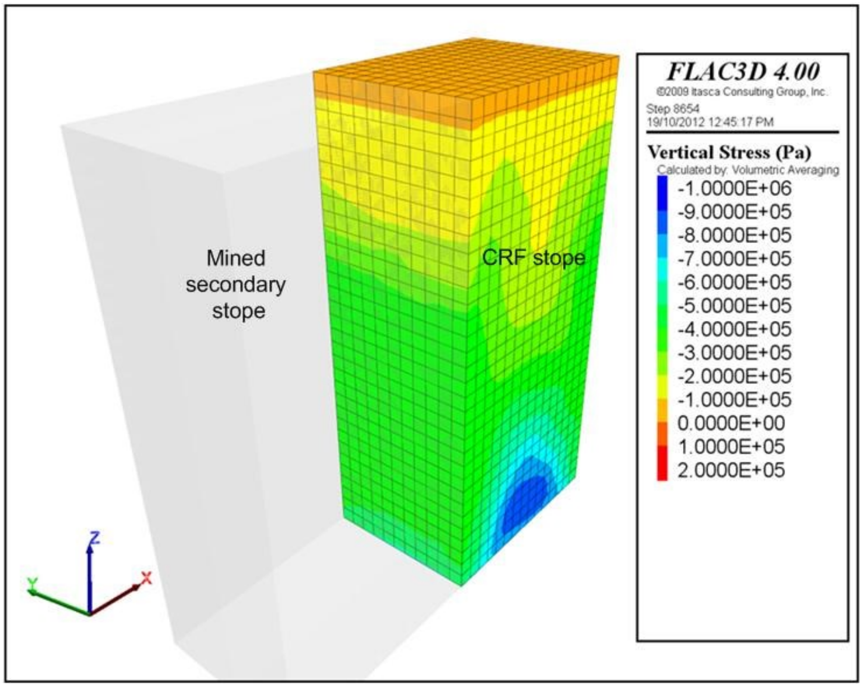

Figure 3-44 – Vertical stress contours after extraction of entire secondary stope – static analysis

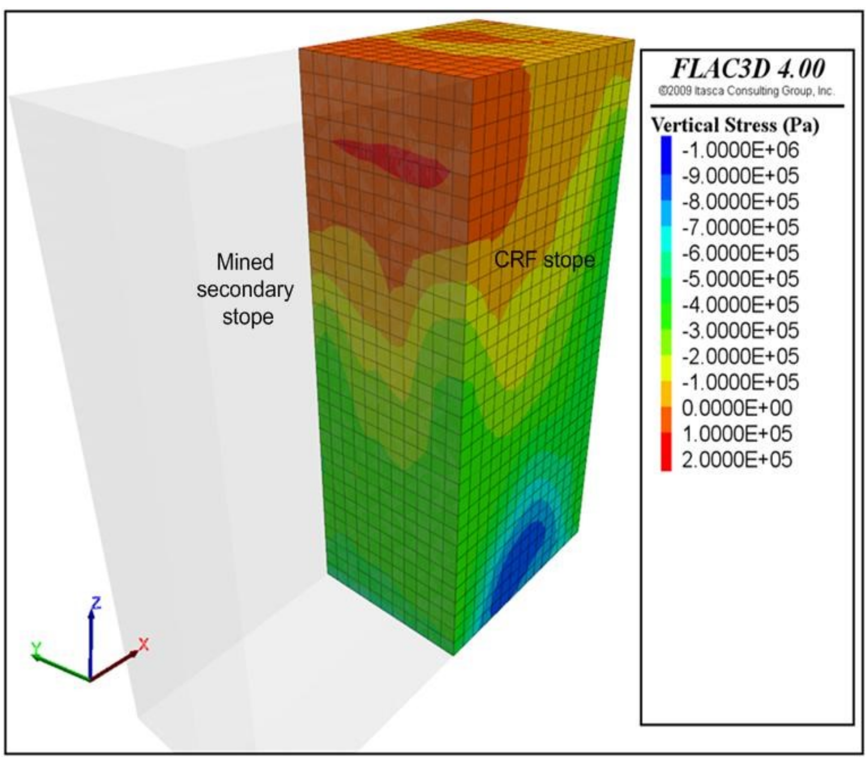

Figure 3-45 – Vertical stress contours after extraction of entire secondary stope – dynamic analysis

A comparison between major principal stress distribution with stope depth after static and dynamic analysis has been presented in Figure 3-46. The stress distribution has been computed at the center line of the exposed CRF face. The plot contains tensile stress region on the right side. It can be observed that the dynamic analysis stress profile presented intersects with vertical axis at a depth of 7 meters and continues its path in the tension zone. A comparison of minor principal stress distribution has been presented in Figure 3-47. It can be seen that the minor principal stress for dynamic analysis, transforms to tensile stress at a depth of 7 m and it remain inside the tensile stress region at zero depth.

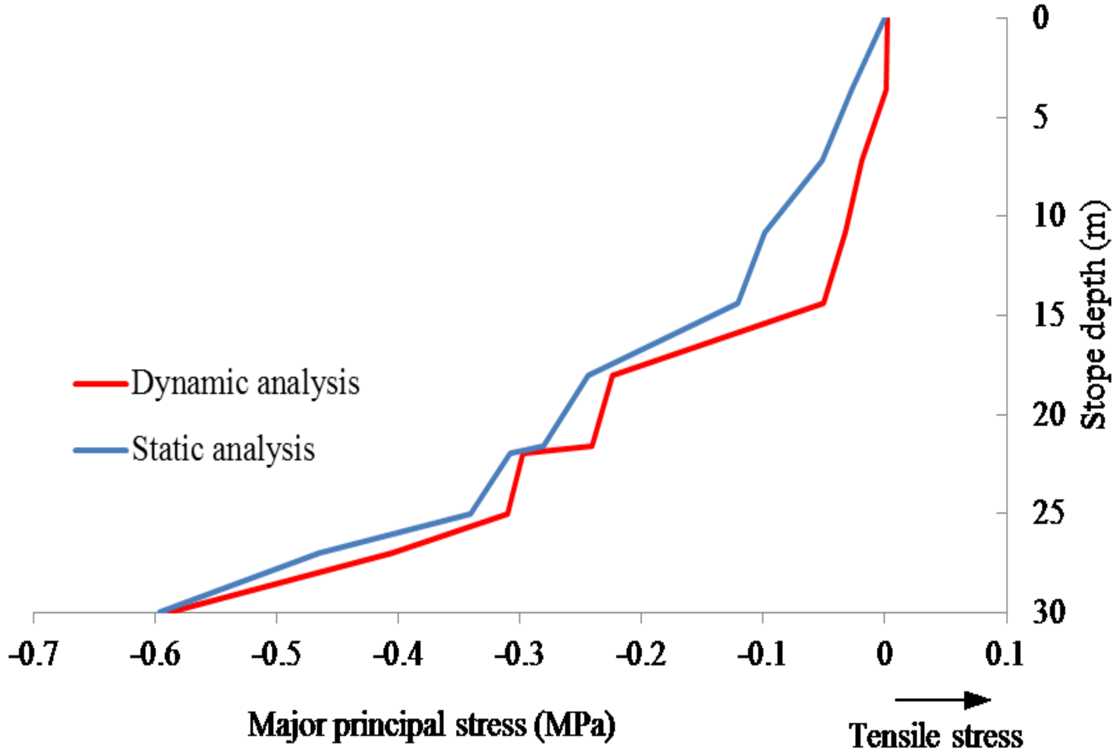

Figure 3-46 – Computed major principal stress distribution on exposed face of CRF

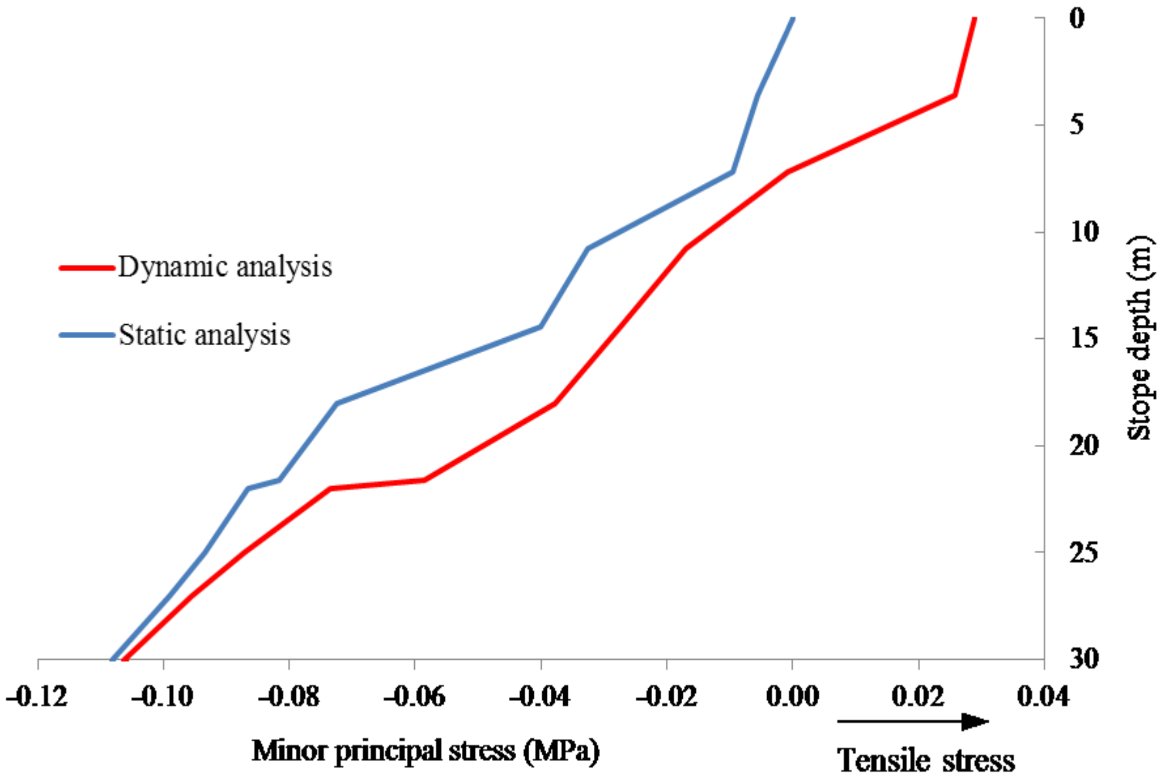

Figure 3-47 – Computed minor principal stress distribution on exposed face of CRF

The results of dynamic loading are also recorded as the total velocity which is sum of the three velocity components that are longitudinal, transverse and vertical. Figure 3-48 presents profile of the vector sum on top of the exposed CRF face during the dynamic analysis. It can be seen that the peak vector sum (PVS) is approaching a value of around 340 mm/s.

Figure 3-49 presents a profile of PVS monitored along the center line of the exposed CRF face. It can be seen that the PVS of top most part of exposed backfill face is have higher magnitudes. This is due to the fact that top of the backfill is less confined and it vibrates more than any other region. The mines use CMS profiles to compute ore dilution from wall slough and backfill. The case study mine's CMS profile of the modeled stope is overlapped with vertical stress contours of CRF stope from dynamic analysis. The overlap of CMS profile and vertical stress contours is presented in Figure 3-50. This may serve as numerical model calibration. In the Figure bold black line is CMS profile showing failure from top of the stope in wedge shape. The numerical modeling results are showing failure in same region.

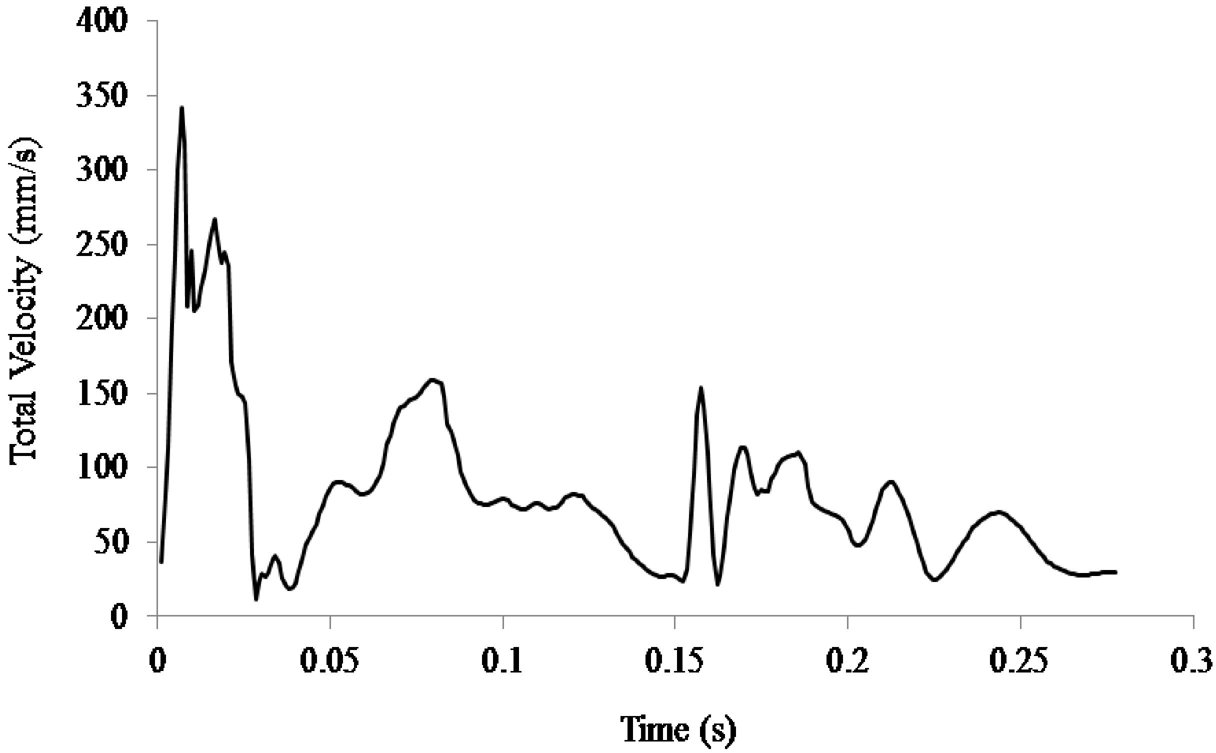

Figure 3-48 – Peak vector sum profile monitored in CRF at a depth of 0 meters, during dynamic analysis

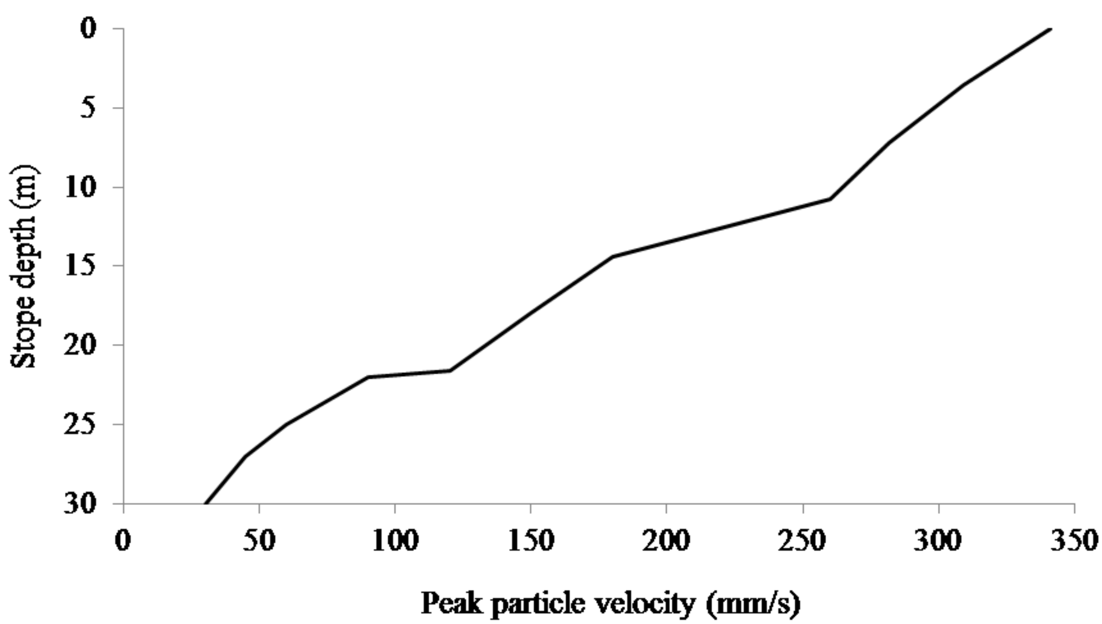

Figure 3-49 – Peak vector sum monitored at the exposed CRF face during extraction of three lifts

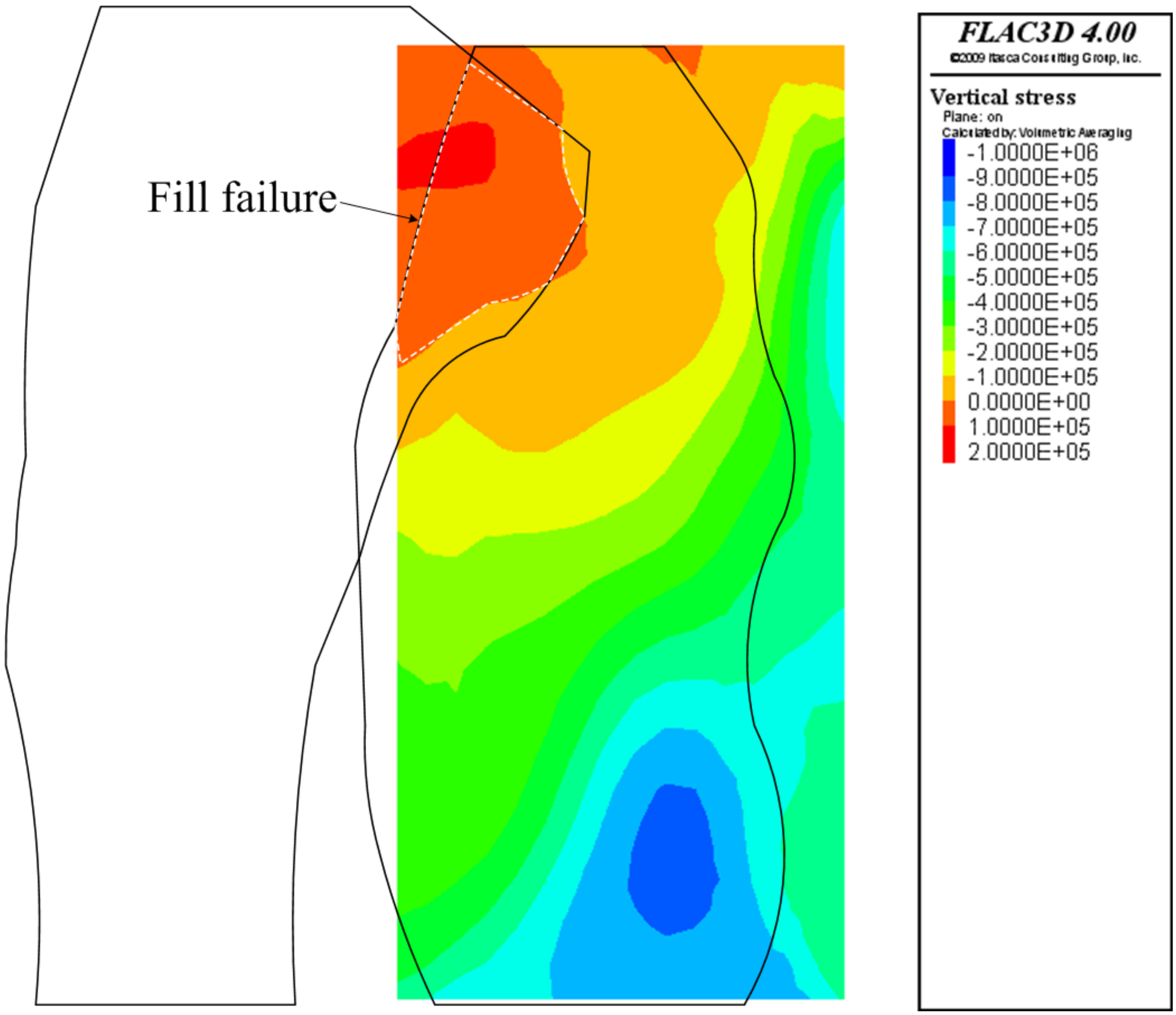

Figure 3-50 – CMS profile overlapping tensile stress contours of numerical model

3.7 SUMMARY

This Chapter presents numerical modeling results for dynamic analysis followed by dynamic modeling setup in FLAC^{3D}. A literature review of blast loading on backfill has also been presented. A dynamic model has also been formulated and dynamic modeling results of backfill material have also been presented. The results of the studies presented are promising. It was found that CRF blocks are not affected by both the static loading and dynamic loading due to sudden extraction of stope or loss of confinement. Blast loading however was found to be among the causes of destabilization in exposed CRF. Parameters like stope dimensions, rock mass deformation modulus and Poisson's ratio have direct relationship with CRF failure. As expected, higher cohesion in CRF results in less failure. A variation in blast load has also been studied and it was found that greater the magnitude of blast vibrations results in greater failure in CRF. Segregation in CRF has also been studied by assuming improper mixing of CRF developing high strength zones near the hanging-wall and weak zones near the footwall in backfill. It was found that there is high yielding in segregated fill. Vertical block mining is simulated and the results showed that only the top blasting lift of VBM initiates CRF failures while lower lifts of VBM did not produce any failure. Tensile stress development and yield in backfill were considered as a failure criteria. Lateral displacement in backfill produced some movement in backfill, which was found to be incompatible with the field observations and backfill failure profiles from CMS.

4 THE BIRCHTREE MINE

4.1 INTRODUCTION

The Birchtree mine is a nickel mine, owned and operated by Vale Manitoba Operations, Thompson MB, Canada since 2005. Before 2005 the mine was owned by International Nickel Company (INCO). The Birchtree mine is located 732 km north of Winnipeg and 8 km south of the city of Thompson as shown in Figure 4-1.

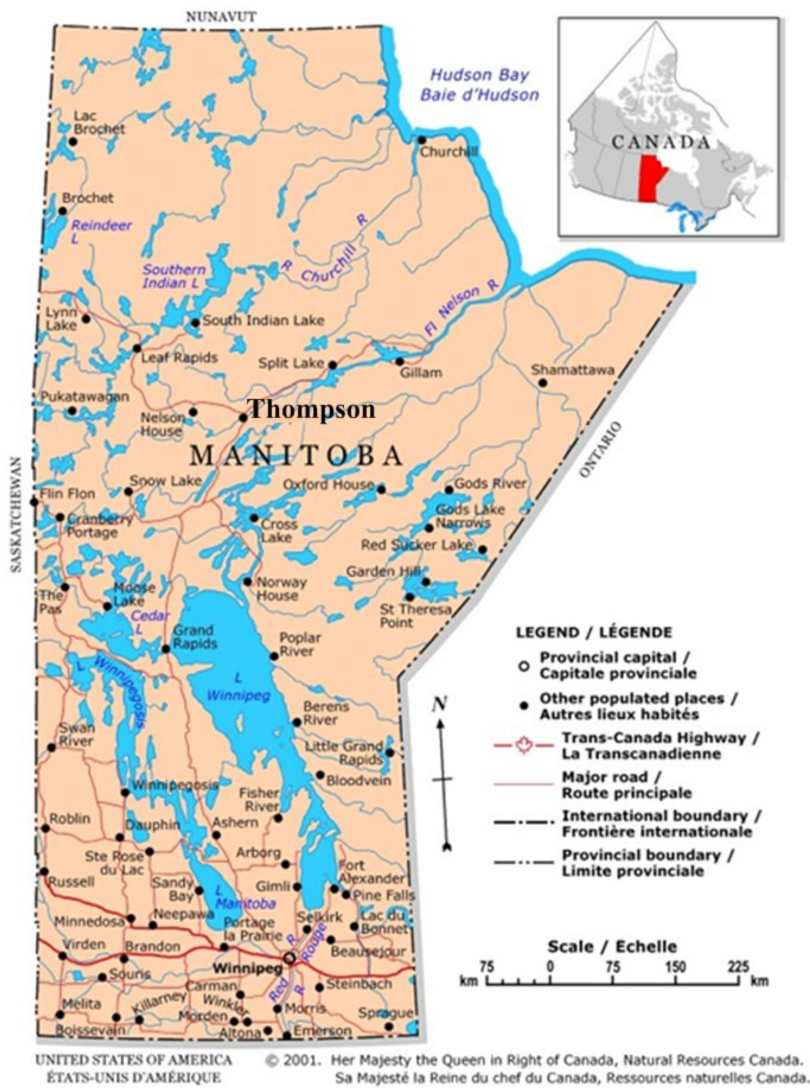

Figure 4-1 – Map of Manitoba showing location of Thompson [137]

The mine produces around 2300 tonnes of nickel ore per day at an average grade of around 1.5% nickel. It is presently one of three producing underground mines in the Thompson MB. Although the economic nickel-bearing SUM deposit was discovered in 1969, production did not begin until 1974. In 1977, low nickel prices moved INCO to concentrate efforts on the higher grade deposits, forcing the closure of Birchtree. Strong demand and higher prices in the mid 80's revived the possibility of reopening the Birchtree Mine in 1989. In the same year the mine management and engineers decided to change the mining method from cut and fill to sublevel stoping method with delayed backfill. They also changed the backfilling system from sand fill to cemented rockfill for simplicity and higher strengths. Since then the Birchtree mine is producing only nickel, which is processed to 99.9% pure nickel at milling and smelter facilities near Thompson mine.

4.2 GEOLOGY OF THE AREA

The Thompson Nickel Belt is located in Central Manitoba north of Winnipeg. It is a linear geological unit with a strike of 45 degrees north or it has a tectonic feature with north-east trend. Geologically it is situated at the borderline of the Superior and Churchill Provinces. It comprises of gneiss, meta-sediments, meta-volcanics, ultramafic rocks and felsic plutons. The serpentinized ultramafic (SUM) and metamorphic volcanic rocks are present in the western limb of the belt. The western limb also contains all nickel deposits [138], and it was explored by International Nickel Company (INCO) in 1940s. Consequently, there are many nickel sulphide ore discoveries in the region. Thompson 1, Thompson 3 and Birchtree are the three mines currently in operation. The Thompson Nickel Belt is very rich with sulphide mineralization at many locations, which is meticulously associated with magnesium-rich ultramafic rocks mainly peridotites. Most of the peridotite has been altered to serpentines [139]. Figure 4-2 presents geology of the Thompson Nickel belt [140]. The geology of Birchtree ore body can be generally described as a brecciated ultramafic rock in a sulphide matrix. The mine’s geological department terms this ultramafic rock as peridotite. There are three main categories of peridotites. First one is core peridotite encompass the mining hanging-wall for more than 50% of the Birchtree 84 ore zone, bearing an average nickel grade of 0.20%. The second category is mineralized peridotite, located within the Birchtree 84 ore body. The mineralized peridotite is scattered with the presence of sulphide and with range of grades from 0.50 to 3.0% nickel. The third type is termed as barren peridotite which hosts the brecciated ultramafic rock within the Birchtree 84 ore zone. It has an average grade of 0.35% Nickel. The barren peridotite subsidizes most of the dilution in the ore produced, and this has 33% MgO [141]. Pyrrhotite is the main constituent of sulphides with very little pentlandite, chalcopyrite and magnetite.

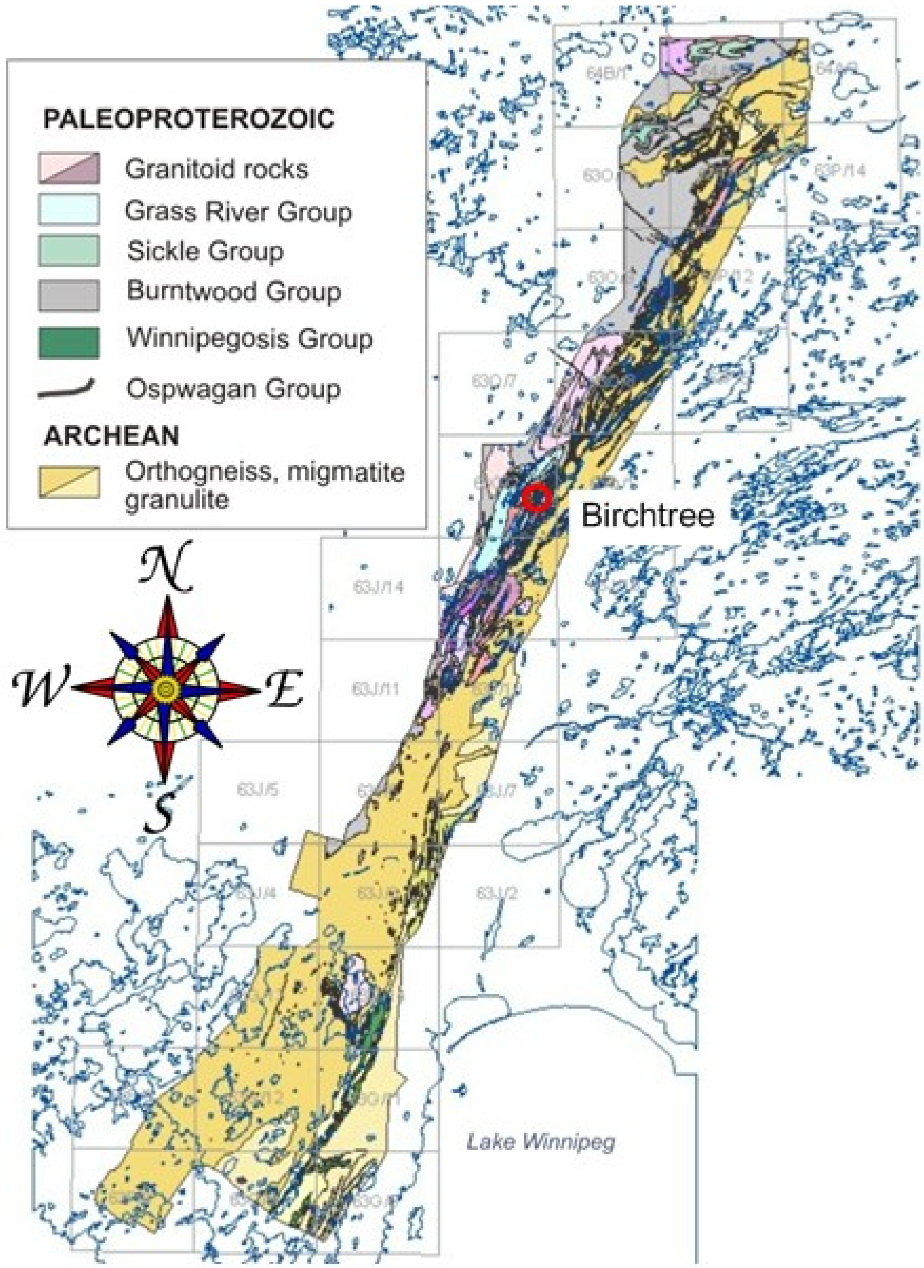

Figure 4-2 – Map presenting location and simplified geology of Thompson nickel belt [142]

Metamorphic rock with biotite, plagioclase, pyrrhotite, and quartz are present in footwall of ore body with minor traces of talc, and serpendite. The hanging-wall rock is schist in major portion of 84-lower ore zone [143]. The comparison of the average grades from the Thompson-1 ore bodies and Birchtree ore bodies are presented in Table 1. Notably nickel percentage is higher for Thompson-1 mine and Fe, S, MgO and Po values are higher for Birchtree mine ore. The noted differences between the two are the higher nickel grade in Thompson ore, and the much higher MgO grade in Birchtree [144].

Table 4-1 – Constituents of different elements in Thompson and Birchtree ore [144]

Mine	Cu	Ni	Fe	S	MgO	Cp	Pn	Po	Rock
Thompson-1	0.16	2.6	15.3	8.9	3.8	0.5	7.3	16.1	76.2
Birchtree	0.10	1.7	21.1	10.2	16.5	0.3	4.9	21.7	73.1

4.3 MINING METHOD

In general the Birchtree mine has employed sublevel stoping method or more specifically one of its variations termed as vertical block mining (VBM) for the extraction of steeply dipping ore bodies [1, 46]. In sublevel stoping methods the ore body is divided into rectangular blocks or stopes. The blocks are mined out while following a pyramid mining sequence in a transverse-retreat direction. A transverse primary-secondary stope sequence is presented in Figure 4-3. Here P-1 represents primary stope sharing no face with backfill. S-1 is a secondary stope sharing only one face with backfill. Similarly, S-2 and S-3 stopes are sharing 2 and 3 faces with previously backfilled stopes. Figure 4-4 presents a vertical section along strike of the ore body, showing the mining sequence. Typical level and sub-levels are presented in the Figure. Notably the primary stope at main level is numbered P0, the one on first sublevel is numbered P1. Similarly P2 and P3 are numbered with respect to their respective sublevels. Mining is progressed from bottom up in a pyramidal sequence. The primary stopes at all the levels are separated by S-2 stopes. The mining of S-2 stopes will also progress from bottom up. A stope is developed by driving top and bottom sill drifts or crosscuts across the ore body from the haulage drifts. The sill drifts are employed for conducting drilling, blasting and backfilling at a later stage.

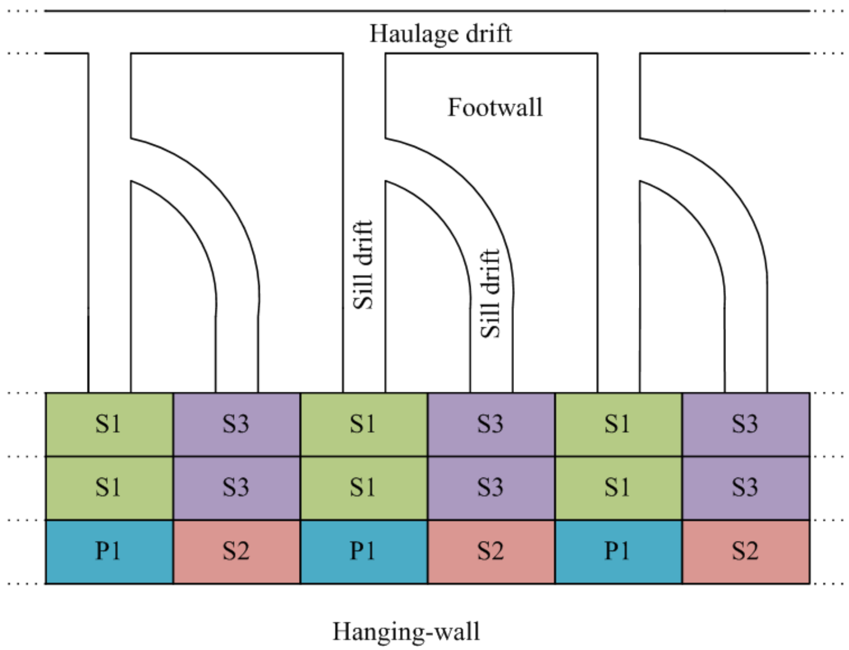

Figure 4-3 – Plan view of transverse primary-secondary stope sequence hanging-wall to footwall

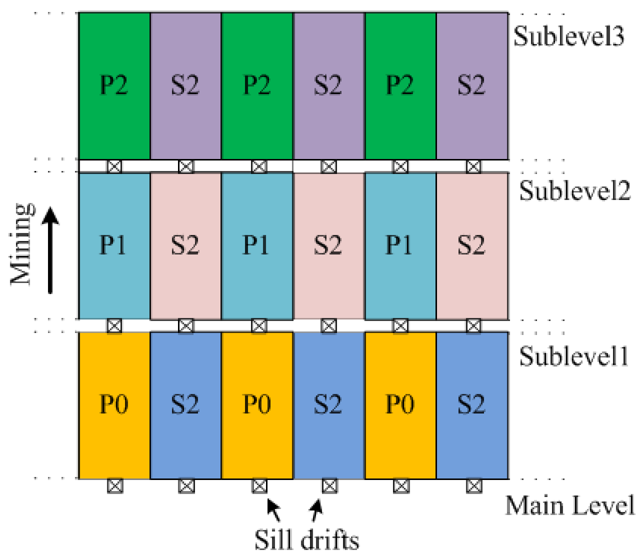

Figure 4-4 – Vertical section showing primary secondary sequence along strike

Generally VBM stope production is carried out in three or four blasts or lifts. Before blasting a large diameter hole is drilled in the stope termed as raise bore. This is done to develop a free face for facilitating blasting process and this hole remains unoccupied. All the other blast holes are blasted while slashing in the raise. Each lift is blasted and mucked one after the other. Once the stope is completely extracted, it is filled with waste material known as backfill while using the top sill drive. Backfill is cemented when there is a possibility of it being exposed in future.

Backfill is cured for at least 28 days before blasting adjacent to it. Details of the backfill system at Birchtree are presented in Section 4.5 of this Chapter. The perspective view of vertical block mining is presented in Figure 1-6.

4.4 TYPICAL STOPE DESIGN

Stope design at the Birchtree mine is based on empirical design that is the stability graph method. The stability graph method is extensively practiced in underground hard rock mines as a basis for open stope support design and is frequently used in the mine planning phase as a tool to assess the viability of stope geometries and to determine maximum permissible spans. This method is well accepted due to its simplicity and suitability to almost all of the sublevel stoping methods. Potvin [145] revised the stability graph method which was presented by Mathews [146] using case studies from Canadian underground mines. Nickson [147] added cablebolt support requirements to the same method. It has been observed that the stability graph method is compatible when the critical face has sufficient compressive stress to hold the buckling blocks. The method has been modified for low compressive and tensile stress environment by Mitri et al. [50]. This method utilises hydraulic radius of the critical face and modified stability number N as proposed by Potvin [145]. The hydraulic radius, HR, can be represented by the following equation:

$$\boldsymbol{HR} = \frac{\boldsymbol{Length \times width}}{\boldsymbol{2 \times (Length \times width)}} \qquad (4\text{-}1)$$

The modified stability number, N is a product of four factors

$$\boldsymbol{N' = Q' \times A' \times B \times C} \qquad (4\text{-}2)$$

Where, Q incorporates rock mass quality, and can be computed from the famous Q chart based on rock tunnelling index by Barton [148]. A induces the effects of stress, B includes the weakness due to the direction of the dominant joint system, and C accounts for the orientation of the critical face and the impact of gravity upon it. Figure 4-5 presents a flow diagram demonstrating the procedure to follow for designing stope using the stability graph method.

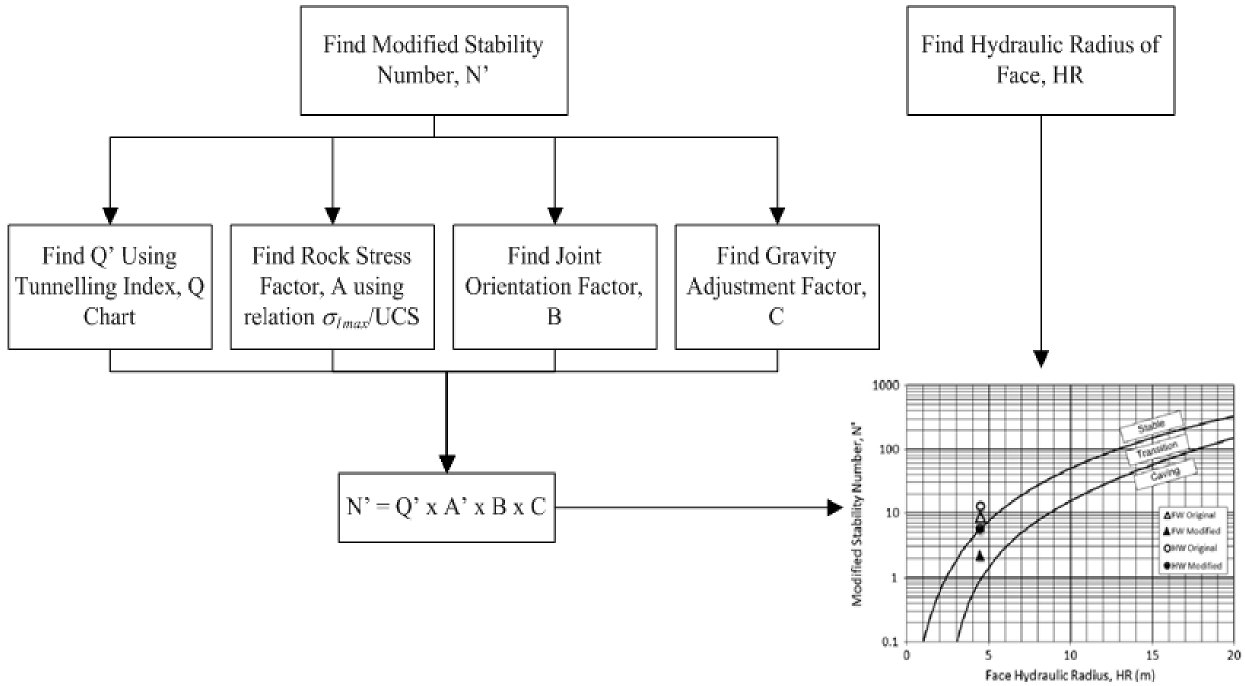

Figure 4-5 – Flow diagram presenting empirical stope design using the stability graph method

The Birchtree mine employs transverse open stoping method which is applied to ore bodies having thicknesses greater than 4 m. The ore zones are divided into grid with 18 m length by 30 m high blocks. Stope widths are designed to be 12 m. Stope production sizes are typically around 10,000 tonnes. In the transverse open stope mining method, an expansion slot is developed by enlarging a 1.07 or 1.30 m diameter slot raise to the width of the stope. Ore is fragmented in the stope using fan drilling pattern (for both primary and secondary stopes) and blasted ore is mucked from the lower sill drift, oriented normal to the stope strike. The top sill drifts are excavated to the contact of hanging wall and ore zone. Explosive is contained by 100 mm diameter fan-drilled blast holes, typically around 2.5 m burden and 2.0 m spacing, with a 1.07 or 1.30 m diameter raise-bore. A typical schematic of stope drilling pattern and explosive loading practice is presented in Figure 4-6. The raise bore is the white thick vertical line surrounded by fan pattern drill hole indicated by inclined thin lines in Figure 4-6 a. The red thick lines are representing explosive charge in Figure 4-6 b), and a disconnection in a single blast hole indicates double priming.

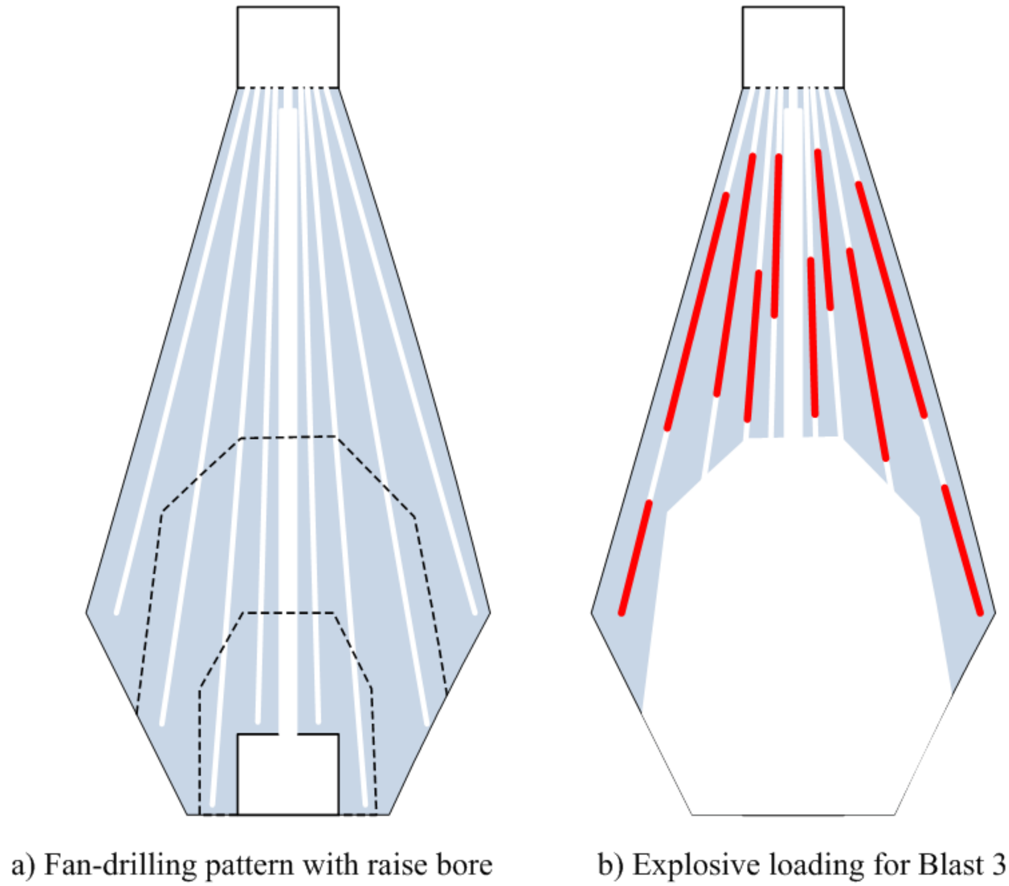

Figure 4-6 – A schematic of stope drilling and explosive loading practice at Birchtree

4.5 BACKFILL SYSTEM

Cemented rockfill is being used as a backfill material, which is prepared by mixing rock aggregate with binder slurry (which is a blend of type 10 Portland cement and type C fly ash in 30:70). The overall binder content in CRF is around 4% to achieve the desired strength. The rock aggregate used is graded and generally comes from developmental work and open pit near the Thompson mine. The type of rock is biotite schist, with minerals biotite 16 – 24%, Silica 28 – 42% and feldspar 35 – 55% which has a low porosity with an average UCS of 90 MPa and Young's modulus of 50 GPa. The rock is graded and passed through sieves to achieve – 8" + 1¼" (– 20.32 cm + 3.2 cm) size range, no additional fines are added and fines created during handling are relied on for filling the void spaces. Rock aggregate is then conveyed to the mine using trucks. The rock is then dumped in rockfill raise, which divides into many finger raises ending at different levels. Fill raise is filled to the surface in summer but in winter the level of rock is dropped to 300 feet from surface to avoid freezing of aggregates. The level is maintained within 500 feet from surface to avoid impact damage. An estimated capacity of rockfill raise is nearly 9 tons/ft. A 20 ton binder silo underground is connected with an 8” binder line via main shaft. Binder is conveyed pneumatically through binder line and compressors are used to supply pressure to keep the binder suspended. The water to binder ratio is generally kept at 0.5 using the flash mixer. The water used for binder preparation comes from nearby river. A flash mixer is used for mixing binder slurry and a pump is used for pumping slurry to stope. Slurry line is flushed after every shift to avoid plugging of slurry line. The ore body is mined transversely, by developing sill drifts on top and bottom of the planned stopes. The stopes are then drilled and blasted from the top or bottom drifts, the dimensions of stope are 18 m long × 12 m wide × 34 m high and there are generally three stopes across the thickness of the ore body. The ore is mucked from bottom sill and the stope is then backfilled from top sill drift using load haul dump machine (LHD). The binder slurry is prepared in colloidal mixers at different levels with a mixture of Portland cement, fly ash and water. The binder slurry is then pumped to each sub-level. There are two mixing methods being practiced at the case study mine. First method is termed as “sump method” in which a LHD loads aggregate from a finger raise, it then dumps aggregates in a sump and showers binder slurry over it. Then the LHD loads CRF from sump and dumps it in an open stope. This method has also been in practice by Junction mine in Australia [19]. The backfilled stope is cured for at least 28 days before mining adjacent secondary stopes. Second method used for mixing of backfill is termed as “bucket method” in which a bucket load of aggregate is showered by binder slurry before placement in the stope. The mine has two 12 hour shifts per day. The current average placement rate of backfill is 500 tons per shift. The stope which will not be exposed in the future are filled with unconsolidated rockfill. A typical flow diagram of a cemented rockfill system is presented in Figure 4-7.

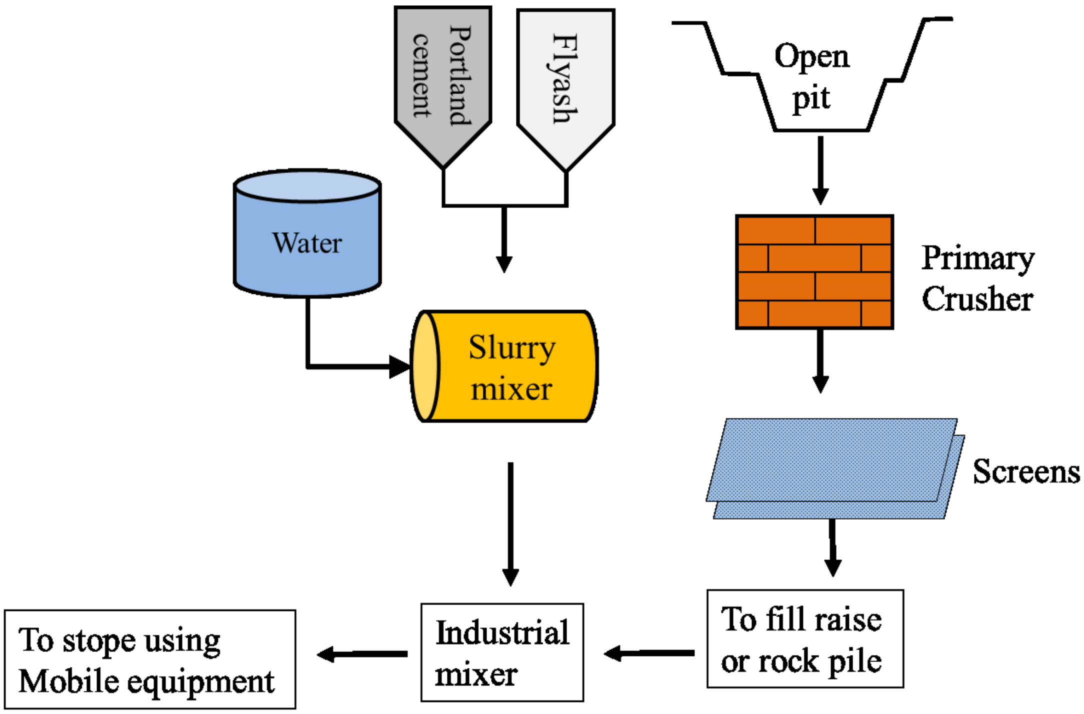

Figure 4-7 – Flow diagram showing different processes in backfill system

4.6 BACKFILL FAILURES

The problem of backfill failure is very common in Canadian mines practicing primary-secondary extraction sequence in sublevel stoping method with delayed backfill. Backfilling practice and design has been studied in the past to resolve backfill failure as discussed earlier. Such studies generally deal with operational issues and they emphasize on following static design procedures. Static designs are based on gravity loading with its maximum magnitude at the base of stope and they do not take into account any blast loading from adjacent production stopes. Stopes designed with static loading criteria generally fail from top. Similar failures in backfill from the top of the exposed face have been observed and presented by Chen et al. [18], Gool [20] and Ran and Watunga [30].

A number of backfill failures were observed at Birchtree, CMS profiles of such stopes are presented in Figure 4-8. The failure shape has been highlighted with a white dashed line, and it can be seen that the location of failure is at the top of the exposed backfill face. The failure shape can be termed as wedge shape failure. Some authors suspect production blasting right next to fill as the main cause of fill failure. Many authors suggested that static design for backfill is insufficient when practicing primary-secondary mining sequence and the static design must be enhanced by increasing the safety factor to 2, in order to reduce the impact of blasting.

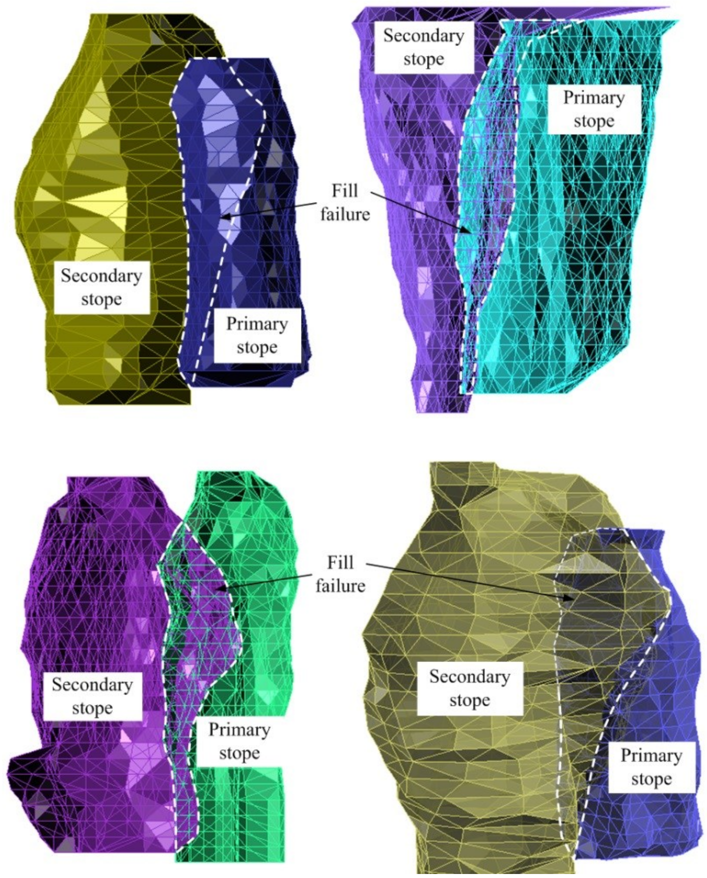

Figure 4-8 – Cavity monitoring survey showing backfill failures observed at the case study mine

4.7 LOCATION OF STUDIED AREA

The Birchtree mine encompass several ore-bodies including 83, 84 upper, 84 lower, 84 deep and 108 ore bodies. The names of these ore bodies are in relation to their longitude values. Major portions of ore zones 83, 84 upper and lower have been mined out and the mine is now planning to extend the mining horizon to 84 deep ore zone. The Birchtree mine management and engineers designated two stopes in 84 lower ore zone for this study. The stope studied is located on level 3200, bearing stope id 952-1 was backfilled with 4 % (Potland cement and flyash in 30:70) CRF in September 2012. A typical level plan is presented in Figure 4-9 and a zoom in view of instrumented area is presented in Figure 4-10.

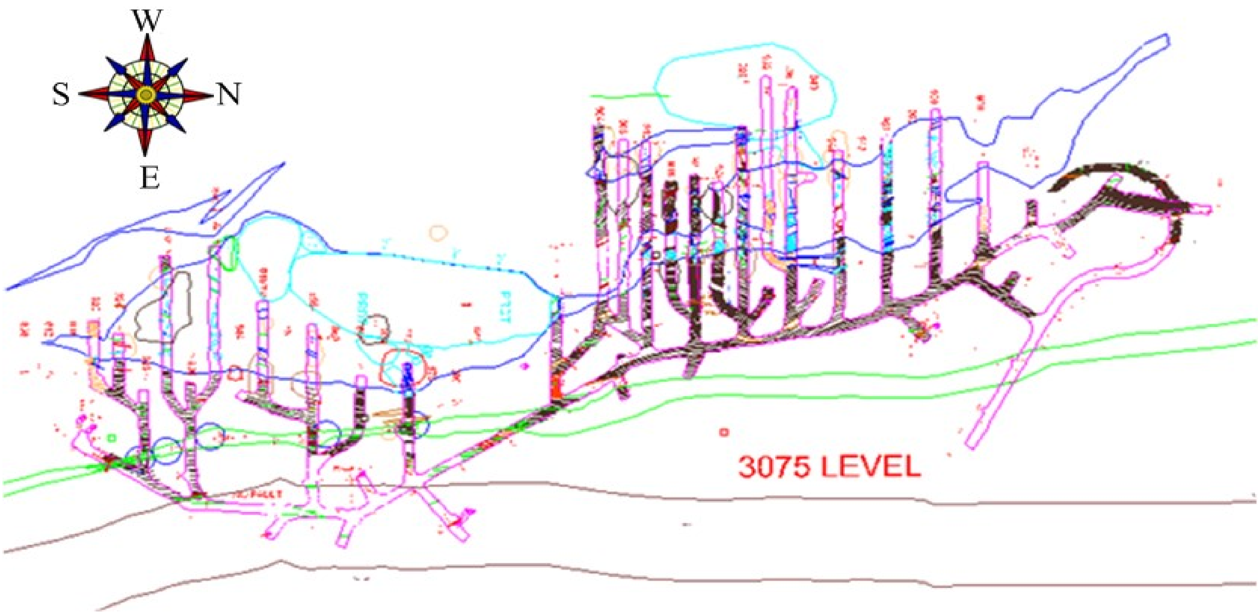

Figure 4-9 – A typical level plan at Birchtree

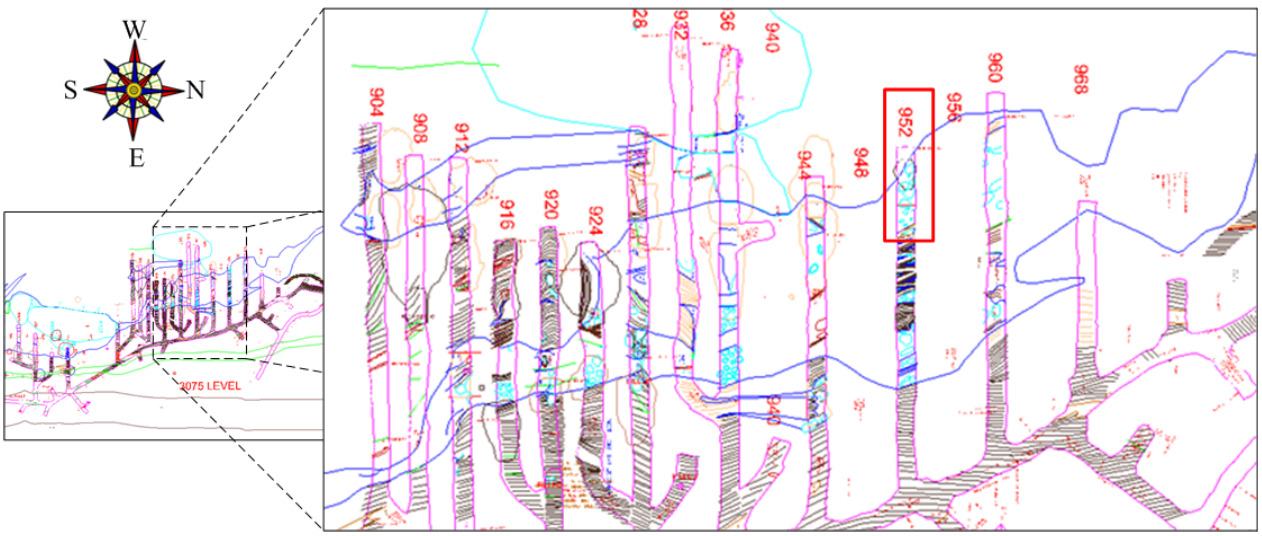

Figure 4-10 – Zoom in view of instrumented sill drift 32-952

Here 952 is the id designated to draw point based on northing and 1 designates extraction sequence while retreating from hanging wall to footwall. The stope 952-1 is a primary stope which was extracted in August 2012 using vertical block mining method explained earlier. The stope 952-1 was immediately backfilled in September 2012 with cemented rockfill. The backfilled stope 952-1 present right next to production stope 952-2, was instrumented with two geophones before blasting. The results and procedure of the instrumentation program is laid down in Chapter 5. The cavity monitoring survey was performed to check for any over-break or under-break and compute dilution levels from wall sloughage or backfill. The stopes 952-1 and 952-2 were later modelled with FLAC^{3D} software and CRF stope was assessed for stability using back analysis. The results of FLAC^{3D} are presented and discussed in detail in Chapter 6.

4.8 GEOMECHANICAL DATA

Several studies have been performed by the Birchtree mine engineering, Vale special services, and third parties to understand and assess the rock mechanics and post mining scenario. During such studies a series of laboratory tests have been conducted by third parties and research laboratories in Canada. The results of such testing were obtained during site visits and online collaboration with the mine. The results of geo-mechanical properties of ore and rock mass have been presented in Table 4-2. Rock cores were tested for unconfined compressive strength (σ_c), tensile strength (σ_t), young's modulus (E), Poisson's ratio (υ), friction angle (ϕ), cohesion (c) and density (ρ). Besides the above properties the rockmass was also characterized using rock mass ratings (RMR). The intact rock properties are converted into rockmass properties using Rocscience software named "RocData" which is embedded with conversion equations [149-152]. The rock mass is considered homogeneous and isotropic for this analysis. The rockmass properties are presented in Table 4-3. In-situ stress determination at Birchtree was carried out by Herget and Miles [153]. The results of in-situ stress tensor are extracted from the report and are presented in Table 4-4.

Table 4-2 – Geo-mechanical properties for intact rock of geological units at Birchtree

Rock type	ρ (g/cm^3)	σ_t (MPa)	σ_c (MPa)	E (GPa)	υ	RMR	ϕ (^{o})	c (MPa)
Sumx	3.49	10.63	67.00	51.70	0.30	60.51	13.71	19.56
Masu	4.54	4.48	74.14	58.25	0.25	-	-	-
Ultramafic	3.10	8.07	157.46	59.90	0.30	60.34	9.94	14.57
Biotite Schist	2.83	10.39	72.23	48.84	0.29	65.86	5.01	27.29
Quartzite	2.67	9.35	213.70	72.40	0.25	68.35	14.27	26.32
Amphibolite	2.97	9.67	101.00	102.90	0.27	-	-	-
Iron Formation	2.74	12.77	83.47	53.30	0.16	64.08	11.18	18.13

Table 4-3 – Rockmass properties for different geological units at Birchtree

Rock type	σ_τ (MPa)	σ_c (MPa)	E (GPa)	υ	c (MPa)	ϕ (^{o})
Sumx	0.19	9.51	32.70	0.30	5.39	43.0
Masu	0.25	11.78	39.30	0.25	6.14	43.5
Ultramafic	0.45	22.36	37.80	0.30	12.70	42.9
Biotite Schist	0.30	13.60	35.80	0.29	6.25	44.4
Quartzite	1.12	47.53	56.85	0.25	19.38	45.0
Amphibolite	0.29	14.34	65.00	0.27	8.12	42.9
Iron Formation	0.32	14.84	38.05	0.16	7.12	44.1

Table 4-4 – In-situ stress tensor magnitude at level 2750

Stress Tensor	Value (MPa)	Orientation
σ_1	31.60	Normal to ore body strike
σ_2	26.80	Parallel to ore body strike
σ_v	15.00	Vertical

4.9 SUMMARY

This Chapter presents an overview of the Birchtree mine, geology of Thompson Nickel Belt area and the Birchtree mine. This Chapter includes mining method, typical stope design and backfill system of the case study mine. Study problem has been discussed with the help of some backfill failure profiles. The location of studied ore zone and experimental stope location using typical level plans is presented. Geomechanical properties of different geological units at the Birchtree mine have also been presented with in-situ stress tensor values. The geomechanical data will be used for numerical modelling of backfill material.

5 IN-SITU BLAST VIBRATION MONITORING EXPERIMENT IN CEMENTED ROCKFILL

5.1 INTRODUCTION

Rock breakage with blasting produces seismic vibrations in ground that are termed as blast-induced vibrations. These vibrations are the part of the explosive energy transmitted through ground and was not used for fragmentation process. Major share of the vibrations produced during blasting are considered as waste product and they may damage structures at a certain level of magnitude and distance. During the blasting process some of the energy released propagates in all directions at different frequencies. The damping effect of materials and distance from a certain structure decreases the effect of blast vibrations and it has been observed that the frequencies are higher at shorter distances. The magnitude of ground vibrations is a product of multiple factors like quantity of explosive charge, compaction, characteristic of rocks, distance from the blasting site and geology of the region. Blast vibrations can be controlled by drilling and firing patterns. In a blasting process chemical energy is converted into fragmentation, but most of the energy converted is wasted away in the surroundings as ground vibrations, air-blast and fly rock. Air-blast and flyrock are not considered as major concern for underground mines. Generally ground vibrations from blasting in underground mines do not influence nearby surface structures, and are thus considered harmless. However, excessive ground vibration magnitude may lead to over-break in adjacent material and may lead to failure in hanging-wall, footwall and backfill, thus diluting precious ore. The blast vibration magnitude is classified in to two main types far field vibration and near field vibration. Far field vibration is the term used for vibration magnitude approaching a structure located relatively far away from the blasting site. Far field vibrations are generally a concern for the residents living nearby a surface mine or quarry. Mines are bounded by law to regulate the vibration levels to minimum for nearby structures and houses, by varying charge weight per delay and blast design. These regulations are established by using blast monitoring technique in tandem with charge weight scaling laws. Mining regulations for blast vibrations only limit the blast vibrations magnitude for far field vibrations. In the United States peak particle velocities and distance between blast source and structures are used to define the blast-induced vibration limits. A limit of 31.75 mm/s is valid at a distance of less than 91.4 meters. A limit of 25.4 mm/s is levied for distance range of 91.5 m to 1524 m. A maximum peak particle velocity of 19 mm/s is allowed for a distance above 1524 m [148] In Canada there are no laws governing blast-induced vibrations with exception of two provinces Nova Scotia and Newfoundland. Regulations 82.64 of Nova Scotia [154] and 19.437 of Newfoundland [79] for blast vibrations do not provide much detail on peak particle velocities and distance between structures and blast source.

Near field vibrations are defined as vibration magnitude approaching a structure situated in the near vicinity of the blast. Near field vibration levels are responsible for over break in nearby geo-materials. Notably there are no regulations laid down for near field vibration levels. The mines generally measure and derive some blast vibration limits to reduce loss of ore as a result of over-break due to excessive blast-vibration levels. Saharan (2004) [83] estimated that a peak particle velocity of 600 mm/s initiates failure in nearby rock. At the Birchtree mine blast vibrations are measured and studied frequently by Vale Manitoba blasting specialist termed as blasting audits. To perform a blast audit, blast-induced vibration monitoring devices, sensors and recorders are installed near the experimental area.

In order to assess a backfill under dynamic loading and to accommodate the effect of blast loading on backfill it is necessary to measure blast-induced vibrations in backfill. A blast vibration monitoring program is devised and geophones are installed in one of the CRF blocks. This aims to address the issue of dynamic loading on backfill due to blast vibrations. The results of vibrations in backfill can be correlated with cavity monitoring survey profiles in order to quantify backfill failure. Similar experiments will enhance the quantification of backfill failure due to blast-induced vibrations. Blast-induced vibration monitoring data obtained during this experimental program is later used as a FLAC3D numerical model calibration. The complete procedure of model calibration using blast vibrations is explained in Chapter 6.

5.1.1 Blasting Theory

Blasting is a process of achieving rock fragmentation by utilizing sudden combustion of chemicals. Detonation of explosives produces immense pressure inside the borehole, which crushes and pulverizes the rock as shown in Figure 5-1. This is followed by compressional stress shock waves having a velocity comparable to sonic velocity in rock are propagated through the rock medium. In the last step high gas pressure is developed which penetrates in fractured zones and is responsible for fragmentation [155]. Shock waves produced by blasting are compressive in nature and these waves are reflected from a free face and are transformed in to tensile stress. Reflection of these waves changes their nature to tensile stress wave which is basically responsible for coarse fragmentation. The coarse fragmentation is followed by the application of immense gas pressure breaking apart the larger fragments into smaller pieces. Figure 5-1 [155] presents the process of blasting an explosive in rock.

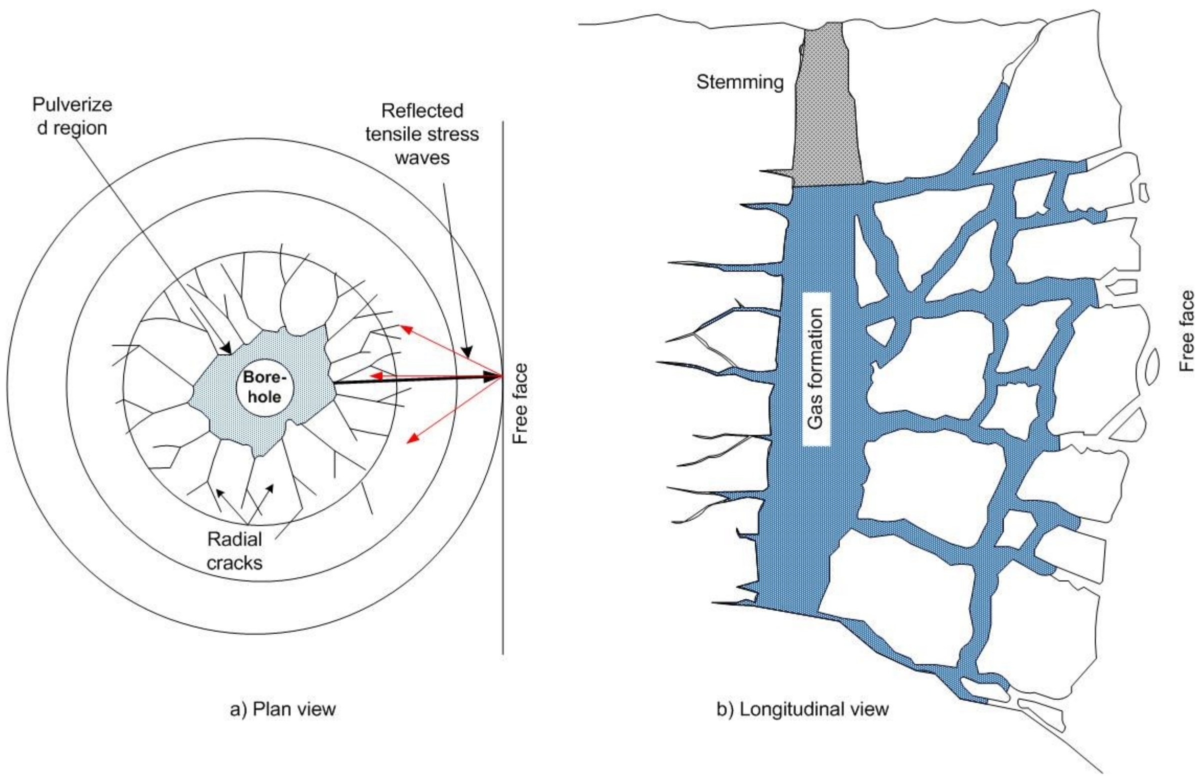

Figure 5-1 – Different zones formed around borehole during blasting [155]

5.1.2 Recommendations for Blast Monitoring – ISRM Suggested Method (1992)

Dowding [156] compiled ISRM suggested methods for blast vibrations monitoring in 1992. In this work it has been recommends that blast vibration monitoring should be performed with portable blast-vibration monitoring instrument only. Instruments for measuring mechanical vibrations are not good enough to measure blast-induced vibrations and thus must not be used blast vibration monitoring. Geophones must be installed on the structure or adjacent to structure. Preferably ground vibrations should be measured in terms of velocity history which is the conventional way of recording blast vibration data. Location of geophone installation varies with region throughout the world. In North America sensor is placed adjacent to the desired structure, in Europe sensor is installed on the structure foundation. If it is impossible to install the sensors on these locations then the most responsive structural member is used for installation of sensor. All three components of vibrations transverse, longitudinal and vertical must be measured, which enables the determination of dominant frequency along with peak particle velocities. Mounting of sensor is deemed to be the most critical part of vibration monitoring. Mounting a geophone on horizontal surface is the least critical when the expected acceleration from blast are less than 0.2 g. If the range of acceleration is between 0.2 g and 1 g then the sensor must be buried completely [157]. When mounting a sensor on concrete or rock, epoxy or quick setting cements should be used to fasten it. Sensors to be mounted on vertical surface should be bolted to the surface. The instruments to be used must be calibrated before installation. Two tri-axial instruments are recommended for blasts within a range of 100 m. Two geophones will be necessary for a thorough analysis of blast vibrations, but one tri-axial instrument will detect blast vibration levels if installed at a critical location. If there are two blasts separated by more than 100 m to be monitored then the minimum number of geophones must be four. Structural response has been classified as major, minor and threshold. Major is termed as permanent damage at high peak particle velocity, minor is term used for small superficial cracks and threshold is the term used when peak particle velocity magnitude only opens up cracks and dislodges loose material. It has been observed that a lower frequency range of 5-10 Hz affects the skeleton of the structure located far away from the site and a higher frequency damages the walls and floor of structures.

5.2 BLAST VIBRATION MONITORING IN BACKFILL

Blast vibration in backfill have been monitored and reported by Yu [5]. He [5] mounted geophones inside CRF stopes of sublevel stoping system, to test CRF for impact damage. The purpose of studying vibrations in fill was to determine vibration levels in fill from blasting. In the first step CRF was tested for vibrations from a sledge hammer (impact loading). It was found that 35% of the impact load could penetrate inside the CRF. The next step is to monitor blast vibrations in backfill and the results show that almost 70% blast vibrations transmitted inside backfill. It was concluded in the study that a ppv magnitude of around 300 mm/s damages backfill. Blast vibrations in CRF were also monitored at the Williams mine [158]. The geophones were mounted inside a drift driven through backfill at Williams mine. It was found that CRF received blast vibrations with a peak particle velocity of 170 mm/sec. Gool [20] installed five tri-axial geophones to monitor the blast. Four geophones were installed in backfill and one of them was installed in rock. To install the instruments the mine excavated a 20 m long drift inside paste fill. The aim was to monitor blast vibrations in fill for studying the dynamic response of fill due to blast loading. The results of blast vibration monitoring were utilized for 2D dynamic numerical model calibration. The analysis by Gool [20] showed that a peak particle velocity of 250-350 mm/s initiates failure in backfill. It was also found that blast vibration penetration in backfill was within 55 – 85 %.

5.3 SITE SELECTION AND LOCATION

The Birchtree mine management and engineers designated two stopes in 84 lower ore zone for this study. The CRF block studied is located on level 3200 bearing stope id 952-1. Here 952 is the id designated to draw point and 1 designates extraction sequence. The stope 952-1 is a primary stope which was extracted in August 2012 using vertical block mining method explained earlier. The stope 952-1 was immediately backfilled after extraction in mid-September 2012 with cemented rockfill. This stope was provided for blast vibration monitoring study by the Birchtree Mine management. The block was instrumented with two geophones before blasting secondary stope 952-2 right next to the stope 952-1.

5.4 TYPICAL BLAST DESIGN AT BIRCHTREE

The Birchtree mine practices vertical block mining method (VBM) which is a variation of sublevel stoping method. VBM stope production is carried out in three or four blasts or lifts. Before blasting the stope, large diameter hole termed as the raise bore is drilled in the block. This is generally drilled to develop a free face for facilitating blasting process and this hole remains unoccupied. All the other blast holes are blasted while slashing inside the raise. There are three blast lifts and each lift is blasted and mucked one after the other. Once the stope is completely extracted, it is filled with waste material known as backfill. The bottom of the stope is blasted first followed by middle portion and at last the deck is blasted as shown in Figure 5-2.

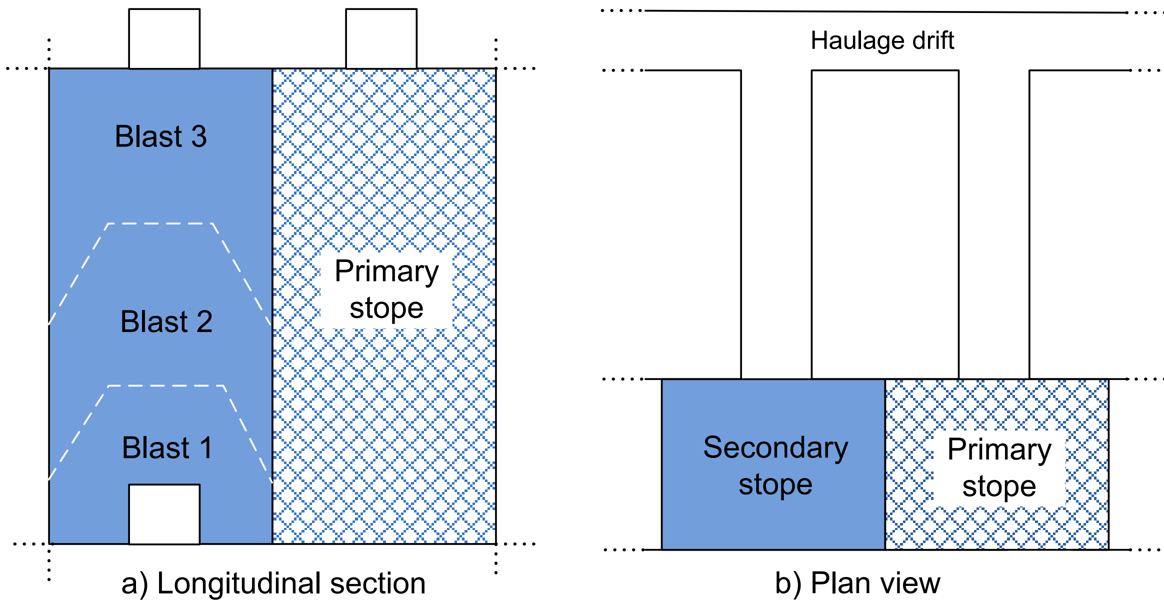

Figure 5-2 – Vertical block mining method

Stope drilling starts with drilling of a large diameter (ψ=1.07 m) raise bore followed by regular drilling of regular blast holes having smaller diameter (ϕ= 0.114 m) in a fan pattern to host explosive for blasting. During blasting of each lift the raise bore is used as a free face and blast holes are slashed in the raise bore. A typical blast design layout at the Birchtree mine was studied during the analysis of blast vibration monitoring in CRF. The studied block was located at level 3200 selected by the Birchtree mine. The block id was 952-2 and the stope type was S – 1 stope (sharing only one side with CRF). The details of blast layouts, blasting sequence etc. for all three blasts are presented in the following sub-sections.

Ammonium nitrate and fuel oil (ANFO) with a trade name of AMEX is used as a prime explosive. AMEX_LE is a trade name given to lower energy ANFO with strength 40% less than the standard ANFO, LE stands for low energy. AMEX_LE is employed to reduce over-break in poor ground conditions. ANFO is a primer sensitive explosive and at Birchtree uses DynoNoble cap sensitive explosive as a primer. The primer is initiated with nonel (non-electric) shock tube initiation system with IKON detonators. The shock tube initiation system detonators are state-of-the art pre-programed devices for a certain delay having specific fourteen digit mac-address. The nonel shock tubes are connected to junction box, present at every level. The junction box is connected to the main blasting box present on surface. The blasting box is linked to a phone line and a computer. Blast is initiated by a computer program which calls the blasting box to initiate the blasting process. The blasting box controls blasting sequence at the time of blast. At Birchtree the blast is centralized and is initiated from the surface, and it is ensured that there is not a single person inside the mine at the time of blast. Production blasting leads the blasting sequence followed by any developmental blasting. ANFO, primer cartridge and nonel shock tube are presented in Figure 5-3.

Figure 5-3 – Explosives used at the Birchtree mine

5.4.1 Blast 1

Blast 1 is generally the smallest blast in terms of explosive used and volume of rock blasted. It is the first to be blasted. As a conventional way of blasting at Birchtree a slot raise bore was drilled through block 952-2. Unfortunately the raise bore drilled was collapsed due to poor ground conditions. Second raise bore was drilled adjacent to the first one, to be used as a free face during blasting. Blast 1 has 15 blast holes, having different firing sequence. A total length of 135 m was drilled and drilled holes were loaded with explosive. The blast holes were charged with a total of 1219 kilograms of explosives. The estimated tonnage from this blast was 1155 tons. Calculated powder factor for this blast was 1.06 Kg/ton (2.32 lb/ton). A layout of blast holes and slot raises at level 3075 are presented in Figure 5-4.

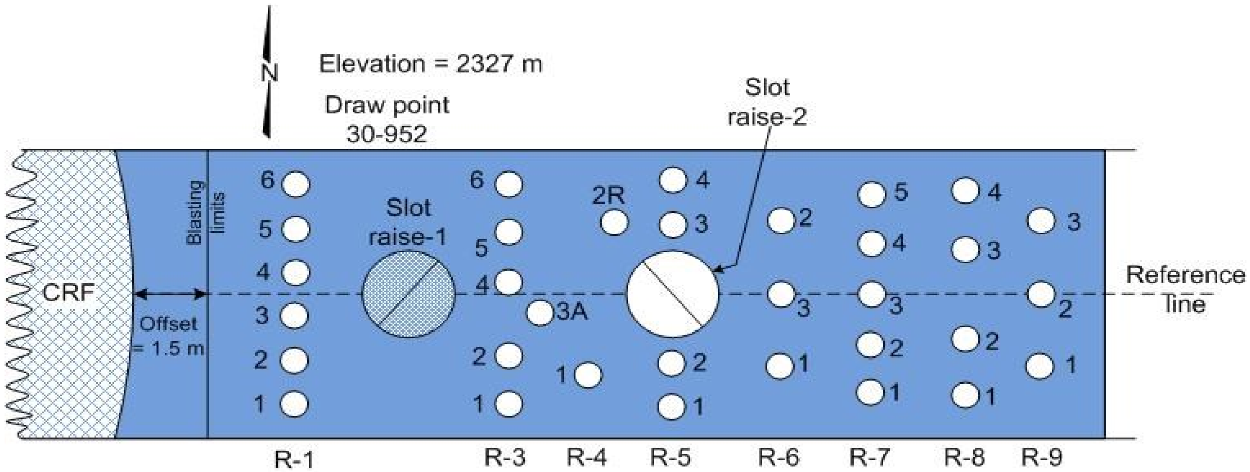

Figure 5-4 – A layout of blast holes and slot raises drilled for blasting block 32-952-2

It can be seen that there is a 1.5 m offset between the CRF and blasting limit due to poor ground conditions. In block 32-952-2 there are two offset blast holes located in rows 3 and 4, with ids 3A and 2R respectively. The blasting sequence is very important for an efficient blast and to reduce over-break in surrounding rock materials. Efficient blasting practices lead to better fragmentation and lesser over-break. Improper blasting sequences leads to wastage of energy as ground vibrations. The blast hole firing sequence is presented in Figure 5-5. Notably most of the blast holes were not charged and only fifteen holes were charged and blasted. The blast holes spacing is changed because of the fan pattern. The vertical section presenting expected ground break as a result of firing sequence is presented in Figure 5-6. The Layout presented shows that the sequence employed enabled slashing the blast holes in the raise. The raise bore has been efficiently used for the case of blast number 1. It can be noticed that the ore is sitting on top of the rock for this block and blast 1 is intended to remove as much rock as possible. A vertical section of 32-952 stope is presented in Figure 5-6. The two raise bore holes are also presented along with the blast-hole rows. The Figure also presents the location of ore and blast-1. It is clear from the Figure that Blast 1 is employed to blast away unnecessary rock to access ore zone on top of rock.

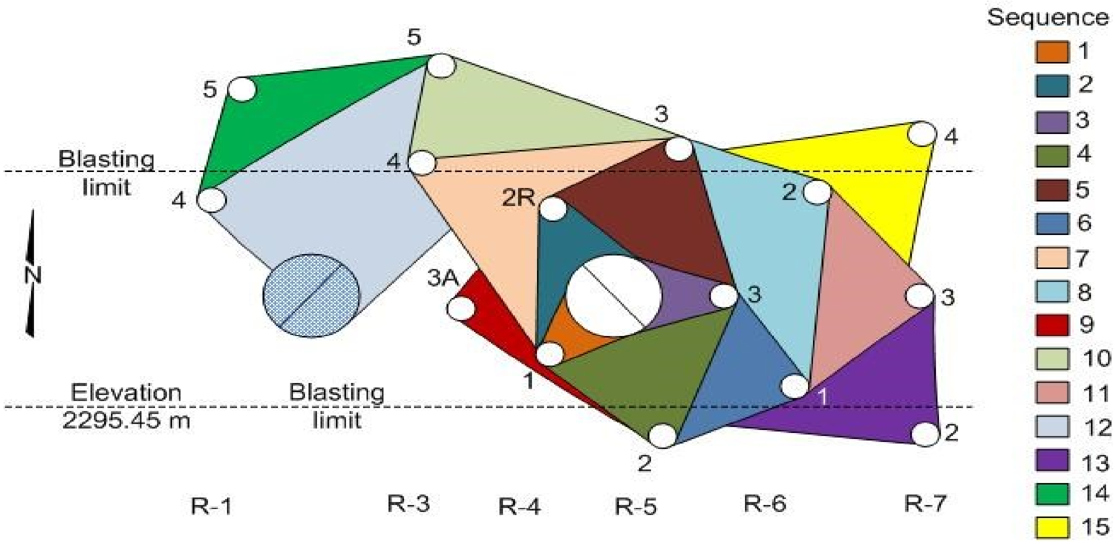

Figure 5-5 – Layout of blasting sequence and intended blast area for blast-1

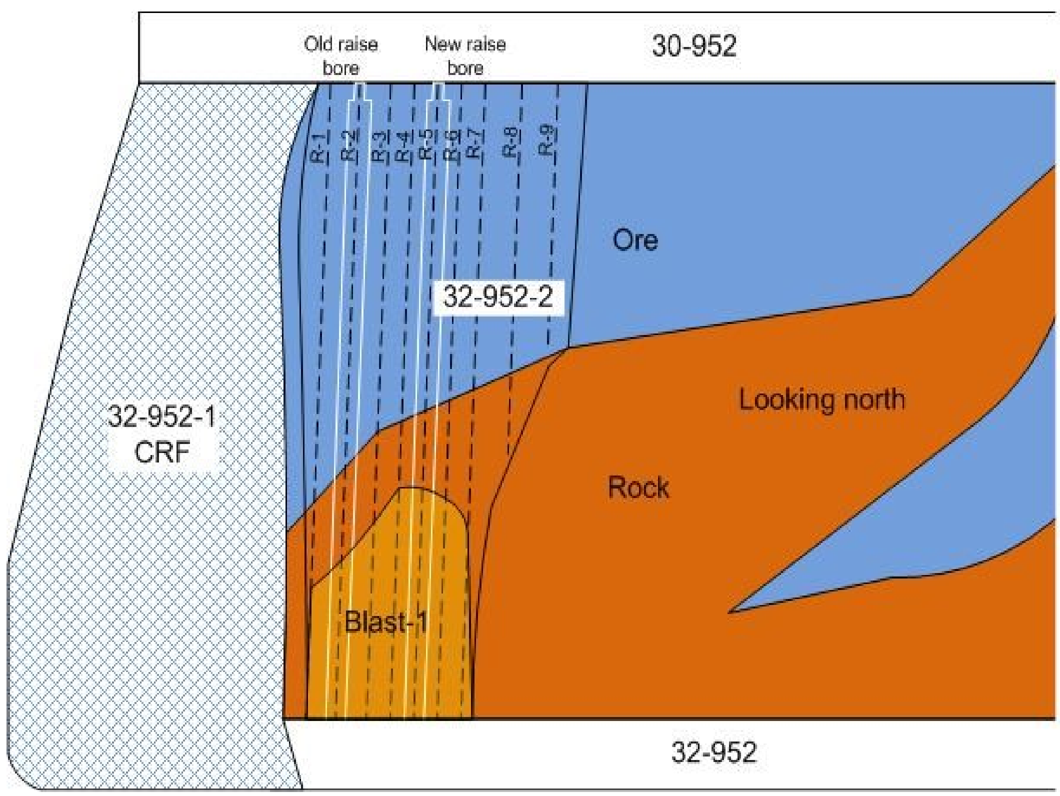

Figure 5-6 – Vertical section of stope 32-952 presenting intended blasting area for blast-1

5.4.2 Blast 2

Blast 2 is generally an intermediate blast in terms of explosive quantity and volume of blasted rock. It is the second blast in sequence of extraction. Slot raise bore and blast holes drilled earlier for blast 1 are generally utilized again for the second blast only if they are in good condition. The holes are reamed in case any of them are collapsed during blast 1. For the case of blast 2 there were only a couple of blast holes to be re-drilled. The holes were reamed and then charged with ANFO. Blast 2 comprised of 21 blast holes, having different firing sequences. A total length of 271.9 m was loaded with explosive. The blast holes are charged with a total of 2481 kilograms of explosives. The estimated tonnage from this block is 3304 tons. Calculated powder factor is 0.75 Kg/ton (1.65 lb/ton) for the second blast. The layout of blast holes and slot raises at level 3075 is presented in Figure 5-4. The expected ground break with respect to following sequence is presented in Figure 5-7. Notably most of the blast holes were charged for blast 2 (21 holes were charged and blasted, out of 32 holes). The blast hole spacing has been changed from Figure 5-4, because of the fan pattern and drilling deviation. The Layout presented in Figure 5-7 shows that the sequence followed enabled slashing the blast holes in the raise. The raise bore has been effectively utilized for second blast as well. A vertical section of stope 32-952 is presented in Figure 5-8 displaying intended blast area for blast-2. It can be seen from the Figure that Blast 2 is removing away some of the unnecessary rock as well to make room for the ore sitting on top. The removal of rock will enable access ore zone and rock removed with this blast will be mucked with ore and is considered as planned dilution.

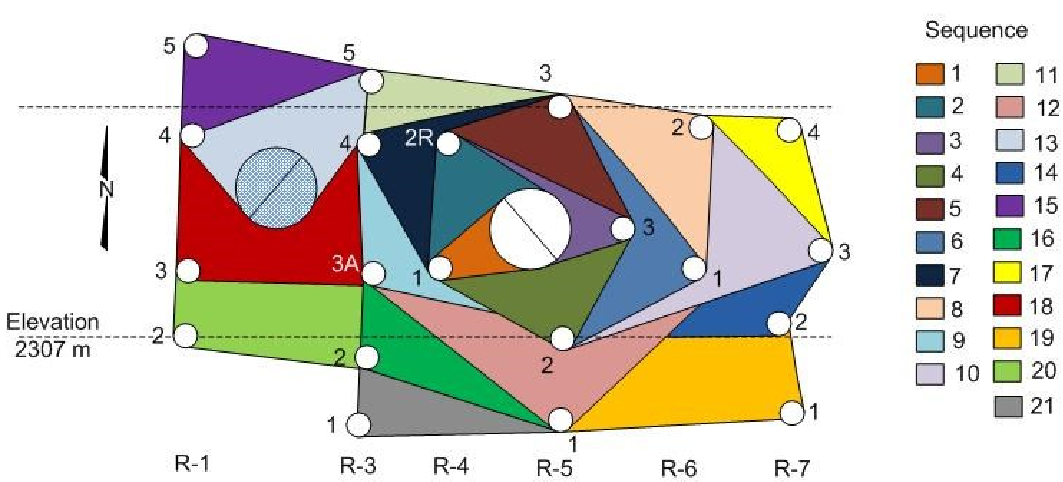

Figure 5-7 – Layout of blasting sequence and intended blast area for blast-2

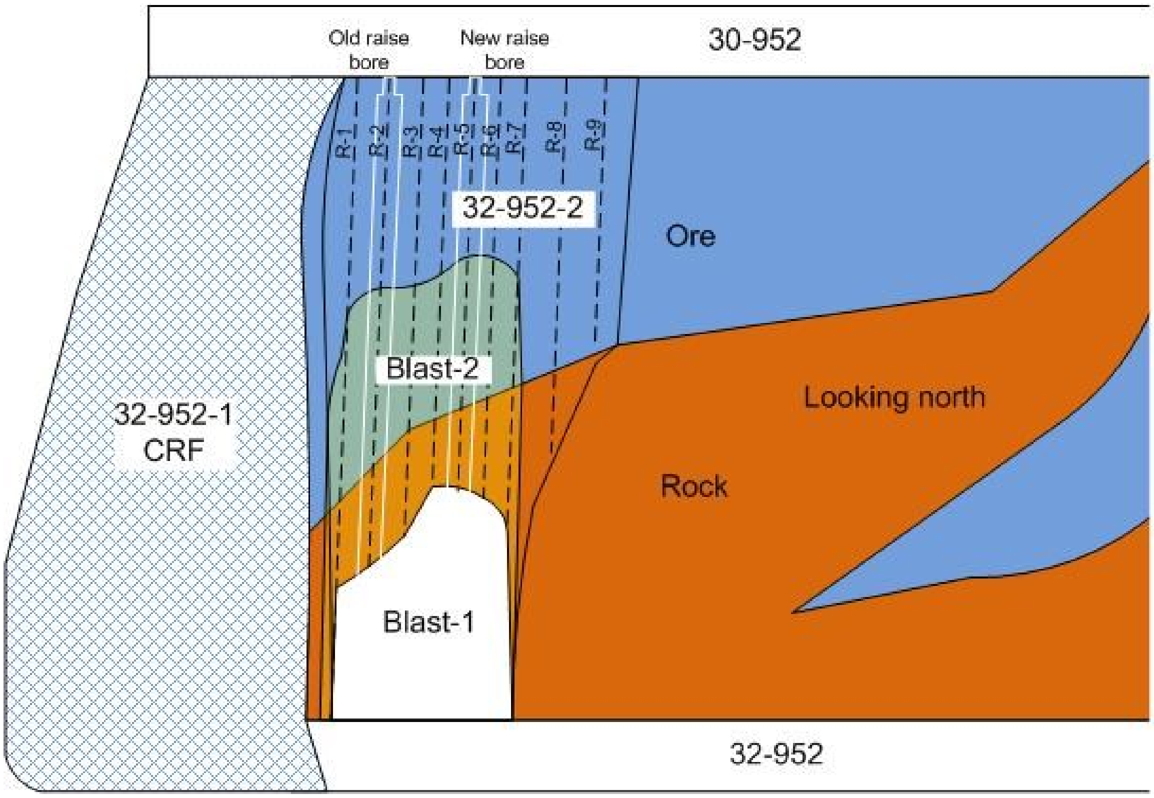

Figure 5-8 – Vertical section of stope 32-952 presenting intended blasting area for blast-2

5.4.3 Deck Blast or Blast 3

In terms of explosive quantity and volume of blasted rock blast 3 is the largest amongst the three blasts. It is the third blast in sequence of extraction and is termed as a deck blast. Slot raise bore and blast holes drilled earlier for blast 1 and 2 are utilized again for the third blast. The holes are reamed once more, in case any of them are collapsed during blast 1 or blast 2. For the case of blast 3 of block 32-952-2 there were only a few blast holes blocked. The holes were reamed and then were charged with regular and low energy ANFO. A total drill hole length of 349.3 m is then loaded with explosive. The blast holes are charged with a total of 3181.4 kilograms of explosives. The estimated tonnage from this block is 5404 tons. Calculated powder factor was 0.591 Kg/ton (1.30 lb/ton). Notably the powder factor has been reduced as there are more free faces available. Refer to Figure 5-4 for the complete layout of blast holes and slot raises at level 3075. Figure 5-8 presents blasting sequence of charged holes. Majority of the blast holes were charged for blast 3 (a total of 29 holes were charged and blasted, out of 32 holes). The blast hole spacing has been changed from Figure 5-4, because of the fan pattern and drilling deviation. The Layout presented in Figure 5-9 shows that the sequence followed enabled slashing the blasted rock in the raise. The raise bore has been effectively utilized once again for the third blast. A vertical section of stope 32-952 is presented in Figure 5-10. The Figure presents the intended blast area for blast-3. The two raise bore holes are also presented along with the blast hole rows. Figure 5-10 also presents the blasted areas from blast 1 and 2, and the intended blast area of blast 3 or the deck blast. It can be seen from the Figure that Blast 2 is removing away some of the unnecessary rock to make room for the ore. The removal of rock will enable LHD access to ore zone.

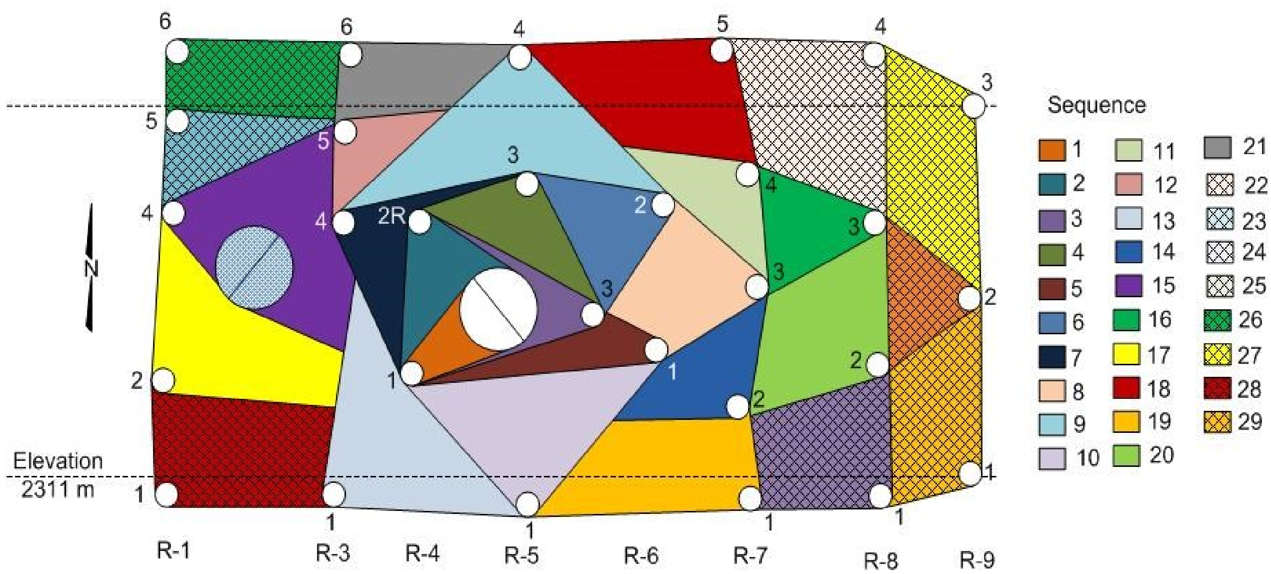

Figure 5-9 – Layout of blast 3 showing the intended area to be blasted by each hole

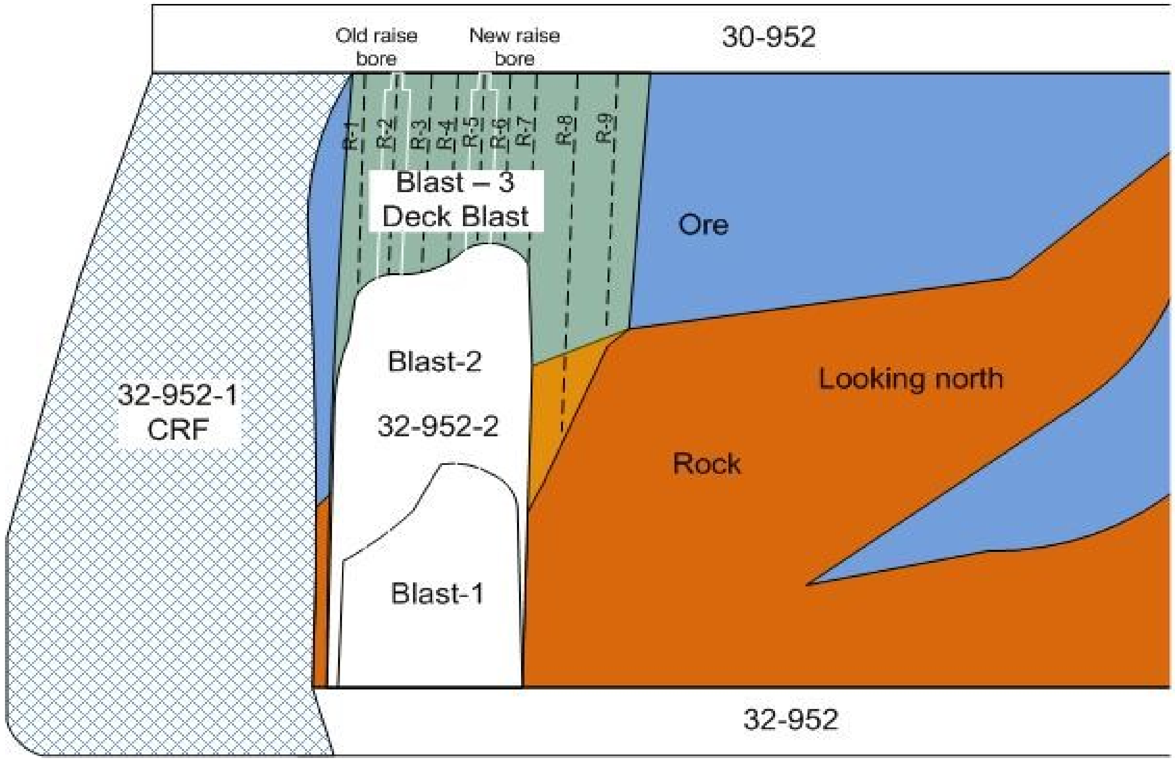

Figure 5-10 – Vertical section of stope 32-952 presenting intended blasting area for blast-3

5.5 BLAST MONITORING EQUIPMENT

ISRM Suggested Methods [156] guidelines were used for selecting a blast monitor. The blast monitoring equipment consists of a transducer which can convert physical motion into electric signal. The signal is transmitted through cables to an amplifying unit and the signal is recorded on a digital computer disc, which can be connected to a computer for data transfer. Two Instantel's Minimate Plus monitors with 4 channels (series III) are used for blast vibration monitoring program in backfill. One of the monitors is connected with 3D borehole geophone installed inside CRF. The other monitor was connected with regular 3D geophone for monitoring the blast induced vibrations on the surface of CRF. Minimate Plus, has a capability of measuring low range vibration levels (0 to 30 mm/sec) and high range vibration levels (>31 mm/sec). Low range vibration levels were selected when measuring blast-induced vibrations in CRF. This is because it is a common belief that CRF receives low magnitude of vibrations due to low coupling of CRF and rock at rock/CRF interface. The interface reflects most of the vibrations back in the rock. A FLAC^{3D} preliminary model was applied with simulated blasting load to find the position for installation of borehole geophone. The borehole geophone is selected because of the initial assessment done using FLAC3D and due to the ease of mounting it inside a borehole deep inside CRF. The regular geophone was mounted on top of the CRF with concrete and was bolted as well to achieve maximum coupling. The blast vibration analysis is performed with the help of blast vibration advanced software. The software enables analysing wave forms and it determines Peak Vector Sum (PVS) and Fast Fourier Transmission (FFT) for further analysis.

5.6 EXPERIMENTAL SETUP

A total of four geophones are used in the experiment for monitoring blast vibrations, two of them are mounted in CRF and rest of the two are mounted on drift wall on rock. Three (6” diameter) boreholes are drilled in CRF and cased with poly vinyl chloride (PVC) pipes to increase the stand-up time of CRF, two of the holes are used for mounting geophones and third one is drilled, in-case one of the holes collapses. The boreholes drilled have a depth of 2 meters and are drilled 3 meters away from ore/backfill interface in CRF. Two of the boreholes are used for mounting borehole geophones. To mount the borehole geophone, some concrete is initially placed in borehole to prepare a horizontal platform for geophone. Then the geophone is placed at a depth of 1.3 meters in CRF and concrete was slowly poured. In the next step PVC casing of borehole was pulled out in order to attain maximum coupling with CRF. The rest of the two boreholes are also filled with concrete, and PVC casing is pulled out. One of the other drilled holes filled with concrete is used for mounting a regular geophone with the help of a nut and bolt. Two additional geophones are also mounted for monitoring the second blast at the left and right drift wall surfaces using the nut, bolt and resin. The results from geophones on walls of sill drift confirmed that the geophones are installed inside the CRF. A horizontal (4” diameter) hole was also drilled through the right wall of sill drift to adjacent sill drift. This was done to house geophone cables and securing monitoring instruments in a safer place during the blasting process. The experimental setup is presented with the help of a schematic in Figure 5-11. Figure 5-12 presents borehole geophone and its installation on site. The arrow on top of geophone facilitates the orientation of 3D geophone with respect to blast.

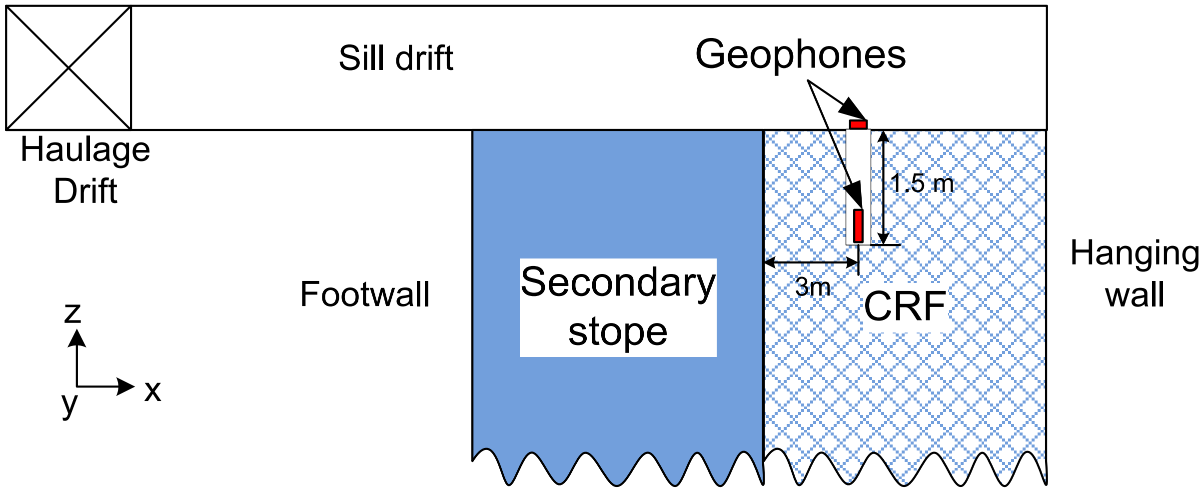

Figure 5-11 – Schematic showing the blast vibration experimental setup

Figure 5-12 – Experimental setup for blast vibration monitoring in CRF

After instrumenting the stope the blast monitors are programmed for automatic switch on and off such that the instruments switch on before blast and switch off after blast. This was accomplished because the Birchtree mine has a central blasting system initiated from surface blast box. The mine management do not allow any personnel inside the mine during a blast for safety reasons. Production blasting is the first in sequence followed by developmental blasting. Blasting is generally performed at the end of every shift that is at 6 am and 6 pm. After blasting each lift, the monitored data was downloaded into a computer on mine site.

5.7 RECOVERY OF GEOPHONES

Right after the blast, a ventilation check is performed by the next shift, the area is cleared, stope mucking is performed. When the stope is empty, cavity monitoring survey (CMS) from top sill drift is performed. CMS surveys generate a stope profile which indicates blast performance. The stope is then backfilled with cemented rockfill and was cured for 28 days. An attempt for recovery of geophones was made when CRF block 32-952-2 was completely cured. An initial site survey showed that the back of the sill drift had remained stable. It was decided to dig out both the geophones and use them for another experiment. The regular geophone mounted on surface of CRF was successfully recovered using a wrench and little hammering. Unfortunately, the borehole geophone could not be recovered and was lost in the experiment.

5.8 RESULTS

The selected ore block bearing id 952-1 is located at level 3200. The adjacent stope with id 952-1 is blasted in three blasts lifts as explained in Section 5.5. The first blast is carried to remove the rock from the lowest portion of the block to access ore. The lowest portion is the smallest with approximately 2700 tons of rock. The second blast is conducted after two days which was planned to yield to a total of 3300 tons of ore and planned rock. The third blast also termed as deck blast was conducted after four days from the first blast and a total tonnage of 5400 tons was acquired from deck blast. The geophones were installed and monitors were set prior to blasting before all three blasts. The monitored results are downloaded right after every blast. The results are analyzed using advanced blasting software "Blastware" by Instantel Canada. Blastware software with analysing dongle is used to process, understand and analyse blast vibration data. The software can perform functions like vector sums, Fast Fourier Transformation, differentiate, integrate, scale, add and subtraction on wave forms. Peak vector sum of the three components of blast load has been used to present results. The results of monitoring blast 1 showed that peak particle velocities of individual components of velocity are recorded to be 24.3, 25.4 and 24.1 mm/s by longitudinal, vertical and transverse channels respectively. Vector sum (VS) values of the first blast are computed using blastware software. The vector sum of blast 1 was computed and results are presented in Figure 5-13. It can be seen from the Figure that peak vector sum of blast 1 is 33 mm/s observed within CRF at a perpendicular distance of 27 m from blast. There are five other peaks approaching 30 mm/s mark. The blast vibration magnitude observed is comparatively small from the past studies on backfill, as this magnitude is way below the damaging magnitude. The total length of blast was 2 seconds. Notably the greater velocity is recorded for the first few blast holes, because there are very few free faces available and much of the blast vibrations are wasted.

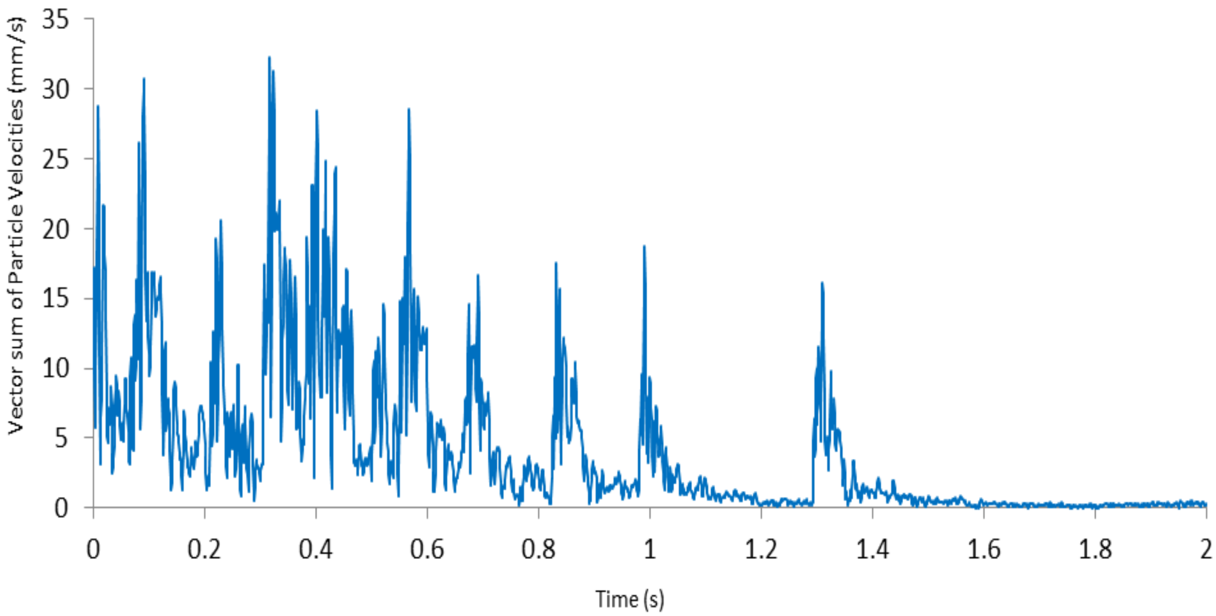

Figure 5-13 – Vector sum of longitudinal, transverse and vertical components of blast 1

The results of monitoring blast 2 showed that peak particle velocities of individual components of velocity are recorded to be 49.5, 72.6 and 50.0 mm/s by transverse, vertical and longitudinal channels respectively, at the observational point in CRF. The vector sum of blast 2 was computed and results are presented in Figure 5-14. From the Figure it can be seen that peak vector sum of blast 2 is 85 mm/s observed within CRF at a perpendicular distance of 18 m from blast. It can be noticed that a total of three peaks crossed 60 mm/s. The peak particle velocity measured is again very low level and it cannot damage CRF stope as much higher magnitude of vibration is required for initiation of failure. The total duration of blast was found to be 2.8 seconds. It can be seen that the few initial blast holes produced more vibrations than the others because of lesser free faces available.

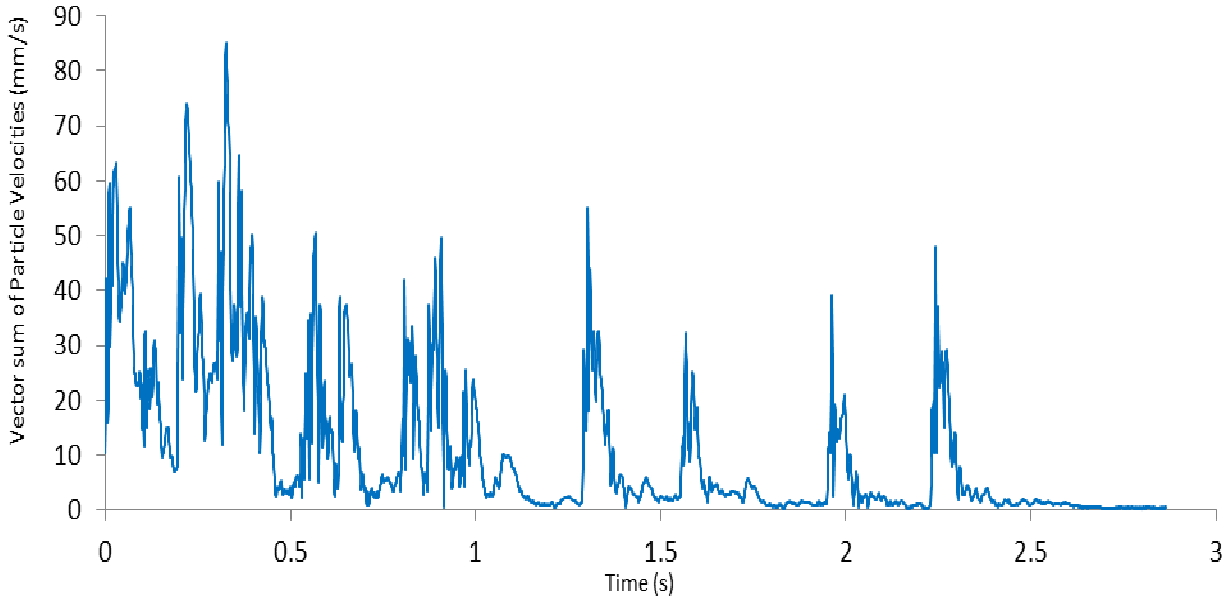

Figure 5-14 – Vector sum of longitudinal, transverse and vertical components of blast 2

The third blast or deck blast was also recorded by the geophone installed in CRF. The results of monitoring blast 3 showed that peak particle velocities of individual components of velocity are recorded to be 266.7, 259.1 and 267.97 mm/s are recorded by the transverse, vertical and longitudinal channels respectively, at the observational point in CRF. A complete event report for blast 3 was also generated with Blastware software. The vector sum of blast 3 was computed and results are presented in Figure 5-15. From the Figure it can be seen that peak vector sum of blast 3 is 425 mm/s observed within CRF at a perpendicular distance of 10 m from blast. It can be noticed that all the eight major peaks are approaching 300 mm/s and over, and most of these are being initiated from the holes closer to CRF. The total time duration is found to be 2.8 seconds for the third blast, The blast vibration magnitude is very high according to the observations of Gool [20] and Yu [5] who suggest backfill failure around the ppv magnitude of 250 mm/s and 300 mm/s respectively.

The cavity monitoring survey profile of the stope is not presented in this work because the CRF stope monitored for this research is not exposed to stabilize the CRF. The stope is under blasted and no failure is observed, although the blast vibration magnitude is very high.

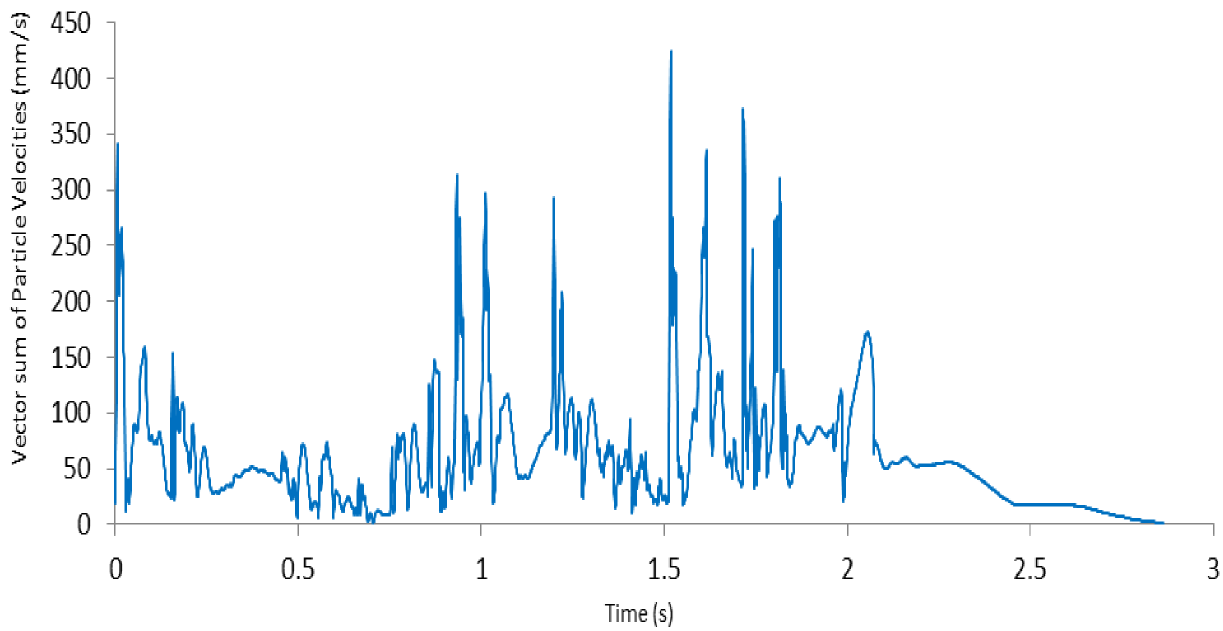

Figure 5-15 – Vector sum of longitudinal, transverse and vertical components of blast 3

PPV in rock are also recorded for blast 2 and it is found that a very low magnitude of vibrations transfers through the CRF/rock interface. Figure 5-16 presents a comparison of peak particle velocity measured in rock and CRF for the blasting sequence presented in Section 5.5. As can be seen only 18 to 30 % blast vibrations are transmitted inside backfill. This confirms the installation of geophones in CRF.

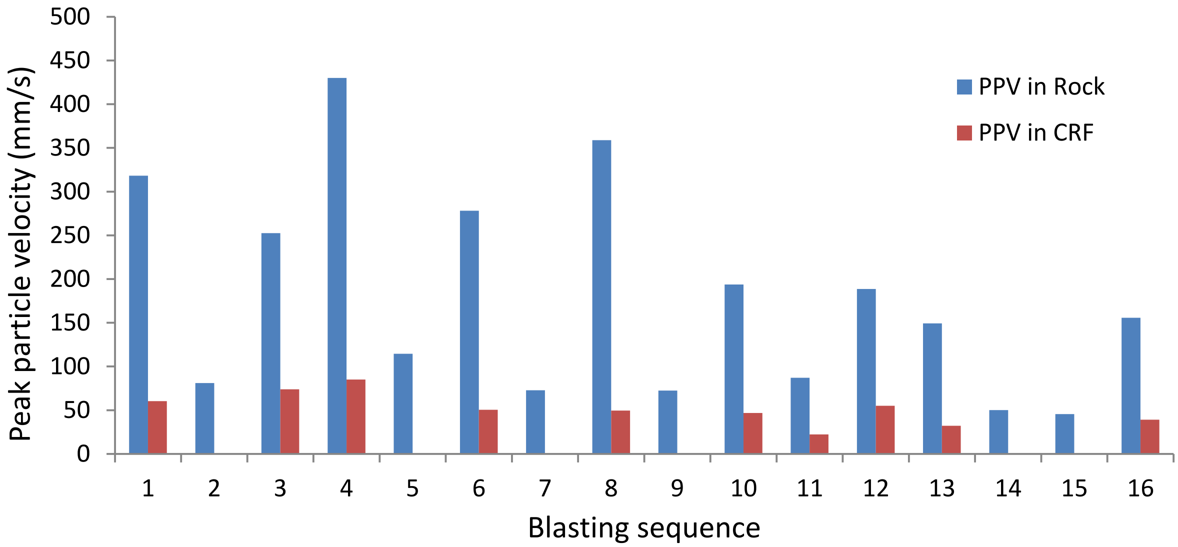

Figure 5-16 – Comparison of peak particle velocities in rock and CRF

5.9 SUMMARY

In-situ blast vibration monitoring experiment for cemented rockfill study is extremely useful to quantify blast loading on CRF. This Chapter presents a detailed review of blasting theory and blast monitoring in mines. ISRM standard monitoring guidelines are laid out in this Chapter. Past studies on blast monitoring in backfill have also been reviewed. Experimental setup and location for blast vibrations monitoring in CRF are also discussed. Blast design has been studied. Blast monitoring equipment and sensors is also included in the discussion. The results obtained have been discussed in the later part and it was found that the CRF is bearing maximum vibration levels of around 425 mm/s. Maximum peak particle velocities of around 268 mm/s were observed for all the three channels. Some of the limitations of the experimental program were unavailability of experimental blocks, cost of experimental program and data validation. Data validation is covered by mounting a regular geophone within 1 meter perpendicular distance and the results are correlated. It is found that the two geophones produced similar results. Two geophones installed in drift walls also helped comparing velocities in rock and CRF.

6 BACKFILL FAILURE CONTROL STRATEGIES

6.1 INTRODUCTION

Limit equilibrium methods for backfill design also known as the fill strength requirement (FSR) models [9] are extensively used for designing backfill stopes. These methods provide a good estimate of static strength requirements by backfill. FSR models consider limited factors influencing stability of fill including stope dimensions, density of fill, cohesion of fill, mining depth and horizontal to vertical stress ratio. Unfortunately the current approach does not quantify the amount of dilution when the backfill is exposed to production blasting in adjacent stope. This is because all parameters incorporated in FSR design methods certainly affect over-break but these models represent overly simplification of a complex condition. To address this problem available data from case study mine in combination with numerical modelling is used to adjust these generalizations to specific conditions. An intelligently fine-tuned model can be of great benefit and it allows mine planners and operators to anticipate future challenges. This Chapter presents numerical modelling setup for the second dynamic model, including numerical model calibration, using the blast-induced vibrations and in-situ stresses, selection of failure criteria and discussion of numerical modelling results. The model validation process encorporates a third FLAC3D dynamic model, in which an equivalent cavity concept is used to determine the damping coefficient and blast vibration distributions to be applied on walls of CRF. The numerical modelling study is followed by a detailed investigation on backfill dilution control.

6.2 NUMERICAL MODELLING SETUP FOR SECOND DYNAMIC MODEL

Numerical model is prepared using ITASCA's finite difference software FLAC^{3D} with dynamic option. The primary and secondary stopes adjacent to each other have been created with fine mesh and rest of the mesh is graded for reduction in solving time. The stope size is extracted from mine plans and the size of stope modelled have a length of 18 m, a width of 12 m and a height of 34 m. The zone modelled comprise of Biotite-Schist in footwall, Peridotite and Ultramafic as ore with significant grade and hanging wall as quartzite. Zones with a thickness of five centimeters surrounding primary stope are created to simulate an interface between rock and CRF, when it is in place. The properties of interface zones and CRF used for this work are presented in Table 3-1. The rock material and CRF are considered as homogeneous and isotropic for this analysis. A small gap of 1 meter on top of backfill is also modelled to limit stress load transfer from and to the top of the backfill. After setting boundary conditions and material properties, the model is solved for equilibrium using linear elastic constitutive model. Rockmass properties for footwall (FW), hanging wall (HW), ore and CRF used for this work are presented in Chapter 4. In-situ stress tensor values at a depth of 840 meters (2750 level) are also presented in Chapter 4. Notably, the horizontal to vertical stress factor K that accounts for tectonic force in the model is accommodated from in-situ stress tensor values obtained from the case study mine. The newly developed boundary traction method by Shnorhokian et al. [159] is used to obtain the stress tensor values inside the model. In this method the model boundaries are kept free and low level compressive stress is applied on face of model boundaries, the load is adjusted by trial and error to obtain the required stress level. Linear-elastic constitutive model is employed and the model is solved for approaching equilibrium initially. The numerical model is then solved with elasto-plastic constitutive model (Mohr-Coulomb) to attain equilibrium conditions. Once equilibrium state is established the stope mining and backfilling sequence is followed. The CRF and other geomaterials are modelled as Mohr-coulomb material for this analysis. The CRF material is assumed to be homogeneous for this analysis. The properties of CRF are extracted from the in-situ measurements and tests conducted by Yu and Counter and Yu [5, 8]. The CRF is assumed to be homogeneous material for this analysis. The stope mining sequence at Birchtree is shown in Figure 6-1. As can be seen, a primary stope is mined out in the first stage, followed by backfilling it. In the next stage secondary stope is extracted and primary backfilled stope is exposed to production blasting. Failure condition for the analysis is described in detail in Chapter 3.

The failed CRF stope and adjacent stopes are constructed at the same location and depth. Model boundaries are constructed ten times the dimensions of excavation in order to diminish the effect of excavations and absorb dynamic pulse to be applied at a later stage in the model.

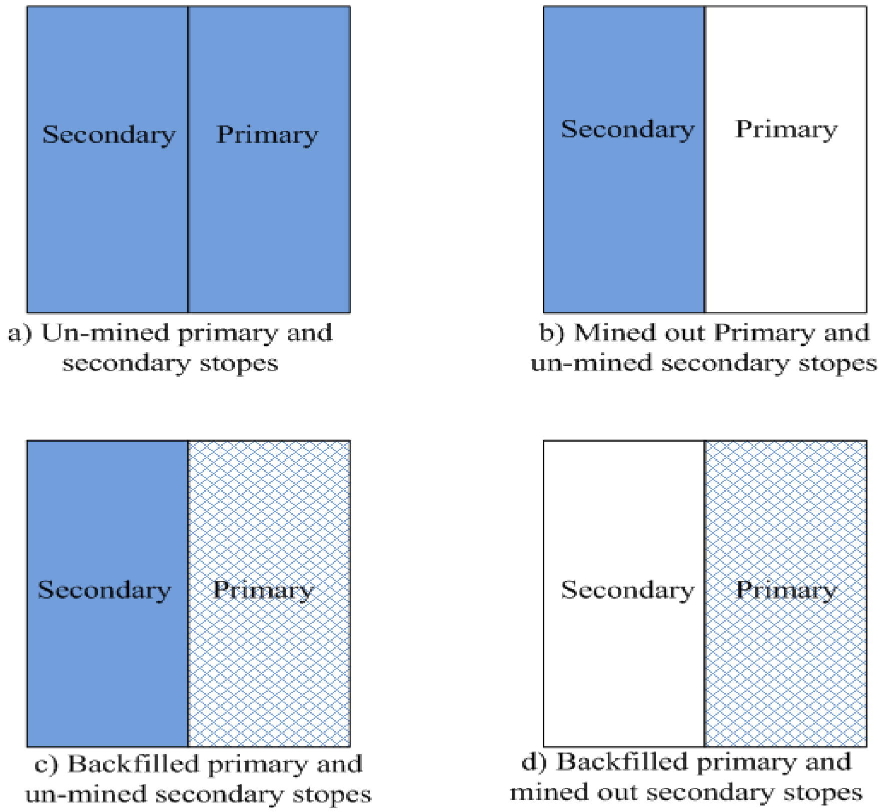

Figure 6-1 – Mining sequence used for the model

6.2.1 ASSUMPTIONS

Some of the assumptions used in modelling the backfill material include considering the geomaterials to be isotropic-homogeneous. In reality geomaterials can be heterogeneous and anisotropic. The direction of the minor principal in situ stress tensor value has a plunge of 75 degrees on site. The minor principal stress tensor value is considered vertical for this analysis.

6.2.2 MESH SENSITIVITY ANALYSIS

Mesh sensitivity analysis is performed for greater precision and accuracy of mesh. For sensitivity analysis the mesh is constructed with different mesh densities (50 thousand to 200 thousand zones). A stope 18 m x 12 m x 34 m opening is mined, and model is solved for different mesh densities one after the other. After solving the model the mesh displacements are observed at the center of stope walls. The process is repeated again and again until relatively consistent displacement values are obtained. Numerical model mesh selected for this analysis contained 135,000 zones and the backfill stope is constructed with fine mesh size, as shown in Figure 6-2.

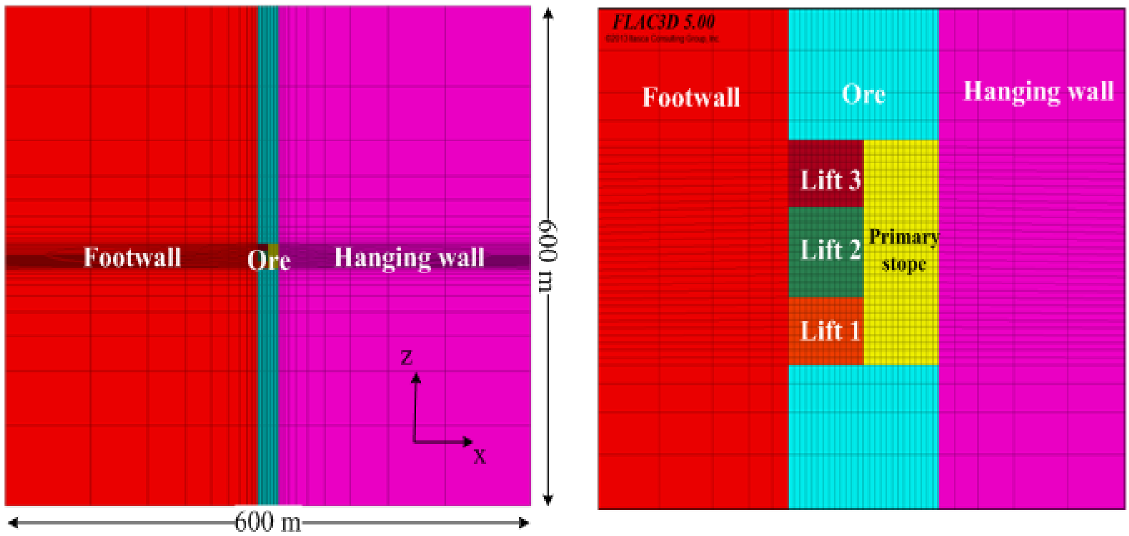

a) Cross-sectional view showing mesh gradation

b) Stopes modelled with fine mesh

Figure 6-2 – FLAC^{3D} model geometry and stopes showing fine mesh

6.2.3 DYNAMIC ANALYSIS SETUP

Dynamic loading effects due to blasting on CRF stope are integrated in the numerical model by following simple procedure laid down in Chapter 3. The procedure includes conversion of model boundaries to viscous boundaries, this helps absorbing excessive vibrations approaching boundaries of the model. In case the model boundaries are non-absorbing the dynamic load is partially reflected back from model boundaries which may lead to model failure in tension. Local damping value of 10% found from calibration process is considered for this analysis. To apply the dynamic load on CRF stope, a series of blast pulses are applied as a stress history on the CRF stope. A blast pulse profile presented in Figure 6-3 is used to apply series of different blast loads according to the blasting sequence provided by the case study mine. The profile of dynamic load can be represented as a decaying blast pulse (skew Gaussian curve) as used in the numerical modelling study by Gool [20] and presented in Figure 3-3. The details of blast load magnitude and procedure are discussed in Section 6.4 model validation. The blast load is applied on the boundary walls of stope including backfill and rock faces as presented in Figure 6-3. Blasting sequence can be incorporated in FLAC3D using Fish function and table command. Different blasting sequences for each of the three blast lifts are followed and magnitude of blasting load applied is in proportion to quantity of charge in blast holes.

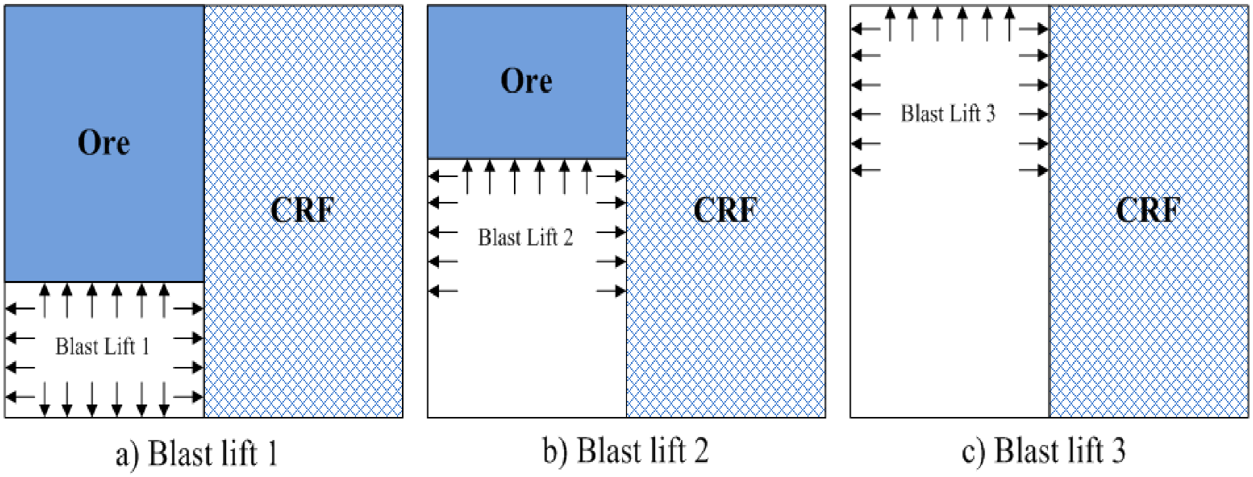

Figure 6-3 – Application of blast load on stope walls of the dynamic model

6.3 NUMERICAL MODEL CALIBRATION WITH IN-SITU STRESS

The numerical model is calibrated with the field observations measured during the in-situ stress determination program at Birchtree conducted by Herget and Miles [153]. The in-situ stresses tensor values were presented at level 2750 of the Birchtree mine. The model calibration is accomplished by applying a compressive stress load and observing the stress tensors inside the FLAC3D model at the same depth. The compressive stress load is applied to the model boundaries with no other boundary conditions. The applied stresses are fine-tuned using trial and error method. The iterative process continued until the error ratio is reduced to acceptable range ($\pm$ 10%) of measured stress tensor values attained during the in-situ measurements at the same location in the model. This serves as numerical model calibration. Once the model is calibrated the mining and backfilling sequence is simulated followed by dynamic analysis. Figure 6-4 presents results of the calibrated numerical model using stress tensor values. The magnitude of stress tensor values are presented in Table 4-4.

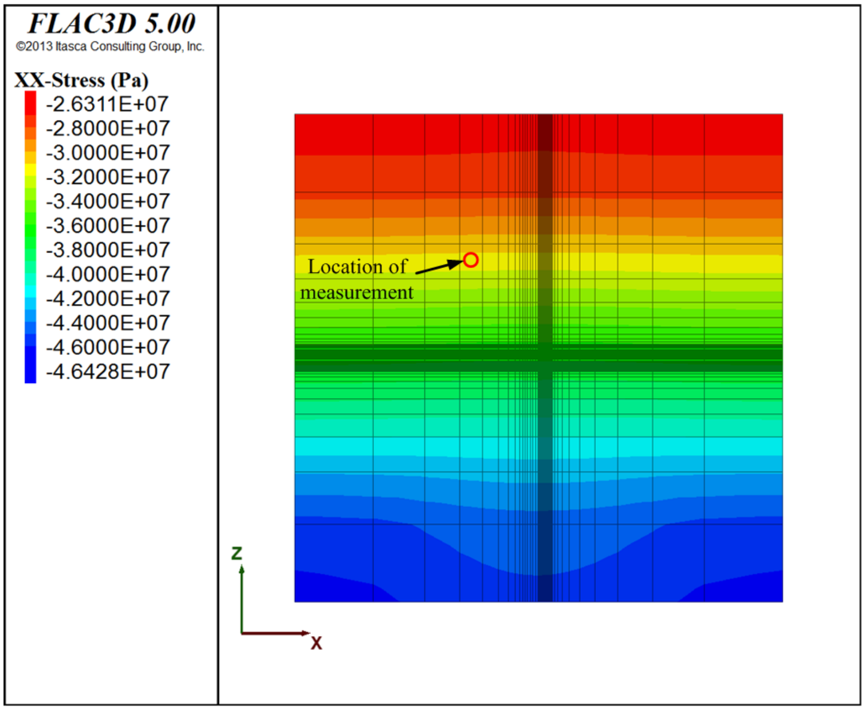

a) Calibrated model presenting σ_{xx}

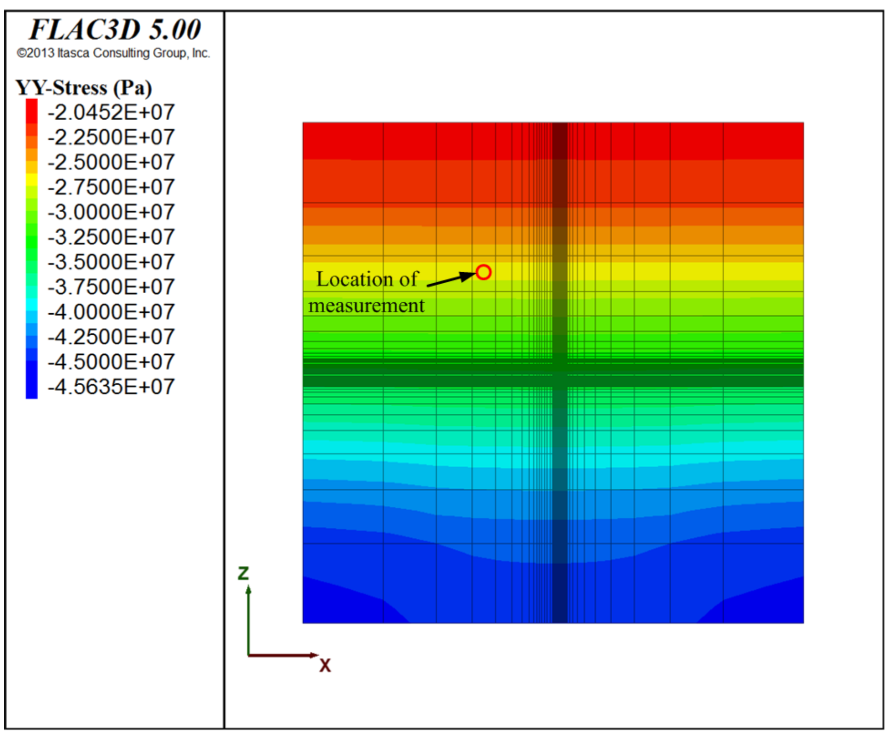

b) Calibrated model presenting σ_{yy}

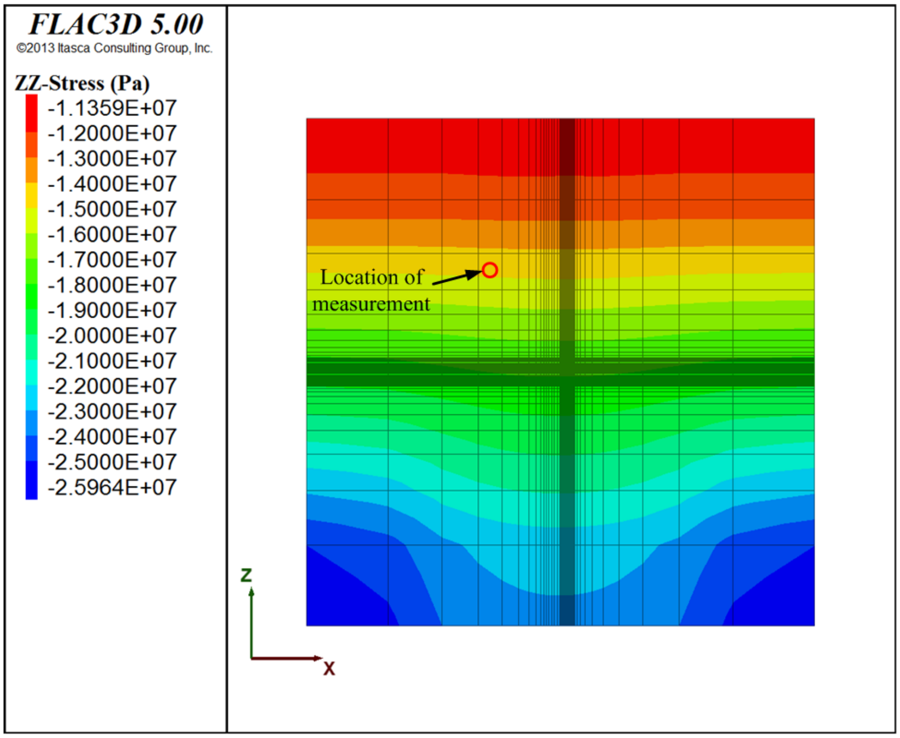

c) Calibrated model presenting σ_{zz}

Figure 6-4 – Results of calibration using in-situ stress tensor values

6.4 NUMERICAL MODEL CALIBRATION WITH BLAST-INDUCED VIBRATIONS

The numerical model is calibrated with the help of a blast-induced vibrations observed during field monitoring program at the mine site while using the method of equivalent cavity, the details of the in-situ blast vibration monitoring experiment conducted at the case study mine are presented in Chapter 5. The equivalent cavity method has been used by Sharpe [97], Kutter and Fairhurst [98], Blair and Jiang [101], Gool [20] and Sainoki and Mitri [160] for simulating blast-induced vibrations. This method replicates the effect of blast vibrations only while neglecting formation of cracking in zones surrounding blast hole. This improves the model efficiency as modelling cracked zones require more solving time and a very fine mesh size. The technique of equivalent cavity is employed for model calibration with blast-induced vibrations and a third model is developed as shown in Figure 6-5.

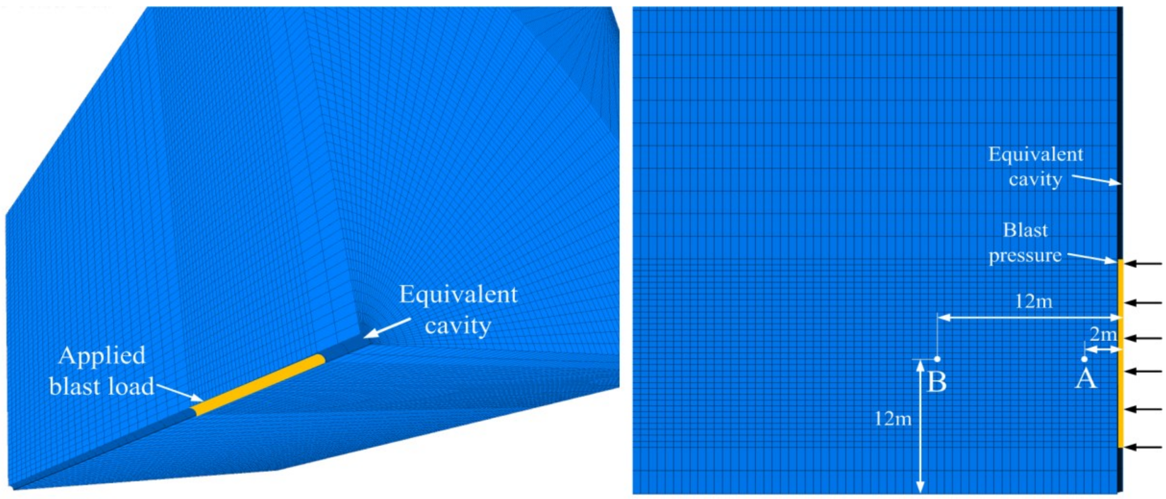

a) Modelling equivalent cavity b) Sectional view

Figure 6-5 – Equivalent cavity used for determining blast load and damping for the model

The radius of equivalent cavity depends on the material dynamic properties in which the blast hole is located, but generally it is taken within three to nine times the diameter of blast hole [98]. The equivalent cavity model will provide the blast loading distribution to be applied on secondary stope faces. Since, CRF is affected by the blast vibrations and not reproduce cracking due to blasting, the approach of equivalent cavity suits well to the requirements. In the first step of numerical model calibration the blast load is computed for explosives used at Birchtree with the help of the equation 6-1 [161-163].

$$P_d = \frac{\rho_e D^2}{4} \tag{6-1}$$

Where P_d is the borehole pressure, ρ_e is the density of explosive and D is the detonation velocity of explosive. ANFO and low energy ANFO are the explosive products being used by the case study mine and P_d for these explosives are found to be 1560 MPa and 930 MPa respectively. The blast load profile used increases very quickly and then decays down slowly. The load profile on equivalent cavity of the model can be determined using the equation 6-2 [101, 105], φ = 2000 and t is the time interval.

$$p(t) = p_0 t^n e^{-\varphi t} \qquad (6\text{-}2)$$

The initial stress load p_0 in the model is considered to be around 101 MPa in the rock and peak particle velocities (ppv) at different distances are calculated from the model for each blast hole present in the blast design. The applied blast load is varied in equivalent cavity model, to attain the ppv computed from the charge weight scaling law presented in equation 6-3 [161]. This exercise also helped determining suitable damping coefficient and blast pressure distribution to be applied on backfill face in terms of particle velocities in mm/s.

$$ppv = K\left(\frac{R}{W^{0.5}}\right)^{-s} \qquad (6\text{-}3)$$

The values of constants K = 141 and s =1.20 for ANFO are extracted from the work of Henning and Mitri [164], the value of radial distance (R) in meters, and charge per delay (W) in kg, are extracted for each production blast hole from the blast design provided by the case study mine. Figure 6-5 presents the equivalent cavity modelled in FLAC3D and parameters used in the charge weight scaling law [20]. The dimensions of the block are 20 m × 20 m × 35 m in length, width and depth respectively. The borehole pressure is applied on equivalent cavity and damping coefficient is varied to obtain the blast vibrations at points A, and B calculated from charge-weight scaling law presented in equation 6-3. Locations A and B are selected based on the blast design provided by the mine. Point A represents location of CRF and rock interface from the nearest blast hole and point B is the farthest blast hole. The applied load is adjusted such that the model obeys charge-weight scaling law. Once the blast vibration magnitude is attained the particle velocities are calculated at different radial distances depending upon the blast design. The explosive charge length is varied according to the blast design of the case study mine. The blast hole inclination is simplified to 70, 80 and 90 degrees. The damping coefficient is found to be 10% for the built-in local damping in FLAC3D. The blast load in the form of peak particle velocity components (x, y and z) are computed for different blast holes in blast design and are then exported to the main CRF model along with the damping coefficient.

The contours of x, y and z-velocity computed by the equivalent cavity model for one of the boreholes in the blast design of lift 3 is presented in Figure 6-6. The section is taken at a distance of 12 meters from equivalent cavity. The distributions of velocities to be applied on exposed

CRF face are simplified for ease of application from such contours for all the blast holes. From Figure 6-7 it can be seen that the velocity is resolved into three velocity components at the CRF and rock interface. In the next step blast load is applied in terms of x, y and z-velocity and ppv is monitored inside the CRF model at observational point presented in the Figure 6-8. The local damping coefficient imported from the equivalent cavity model is also applied to the main CRF model to simulate blast wave transmission accurately.

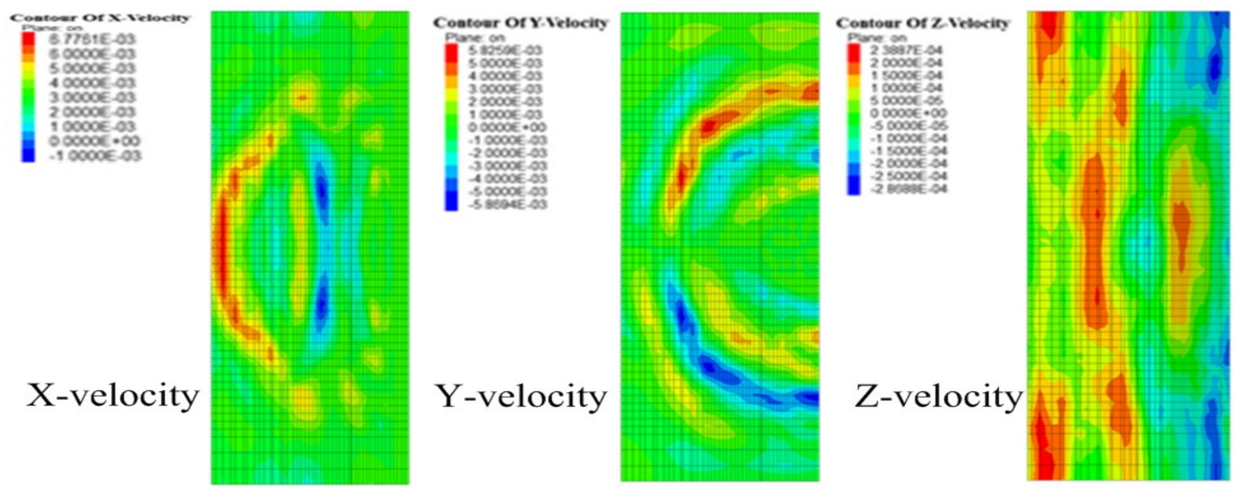

Figure 6-6 – Blast load distribution for one of the blast holes on the face of exposed backfill face

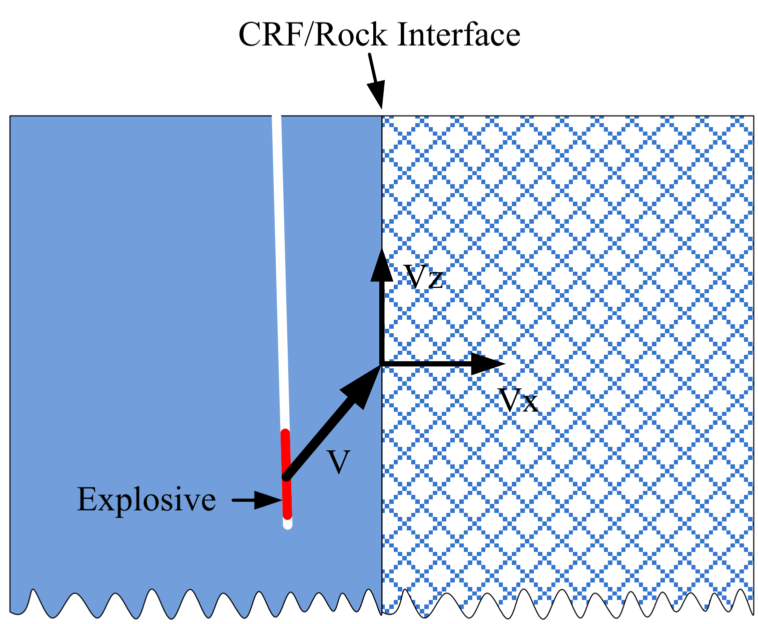

Figure 6-7 - Resolution of velocity into components at rock CRF interface

The damping coefficient for backfilled zones and blast load from equivalent cavity model are varied to $\pm$ 20% to equate the peak particle velocities observed on site and calculated ppv from the FLAC3D model. Figures 6-8 to 6-10 present numerical model calibration results as a comparison of the peak particle velocities computed from the FLAC3D model and PPV measured during in-situ blast vibration monitoring program in CRF for all the three blast lifts. The horizontal axis represents blast sequence as discussed in Section 5.5. This process serves as numerical model calibration with blast vibration monitoring results. It can be seen that the numerical model behavior is very close to the field conditions.

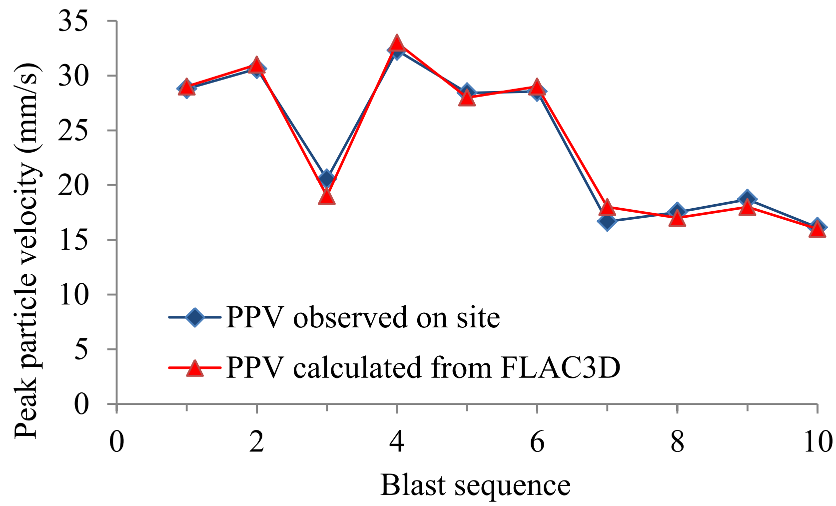

Figure 6-8 – Peak particle velocity monitored versus computed for blast lift 1

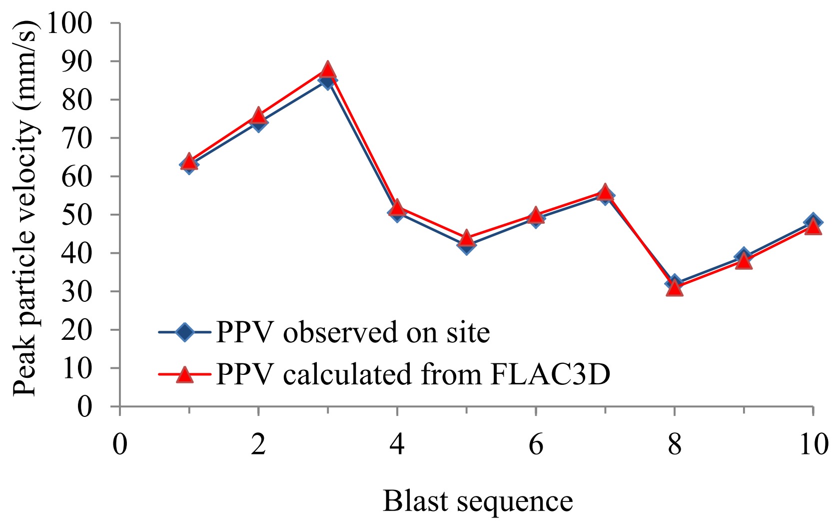

Figure 6-9 – Peak particle velocity monitored versus computed for blast lift 2

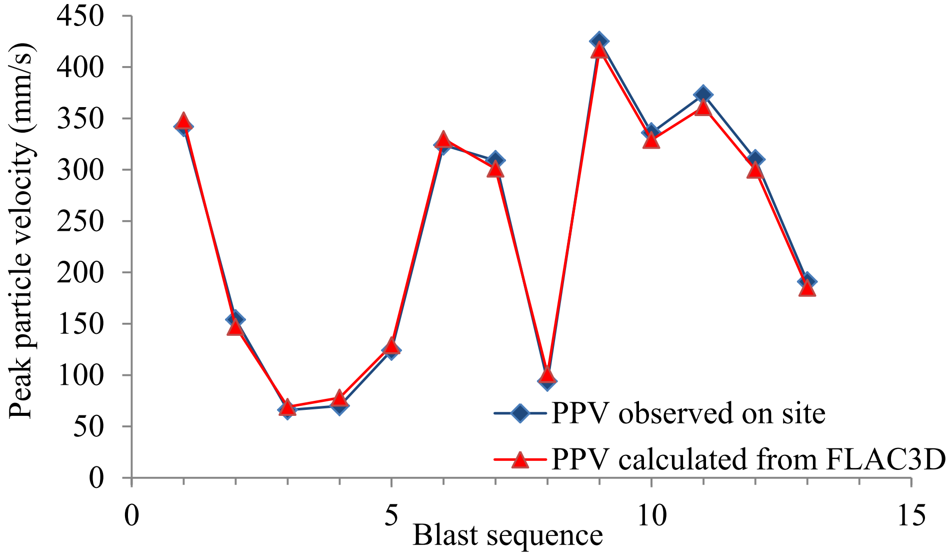

Figure 6-10 – Peak particle velocity monitored versus computed for blast lift 3

6.5 BACKFILL FAILURE CONTROL STUDY USING SECOND DYNAMIC MODEL

Collected data, field measurements, numerical modelling technique and numerical model calibration process are combined to form a second 3-D backfill planning and design numerical model capable of simulating various field conditions for studying the problem of backfill failure in detail. Notably the cavity monitoring survey (CMS) profile of the blasted stope is not presented due to the fact that a thin ore skin was planned to be left in place by the mine. The CMS profile of the stope shows no failure. The following section presents a study on CRF failure and its control using the calibrated and calibrated numerical model. The base case scenario representing the planned mining and blasting method and base case is presented in the following Section. The results are presented in terms of vertical stress contours and peak particle velocities at the end of a dynamic analysis.

6.5.1 Base Case – Exposed Backfill

The base case scenario is the calibrated model for the case study mine. It is the actual scenario being planned at the case study mine for extraction of secondary stopes as discussed in Chapter 4. The stope is extracted in three blast lifts and once the blasted ore is mucked out the stope is backfilled. The stope is then cured for 28 days and adjacent secondary stope is mined consequently in a similar fashion. The comparison of gravity loading versus blast loading on backfill for all three lifts is presented. Figure 6-11 shows the contours of vertical stress for the first blast lift. It can be seen that there is no change in the state of backfill due to blast loading and it can be suggested that the backfill is not affected by the first blast, which have the highest powder factor. The first blast is the smallest blast with respect to the quantity of explosive and volume of rock blasted. The reason for backfill to remain stable under dynamic load is because of the support to the backfill and damping of blast vibration reaction provided by the ore block sitting on top of blast 1.

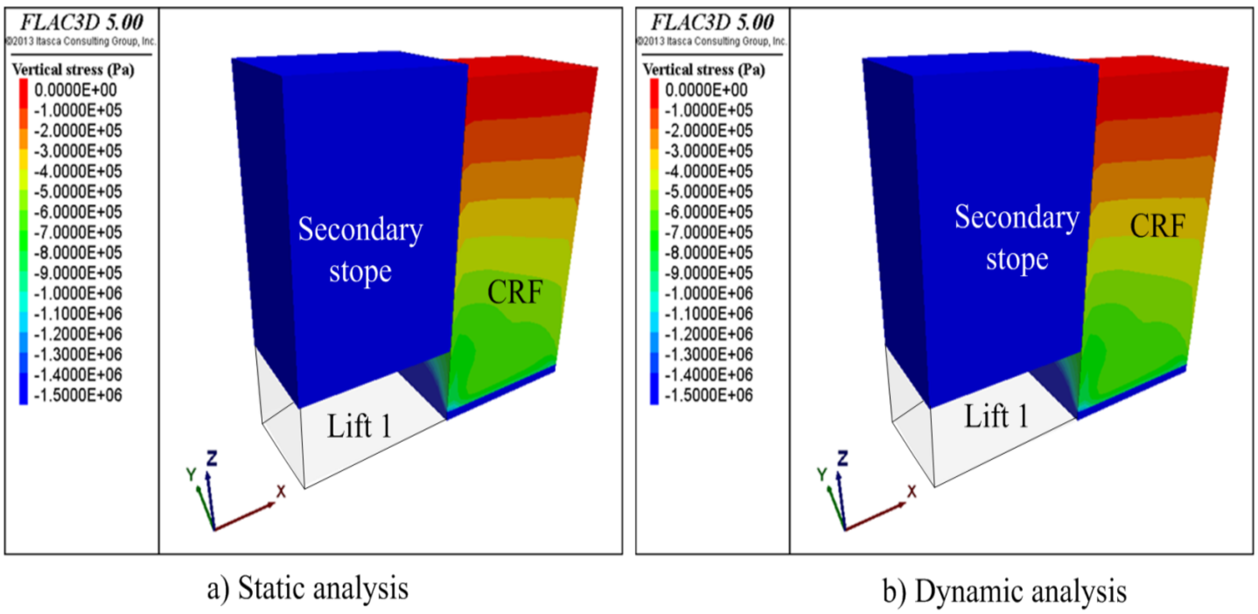

Figure 6-11 – Vertical stress contours plotted after the first blast lift

The second blast is simulated in a similar fashion and the results of the dynamic analysis are presented in terms of vertical stress contours in backfill and are displayed in Figure 6-12. It can be seen that there is no change in backfill except a thin band of tensile stress near the top of the exposed backfill face area from blast 2 for dynamic analysis. Static analysis still shows CRF to be very stable. It can be suggested that the backfill is not much affected by the second blast and a small tensile stress band is a sign of instigation of backfill failure. The second blast is an intermediate blast with respect to the quantity of explosive and volume of rock blasted as discussed in Chapter 5. The reason again for no failure is the fact that backfill is supported by remaining ore block present in third lift. The ore block is also a source of damping blast vibration reaction.

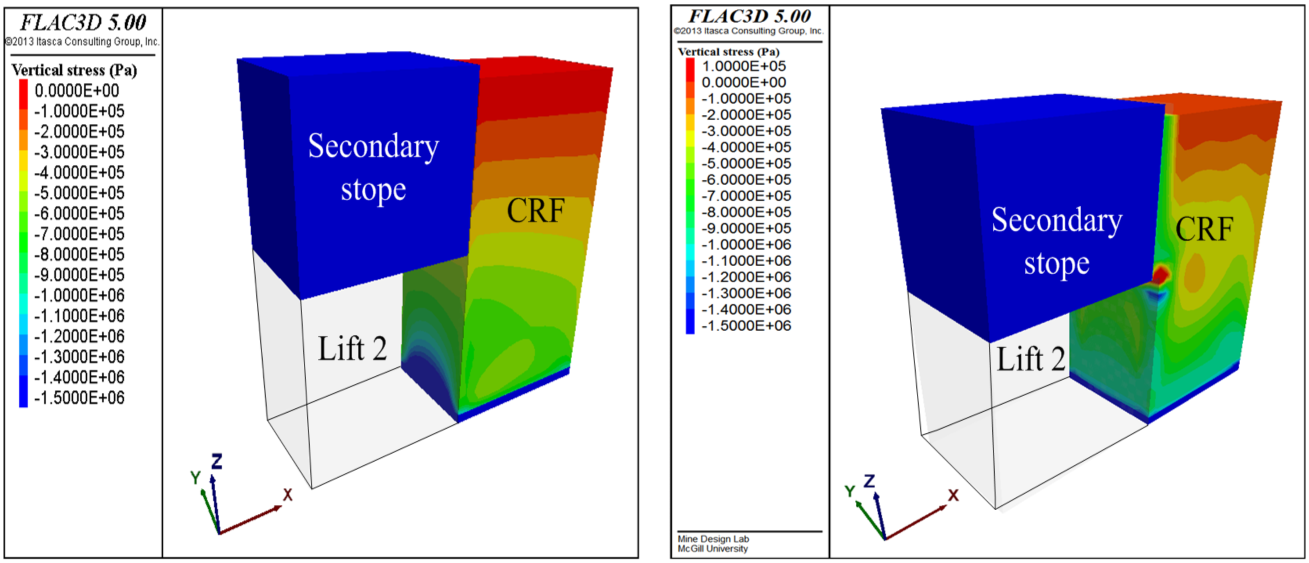

a) Static analysis b) Dynamic analysis

Figure 6-12 – Vertical stress contours plotted after the second blast lift

The third blast also known as the deck blast is simulated and results are presented in Figure 6-13. It can be seen that the top portion of the exposed backfill is under relaxation due to development of tensile stress for dynamic analysis. This is an indication of backfill failure as described in the failure criteria in Chapter 3. The blast 3 is the largest blast in terms of volume of ore blasted. The reason for failure is clear for the third blast as there is no more ore left on top of this blast to support backfill and also to counteract the reaction from excessive blast vibrations. The reaction from blast vibrations destabilizes backfill from the top of the exposed face as there is very little confinement. As can be seen from Figure 6-14, the CRF is failing from top of the exposed face and the failure shape is in wedge shaped. The term wedge shape failure is a generic term applied to CRF failures but circular failure is the most common mode of failure in CRF. The wedge shape failure is in accordance with the field observations [2, 6, 18, 30] and laser survey profiles obtained from the case study mine presented in Chapter 4.

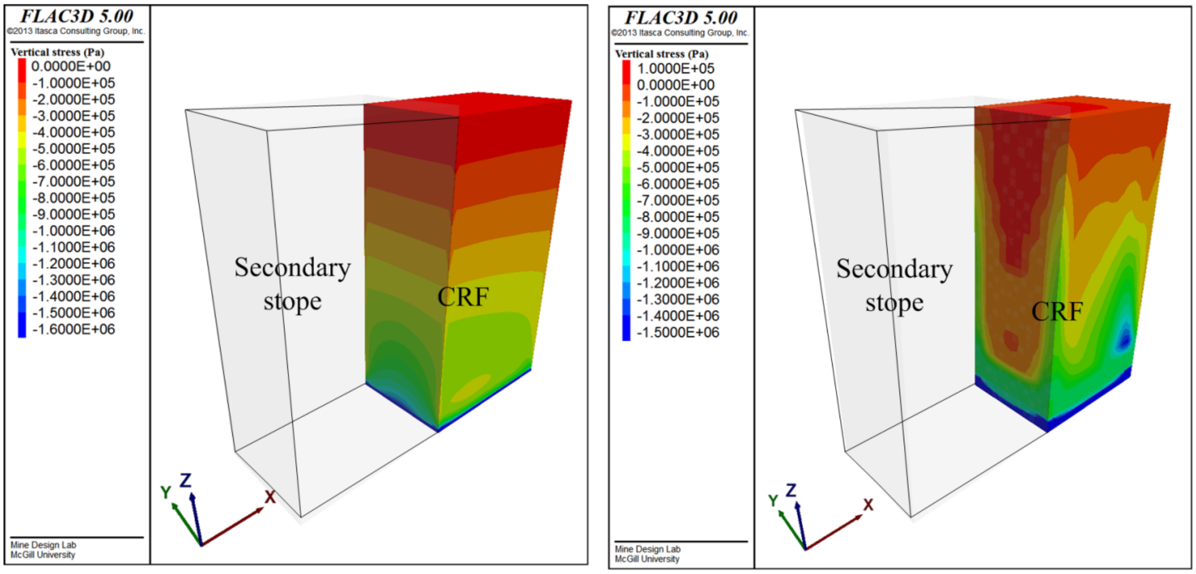

a) Static analysis b) Dynamic analysis

Figure 6-13 – Vertical stress contours plotted after the third blast lift

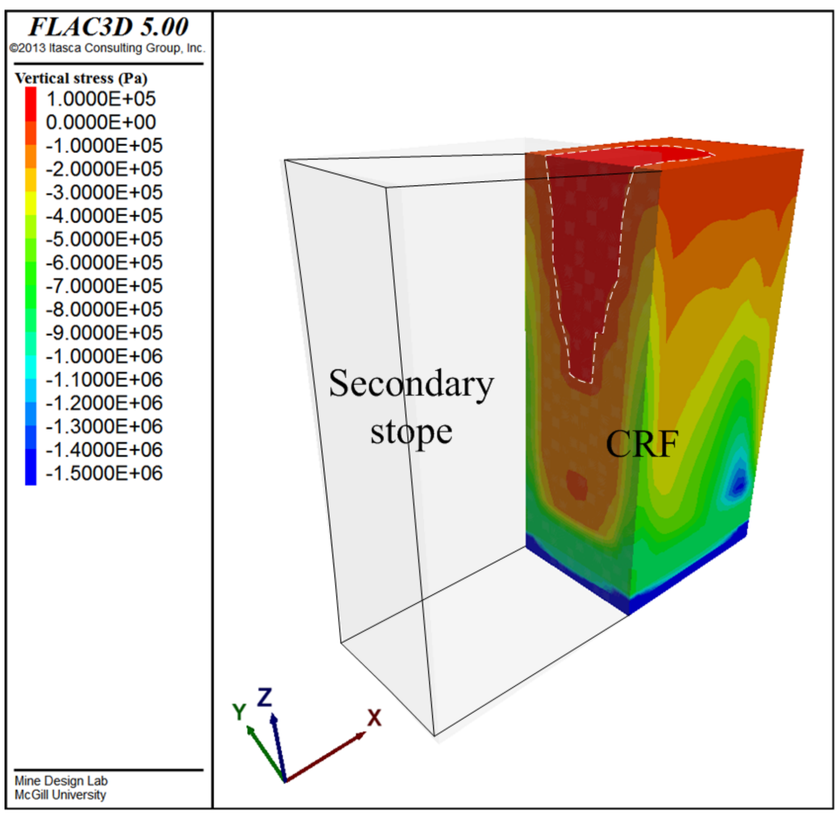

Figure 6-14 – CRF failure shown by dashed line on exposed face

The profile of minor principal stress along the center line of exposed backfill face for both static and dynamic analysis is presented in Figure 6-15. It can be seen that the top portion of backfill is under zone of relaxation as indicated by the tensile stress region of the curve for dynamic analysis. However the static analysis shows backfill to be pretty stable. Notably the CRF stope is failing from the top of the exposed face, as observed from case study and other mines [20, 43, 96]. The profile of major principal stress along the center line of exposed backfill face for both static and dynamic analysis is presented in Figure 6-16. The static analysis presents no failure in backfill. It can be seen that the top portion of backfill is under relaxation zone indicated by the tensile stress for dynamic analysis. CRF failures are generally observed at a similar location that is top of the exposed face having wedge shape.

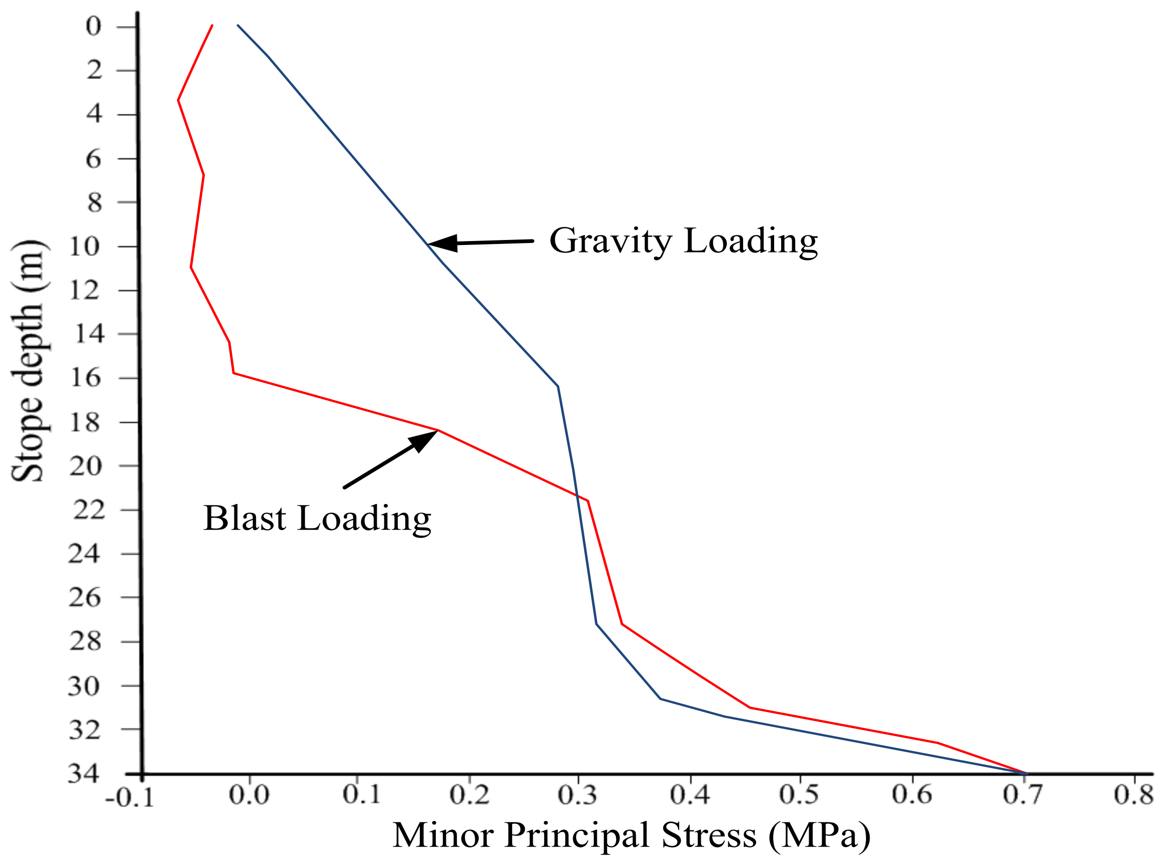

Figure 6-15 – Profile of vertical stress computed at the center line of exposed face

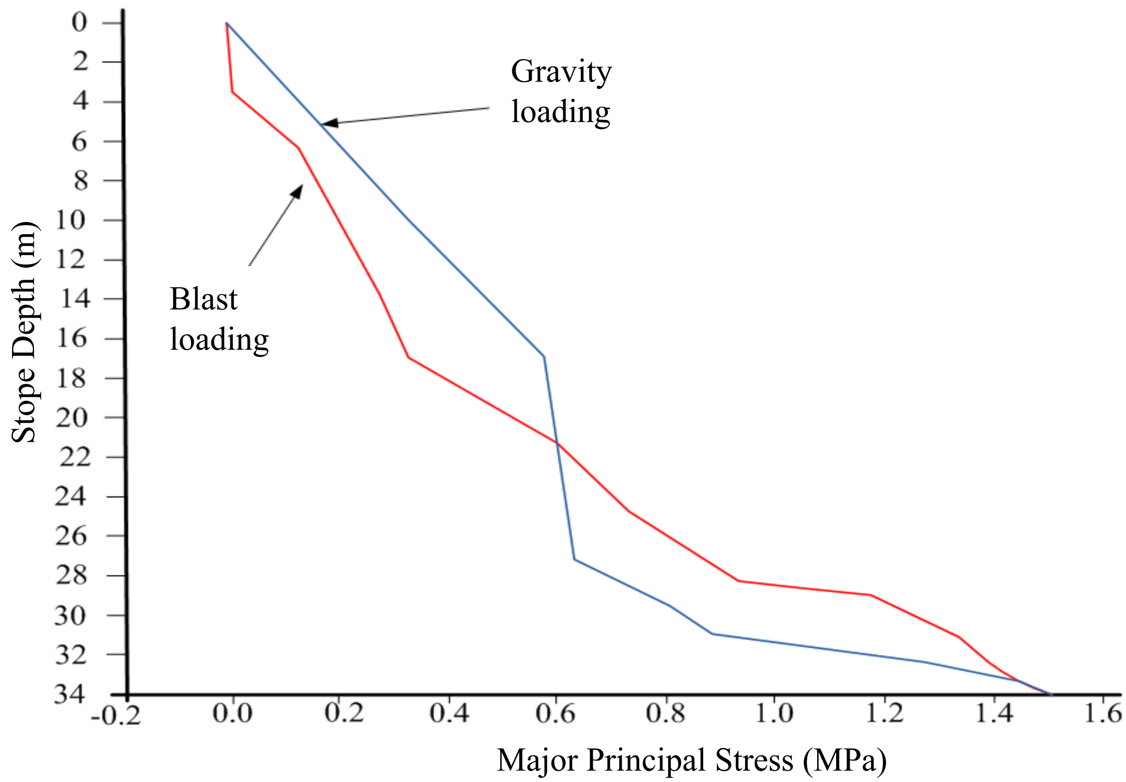

Figure 6-16 – Profile of major principal stress computed at the center line of exposed face

The profile of the peak particle velocity computed from FLAC3D results along the centerline of the exposed CRF face during the dynamic analysis is presented in Figure 6-18. It can be seen that the higher peak particle velocities are computed near the top most part of the exposed CRF face, in the failed zones. By comparing Figure 6-17 and Figure 6-15 it can be noted that CRF is under tensile stress region between a depth of 0 m to 16 m, and there is a sharp decrease in PPV at the same location. This suggested that the peak particle velocities around the magnitude of 278 mm/s are initiating failure in backfill when it is exposed. This is in accordance with the observations of Gool [20] who suggested that a backfill experiences failure at a ppv greater than 250 mm/s and by Yu [5] who suggested that a magnitude of around 300 mm/s damages CRF.

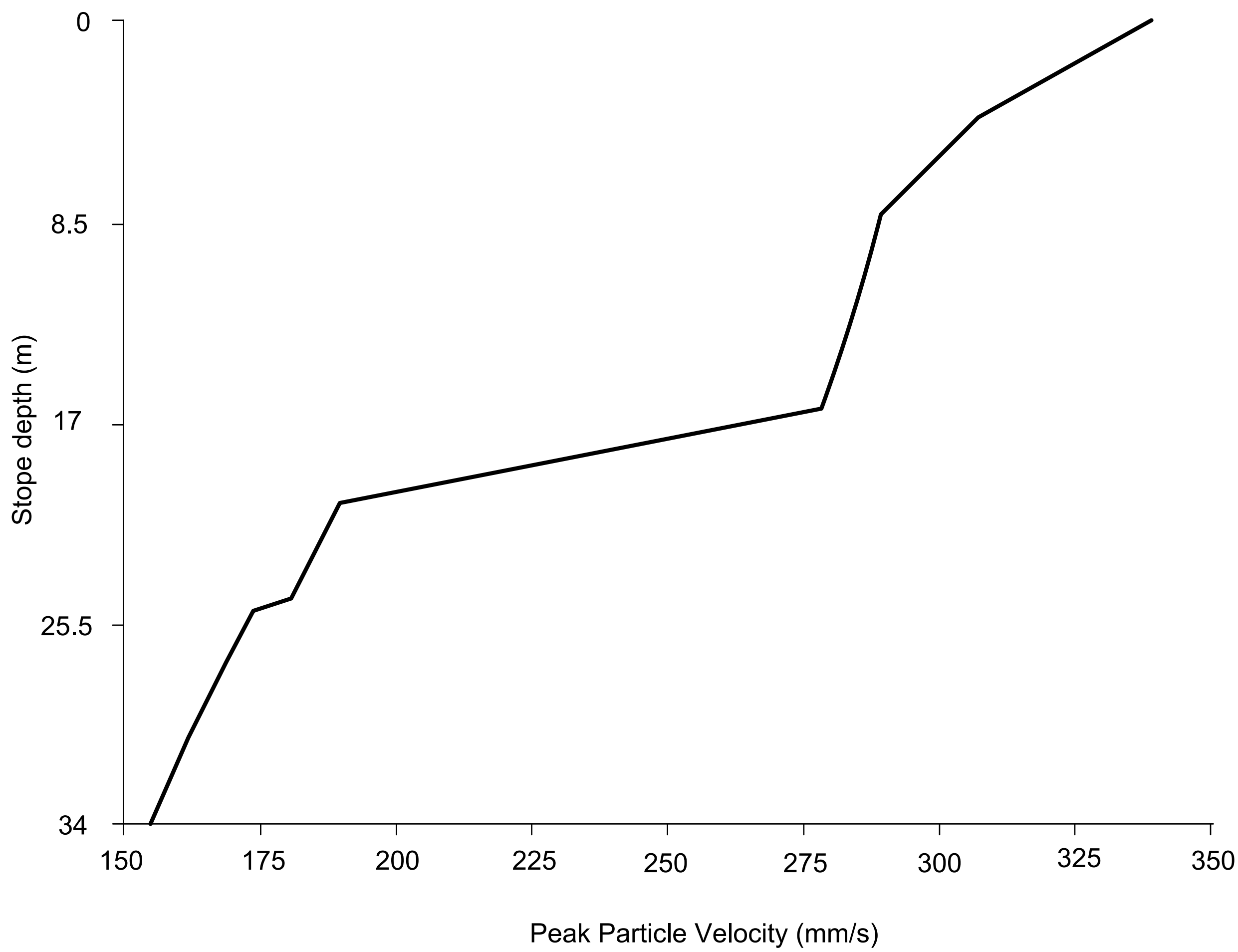

Figure 6-17 – Profile of the peak particle velocity plotted at the centerline of the exposed fill face

6.5.2 Tactically Leaving a Thin Ore Skin between Production Stope and CRF Stope

Generally, a thin ore skin also termed as diaphragm is tactically used by some operations in North America. It can be used as a support for backfill when the ore grade is very low or when there are bands of barren rock. In such a situation the stopes must be designed in such a way that the barren rock bands can be used as a skin for supporting backfill. This method will not allow backfill to be exposed in future. This approach can also save significant binder costs while reducing backfill dilution to zero. However, leaving an ore skin will decrease the recoverability to some extent but will also decrease the dilution costs. A mine planner must decide on leaving the ore by equating cost due to backfill dilution tonnage that can incur versus the potential revenue from the ore that is left in place. A schematic of leaving an ore skin is presented in Figure 6-18.

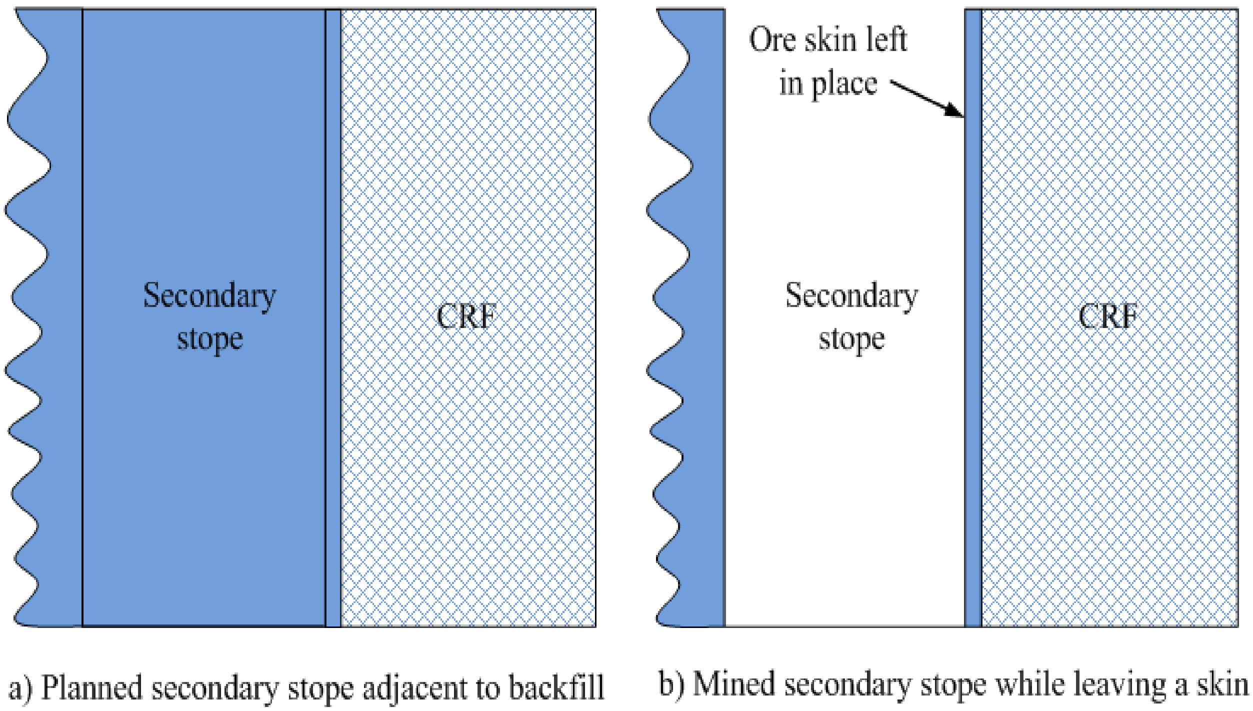

Figure 6-18 – Schematic diagram of leaving an ore skin between backfill and production stope

The practice of North American mines of leaving 2 meters ore skin is modelled with the help of FLAC3D. The contours of vertical stress are presented in Figure 6-19. It can be seen from the Figure 6-19 that the backfill remains stable for both static and dynamic analysis. The un-mined ore skin between a backfill and production stope not only takes away the reaction of blast loading from backfill but it supports backfill as well. The numerical modelling results suggest that a skin can be efficiently used to support backfill when practicing sublevel stoping methods. The practice of leaving a skin is highly recommended when it is feasible to leave the low grade ore in place for stability of CRF material.

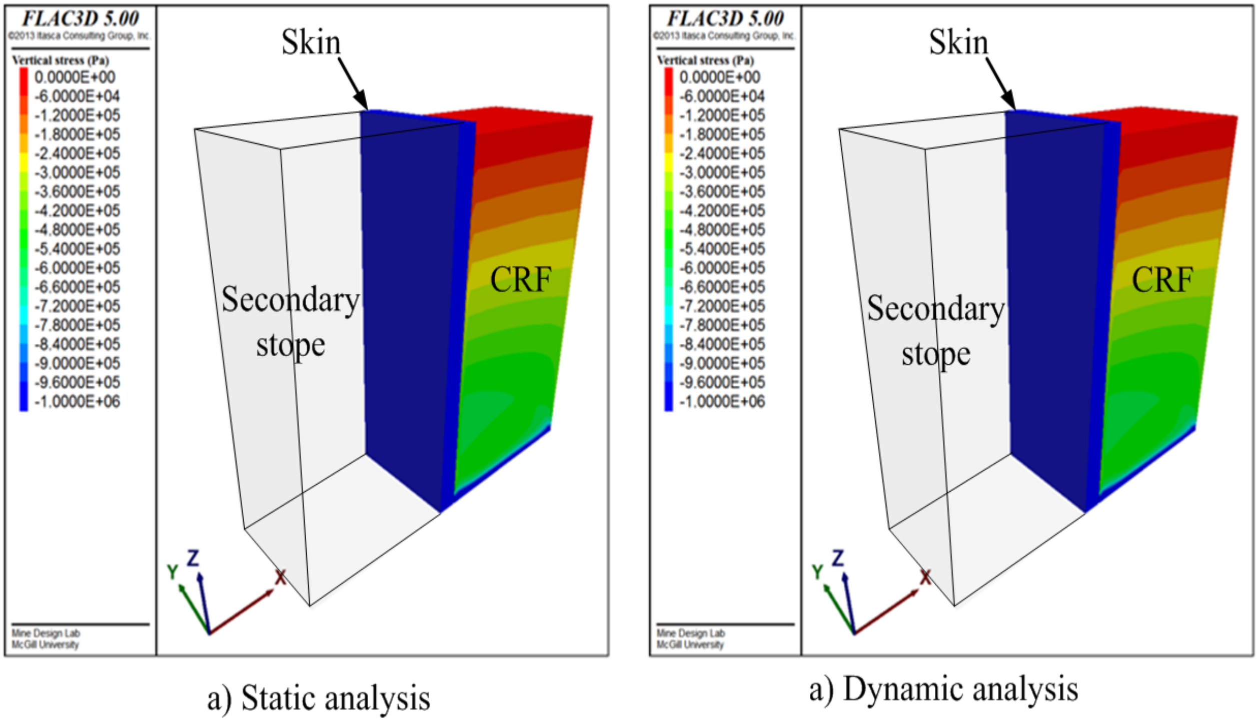

Figure 6-19 – Contours of vertical stress contours presenting no failure in backfill

6.5.3 Strategic Approach of Selective Mining

Selective mining is defined as a methodology of mining only high grade ore while leaving low grade ore or rock material in place. In this section two selective mining scenarios are simulated that are observed at Canadian mines. In addition to current approach of selective mining an improved approach is simulated and presented. The improved approach for both the cases provides greater backfill stability without adding extra costs. Results of different situations observed at Canadian mines and an improved approach of selective mining for each scenario are presented in the following sections.

6.5.3.1 Ore on Top of Rock

Generally the blast holes used for probing the stope and block modelling softwares may show different geological feature including discontinuous ore body. At one of the mines in North America it was found that a large ore block is located on top of the barren rock. The stope was mined in a fashion shown in Figure 6-20. In such a situation ideally the mine would like to remove all the ore without blasting and mucking out the waste material. In reality this is not possible as the load haul dump machine requires some access to muck out blasted ore. As can be seen there is a need to blast and muck some portion of rock to facilitate the mucking of blasted ore at a later stage. The same scenario is modelled to assess the stability of backfill and results are presented in terms of vertical stress in Figure 6-21. It can be seen from the Figure that the backfill is failing from top of the exposed backfill face because the backfill has been completely exposed by this approach of selective mining. It can be concluded that the approach used by the mines to extract the stope partially in this manner may initiate backfill failure from the exposed backfill face.

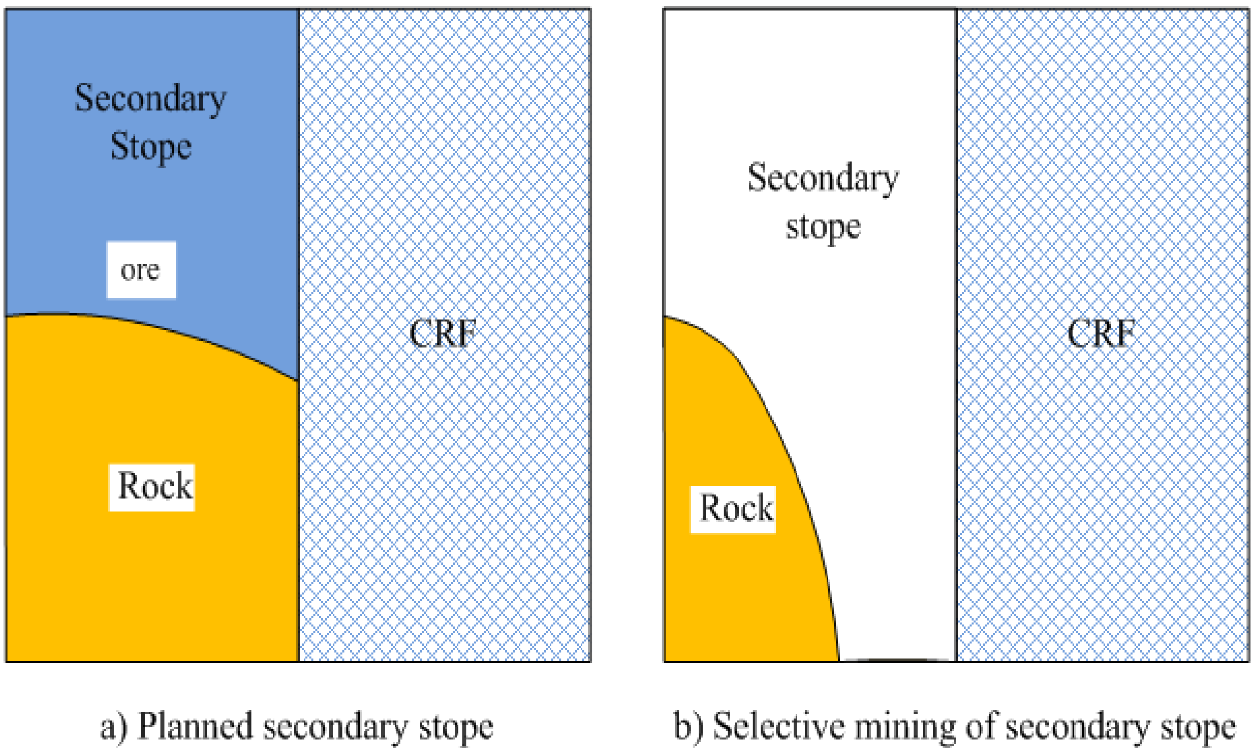

Figure 6-20 – Selective mining while exposing entire backfill face

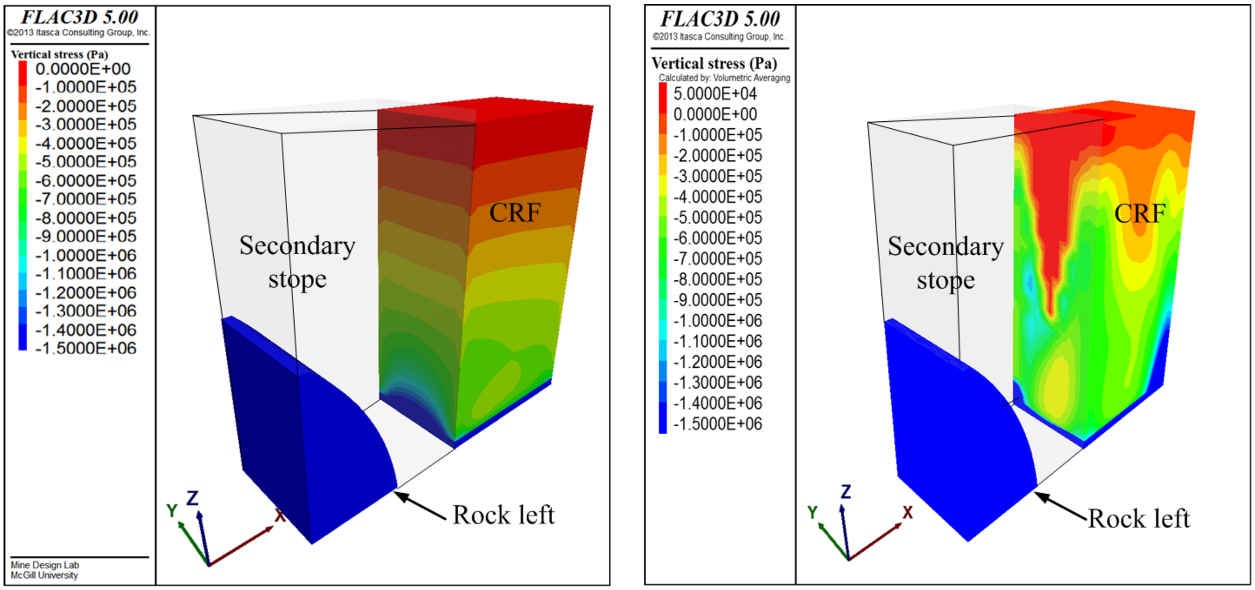

a) Static analysis   b) Dynamic analysis

Figure 6-21 – Contours of vertical stress when selective mining and exposing backfill

It can be seen from Figure 6-21 that blast vibrations are destabilizing the top most part of the exposed CRF face. A better approach of mining the ore sitting on top of waste rock will be to leave a large rock block on from the barren waste rock sitting on top of ore instead of blasting adjacent to backfill. Figure 6-22 presents a schematic of this approach. The approach is modelled using the calibrated model and results are presented. Figure 6-23 presents the contours of vertical stress showing no failure. The big rock wedge left adjacent to backfill is behaving as a partial skin as some part of the backfill is not exposed. The rock wedge is absorbing blast vibration reaction from backfill and it is also supporting toe of the backfill. Notably there is some tensile stress development in the rock wedge for dynamic analysis. According to the numerical modelling result this approach seems to be a better approach because of the fact that major portion of backfill is stable as it is being supported by barren waste while the stope is recovering most of the high grade ore.

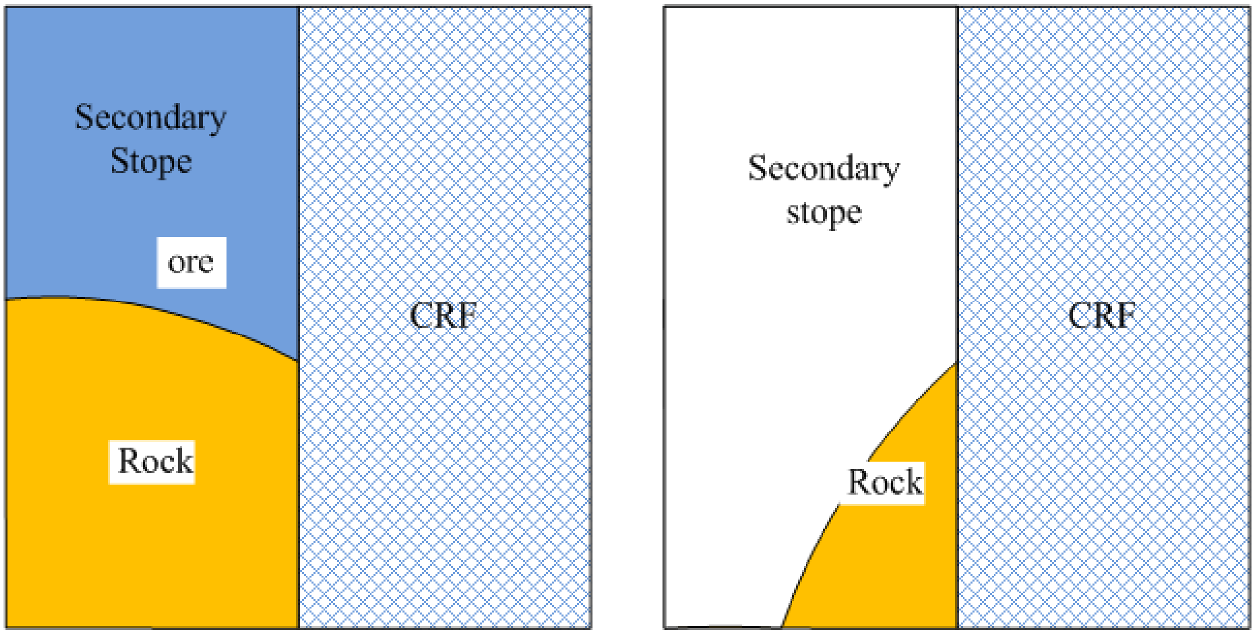

a) Planned secondary stope   b) Selective mining of secondary stope

Figure 6-22 – Selective mining while partially exposing backfill

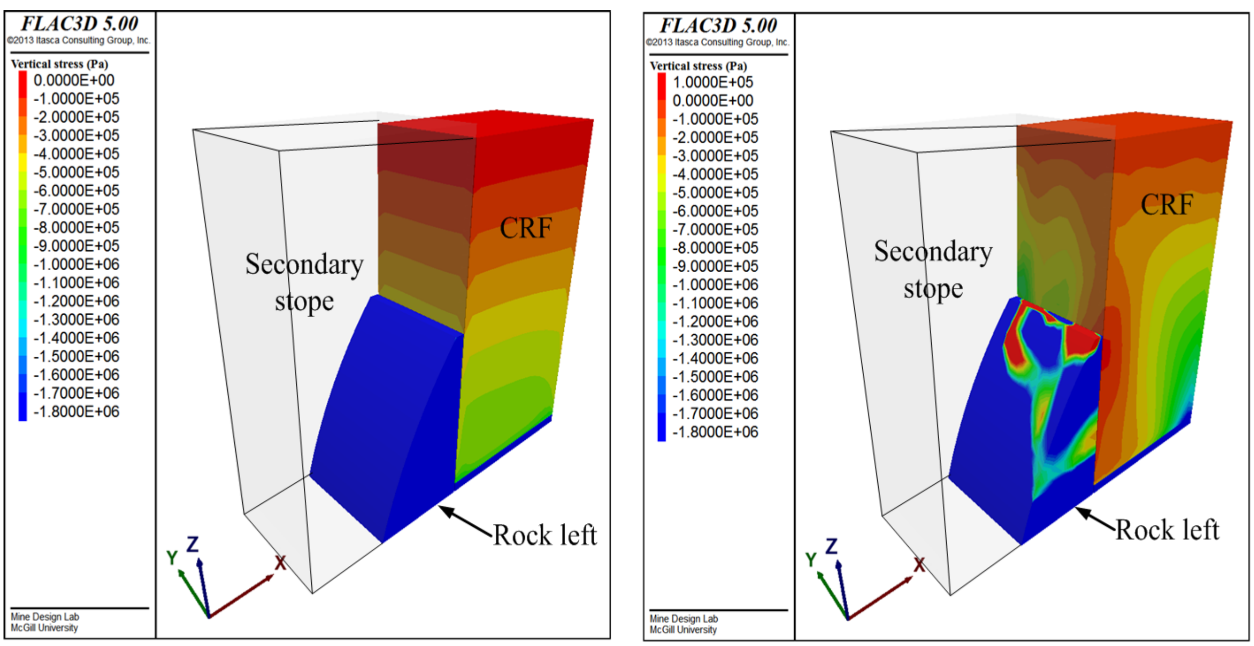

a) Static analysis   b) Dynamic analysis

Figure 6-23 – Contours of vertical stress when selective mining and exposing backfill partially

6.5.3.2 Ore beneath the Rock

Figure 6-24 presents another scenario found during probing of a stope at one of the mines in North America. It can be observed that the geological settings comprised of a large rock block sitting on top of the high grade ore as shown in the Figure. As can be seen a small portion of rock will required to be blasted to facilitate the backfilling from sill drift. Blasts lifts 1 and 2 can be planned in a traditional way, however blast 3 or deck blast was planned to blast away the low grade ore or rock partially in order to create sufficient space for placing the CRF. This is the reason why blast 3 is relatively smaller for this particular case compared to other two blasts. In the Figure the blast holes for facilitating CRF placement are blasted right adjacent to backfill. The exact same scenario is modelled to assess the stability of backfill and results are presented in terms of vertical stress in Figure 6-25. The Figure shows that the backfill is stable for both static and dynamic analysis. No failure is observed from the numerical modelling analysis but there is a chance of backfill failure with a slightly greater magnitude of blast vibration as the backfill is completely exposed with this approach.

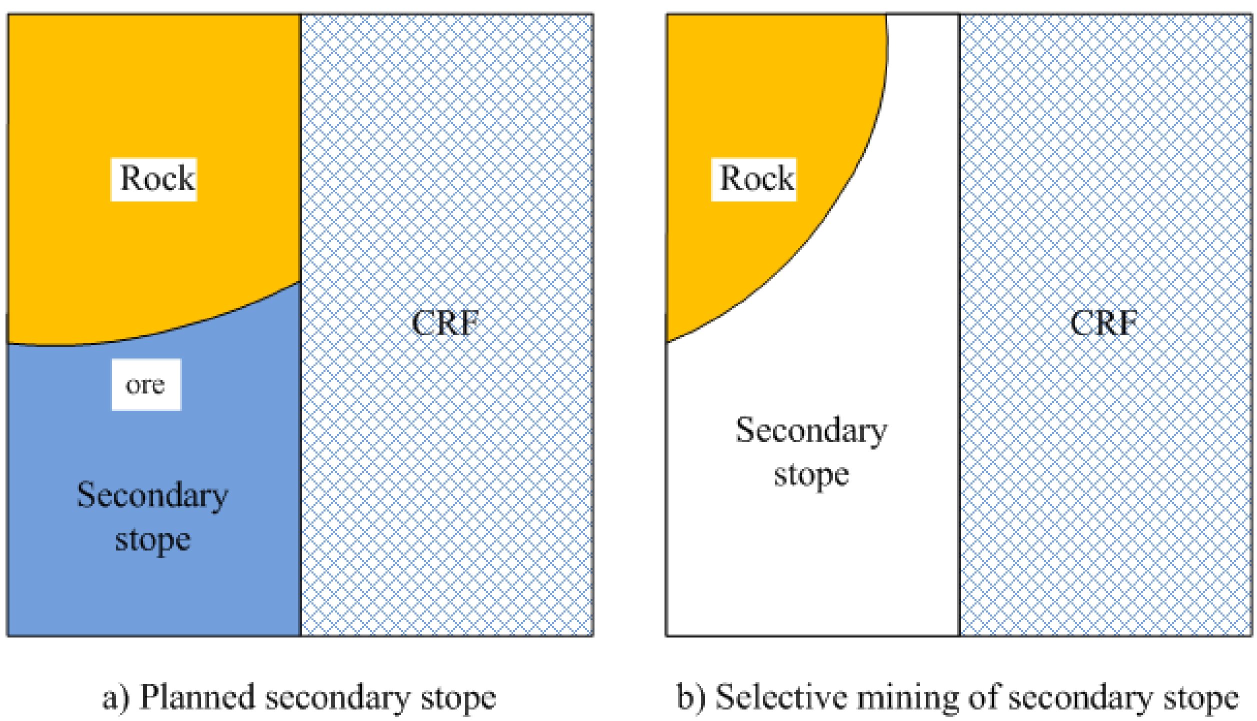

Figure 6-24 – Schematic showing selective mining while exposing entire CRF face

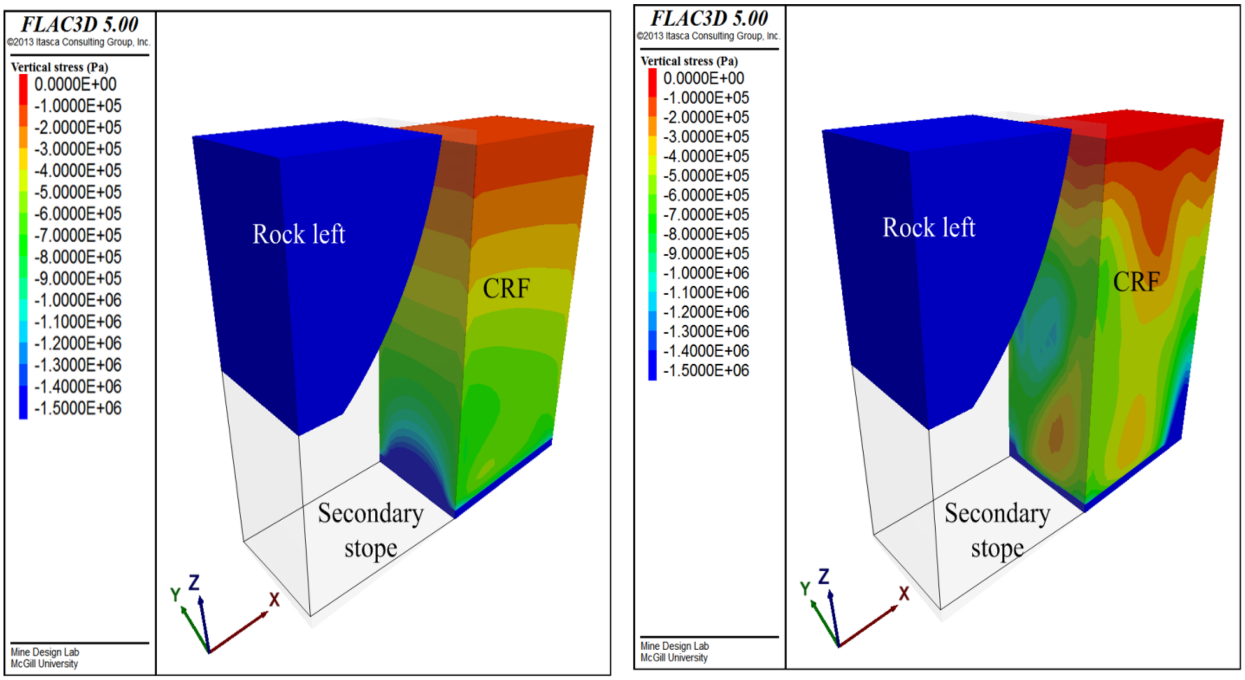

a) Static analysis

b) Dynamic analysis

Figure 6-25 – Vertical stress contours in CRF presenting selective mining of ore beneath rock

A better approach of removing the waste rock for facilitating backfilling will be to blast the rock away from previously backfilled stope instead of blasting right next to it. Figure 6-26 presents a schematic diagram of this approach. It can be seen that the deck blast is still the smallest but it is fired away from previously backfilled stope. The approach is modelled using the calibrated model and results are presented. Figure 6-27 presents the contours of vertical stress. The Figure shows no failure as the backfill is not exposed to a large deck blast also there is a big chunk of rock supporting backfill. This approach is better because of the fact that major portion of backfill is stable as it is being supported by barren waste while the stope is recovering most of the better grade ore. This approach ensures that the CRF remains stable during the extraction of secondary stope.

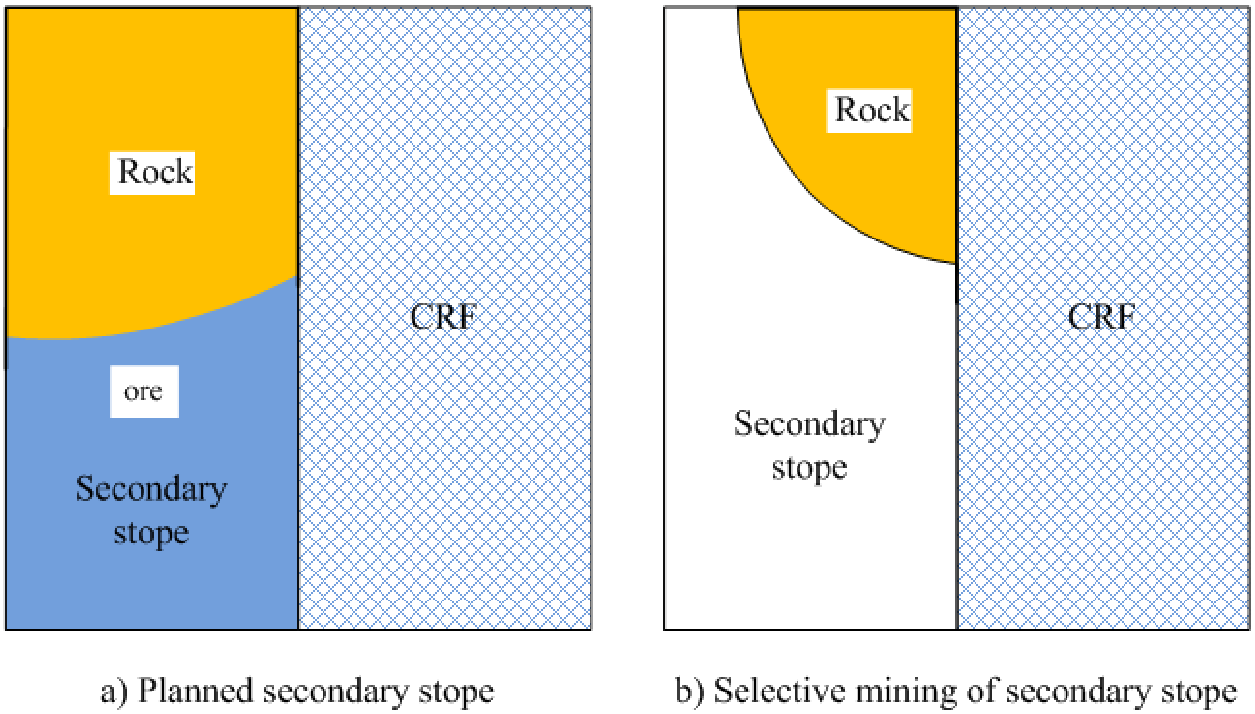

Figure 6-26 – Schematic presenting selective mining approach of mining ore under rock

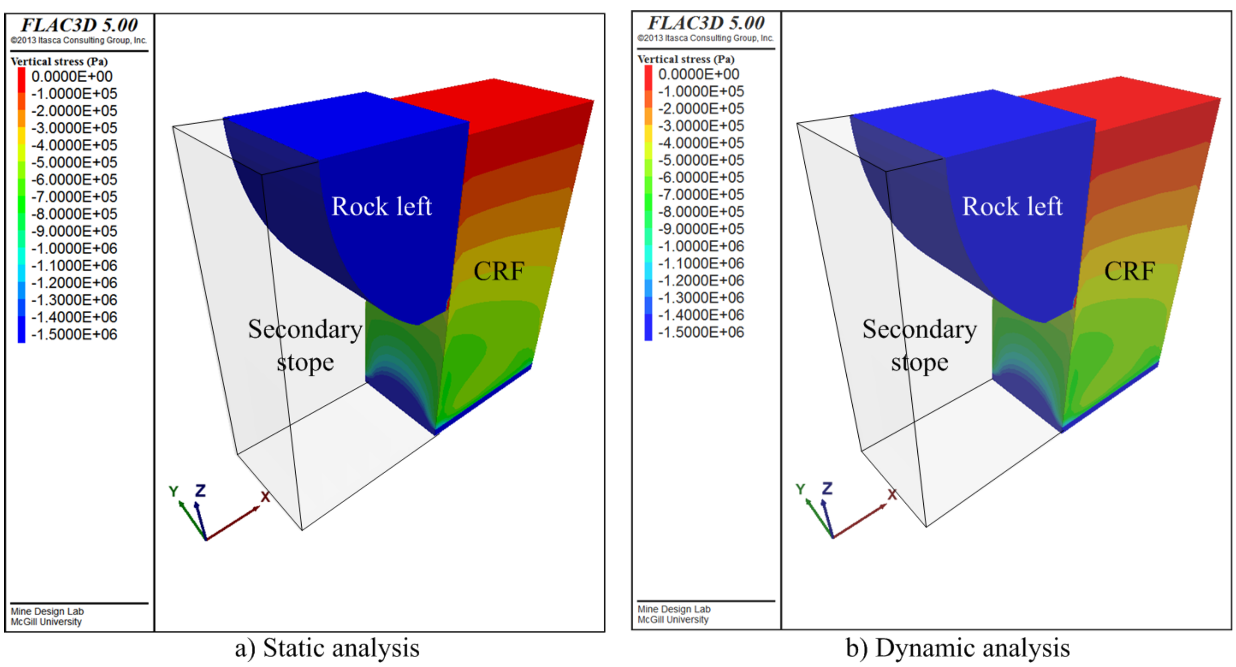

Figure 6-27 – Vertical stress presenting the selective mining scenario of ore under rock

6.5.4 Varying Binder Contents Vertically in Backfill

Some of the CRF operations in North America pour backfill with variable binder contents that is high binder contents at the bottom and lesser on top. This approach is adopted to save cost on binder while fulfilling the FSR design criteria for backfill. The practice has been observed to vary in terms of binder percentages for each pour from mine to mine. The schematic of this approach being practiced is presented in Figure 6-28. As can be seen the binder quantity is reduced from bottom to top by one percent in each shift. This approach is based on the fact that the compressive stress approaches its highest value at the foot of backfill and it can be reduced with reduction in depth of fill. Thus the binder can be reduced as gravity loading is decreasing on the CRF with vertical distance. The scenario is modelled by varying cemented rockfill properties for the five backfill layers with overall binder contents of 4%. The results are presented in Figure 6-29 in terms of vertical stress in backfill. The properties of CRF varied with binder percentage are computed from the theoretical equations presented in Section 2.3. The properties of un-cemented rockfill modelled in the second approach are extracted from the work of Alavez [164].

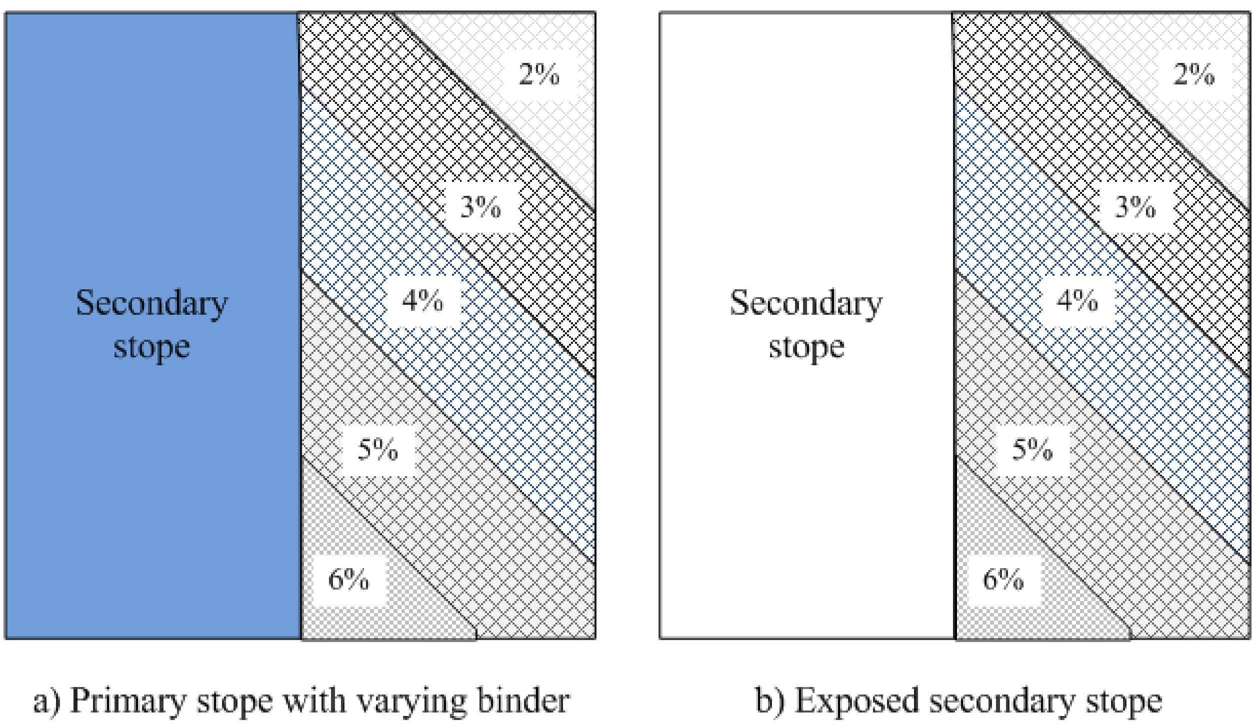

Figure 6-28 – Schematic presenting backfill placed with different binder contents for each pour

Table 6-1 – Assumed properties of CRF

Binder %	UCS MPa	Cohesion MPa	Deformation Modulus GPa	Poisson's Ratio	Tensile Strength MPa
6	5.41	2.71	3.1	0.35	0.041
5	4.18	2.09	2.8	0.35	0.036
4	2.94	1.47	2.6	0.35	0.030
3	1.71	0.85	2.3	0.35	0.023
2	0.47	0.24	2.1	0.35	0.012
URF	0	0	0.15	0.35	0

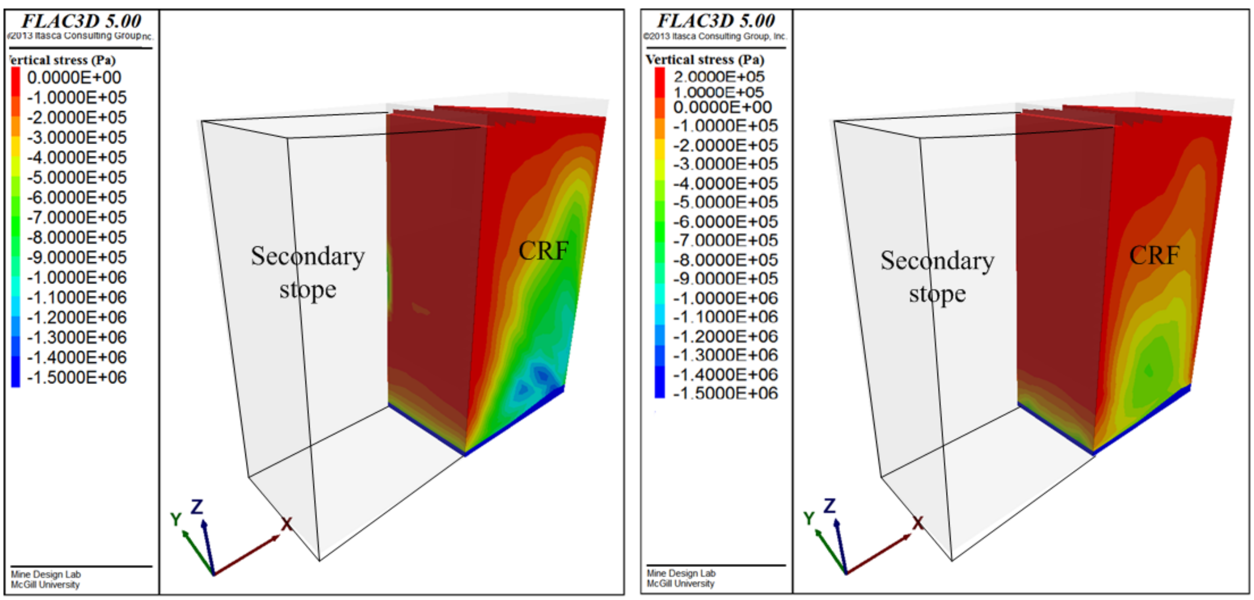

a) Static analysis b) Dynamic analysis

Figure 6-29 – Vertical stress presenting failure due to variable binder in backfill

It can be seen from Figure 6-29 that the backfill is stable at the bottom and it is at transition state on top for the static analysis. The dynamic analysis show failure in the top most zones of backfill that are poured with lowest binder. The next scenario that is observed at a Canadian CRF operation is somewhat opposite to the one discussed above. In this approach bottom portion of the backfill is poured with zero binder termed as un-cemented rockfill (URF) and rest of the stope is filled with the regular binder, as shown in Figure 6-30. The mine planners believe that by adopting this approach some of the binder will seep in the zero binder regions and thus will consolidate it partially. In the current study the binder seeping in URF is not simulated. Rest of the stope is poured with regular CRF except the top part, which is URF. It is believed that the top part of the exposed CRF will not be exposed at a later stage. As can be seen in the Figure, the top most portion of backfill is poured with URF. The scenario discussed is modelled with calibrated FLAC3D model. The contours of vertical stress are presented in Figure 6-31. It can be seen that the backfill destabilizes under gravity loading from the bottom URF zones, however the remaining part of exposed face is under transition zone. For the dynamic analysis the CRF is failing not only from the bottom but also from middle and top of the exposed face of backfill. This is because the URF is unconsolidated and when exposed fully it causes relaxation under gravity loading in the exposed backfill face.

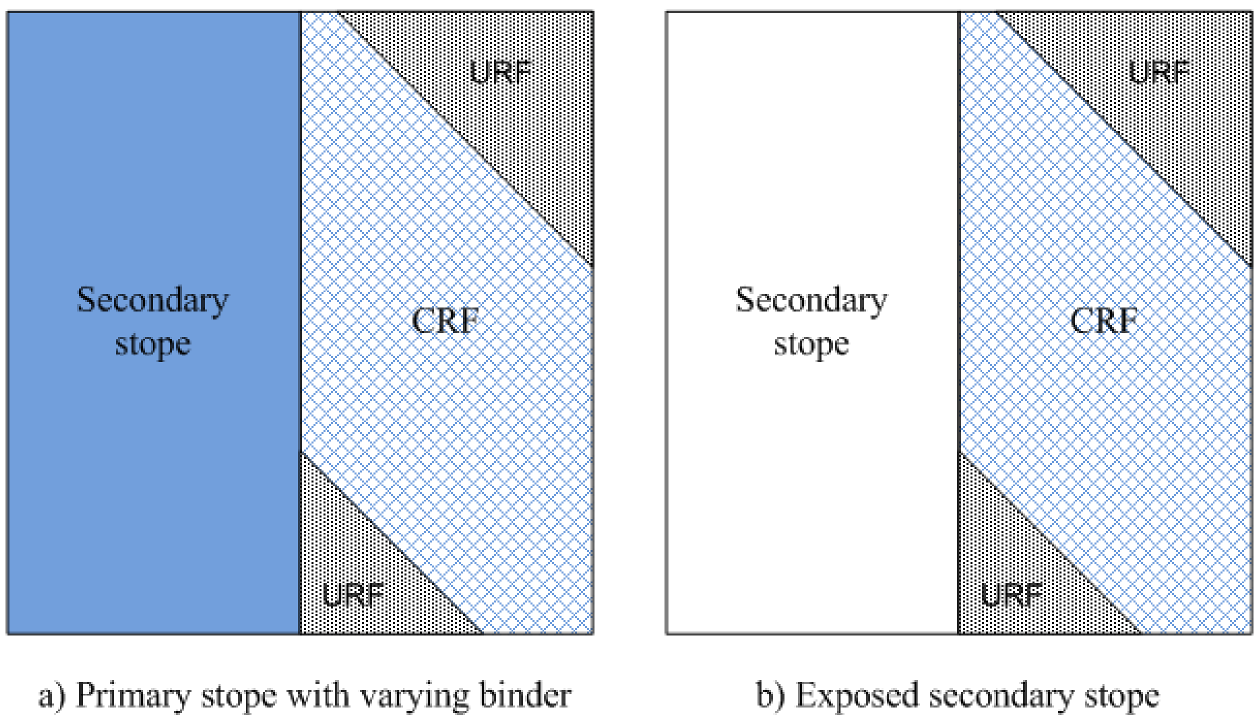

Figure 6-30 – A schematic presenting CRF practice of using URF to save binder cost

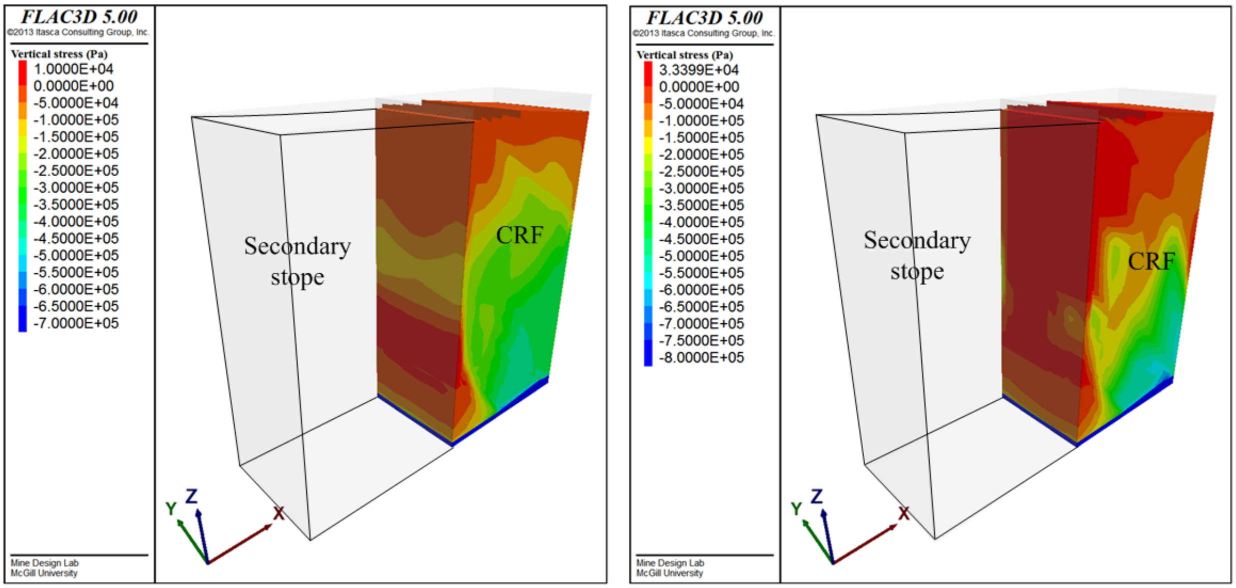

a) Static analysis

b) Dynamic analysis

Figure 6-31 – Vertical stress contours presenting failure in weak zones

6.5.5 Improving Backfill Performance by Studying Its Properties

The literature review of backfill suggested that the properties of backfill which control its performance include cohesion-friction angle, tensile strength, deformation modulus and Poisson's ratio. These properties are varied in the calibrated numerical model to study the impact of each property and results are presented. The tonnage of the failed zones is computed with the help of IsoZone plot of stress in FLAC3D. The IsoZone plot is exported as a DXF format to CAD software for computation of failed volume which is then used for computation of failed tonnage. Failed tonnage of CRF that is below the friction angle of CRF is not considered for this analysis.

Results of varying cohesion in CRF are presented in Figure 6-32, quite obviously it can be seen that the cohesion have an inverse relationship with failure in CRF. The dynamic analysis of CRF stope shows that more CRF zones are failing with low cohesion value but with increase in cohesion will decrease CRF failure. The cohesion in CRF can also be improved by controlling the particle size distribution as described by Stone [7]. The coefficient of determination of the data is found to be 97.34%.

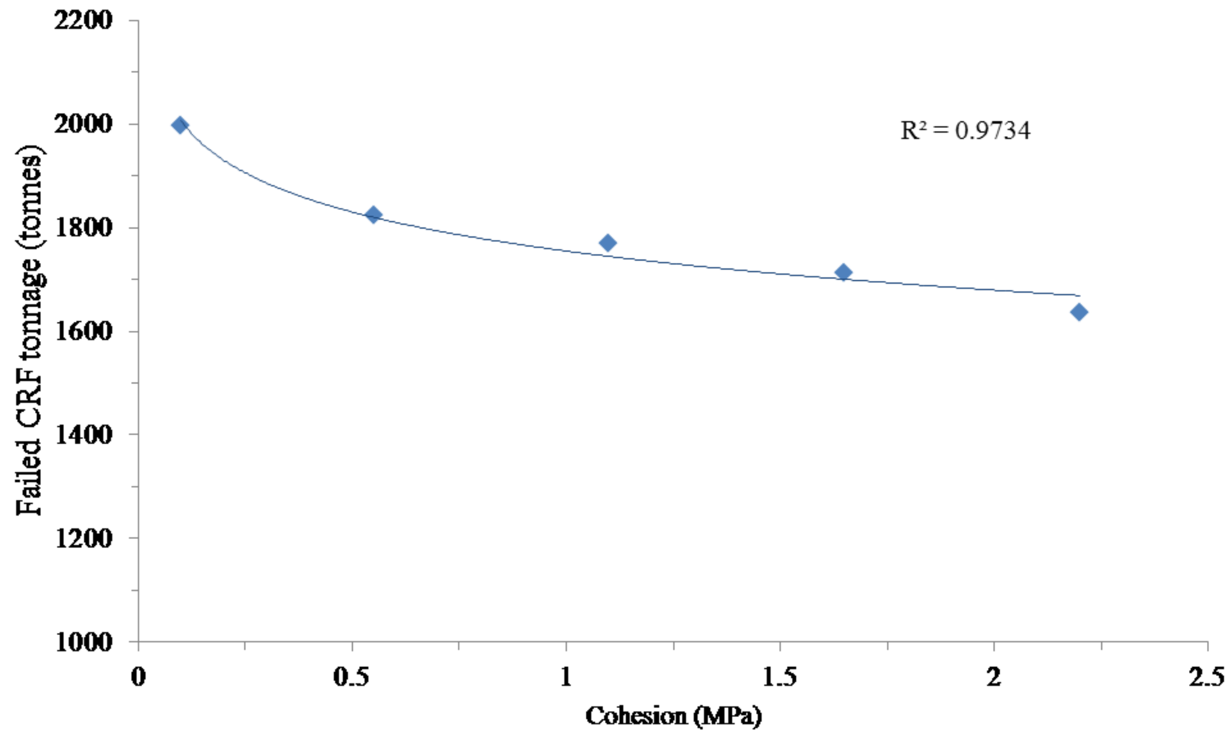

Figure 6-32 – Effect of varying cohesion on failed tonnage

Tensile strength of CRF is also varied in this analysis and results are presented in Figure 6-33. It can be seen from the Figure that the tensile strength of backfill have a negative relationship with failed CRF tonnage. The CRF rely on binder contents totally for improving tensile strength, and to improve tensile strength the binder must be increased along with finer particles to decrease void spaces and porosity of CRF [7, 8]. The coefficient of determination is found to be 92.21% for varying tensile strength. The results of varying deformation modulus of CRF are presented in Figure 6-34. It can be seen that the CRF failure has an indirect relationship with deformation modulus, that is the stiffer the backfill the lesser will be the failure in CRF. The coefficient of determination value of 96.75% is found for deformation modulus versus failed CRF tonnage. Results of varying the Poisson's ratio of CRF are presented in Figure 6-35. It can be observed that Poisson's ratio have an adverse effect on failure in CRF, the failure increases with increase in Poisson's ratio. The determination coefficient for the data is 93.73%.

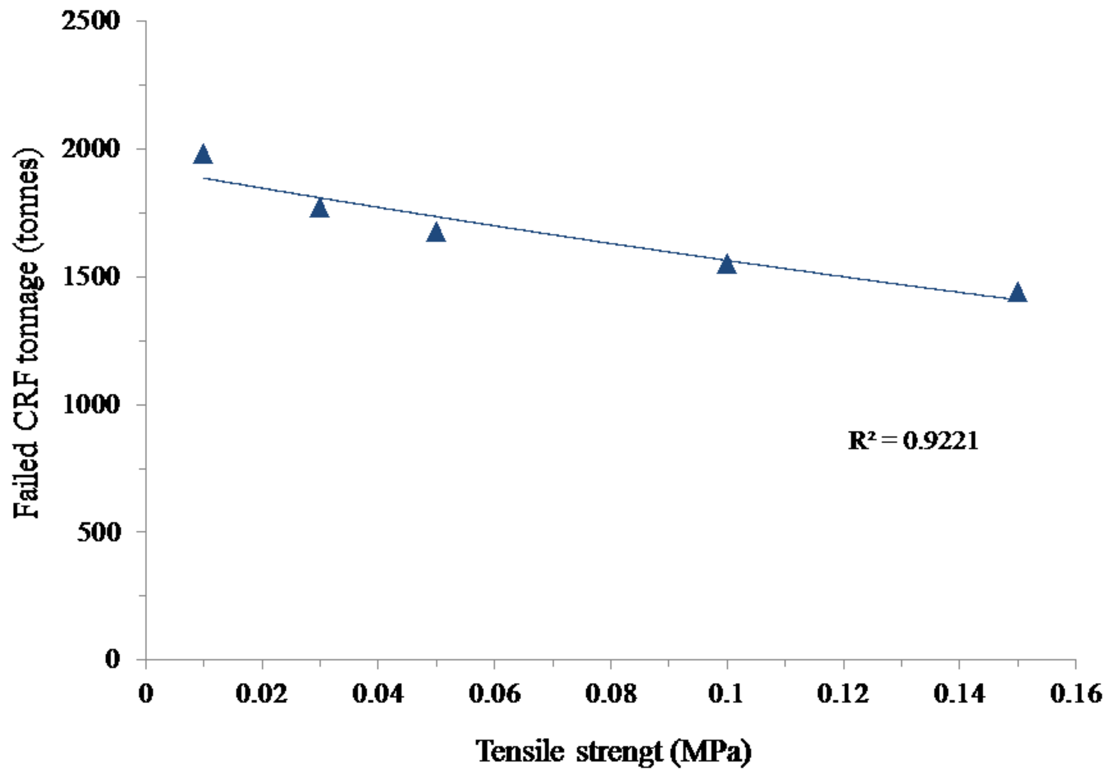

Figure 6-33 – Effect of varying tensile strength on failed tonnage

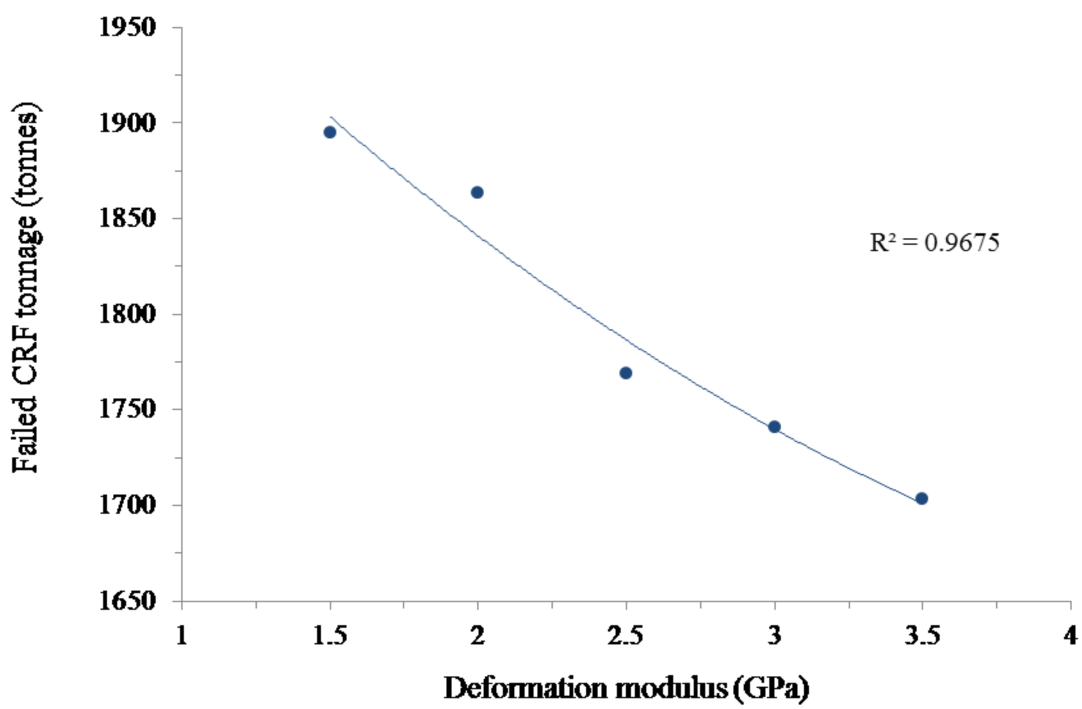

Figure 6-34 – Effect of varying deformation modulus on failed CRF tonnage

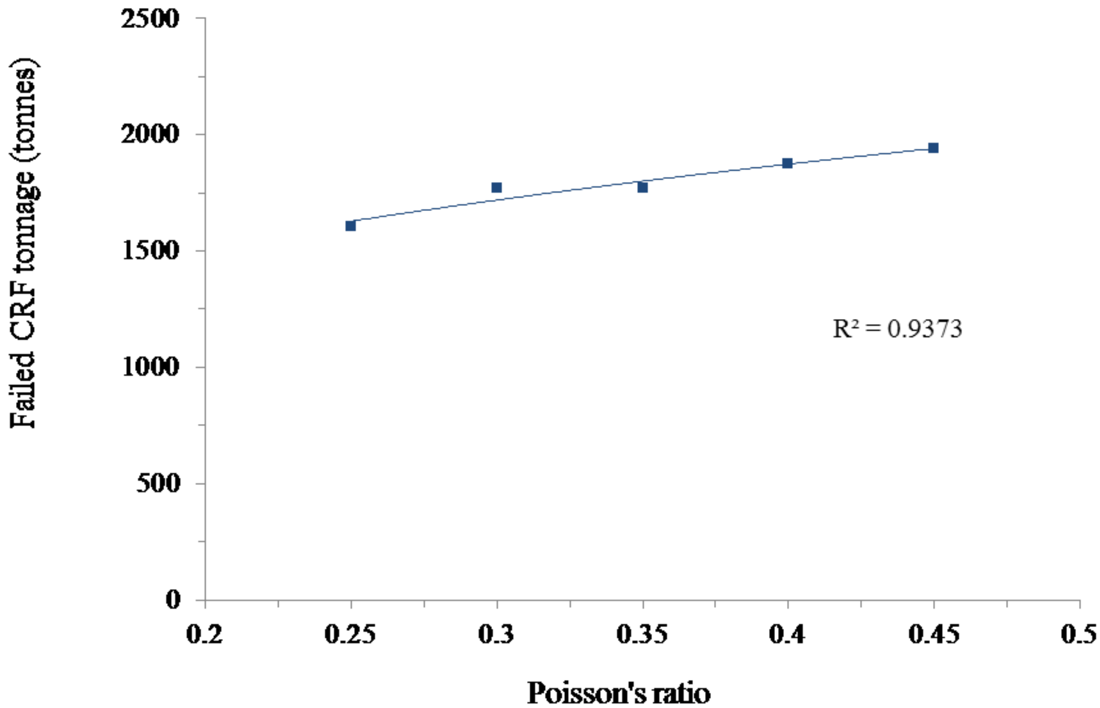

Figure 6-35 – Effect of varying Poisson's ratio on failed tonnage

6.6 DISCUSSION AND SUMMARY

The current practice for the design of mine backfill is largely based on static analysis of limit equilibrium models that are known as fill strength models (FSR). The practice is also dependent on experience gained from field observations. FSR models employ a factor of safety that ranges from 1.0 to 2.5 in order to account for the inherent variability of the in situ fill mechanical properties. FSR methods however are inadequate for the design of backfill against dynamic loads that are exerted on the exposed fill face due to production blasting of adjacent stopes. Numerical modelling with dynamic analysis option has been used in this work for assessing CRF stopes in sublevel stoping environment. The results show that the incorporation of blast-induced vibrations is crucial for adequate design of backfill.

The 3D dynamic numerical modelling technique laid down in this Chapter investigates CRF failure when subjected to blast loading. The approach adopted and results obtained are first of their kind as to date CRF is designed on gravity loading only and blast vibrations were never incorporated the design. This methodology incorporates three dimensional modelling in tandem with detailed literature review and on-site experimentation programs to simulate CRF material underground. The numerical model is calibrated using in-situ stress tensor values obtained from the study performed in late 70s. The model calibration technique used in this Chapter incorporates development of a smaller equivalent cavity model to study the transmission of blast vibrations and computation of blast load to be applied on CRF face. The equivalent cavity model also yielded to damping coefficient to be used for the main backfill model. Normal stress is applied on the walls of equivalent cavity and x, y and z components of velocity are monitored at two points in the model separated by a distance of 10 m. The length of explosive charge is also varied based on the blast design supplied by the case study mine. The peak particle velocity is computed at the two point monitored using charge-weight scaling law and is compared with FLAC3D results. The two particle velocities are equated by adjusting the applied normal stress and damping coefficient. Once the desired values are obtained the required data is extracted and imported in to the main CRF model. The main model is calibrated by comparing the onsite in-situ blast vibration monitoring experiment results and output of the FLAC3D. The calibrated model is then used to study various scenarios observed at North American mines. One of the planned stope at the Birchtree mine is taken as a base case scenario. It is shown that the CRF stope is stable during the static analysis but the same stope fails from the top of the exposed face when applied with blast load. The case of leaving a thin skin is also studied and it is found from the results that the approach is very good for minimizing backfill failure. Selective mining scenarios observed at Canadian mines are also simulated and better approach of mining with respect to CRF stope are laid down with the help of calibrated numerical model. The cases of varying binder contents in each shift to reduce cost are also modelled. It is found that such practices are not good for the stability of CRF. In the end a small parametric study is performed for geo-mechanical properties to appreciate the trend with CRF failure. The modelling approach laid down is a platform for developing a better CRF design tool capable of incorporating various conditions that are observed underground.

7 CONCLUSION, LIMITATIONS AND FUTURE WORK

7.1 CONCLUSIONS

A comprehensive review of backfill literature is conducted to develop an understanding of the cemented rockfill practices, properties and research. The review also shed light on other backfill types in use by the industry. Flaws in practices and design are highlighted from different operations, which enabled developing a 3D backfill model. It is found from the review that the CRF practitioners are well aware of the consequences of excessive blast vibrations when the fill is exposed for greater recovery. The review of CRF operations suggested that the backfill static design is insufficient to coup up with the strength requirements by CRF under dynamic load. The numerical modelling strategy for backfill material is also presented and it is recommended to use interface zones around backfill and a small gap of less than 1 meter on top of backfill. To decrease the solving time only backfill can be modelled as mohr-coulomb material, the rockmass may stay as elasto-plastic material. A small gap must be modelled on top of the backfill material to limit transformation of stress from top of the backfill.

Dynamic modelling technique is discussed in detail in Chapter 3. This Chapter includes theoretical equations solved for dynamic analysis, dynamic setup in FLAC3D, model boundary conditions, blast load application and damping. The chapter also reviews dynamic modelling studies on backfill and development of a CRF model for studying blast vibrations. The CRF is used to study various parameters including static and dynamic loading, stope dimensions, fill properties, segregation, mining method and magnitude of blast vibrations. The results of CRF model developed showed wedge shape failure from top of the exposed face, as recorded on site and discussed in the literature.

Chapter 4 present an overview of case study mine, location, geology of the area, mining method, typical stope design, backfill system employed, problems encountered with backfill system, backfill failure CMS profiles showing fill failure and geo-mechanical data provided by the mine for CRF study.

Details of in-situ blast vibration monitoring experiment conducted at the mine site are presented in Chapter 5. The standard guidelines, procedure for blast vibration monitoring as well as review of vibrations monitoring in backfill are shown. The blast design at the case study mine is discussed along with experimental setup adopted. The results of experiment performed are presented for all the three blast lifts conducted. As presented the blast 1 and 2 produced low magnitude of blast vibrations in CRF that is 33 mm/s and 86 mm/s. The third blast produced high level of blast vibration magnitude of 426 mm/s and this may produce big failures as vibration magnitude of 250 mm/s or more produces fill failure in exposed backfill.

FSR models can only be used for the assessment of required compressive strength to sustain the own weight of the backfill stope. Chapter 6 presents numerical model setup for CRF at the Birchtree mine. The numerical model is calibrated using the in-situ stress tensor values at a depth of 1090 meters (2750 level) provided by the mine. Model calibration is followed by calibration process, which includes development of an equivalent cavity model, applying blast load and equating vibration levels in the model with charge-weight scaling laws. The blast vibration magnitude is extracted from equivalent cavity model and is then applied to the main calibrated CRF model. The blast vibrations in CRF are computed and the blast load is varied to $\pm$ 20% to achieve the blast vibration magnitude obtained during the in-situ experiment conducted at the case study mine. The process is repeated for all blast holes of three blast lifts. Once the CRF model is calibrated it is ready for performing a detailed study on different scenarios encountered at different operations. The results of base case scenario are also presented which is the scenario of the planned stope at the case study mine. The results presented failure of exposed CRF face from top of the stope in wedge shape. This is in-accordance with the CRF failures observed at the Birchtree mine and other CRF operations. The case of leaving a thin ore skin in between production stope and CRF is modelled. It is shown that the thin skin is supporting CRF under high blast vibrations. Similarly two cases of selective mining and better approaches of selective mining are presented. It is shown that the current practices of selective mining at CRF operations are exposing backfill and better approach presented in this thesis can assist supporting CRF stopes. The scenario of modelling the practice of varying binder for each backfilling shift is modelled and results are presented. It is found that the lower binder zones on top of fill produced greater failure. Similarly the greater binder zones are strong and stable at the bottom of the stope. A common practice of using un-cemented rockfill (URF) at the bottom as a barricade is also modelled and it is found that the practice is not very good. As when the CRF block is exposed, major portion of URF will be removed and the exposed face will be under tension. The last part includes a parametric study incorporating the geo-mechanical properties of CRF. The parameters studied including cohesion, tensile strength, deformation modulus and poisson's ratio. The parameters studied showed an inverse relationship with failed CRF tonnage with exception of Poisson's ratio that showed a direct relationship.

7.2 LIMITATIONS

The stope monitored for blast vibrations was not planned to be exposed by the case study mine, and the CRF remained stable under blast load. FLAC3D models zones as cuboid, pyramid and prism however CRF can be better represented by spheroid or oblate spheroid particles of different sizes. Each spheroid can be made with a combination of smaller balls assigned different properties and binder coating on aggregate can be modelled in PFC3D using combination of very small balls. This will help modelling and studying segregation in CRF. Blasting is a thermo-mechanical process, and thermal effects of blasting are not simulated in this analysis. This study includes fewer data points from in-situ experiment. Each in-situ experiment requires remote site visits for longer duration for planning, setup and acquisition of results. Purchase of geophones and calibration of equipment are also costly. The in-situ properties of CRF are unavailable for the case study mine and this is a limitation of this work. The determination of in-situ properties is a troublesome job of extensive sampling and testing of backfilled stope. This project incorporated monitoring only primary (P-1) stope for blast vibrations. The model calibration with in-situ stresses needs two measurements, in this work only one location is available for calibration.

7.3 RECOMMENDATIONS FOR FUTURE WORK

In future a CRF stope to be exposed must be monitored for blast vibrations. If the CRF stope fails then the failure surface produced can be used for calibration of the numerical model. PFC3D is highly recommended for simulating backfill. Segregation in backfill can be measured from core drilling of CRF stopes and the results should be incorporated in CRF model. Blasting process must be simulated as close to reality as possible. Extensive in-situ testing of geo-materials and blast monitoring programs are recommended to support and calibrate the findings. Similar studies on S-2 stopes can be conducted with greater efficiency, as S-2 stope is exposed on two sides. Thus the same geophone installed in S-2 stope can be used twice.

8 STATEMENT OF CONTRIBUTIONS

This study is the first to adopt 3D dynamic modelling approach for the stability analysis of CRF stope subjected to dynamic loads due to production blasts in an adjacent stope. This study provided a methodological approach for the complete stability assessment of cemented rockfill stope. As a result the mine planner will foresee any upcoming fill failures and will counteract as required. The CRF material is monitored for blast vibrations from adjacent production stope for the first time, and the results are used to calibrate the numerical model and assess the possible extent of fill failure should the fill stope be completely exposed. The calibrated 3D-dynamic CRF model is used to examine various other scenarios that result from different backfilling practice.

9 REFERENCES

1. Zhang, Y. and H.S. Mitri, *Elastoplastic stability analysis of mine haulage drift in the vicinity of mined stopes.* International Journal of Rock Mechanics and Mining Sciences, 2008. **45**(4): p. 574-593.
2. Aitchison, G.D., M. Kurzeme, and D.R. Willoughb, *Geomechanics considerations in optimising the use of mine fill: Part A: The investigation of the response of fill as a structural component*, in *Jubilee Symposium on Mine Filling, Mount Isa*1973, The Australasian Institute of Mining and Metallurgy, North West Queensland Branch: Mount Isa. p. 35 - 48.
3. Bagde, M.N., et al., *Examining the influence of stope dimensions and mining sequence on backfill dilution: a review with case study* In Int. Conf. on Technological Challenges and Management issues for sustainability of Mining Industries (TMSMI), August 04-06, 2011, organized by Dept. of Mining Eng., NIT Rourkela, India, B. K. Pal and S. Chatterjee (Eds), 2011: p. 13-28.
4. Hassani, F. and J. Archibald, *Mine Backfill*, 1998, Canadian Institute of Mining, Metallurgy, and Petroleum: Montreal Canada.
5. Yu, T.R., *Some factors relating to the stability of consolidated rockfill at Kidd Creek*, in *Proceedings of the 4th International Symposium on Mining with Backfill*, F. Hassani, M.J. Scoble, and T.R.YU, Editors. 1989, A.A. Balkema: Montreal Canada. p. 279 - 286.
6. Emad, M.Z., H.S. Mitri, and J.G. Henning, *Effect of blast vibrations on the stability of cemented rockfill.* International Journal of Mining, Reclamation and Environment, 2012. **26**(3): p. 233-243.
7. Stone, D., *Factors that affect cemented rockfill quality in Nevada mines*, in *Minefill 2007 : The 9th International Symposium on Mining with Backfill*, F. Hassani, et al., Editors. 2007, Canadian Institute of Mining and Metallurgy: Montreal QC Canada. p. 1 - 6.
8. Yu, T.R. and D.B. Counter, *Backfill practice and technology at Kidd Creek Mines.* The Canadian Mining and Metallurgical Bulletin, 1983. **76**(856): p. 56 - 65.
9. Yu, T.R., *Mechanisms of fill failure and fill strength requirements*, in *16th Canadian Rock Mechanics Symposium*, P.K. Kaiser and D.R. McCreath, Editors. 1992: Sudbury ON Canada. p. 43 - 46.

10. Henning, J.G., *Evaluation of Long-Hole Mine Design Influences on Unplanned Ore Dilution.* PhD Thesis, McGill University, Montreal Canada, 2007.
11. Smith, J.D., C.L.D. Jongh, and R.J. Mitchell. *Large scale model tests to determine backfill strength requirements for pillar recovery at the Black Mountaine Mine*. in *Minefill 83: Proceedings of the International Symposium on Mining with Backfill* 1983. Lulea Sweden: A.A.BALKEMA/ROTTERDAM/1983.
12. Mathews, K.E. and F.E. Kaesehagen, *The development and design of a cemented rock filling system at the Mount Isa Mine Australia*, in *Jubilee Symposium on Mine Filling, Mount Isa*1973, The Australian Asian Institute of Mining and Metallurgy, North West Queensland Branch Mount Isa. p. 13 - 23.
13. Tatman, C.R., *Mining dilution in moderate- to narrow-width deposits*, in *Underground Mining Methods: Engineering Fundamentals and International Case Studies*, W.A. Hustrulid and R.L. Bullock, Editors. 1998, Society of Mining and Metallurgical Engineering: United States of America. p. 615 - 626.
14. Miller, F., Y. Potvin, and D. Jacob, *Laser Measurement of Open Stope Dilution* CIM Bulletin, 1992. **85**: p. 96-102
15. Vallée, M., M. Dagbert, and C. Desrochers, *Guide to the evaluation of gold deposits* CIM Special 1992. **45**(ISBN 0-919086-31-4).
16. Scoble, M.M.A., *Dilution in underground metal mining: implications for grade control and production management.* Geological Society special publication., 1994. **79**: p. 95.
17. Farsangi, P.N., *Improving cemented rockfill design in open stoping*, in *Department of Mining and Metallurgical Engineering*1996, McGill University: Montreal Canada.
18. Chen, D., M.L. Messurier, and B. Mitchell, *Application of cemented aggregate fill at Barrick's Darlot Gold Mine*, in *Minefill 2004: Proceedings of the 8th International Symposium on Mining with Backfill.*, Z. Aimin, Editor 2004, The Nonferrous Metal Society of China: Beijing China. p. 82 - 89.
19. Grice, A.G. *Recent Minefill Developments in Australia*. in *Minefill 2001: Proceedings of the 7th International Symposium on Mining with Backfill* 2001. Seatle WA USA: Society of Mining, Metallurgy & Exploration.
20. Gool, B.S.v., *Effects of blasting on the stability of paste fill stopes at Cannington Mine*, in *School of Civil and Environmental Engineering*2007, James Cook University: Australia.

21. Yumlu, M., *Backfill Practices at Çayeli Mine.* 17th International Mining Congress and Exhibition of Turkey- IMCET2001, 2001: p. 333 - 340.
22. Doerner, C.A.C., *Effect of delayed backfill on open stope mining methods*, in *Mining Engineering*2005, University of British Columbia: Vancouver BC Canada.
23. Tesarik, D.R., J.B. Seymour, and F.M. Jones. *Determination of in situ deformation modulus for cemented rockfill* in *Technology Roadmap for Rock Mechanics, 10th Congress*. 2003. Johannesburg: International Society for Rock Mechanics, S. African Institute of Mining and Metallurgy Symp. Series, 2003.
24. Kockler, M., *Design of cemented rockfill spans for longhole stoping at the Rain Mine, Carlin, Nevada.* PhD Thesis, University of Idaho, 2007.
25. Lilley, C.R. and G.P.F. Chitombo, *Development of a near field damage model for cemented hydraulic fill.* Minefill'98, Brisbane, 1998: p. 191 - 196.
26. O'Hearn, B. and G. Swan, *The use of models in sill mat design at Falconbridge.* Innovatins in Mining Backfill Technology, Proceedings of the 4th International Symposium on Mining with Backfill, Montreal 1989: p. 139 - 146.
27. Coulthard, M.A., *Applications of numerical modelling in underground mining and construction.* Geotechnical and Geological Engineering, 1999. **17**(3): p. 373-385.
28. Napier, J.A.L., et al., *Quantification of stope fracture zone behaviour in deep level gold mines.* J. the South African Inst. of Min. and Met. (SAIMM), 1997 **97**: p. 119-134.
29. Hazzard, J.F., R.P. Young, and S.C. Maxwell, *Micromechanical modeling of cracking and failure in brittle rocks.* J. of Geophy. Res. , 2000. **105**(B7): p. 16683-97.
30. Ran, J. and T. Watunga, *Application of Consolidated Rockfill to Open Stoping in Underground Mines*, in *RockEng12 - Rock Engineering for Natural Resources*, C. Hawkes, Editor 2012, Canadian Institute of Mining and Metallurgy: Edmonton AB Canada. p. 197 - 207.
31. Hustrulid, W.A.B.R.C., *Underground mining methods : engineering fundamentals and international case studies*2001, Littleton, Colo.: Society for Mining, Metallurgy, and Exploration.
32. Kurakami, T., et al., *Mining with backfill at the Hishikari Mine, Japan.* Gospodarka Surowcami Mineralnymi 2008. **24**: p. 197 - 212.

33. Henderson, A., G. Jardine, and C. Woodall, *The implementation of paste fill at the Henty gold mine*, in *Minefill98: The Sixth International Symposium on Mining with Backfill*, M. Bloss, Editor 1998, Australasian Institute of Mining and Metallurgy: Brisbane Australia. p. 299 - 304.
34. O'Toole, D., et al. *Backfill - Queens Mine Design Wiki*. 2011.
35. Currie, R., *The preparation of pastefill and its use at some Canadian mines*, in *Minefill98: The Sixth International Symposium on Mining with Backfill*, M. Bloss, Editor 1998, Australasian Institute of Mining and Metallurgy: Brisbane Australia. p. 325 - 330.
36. MacKenzie, A.T. and P.A. Rantala, *Pastefill transportation techniques and predictive rheology*, in *Minefill 2001: The 7th International Symposium on Mining with Backfill* D. Stone, Editor 2001, Society for Mining, Metallurgy & Exploration: Seatle Washington. p. 57 - 62.
37. Jewel, R.J. and A.B. Fourie, *Paste and thickened tailings - a guide.* 2nd Ed, Australian Centre for Geomechanics, 2005.
38. Slottee, J.S., *Update on the Application of Paste Thickeners for Tailings Disposal - Mine Paste Backfill.* International Seminar on Paste and Thickened Tailings Paste and Thickened Tailings Paste 2004, 2004.
39. Skeeles, B.E.J., *Design of paste backfill plant and distribution system for the Cannington project*, in *Minefill98: The Sixth International Symposium on Mining with Backfill*, M. Bloss, Editor 1998, Australasian Institute of Mining and Metallurgy: Brisbane Australia. p. 59 - 63.
40. Bloss, M.L. and R. Mathew B, *Mining with paste fill at BHP Cannington* in *Minefill 2001: The 7th International Symposium on Mining with Backfill* D. Stone, Editor 2001, SME: Seatle Washington. p. 209 - 221.
41. Archibald, J.F., E.M.D. Souza, and L. Beauchamp, *Safe Canadian practices in mine backfill operations*, in *Minefill 2011, 10th International, Symposium on Mining with Backfill, The Southern African Institute of Mining and Metallurgy*2011. p. 249 - 256.
42. Dorricott, M.G. and A.G. Grice, *Backfill – The Environmentally Friendly Tailings Disposal System.* Proceedings Green Processing, The Australasian Institute of Mining and Metalurgy: Melbourne, 2002: p. 265 - 270.

43. Reschke, A.E., *The use of cemented rockfill at Namew Lake mine, Manitoba, Canada*, in *Minefill 93: The 5th International Symposium on Mining with Backfill*, H.W. Glenn, Editor 1993, The South African Institute of Mining and Metallurgy: Johannesburg. p. 101 - 108.
44. Clough, R.W. and J. Penzen, *Dynamics of Structures*1975, United States of America: McGraw-Hill Book Company Inc.
45. Askew, J.E., P.L. McCarthy, and D.J. Fitzgerald, *Backfill research for pillar extraction at ZC/NBHC*, in *Mining with Backfill - Minefill 1978*1978, CIM: Sudbury. p. 100 - 110.
46. Terzaghi, K., *Theoretical Soil Mechanics*1961: Wiley and Sons.
47. Coates, D.F., *Rock Mechanics Principles*. Vol. 874. 1981: EMR Canada Monograph.
48. Mitchell, R.J., R.S. Olsen, and J.D. Smith, *Model studies on cemented tailings used in mine backfill.* Canadian Geotechnical Journal, 1982. **19**(1): p. 14-28.
49. Pirapakaran, K., *Load-deformation characteristics of minefills with particular reference to arching and stress developments*, in *Civil Engineering*2007, James Cook University: Townsville Australia.
50. Mitri, H.S.H.R.Z.Y., *New rock stress factor for the stability graph method.* RMMS International Journal of Rock Mechanics and Mining Sciences, 2011. **48**(1): p. 141-145.
51. Donze, F.V. and N.H.P. Bemasconi, *Optimization of the blasting patterns in shaft sinking*, in *In Proc. 5th North American Rock Mech. Symp. - NARMS-TAC 2002*, R. Hammah, et al., Editors. 2002, Univ. of Toronto press: Toronto, Canada. p. 999-1005.
52. Mitchell, R.J. and J.D. Smith, *Mine backfill design and testing* CIM Bulletin, 1979. **72**(8018): p. 82-89.
53. Mitchell, R.J. and B.C. Wong, *Behaviour of cemented tailings sands* Canadian Geotechnical Journal, 1982. **19**(3): p. 289-295.
54. Brady, A.C. and J.A. Brown, *Hydraulic fill at Osborne mine*, in *In Proc. 8th AUSIMM Underground Operators Conference, 29-31 July* 2002, The Australian Institute of Mining and Matellurgy: Townsville, Qld Australia. p. 161-165.
55. Dirige, A.P.E., *Engineering design of paste backfill systems* in *Mining Engineering*2003, Queen's University: Kingston ON Canada.

56. Li., L., et al., *Modeling arching effects in narrow backfilled stopes with FLAC*, in *In FLAC and numerical modeling in geomechanics –2003* R. Brummer, et al., Editors. 2003, A.A. Balkema, Rotterdam: The Netherlands. p. 211–219.

57. Rankine, R.M., *The geotechnical and static stability of Cannington mine paste backfill* in *Civil Engineering*2004, James Cook University: Townsville Australia.

58. Eberhardt, E., *The Hoek-Brown failure criterion.* Rock Mech Rock Eng Rock Mechanics and Rock Engineering, 2012. **45**(6): p. 981-988.

59. Roberts, R.R.S.L.M. *Meikle Mine Backfill System -A Case History*. in *Minefill 2001: Proceedings of the 7th International Symposium on Mining with Backfill* 2001. Seatle Washington: Society for Mining and Metallurgy & Exploration.

60. Reschke, A.E., *The development of colloidal mixer based CRF systems.* Minefill'98, Brisbane Australia, 1998: p. 1-11.

61. Kosmatka, S.H. and W.C. Panarese, *Design and Control of Concrete Mixture*. Thirteenth Edition ed1988, Illinois USA: Portland Cement Association.

62. Yu, T.R., J.G. Henning, and D.B. Counter. *Geomechanical assessment of a large open stope at depth*. in *Stresses in Underground Structures: proceedings of speciality conference*. 1990. Ottawa ON Canada: Mining Research Laboratories, Canada Centre for Mineral and Energy Technology, EMR.

63. Swan, G., *A new approach to cemented backfill design.* CIM Bulletin, 1985. **78**(884): p. 53-58.

64. Lilley, A.M.H.C.R., *Backfill Selection and Experience at the Kanowa Belle Gold Mine, Western Australia*, in *Minefill 2001: 7th International Symposium on Mining with Backfill*, D. Stone, Editor 2001, Society of Mining and Metallurgical Engineering: Littleton, Colarado. p. 379-387.

65. Annor, A. and D. Millette, *Laboratory Studies Optimization of Aggregate mix Compositions for Cemented Rockfill.* Submitted to Lac Minerals by CANMET - Mining Research Laboratories, Sudbury Lab, 1991(MRL91-115).

66. Annor, A., D. Millette, and S. Boualavong, *Uniaxial compression testing of cemented rockfill samples.* CANMET, 1993.

67. Walton, T.R., *Project 94037 Bousquet #2 Mine - Cemented rockfill testing* American Barrick Corp., 1994.

68. Piciacchia, L., *Rockfill testing 18" diameter specimen.* Internal report of W.R. Grace & Co. of Canada Ltd., 1989. **TROW Ontario LTD**(Project: S00073R).

69. Seppanen, P. and K.E. Marttala, *Cemented-rockfilling practices at Enonkosko and Visaria mines*, in *Minefill 93: The 5th International Symposium on Mining with Backfill*, H.W. Glenn, Editor 1993, THE SOUTH AFRICAN INSTITUTE OF MINING AND METALLURGY: Johannesburg. p. 333 - 336.

70. Annor, A.B., *A Study of the Characteristics and Behaviour of Composite Backfill Material*, in *Department of Mining and Metallurgy*1999, McGill University: Montreal Canada.

71. Wang, C. and E. Villaescusa, *Factors influencing the strength of cemented aggregate fill*, in *Minefill 2001: The 7th International Symposium on Mining with Backfill* D. Stone, Editor 2001, SME: Seatle Washington. p. 81 - 87.

72. Millette, A.A.D. and S. Boualavong, *Uniaxial Compression Testing of Cemented Rockfill Samples.* Lac Minerals (Macassa) Limited's Cemented Rockfill Project, 1993. **CANMET-Mining Research Laboratories Sudbury Lab**(MRL 93-014CL).

73. Stone, D.M.R., *The optimization of mix designs for cemented rockfill*, in *Minefill 93: The 5th International Symposium on Mining with Backfill*, H.W. Glenn, Editor 1993, THE SOUTH AFRICAN INSTITUTE OF MINING AND METALLURGY: Johannesburg. p. 249 - 253.

74. Magnier, F.V.D.J.B.S.A., *Modeling fractures in rock blasting.* Int. J. Rock Mech. Min. Sei., 1997. **34**(8): p. 1153-1163.

75. Yang, R., W.F. Bawden, and P.D. Katsabanis, *A new constitutive model for blast damage.* Int. J. Rock Mech. Min Sci. Geornech Abstr. , 1996. **33**: p. 245-254.

76. Liu, L. and P.D. Katsabanis, *Development of a continuum damage model for blasting analysis.* lnt. J. Rock Mech. Min. Sci. , 1997. **34**(2): p. 217-231.

77. ITASCA Consulting Group, I., *Dynamic Analysis, FLAC3D Fast Lagrangian Analysis of Continua in 3 Dimensions*, 2009, Itasca Consulting Group: Minneapolis, Minnesota USA.

78. Seed, H.B. and I. Idriss, *Influence of Soil Conditions on Ground Motion during Earthquakes.* J. Soil Mech. Found., Div. ASCE, , 1969. **95**: p. 99-137.

79. Bickford, W.B. *A first course in the finite element method*. 1994. lrwin, USA.

80. Belytschko, T., *An Overview of Semidiscretization and Time Integration Procedures*. Computational Methods for Transient Analysis, ed. T. Belytschko and T.J.R. Hughes1983, New York United States: Elsevier Science Publishers
81. Lysmer, J. and R.L. Kuhlemeyer, *Finite Dynamic Model for Infinite Media.* J. Eng. Mech, 1973. **95**(EM4): p. 859 - 877.
82. Kunar, R.R., P.J. Beresford, and P.A. Cundall, *A Tested Soil-Structure Model for Surface Structures," in Proceedings of the Symposium on Soil-Structure Interaction* Roorkee University, India, January, 1977, 1977. **1**: p. 137 - 144.
83. Saharan, M.R., *Dynamic Modelling Of Rock Fracturing By Destress Blasting*, in *PhD Thesis, McGill University, Montreal Canada*2004, McGill University: Montreal Canada.
84. Lee, E., M. Finger, and W. Collins, *JWL equation of state coefficients for high explosives.* Technical Report UCID-16189, Lawrence Livermore National Library, Livermore, CA, 1973.
85. Duvall, W.L., *Strain wave shapes in rock near explosions.* Geophysics, 1953. **18**(2): p. 310 - 323
86. Jung, W.J., et al., *Effects of rock pressure on crack generation during tunnel blasting. .* IJ Japan Explosives Soc, 2001. **62**(3): p. 138 - 146.
87. Lima, A.D.R., et al., *An adaptive strategy for the dynamic analysis of rock fracturing by blasting.* lnternational Proceedings and International Conference on Computational Engineering & Science (ICES'02) Reno Nevada, 2002.
88. Olatidoye, O., et al., *A representative survey of blast loading models and damage assessment methods for buildings subject to explosive blasts.* Report by Nichols Research Corporation. , 1998. **Report No. CEWES** (MSRCIPET TR/98-36.): p. 14.
89. Robertson, N.J., C.J. Hayhurst, and G.E. Fairlie, *Numerical simulation of explosion phenomena.* Int J. Computer Appl. Tech. , 1994. **7**(3-6): p. 316 - 329.
90. Biggs, J.M., *Introduction to Structural Dynamics.* New York:McGraw-Hill, 1964.
91. Gemant, A. and W. Jackson, *The Measurement of Internal Friction in Some Solid Dielectric Materials.* The London, Edinburgh, and Dublin Philosophical Magazine & Journal of Science, 1937. **XXII**: p. 960-983.

92. Metzger, D.R., *Adaptive damping for dynamic relaxation problems with non-monotonic spectral response.* international Journal for Numerical Methods and Engineering, 2003. **56**: p. 57 - 80.

93. McKay, D.L. and J.D. Duke, *Mining with backfill at Kidd Creek no. 2 mine*, in *Minefill 89: Proceedings of the 4th International Symposium on Mining with Backfill*, F.P.HASSANI, M.J.SCOBLE, and T.R.YU, Editors. 1989, A.A.BALKEMA / ROTTERDAM / BROOKHELD: Montreal Canada. p. 161 - 172.

94. Hassani, F.P., M.J. Scoble, and T.R.Yu, *Innovations in mining backfill technology : proceedings of the 4th International Symposium on Mining with Backfill/Montreal/2-5 October 1989.* Rotterdam : A.A. Balkema, 1989.

95. Grice, A.G., *Fill research at Mount Isa mines limited*, in *Minefill 89: PROCEEDINGS OF THE 4TH INTERNATIONAL SYMPOSIUM ON MINING WITH BACKFILL*, F.P.HASSANI, M.J.SCOBLE, and T.R.YU, Editors. 1989, A.A.BALKEMA / ROTTERDAM / BROOKHELD: Montreal Canada. p. 15 - 22.

96. Emad, M.Z., H. Mitri, and C. Kelly, *Effect of blast-induced vibrations on ore dilution due to fill failure*, in *65th Canadian Geotechnical Conference - GeoManitoba2012*, G. Robinson and K. Bannister, Editors. 2012, Canadian Geotechnical Society: Winnipeg Canada. p. Paper number: 390.

97. Sharpe, J.A., *The production of elastic waves by explosion pressures I. Theory and empirical field observations.* Geophysics, 1942. **7**(2): p. 144 - 154.

98. Kutter, H.K. and C. Fairhurst, *On the fracturing process in blasting.* International Journal of Rock Mechanics & Mining Sciences, 1971. **8**: p. 181 - 202.

99. Starfield, A.M. and J.M. Pugliese, *Compression waves generated in rock by cylinderical explosive charge: A comparison between a computer model and field measurements.* International Journal of Rock Mechanics & Mining Sciences, 1968. **5**: p. 65 - 77.

100. Harries, G., *Development of a dynamic blasting simulation.* The Third International Symposium on rock Fragmentation by Blasting, Brisbane Australia, 1990(175 - 179).

101. Blair, D.P. and J.J. Jiang, *Surface vibrations due to a vertical column of explosive.* international Journal of Rock Mechanics & Mining Sciences & Geomechanics Abstracts,, 1995. **32**(2): p. 149 - 154.

102. Wilcox, T., *Finite Element Simulation of a Blast Containment Cylinder Using LS-DYNA*, 2003, University of Nevada: Las Vegas USA.

103. Kjartansson, E., *Constant Q-wave propagation and attenuation.* Journal of Geophysical Research, 1979. **84**(B9): p. 4737 - 4748.

104. Yang, R.L., W.F. Bawden, and P.D. Katsabanis, *A new constitutive model for blast damage.* International Journal of Rock Mechanics & Mining Sciences & Geomechanics Abstracts,, 1996. **33**(3): p. 245 - 254.

105. Jiang, J.J., D.P. Blair, and G.R. Baird, *Dynamic response of an elastic and viscoelastic full space to a spherical source.* International Journal for Numerical and Analytical Methods in Geomechanics, 1995. **19**: p. 181 - 193.

106. Blair, D. and A. Minchinton, *On the damage zone surrounding a single blasthole.* Rock Fragmentation by Blasting, Rotterdam, 1996: p. 121 - 130.

107. Minchinton, A. and P.M. Lynch, *Fragmentation and heave modelling using a coupled discrete element gas flow code.* Rock Fragmentation by Blasting, Rotterdam, 1996: p. 71 - 80.

108. Preece, D.S. and B.J. Thorne, *A study of detonation timing and fragmentation using 3-D finite element techniques and a constitutive model.* Rock Fragmentation by Blasting, Rotterdam, 1996: p. 147 - 156.

109. Piciacchia, L., *Field and Laboratory Studies on Mine Backfill Design Criteria*, in *Department of Mining and Metallurgical Engineering*1987, McGill University: Montreal, Quebec.

110. Seppanen, P. and K.E. Marttala, *Cemented Rockfilling Practices at Enonkoski and Viscaria Mines*, in *Minefill 1993: International Symposium on Mining with Backfill*1993, South African Institute of Mining and Metallurgy: Johannesburg South Africa. p. 333-335.

111. Schimizze, B., et al., *An experimental and numerical study of blast induced shock wave mitigation in sandwich structures.* Applied Acoustics, 2013. **74**(1): p. 1-9.

112. Ryu, C.H., *Computer modeling of dynamic ground motion due to explosive blasting and review of sorne modeling problems.* J. Japan Explosives Society, 2002. **63**(5): p. 217-222.

113. Taylor, L.M., E.P. Chen, and J.S. Kllsmaul, *Micro-crack induced damage accumulation in brittle rock under dynamic loading* Computer Methodology in Applied Mechanics Engineering, 1986. **55**: p. 301-320.
114. Hao, H., H.W. Ma, and Y.X. Zhau, *Numerical simulation of underground explosions.* Int. J. Blasting by Fragmentation (FRAGBLAST), 1998. **2**: p. 383-395.
115. Hao, H., C. Wu, and Y. Zhau, *Numerical analysis ofblast-induced stress waves in a rock mass with anisotropic continuum damage models Part 1 : equivalent material property approach.* Rock Mech. Rock Engg, 2002. **35**(2): p. 79-94.
116. Curran, D.R., L. Seaman, and D.A. Shockey, *Dynamic failure of solids.* . Physics reports, 1987. **147**: p. 253-388.
117. Thome, B.J., P.J. Hommert, and B. Brown, *Experimental and computational investigation of the fundamental mechanisms of cratering*, in *ln Proc. 3rd Int. Symp. Rock fragmentation by Blasting - FRAGBLAST 3*1990: Brisbane, Australia. p. 412-423.
118. Grady, D. and M. Kipp, *Dynamic fracture and fragmentation*, in *ln - Highpressure shock compression of solids*, J.R. Asay and M. Shahinpoor, Editors. 1993, Springer: New York, United States of America. p. 265-322.
119. Repetto, E., R. Radovitzky, and M. Ortiz, *Finite element simulation of dynamic fracture and fragmentation of glass rods.* Comput. Methods Appl Mech. Engg., 2000. **183**.
120. Freund, L.B., *Dynamic fracture mechanics* 1990, Cambridge university press: Cambridge, UK p. 563.
121. Hart, R., *An introduction to distinct element modelling for rock engineering*, in *ln Comprehensive rock engineering Oxpford*, J.A. Hudson, Editor 1993, Pergoman Press: Oxford UK. p. 245-261.
122. Mortazavi, A. and P.D. Katsabanis, *Modelling burden size and strata dip effects on the surface blasting process.* lnt. J. Rock Mech. Min. Sci. , 2001. **38**: p. 481-98.
123. Toper, A.Z., *Numerical modelling ta investigate the effects of blasting in confined rock simulation of a field study* in *In Proc. 35th US Symp. Rock Mech* J.J.K. Daemen and R.A. Schultz, Editors. 1995, Balekma, Rotterdam: University of Nevada, Reno, USA.
124. Cho, S.H., et al., *Effect of the wavetonn of applied pressure on rock fracture process in one free-face.* J. of Sc. Tech. Energetic Mat. , 2003. **64**(3): p. 116-25.

125. Lilley, C.R., *The likelihood of blast induced near field in for cemented hydraulic fill.* Undergraduate Thesis, The University of Queensland, Brisbane, 1994.

126. Pierce, M.E., *Assessment of the liquefaction potential of saturated hydraulic fill in the 3ES stope at Osborne Mine* Itasca Consulting Group Inc. Minneapolis, 2001.

127. Cundall, P., J.H. Shillabeer, and G. Herget. *Modelling to Predict Backfill Stability in Transverse Pillar Extraction*. in *12th Canadian Rock Mechanics Symposium (Ref: 5)*. 1978. Sudbury Canada: Canadian Institute of Mining and Metallurgy.

128. Villaescusa, E., I. Onederra, and C. Scoot, *Blast induced damage and dynamic behvaiour of hangingwalls in bench stoping*, in *Fragblast*2004. p. 23-40.

129. Sarracino, R.S. and J.R. Brinkmann, *The modelling of shock effects in blasthole liner experiments.* The Third International Symposium on rock Fragmentation by Blasting, Brisbane Australia, 1990: p. 199 - 203.

130. Arjang, B., *Premining ground stresses at the Bousquet/Dumagami mines, Cadillac, Quebec.* CANMET, Energy, Mines and Resources Canada, Div Report MRL 88-132 (TR), 1988.

131. Zhou, X.J. and R.L. McNearny, *Triaxial Shear Characterization of CRF Test Specimens by PFC3D*, in *Golden Rocks 2006, The 41st U.S. Symposium on Rock Mechanics (USRMS): "50 Years of Rock Mechanics - Landmarks and Future Challenges."*2006, American Rock Mechanics Association: Golden, Colorado, USA. p. ARMA/USRMS 06-1074.

132. Emad, M.Z., H.S. Mitri, and J.G. Henning, *Some factors affecting cemented rockfill failure in longhole mining.* Proceedings of the Twentieth International Symposium on Mine Planning and Equipment Selection MPES 2011, Edited by A. ZHARMENOV, R.SINGHAL, S.YEFREMOVA, 2011: p. 163 - 174.

133. Emad, M.Z., H. Mitri, and J.G. Henning, *Effect of Backfill Placement Method on Its Stability: A Dynamic Modelling Case Study.* 21st Canadian Rock Mechanics Symposium, RockEng12 Edmonton AB 5 - 9, May 2012, 2012: p. 187 - 196.

134. Villaescusa, C.W.a.E., *Factors influencing the strength of cemented aggregate fill*, in *Minefill 2001: The 7th International Symposium on Mining with Backfill* D. Stone, Editor 2001, Society for Mining, Metallurgy & Exploration: Seatle Washington. p. 81 - 90.

135. Peterson, S.M., *Cemented Rockfill optimization in Vertical Block Mining.* Master thesis - Submitted to University of Alberta, Edmonton AB, Canada, 1996.

136. Farsangi, P.N., A.G. Hayward, and F.P. Hassani, *Consolidated rockfill optimization at Kidd Creek Mines.* CIM Bulletin, 1993.

137. Shaw-web-space. *http://members.shaw.ca/kcic1/mapmb.html*. 2013 Jan 1, 2013].

138. Crackle, D. and M. Heisel, *Stope Blasting Design and Experience at the Carr Fork Mine*, in *Design and Operation of Caving and Sublevel Stoping Mines*1981, Society of Mining and Metallurgy New York NY, USA. p. 529-38.

139. Donze, F.V., J. Bouchez, and S.A. Magnier, *Modeling fractures in rock blasting.* Int. J. Rock Mech. Min. Sei., 1997. **34**(8): p. 1153-1163.

140. Henderson, A.M. and C.R. Lilley, *Backfill Selection and Experience at the Kanowa Belle Gold Mine, Western Australia*, in *Minefill 2001: 7th International Symposium on Mining with Backfill*, D. Stone, Editor 2001, Society of Mining and Metallurgical Engineering: Littleton, Colarado. p. 379-387.

141. McNearny, R.L. and Q. Li, *Numerical Study of Stope Backfill Behavior in an Underground Mine*, in *AlaskaRocks 2005, Rock Mechanics for Energy, Mineral and Infrastructure Development in the Northern Regions*2003, ARMA. p. paper 824.

142. Manitoba. *www.manitoba.com*. 2013 [cited 2013 Jan 13].

143. Li, Q., R.L. McNearny, and M.M. MacLaughlin, *Stability of Sublevel Fill Stops Under Blasting Load*, in *Fourth International Conference in Computer Applications in Minerals Industries (CAMI 2003)*, R. Singhal and K. Fytas, Editors. 2005, International Journal of Mining Reclamation and Environment: Calgary, Alberta, Canada.

144. Sacrison, R.R. and L.M. Roberts. *Meikle Mine Backfill System -A Case History*. in *Minefill 2001: Proceedings of the 7th International Symposium on Mining with Backfill*. 2001. Seatle Washington: Society for Mining and Metallurgy & Exploration.

145. Hoek, E.D.M.S., *Empirical estimation of rock mass modulus.* International Journal of Rock Mechanics and Mining Sciences, 2006. **43**(2): p. 203-215.

146. Hoek, E., C.T. Carranza-Torres, and B. Corkum. *Hoek-Brown failure criterion - 2002 edition*. in *Proceedings of the Fifth North American Rock Mechanics Symposium and 17th Tunneling Association of Canada Conference, Toronto*. 2002. Toronto, ON Canada.

147. Herget, G. and P. Miles, *Ground Stress Determinations at Thompson and Birchtree Mines, Thompson, Manitoba.*, C.C.F.M.a.E.T.M.R.L.R. Mrp/Mrl., Editor 1979.

148. Washington, G.o. *Washington State Department of Labor & Industries – Rules and Policies, Use of Explosive Materials Chapter 296-52 – Part C Vibration and Damage Control* 2002 [cited 2011 June 8th 2011]; http://www.lni.wa.gov/wisha/rules/explosives/HTML/52-c.htm#WAC296-52-67065].

149. Potvin, Y., *Empirical open stope design in Canada*, 1990, National Library of Canada: Ottawa.

150. Hoek, E. and E.T. Brown, *Practical estimates of rock mass strength.* International Journal of Rock Mechanics and Mining Sciences, 1997. **34**(8): p. 1165-1186.

151. Nickson, S.D. *Cable support guidelines for underground hard rock mine operations*. 2008; Available from: http://hdl.handle.net/2429/1924.

152. Mathews, K., et al., *Prediction of stable excavation spans for mining at depths below 1,000 meters in hard rock*, ed. C.C.f.M.E. Technology and G. Associates1980, Ottawa: Canada Centre for Mineral and Energy Technology.

153. Barton, N., R. Lien, and J. Lunde, *Engineering classification of rock masses for the design of tunnel support Barton, N Lien, R Lunde, J 8F, 14T, 24R Rock mechanics, v6, n4, Dec. 1974, p189236.* International Journal of Rock Mechanics and Mining Sciences & Geomechanics Abstracts International Journal of Rock Mechanics and Mining Sciences & Geomechanics Abstracts, 1975. **12**(5-6): p. 77-77.

154. Scotia, G.o.N. *Blasting Safety Regulations, Part 82 of the Occupational Health and Safety Act Sections 63 to 65 of Firing*. 2008 May 15, 2011]; <http://www.gov.ns.ca/just/regulations/regs/ohsblasting.htm>].

155. Olofsson, S.O., *Applied explosives technology for construction and mining*1990, Arla, Sweden: APPLEX.

156. Dowding, C.H., *Suggested method for blast vibration monitoring.* International Journal of Rock Mechanics and Mining Sciences & Geomechanics Abstracts, 1992. **29**(2): p. 145-156.

157. Peredery, W.V. and G. staff, *Geology and Nickel Sulphide Deposits of the Thompson Belt, Manitoba.* , in *In Precambrian SuIphide Deposits*, H.S. Robinson and R.W. Hutehinson, Editors. 1982. p. 165-209.

158. Macek, J.J., et al. *Mapping the Thompson Nickel Belt and its extensions*. 2009 [cited 2013 February 6th].

159. Shnorhokian, S., H. Mitri, and D. Thibodeau, *Numerical simulation of pre-mining stress field in a heterogeneous rockmass. (revision submitted 2013).* Int. Journal of Rock Mechanics and Mining Sciences, 2013.

160. Sainoki, A. and H. Mitri, *Effect of stope production blast on nearby fault*, in *23rd World Mining Congress* F. Hassani, Editor 2013, Canadian Institute of Mining and Metallurgy: Montreal Canada.

161. Atlas, *Explosives and Rock Blasting*1987, Atlas Powder Company: ISBN 0-9616284-0-5.

162. Nie, S.L. and M. Olsson. *Study of mechanism by measuring pressure history in blast holes and crack lengths in rock.* in *ln Proc. 27th annual conf. Explosives and Blasting Technique*. 2000. Orlando, US. .

163. Clark, G.B., *Principles of rock fragmentation*1987, London UK: John Wiley & Sons Inc.

164. Alavez, A.C., et al. *PROPERTIES OF COMPACTION REACHED IN THE ROCKFILLS OF THE EL CAJÓN DAM* in *The 1st International Symposium on Rockfill Dams* 2009. Chengdu, China: China Institute of Water Resources and Hydropower Research (IWHR).